Performance Analysis for a Shaded-Pole Linear Induction Motor

Innocent Ewean Agbongiague Davidson

Thesis Presented for the Degree of
DOCTOR OF PHILOSOPHY
in Department of Electrical Engineering
University of Cape Town
February 1998

Performance Analysis for a Shaded-pole Linear Induction Motor

by

Innocent Ewean Agbongiague Davidson

B.Eng., M.Eng. *University of Ilorin, Nigeria*

Submitted to the Department of Electrical Engineering
in fulfillment of the requirements of the degree of

Ph.D (Eng)

at the

UNIVERSITY OF CAPE TOWN

February 1998

Dedication

Dedicated to my son,

Kenan Nosagie Osamagbe Davidson.

Declaration

I declare that this thesis is my own original and unaided work, except where otherwise acknowledged. It is being submitted for the degree of Doctor of Philosophy in the Department of Electrical Engineering at the University of Cape Town. It has not been submitted before for any degree or examination at this or any other university. Portions of the work have been published in international journals and conference proceedings. The author confirms that in accordance with the University of Cape Town rule GP7(3) that he was the primary researcher in all instances where work described in this thesis was published under joint authorship.

Innocent Ewean Agbongiague Davidson

12 February, 1998.

Acknowledgement

My sincere thanks go to my supervisor, Prof. Jacek F. Gieras, for his invaluable advice and guidance throughout my research, which enabled me bring this work to completion.

Thanks to the University of Cape Town, the Foundation of Research and Development (FRD) and the Federal University of Technology, Akure - Nigeria for their financial assistance.

Finally, my deepest thanks go to my wife, Candace, for her loving support and patient encouragement, and above all, to my Lord and Saviour Jesus Christ, the Author and Perfecter of my faith.

Abstract

The induction motor remains the prime mover of present day industry with it's associated components in drive applications. In many such applications, fractional horse-power motors find ready use in small mechanisms where three-phase power supply is not available. In Southern Africa, these motors can be used is rural areas with simple reticulation systems, hence the renewed interest in the development of these low-power electrical motors, especially specialised models such as linear versions of such motors for special applications.

This research is in the area of single-phase LIMs. The objective has been to model the shaded-pole LIM, in an attempt to enhance it's performance through improved design methods. This was carried out using an integrated analysis approach, involving circuital and field theory in the analysis of the practical motor, and computer simulation of it's equivalent model using the finite element method.

Linear counterparts are possible for all the various forms of rotating electrical machines. All cylindrical machines can be 'cut' along a radial plane and 'unrolled' [32]. LIMs convert electrical energy directly into mechanical energy of translatory motion. Some advantages of linear version of induction motors are: they are gearless and often require minimal material thus minimising cost.

While their scope of application are somewhat limited when compared to rotary versions, they do however give excellent performance in special situations where translatory motion is required. However, the output power-to-mass and output power-to-volume of active materials ratio is reduced compared to rotary induction motors[45]. These disadvantages are caused by the large air-gap and the open magnetic circuit, which produces parasitical effects.

A 4-pole shaded-pole single-sided flat LIM with a 0.52m double layer disc has been analysed and tested. The thickness of back iron is 10mm, the thickness of aluminium cap is 3mm and the airgap thickness is 1.5mm. This thesis presents a study of the shaded-pole single-phase single-sided LIM for industrial applications, performance calculations using two-phase symmetrical components approach, field analysis calculations, 2-D electromagnetic field analysis based on the Magnet 5 finite element software package, and experimental tests.

The experimental tests were carried out on the shaded-pole LIM using sinusoidal excitation for various power frequencies. A comparison of results obtained from FEM, symmet-

rical components and field theory with practical measurements is presented and discussed. The application of FEM seems to be well justified in order to obtain not only the performance characteristics, but also to analyse and optimise the magnetic circuit.

It was found that the performance characteristics of the shaded-pole LIM are rather poor in comparison with a three phase rotary induction motor and a three phase linear induction motor. Although its efficiency is very small at power frequency, it has been found that the efficiency increases with the input frequency. The shaded-pole LIM can find applications in turntables used in industry or in small mechanisms where a three-phase power supply is not available or the price and simplicity of the drive is important.

List of Figures

2.1 General Assembly of the 4-pole Shaded-Pole LIM 7
2.2 Sectional View of the Shaded-Pole LIM 8
2.3 Structure of the 4-pole Shaded-Pole LIM: 1 - secondary back iron, 2 - aluminium cap, 3 - airgap, 4 - short-circuited coil, 5 - main winding, 6 - primary stack . . . 8
2.4 Schematic diagram of shaded-pole LIM parameters 12
2.5 LIM Topology (a) shaded-pole primary stack (b) arc-shaped primary . . . 20

3.1 Asymmetric system of current vectors 23
3.2 Symmetrical components of asymmetric system of current vectors 24
3.3 Phasor diagram of stator phase currents I_a^+ and I_b^+, $\alpha = 90°$ 27
3.4 Phasor diagram of stator phase currents I_a^- and I_b^-, $\alpha = 90°$ 27
3.5 Phasor diagram of stator phase currents I_a and I_b, $\alpha = 90°$ 28
3.6 Phasor diagram of stator phase currents I_a^+ and I_b^+, $\alpha = 75°$ 30
3.7 Phasor diagram of stator phase currents I_a^- and I_b^-, $\alpha = 75°$ 30
3.8 Phasor diagram of stator phase currents I_a and I_b, $\alpha = 75°$ 31
3.9 Phasor diagram of stator phase currents I_a^+ and I_b^+, $\alpha = 45°$ 33
3.10 Phasor diagram of stator phase currents I_a^- and I_b^-, $\alpha = 45°$ 33
3.11 Phasor diagram of stator phase currents I_a and I_b, $\alpha = 45°$ 34
3.12 Phasor diagram of stator phase currents I_a^+ and I_b^+, $\alpha = 29.3°$ 43
3.13 Phasor diagram of stator phase currents I_a^- and I_b^-, $\alpha = 29.3°$ 43
3.14 Phasor diagram of stator phase currents I_a and I_b, $\alpha = 29.3°$ 44
3.15 Equivalent circuit of a shaded pole induction motor, Phase a positive sequence 45
3.16 Equivalent circuit of a shaded pole induction motor, Phase a negative sequence 45
3.17 Equivalent circuit of a shaded pole induction motor, Phase b positive sequence 46
3.18 Equivalent circuit of a shaded pole induction motor, Phase b negative sequence 46
3.19 Equivalent circuit of a shaded-pole induction motor, positive sequence . . . 47
3.20 Equivalent circuit of a shaded-pole induction motor, negative sequence . . 48
3.21 Flow-Chart of Shaded-pole Motor Computer Program 50
3.22 Torque against speed at $f = 75Hz$ 52
3.23 Torque against speed at $f = 60Hz$ 53
3.24 Torque against speed at $f = 50Hz$ 54
3.25 Torque against speed at $f = 40Hz$ 55

4.1 Geometric Model of shaded-pole LIM 59

4.2 Magnetic field distribution of shaded-pole LIM 61
4.3 Normal component of airgap magnetic flux density at standstill,(Magnetostatic), $V_1 = 220V$ and $f = 0Hz$: 1 - FEM computation, 2 - measurements. 62
4.4 Torque against speed at $f = 75Hz$ 65
4.5 Torque against speed at $f = 60Hz$ 66
4.6 Torque against speed at $f = 50Hz$ 67
4.7 Torque against speed at $f = 40Hz$ 68
4.8 Torque against speed at $f = 75Hz$ 69
4.9 Torque against speed at $f = 60Hz$ 70
4.10 Torque against speed at $f = 50Hz$ 71
4.11 Torque against speed at $f = 40Hz$ 72

5.1 Flow-Chart of Shaded-pole LIM using Field Theory 79
5.2 Torque against speed at $f = 75Hz$ 80
5.3 Torque against speed at $f = 60Hz$ 81
5.4 Torque against speed at $f = 50Hz$ 82
5.5 Torque against speed at $f = 40Hz$ 83

6.1 Shaded-pole LIM, Voltage Vs Input Current. 85
6.2 Shaded-pole LIM, Voltage Vs Power Factor. 86
6.3 Shaded-pole LIM, Voltage Vs Input Power. 87
6.4 Torque Measurement Using the Prony's Brake Method. 88
6.5 Shaded-pole LIM, Torque Vs Speed. 89
6.6 Shaded-pole LIM, Efficiency Vs Speed. 90
6.7 Shaded-pole LIM, Input Power Vs Speed. 91
6.8 Shaded-pole LIM, Output Power Vs Speed. 92
6.9 Shaded-pole LIM, Input Current Vs Output Power. 93
6.10 Shaded-pole LIM, Power Factor Vs Speed. 94
6.11 Shaded-pole LIM, Torque Vs Input Voltage. 95
6.12 Shaded-pole LIM, Input Power Vs Input Voltage. 96
6.13 Shaded-pole LIM, Power Factor Vs Input Voltage. 97
6.14 Shaded-pole LIM, Input Current Vs Input Voltage. 98
6.15 Shaded-pole LIM, Voltage Vs Input Current 99
6.16 Shaded-pole LIM, Voltage Vs Power Factor 100
6.17 Shaded-pole LIM, Voltage Vs Input Power 101
6.18 Torque Vs Speed for Varying Frequency 102
6.19 Efficiency Vs Speed for Varying Frequency 103
6.20 Output Power Vs Speed for Varying Frequency 104
6.21 Power Factor Vs Speed for Varying Frequency 105
6.22 Power Factor Vs Input Frequency ($V/f \approx 2.0$) 106
6.23 Shaft Torque Vs Input Frequency ($V/f \approx 2.0$) 107
6.24 Output Power Vs Input Frequency ($V/f \approx 2.0$) 108
6.25 Efficiency Vs Input Frequency ($V/f \approx 2.0$) 109

6.26 Speed Vs Input Frequency ($V/f \approx 2.0$) 110
6.27 Shaft Torque Vs Input Frequency at 220V and rated load 112
6.28 Efficiency Vs Input Frequency at 220V and rated load 113
6.29 Output Power Vs Input Frequency at 220V and rated load 114
6.30 Power Factor Vs Input Frequency at 220V and rated load 115
6.31 Speed Vs Input Frequency at 220V and rated load 116
6.32 Torque Vs Speed for varying γ and σ_1, f=50Hz, V=90V 118
6.33 Torque Vs Speed for varying γ and σ_1, f=75Hz, V=160Hz 119
6.34 Short-circuit Test: Torque Vs Input Voltage 120

7.1 Torque against speed at $f = 75Hz$ 122
7.2 Torque against speed at $f = 60Hz$ 123
7.3 Torque against speed at $f = 50Hz$ 124
7.4 Torque against speed at $f = 40Hz$ 125

List of Tables

2.1 Specification data of the tested shaded-pole LIM 10
2.2 Design Data of LIM 11

3.1 Simulation data of shaded-pole LIM at 90V, 50Hz and $\alpha = 90°$ 26
3.2 Phase current I_a and symmetrical components at 90V, 50Hz, $\alpha = 90°$ . . . 28
3.3 Phase current I_b and symmetrical components at 90V, 50Hz, $\alpha = 90°$ . . . 28
3.4 Simulation data of shaded-pole LIM at 90V, 50Hz and $\alpha = 75°$ 29
3.5 Phase current I_a and symmetrical components at 90V, 50Hz, $\alpha = 75°$ . . . 31
3.6 Phase current I_b and symmetrical components at 90V, 50Hz, $\alpha = 75°$ . . . 31
3.7 Simulation data of shaded-pole LIM at 90V, 50Hz and $\alpha = 45°$ 32
3.8 Phase current I_a and symmetrical components at 90V, 50Hz, $\alpha = 45°$ . . . 34
3.9 Phase current I_b and symmetrical components at 90V, 50Hz, $\alpha = 45°$ . . . 34
3.10 Simulation data of shaded-pole LIM at 90V, 50Hz and $\alpha = 29.3°$ 42
3.11 Phase current I_a and symmetrical components at 90V, 50Hz, $\alpha = 29.3°$ . . 44
3.12 Phase current I_b and symmetrical components at 90V, 50Hz, $\alpha = 29.3°$ . . 44

6.1 Variation of LIM efficiency with Frequency $V/f \approx$ constant 111
6.2 Variation of LIM efficiency with Frequency, V = 220 volts 111
6.3 Variation of LIM torque with γ and σ_1 117

7.1 B-H Curve for Cold Rolled Steel Primary Core 139
7.2 B - Specific Loss Curve for Cold Rolled Steel Primary Core 140
7.3 H_{Fe}, B_{Fe}, a_R, a_X Data for Solid Steel Secondary 141
7.4 Shaded-Pole Flat Linear Induction Motor Load Test Data - 50Hz 144
7.5 Shaded-Pole Flat Linear Induction Motor Load Test Data - 60Hz 144
7.6 Shaded-Pole Flat Linear Induction Motor Load Test Data - 75Hz 145
7.7 Magnetic Flux Density Measurements 147
7.8 Magnetic Flux Density Vs Voltage ($B \propto V$) 148

Contents

Dedication i

Declaration ii

Acknowledgements iii

Abstract iv

List of Figures vi

List of Tables vii

Table of Contents viii

List of Symbols and Abbreviations xi

1 Introduction 1
- 1.1 Background . . . 1
- 1.2 Motivation . . . 2
- 1.3 Objective . . . 3
- 1.4 Literature review . . . 3

2 Construction 7
- 2.1 General Assembly . . . 7
- 2.2 Design Data for shaded-pole motor . . . 9
- 2.3 Main Dimension and Electromagnetic Loading . . . 12
  - 2.3.1 Transformation Factor, k_{tr} . . . 12
  - 2.3.2 Carter's Coefficient . . . 12
  - 2.3.3 Resistance of Primary Winding, R_{1a} . . . 13
  - 2.3.4 Winding Impedances . . . 13
  - 2.3.5 Mutual(Magnetising) Reactance . . . 14
  - 2.3.6 Stator Leakage Reactance as seen from the Main Phase . . . 14
  - 2.3.7 Auxiliary Phase Leakage Reactance . . . 14
  - 2.3.8 Impedance of Vertical Branch for Series Connection . . . 14

2.3.9 Mutual Reactance Between Main and Auxiliary Phases 15
2.3.10 Rotor Impedance 15
2.3.11 Coefficient including Transverse Edge Effect, k_{rn} 16
2.3.12 Linear Speed of LIM 16
2.3.13 Slip 17
2.3.14 Electromagnetic field equations 17
2.3.15 Magnetic Permeability, μ_i 18
2.3.16 Magnetic Flux Density Components, B_{mz_1} 19
2.4 Effect of reaction rail curvature 20

3 Performance Calculation Using Symmetrical Components **21**
3.1 Stator Magnetic Field 21
3.2 Symmetrical Components of Two-Phase System 22
3.3 Equations for Phase Currents I_a and I_b 24
3.4 Circuital Analysis 35
3.4.1 Voltage Equations for Main and Auxiliary Phases 35
3.4.2 Voltage and Current Equations for Angle $\alpha \leq 90°$ 35
3.4.3 Main Phase 36
3.4.4 Auxiliary Phase 37
3.4.5 Verification of Equations 38
3.4.6 Equations for Currents I_a^+ and I_a^- 40
3.5 Resistances and reactances of the equivalent circuit of LIM 45
3.6 Resultant Secondary Impedance 47
3.7 Total Impedance of Motor 47
3.8 Rotor Currents 48
3.9 Electromagnetic Torque 49
3.10 Software Program 49
3.11 Conclusions 51

4 Performance Calculation Using Finite Element Analysis **56**
4.1 Fundamental electromagnetic field equations 56
4.2 Modelling the shade-pole LIM 60
4.3 Magnetostatic Analysis 60
4.4 Eddy Current (Time-harmonic) Analysis of LIM 60
4.5 Comparison of FEM calculation and measurement 63
4.6 Conclusions 64

5 Performance Calculation Using Field Theory Approach **73**
5.1 Defining the LIM problem 73
5.2 Solution of field equations 74
5.3 Electromagnetic field equations 74
5.4 Calculation of forces using Maxwell's stress tensor method 77
5.5 Field analysis software program 78

5.6 Comparison of analytical approach with FEM 78
5.7 Conclusions 78

6 Experimental Tests Using Sinusoidal Excitation **84**
6.1 Testing at rated voltage and frequency 84
6.1.1 No-Load Test of LIM at rated voltage and frequency 84
6.1.2 Load Test of LIM at rated voltage and frequency 88
6.1.3 Short Circuit Test of LIM 95
6.2 Testing for optimum performance of LIM 99
6.2.1 No-Load Test of LIM with V/f $\approx$ 2.0 99
6.2.2 Load Test of LIM with V/f $\approx$ 2.0 102
6.2.3 Analysis of Results 106
6.3 Comments on Measurements and Analytical Results 117

7 Conclusion **121**
7.1 Optimisation 121
7.2 Error Estimation in Measurement and Analysis 121
7.3 Comparison of Measurements and Calculated Parameters 122
7.4 Comparison of Analytical Techniques 126
7.5 Efficiency of Shaded-pole LIM 127
7.6 Applications 128

Appendix A **137**

Appendix B **142**

Appendix C **146**

List of Symbols and Abbreviations

Symbols	Units	
$\mathbf{A}$	Wb/m	magnetic vector potential
a	m	main excitation winding
b	m	shaded pole or auxiliary winding
$\mathbf{B}$	T	magnetic flux density
B_a	T	normal component of magnetic flux density due to phase a
B_b	T	normal component of magnetic flux density due to phase b
$b(x,t)$	T	normal component of magnetic flux density distribution
$B^+_{m\nu}$	T	peak value of magnetic flux density for the ν^{th} space harmonic (forward) wave travelling in the x-direction along the pole pitch
$B^-_{m\nu}$	T	peak value of magnetic flux density for the ν^{th} space harmonic (backward) wave travelling in the x-direction along the pole pitch
d	m	thickness of aluminium (disc) layer
d_{sec}	m	diameter of secondary (aluminium and mild steel rotor disk)
d_w	m	diameter of wire with insulation
$\mathbf{E}$	V/m	electric field intensity
F_x	N	tangential force
F_z	N	normal force
f	Hz	frequency
g	m	air gap
$\mathbf{H}$	A-t/m	magnetic field intensity
H_{ahp}	A-t/m	magnetic field intensity of air half-space
H_{Al}	A-t/m	magnetic field intensity of aluminium cap layer
H_{Fe}	A-t/m	magnetic field intensity of ferromagnetic layer
H_g	A-t/m	magnetic field intensity of airgap layer
h_P	m	height of pole
h_s	m	height of shading ring slot
H_{sec}	m	thickness of ferromagnetic core
I_a	A	current in main stator winding (phase a)

I_a^+	A	positive sequence stator current
I_a^-	A	negative sequence stator current
I_b'	A	current in auxiliary winding (phase b) referred to main winding side
I_b^+	A	positive sequence current in auxiliary winding
I_b^-	A	negative sequence current in auxiliary winding
$I_2'^+$	A	positive sequence rotor current referred to the primary side
$I_2'^-$	A	negative sequence rotor current referred to the primary side
j		complex notation
$\mathbf{J}$	A/m^2	current density
k_{ab}		transformation factor for bringing the auxiliary winding to the main winding side
k_{tr}		transformation factor for bringing the rotor impedance to the stator
k_{w1a}		winding factor of main windings
k_{w1b}		winding factor of auxiliary winding
L_τ	m	length of primary stack
L_i	m	width of primary stack
m_1		number of phases
N_a		number of turns per main phase winding
N_b		number of turns per auxiliary phase winding
p		number of poles
R	Ω	resistance
R_{dc}	Ω	resistance of main winding for dc current
R_{Fe}	Ω	core losses
s		rotor slip
s^+		rotor slip (positive sequence)
s^-		rotor slip (negative sequence)
t_p	m	thickness of insulation paper between windings
v	m/s, rpm	speed
v_s	m/s, rpm	synchronous speed
V_a	V	input voltage across the main phase terminals
V_b	V	induced voltage in short-circuited (auxiliary) winding
w_p	m	width of pole
w_s	m	width of shading pole slot
X	Ω	reactance
X_m	Ω	mutual reactance between primary and secondary side
Z^+	Ω	positive sequence impedance of the vertical branch (Z_o) in parallel with the secondary ($Z_2'^+$)
Z^-	Ω	negative sequence impedance of the vertical branch (Z_o)

		in parallel with the secondary ($Z_2'^-$)
Z_{ab}	Ω	mutual reactance between main and auxiliary windings
Z_a^+	Ω	resultant impedance of the motor together with the main winding for positive sequence current
Z_a^-	Ω	resultant impedance of the motor together with the main winding for negative sequence current
Z_b^+	Ω	resultant impedance of the motor together with the main winding for positive sequence current
Z_b^-	Ω	resultant impedance of the motor together with the main winding for negative sequence current
Z_{1a}	Ω	impedance of the main stator winding
Z_{1b}	Ω	impedance of the auxiliary winding
Z'_{Al}	Ω	impedance of aluminium (disc) secondary
Z'_{Fe}	Ω	impedance of back iron (disc) secondary
Z_t^+	Ω	total impedance of LIM as seen from the input terminals positive sequence
Z_t^-	Ω	total impedance of LIM as seen from the input terminals negative sequence
α		space angle between the two stator windings or symmetry axes of a and b
β_ν		phase angle between the currents in phase a and b
ϵ	F/m	electric permittivity
Φ	Wb	magnetic flux
Θ	A-t	peak value of magnetomotive force
τ	m	pole pitch
σ	S/m	electric conductivity
μ	Wb/A.m	magnetic permeability
μ_o	Wb/A.m	permeability of free space
μ_r		relative permeability
μ', μ''		coefficients of complex magnetic permeability
μ_{rs}		surface relative permeability of ferromagnetic layer
ν		number of space harmonics
ω		angular frequency
ω_1		angular synchronous frequency for fundamental harmonic
ω_2		angular rotor frequency
$\omega_{s\nu}^+$		angular frequency for the forward travelling field
$\omega_{s\nu}^-$		angular frequency for the backward travelling field
∞		infinity
λ		specific permeance of slot leakage
χ_k		propagation constant taking into account space distribution of electromagnetic field

Subscripts

i	1,...., $k-1$, k - number of layer
n	n^{th} space harmonic of field distribution in the y direction
s	surface value
x, y, z	components of vector in the x,y,z directions

Superscripts

k	quantity of layers of the object (secondary)
'+'	forward-travelling field
'-'	backward-travelling field

Abbreviations

A	ampere
a.c.	alternating current
Al	aluminium
d.c	direct current
d-q	direct, quadrature axis
Eqn	equation
FA	field analysis
FEM	finite element method
HGST	high speed ground transport
L.H.S	left hand side
LIM	linear induction motor
LSM	linear synchronous motor
Mea	measurements
MMF	magnetomotive force
R.H.S	right hand side
rpm	revolutions per minute
rms	root mean square
SMC	symmetrical components
V	volt
2-D	two-dimensional

Chapter 1

Introduction

1.1 Background

Fractional horsepower single-phase motors find application as general purpose machines and in automatic control systems. These machines are essential parts of industrial control systems, regulation systems, computer peripherals and domestic appliances. Although three-phase motors are available in ratings as low as 125 W, the majority of small power a.c. motors operate on single-phase alternating current[35].

The most popular single-phase motors are induction motors. They have been developed with varying torque requirements and differ in their starting methods, hence their names are descriptive of their starting methods. This provides for a minimisation of motor cost which satisfies the conditions for a particular application. Such starting techniques include: shaded-pole, split-phase[68], capacitor-start induction-run, single-value-capacitor, capacitor-start capacitor-run and the universal motor. Modern solutions to single-phase a.c. drives include: single-phase rectifiers, filter three-phase inverters and three-phase brushless motors.

Over the years, linear versions of the induction motor, d.c. motor, synchronous motor, permanent magnet motor, stepper motor and reluctance motor have been developed [32, 59, 69]. This can be attributed in part to the development of power electronic converters, new control techniques and materials such as rare-earth permanent magnets[70]. Typical applications of linear drives include high-speed ground transportation (HSGT)[28, 104, 77, 98, 39], material transportation[95, 51, 31, 44, 60], factory automation, office automation, measuring instruments as well as home and medical applications[57, 76].

The competitiveness of linear motors is perhaps reflected in the steady sales by several manufacturers, even though no mass market currently exists for them[69]. The development of linear drives and their increasing application in industry will ultimately minimise the use of several mechanical components. For example in high-speed ground transportation, magnetically levitated electromagnetic and electrodynamic systems are taking precedence to conventional rotary induction motors.

Presently, the cheapest and most reliable electrical machine is the cage induction motor. Since the linear motor may be considered to be an unrolled version of its cylindrical counterpart, the linear induction motor (LIM), with its simple variable voltage controller, is currently the most common in the field of linear drives for industrial applications. LIMs are playing an increasing role in industrial and transportation applications. Typical industrial applications of LIMs include: internal transport systems, transfer systems, impact machines (e.g. hammers, presses), piston pumps, linear tables, textile machinery, vibrators, rammers, saws and separators.

Linear motors show great potential in specialised applications in industry, especially where direct translatory motion is required. A rotary induction motor can theoretically be replaced by a LIM in any translatory motion drive and in some cases in rotating wheels, discs and drums where small torques are transmitted and small friction forces take place[45].

Presently, the range of applications of LIMs, when compared to rotary induction motors is limited by several factors such as: the increased temperature rise of the primary winding, increased energy consumption, and reduced efficiency. In factories and plants for example, LIMs can be used in transportation systems, materials handling, industrial drives, automative control systems, robotics and in industrial testing. However, there are many characteristics of linear motors that cannot be achieved by rotary equivalents[95, 59]. In several industrial applications, LIMs are competitive to rotary induction motors.

1.2 Motivation

The LIM has an open magnetic circuit with an entry and an exit end, while the rotary induction motor has a closed magnetic circuit. LIMs in industry have been confined mainly to low-speed applications, and the influence of the end effect in low-speed applications is not significant[112]. The problems arising from a larger air gap and a secondary solid conductive rail are common to both linear and rotary induction motors[58].

Furthermore, the output power-to-mass and output power-to-volume of active materials ratio in the LIM is reduced as compared to rotary induction motors[45]. These disadvantages are caused by larger air-gap than that of rotary induction motors and the open magnetic circuit, which produces parasitical end effects. Large airgaps means increased magnetising currents and consequently an increase in the input rms current. Thus, the winding losses are high and the efficiency decreases.

The capacity and flexibility in designing linear motors and adapting them for specialised applications is broad. These challenges have resulted in the need for continued analysis and improvement of existing design methods. This is expected to increase the overall performance of linear motors, with improved reliability and reduced power capacity, which will enhance their potential application.

The single-phase single-sided shaded-pole linear induction motor is the linear counterpart of the single-phase rotary shaded-pole motor. It can find applications in turntables used in industry. It also finds ready use in small mechanisms where a three-phase power

supply may not be available or where the price and simplicity of the drive is important. The development of single-phase electric motor is especially important in Southern Africa for example, where vast parts of the country are electrified using single-phase lines.

1.3 Objective

The objective of this thesis is to analyse the single-phase single-sided shaded-pole linear induction motor and determine its performance characteristics, i.e. :

- Performance calculation using two-phase symmetrical components approach
- Analysis of electromagnetic field and forces
- Application of 2-D finite element method (FEM) to performance calculations
- Experimental tests performed on the shaded-pole single-sided LIM
- Evaluation of construction and performance from the point of view of industrial application.

The single-phase single-sided shaded-pole linear induction motor is technically a two-phase motor with a main phase (main stator winding) and an auxiliary phase (shaded-pole) which provides the two phases required for starting and maintaining electromechanical energy conversion. Symmetrical components for two-phase system is normally used in the analysis of such single- or two-phase machines[19, 100, 92, 15].

For the field approach, the general solutions of equations for 2-D electromagnetic field distribution in an induction machine with salient poles is used in the analysis of the single-phase single-sided shaded-pole LIM, with multilayer secondary and distributed parameters[41, 112, 45, 10, 89]. The calculation of forces is carried out using Maxwell's stress tensor method[17].

Recent advances in computer hardware have given remarkable access to electromagnetic field simulation using finite elements. The FEM has been used for the electromagnetic field analysis and calculation of forces[37]. A comparison of different analysis methods, namely finite elements, symmetrical components and field analysis, has been carried out and the results compared with the measurements.

1.4 Literature review

The development of the generalised theory of induction motors with asymmetrical primary windings, i.e. the two-phase rotating field theory and symmetrical components theory for asymmetrical machines, was carried out over 40 years ago[106, 34, 5]. The method of symmetrical components[36] was originally developed in connection with the analysis

of symmetrically wound polyphase induction machines operating under unbalanced conditions. Since its original development, the method has proved to be of immense value in the analysis of problems involving a.c. rotating machines under both steady and transient[64] conditions.

Several early contributions have been made to the revolving field theory[52, 13] and analysis of unsymmetrical two-phase and single-phase induction machines[7, 96]. Morrill[72] presented an accurate theory of the split-phase motor, with regards to both starting and running performance, having derived general equations for an unbalanced two-phase motor and applying them to the special case of the capacitor motor. Puchstein and Lloyd[91] analysed the capacitor motor with windings not in quadrature. Chang and Llyod[18, 65] showed the usefulness of the cross field theory for the design of permanent split-phase motors. Burian[14] analysed the unsymmetrical machine from the viewpoint of the cross-field theory and derived an equivalent circuit for the machine. McCormick, Kuale and Foster's[68] work on the design of auxiliary phase windings for fractional-horsepower induction motors is most helpful from the point of view of practical engineering design.

Shaded pole rotary induction motors[106] have been built for more than ninety years[88]. They are one of the most popular type of single-phase induction motors in the fractional horsepower range[102, 2]. Due to their wide range of domestic and industrial applications, especially for constant speed applications and their low cost, these machines have been subject to continuing research efforts from which a number of analytical models and results have been published. Shaded pole motors are recognised to be among one of the most robust, durable, simple-to-design, and low cost machines with high reliability, yet they are classified to be among the most complicated to analyse[103, 19, 15, 62, 3].

Since it was discovered that a squirrel cage motor with a salient-pole single-phase field would run if a portion of the pole were short-circuited with a winding or coil[102], the saving in the cost of this winding, compared with distributed field winding of the split-phase type, has given the shaded pole motor tremendous popularity in low power, constant speed applications. Trickey[102] carried out a limited analysis of the shaded pole motor for standstill condition and later extended it to cover the running condition with performance calculations[103] using circuital method in calculating motor constants.

Bojer[8] carried out a pre-determination of shaded-pole induction-motor performance. Kron and Chang[55, 19] developed equations and equivalent circuits for the shaded pole motor using both the revolving and cross field theories, including the space harmonics introduced by the stator windings, the uneven airgap, machine parameters such as angle of shift of the shaded coil, turns ratio and influence of the shaded coil. Chang's[19] analysis appears to have found the widest application[15].

Morath[71] developed a mathematical theory of shaded-pole motors, while Kucera[56] also worked on single-phase induction motor with short circuited auxiliary winding. A qualitative analysis of the flux distribution in the airgap of the shaded-pole motor was carried out by Kimberly[53], where he evaluated the influence of the shaded-pole and

saturation on motor performance using both the classical rotating field theory and classical cross-field theory. Several other authors[101, 38, 73, 105] have made contributions to the theory and analysis of shaded-pole rotary induction motor.

Despite all these contributions, there appears to be no established single universal method of analysis to apply to these machines[3]. In the past, the single-phase induction motor was analysed either by the double-revolving-field theory or the crossfield theory. The relative merits and demerits of the two theories have often been debated[4]. Both theories can be blended into one through the field-theory approach[75].

Suhr's[100] analysis employs the resolution of the exciting winding and auxiliary-winding MMFs into quadrature components, and then applies symmetrical components theory in this analysis. If efficiency were a highly important consideration, or a high overload capacity were an application requirement, the shaded-pole motor and linear motors in general, would have few jobs to perform[100]. However, some of the reasons for wide-spread use of shaded pole motors[100] include: (a) it operates from single-phase power supply, (b) it is cheaper to build than other motors and this saving is passed on to the ultimate consumer, (c) it is usually quiet in operation, (d) it lends itself to speed control through simple means, and (e) if it is properly applied it has high reliability.

Possibly the most instrumental work in substantially increasing the rating and application of shaded-pole motors is the work of Sherer and Herzog[97] who studied the effects on performance due to the variation of one parameter while all other parameters were held constant. Using the generalised theory of induction motors with asymmetrical primary windings, Butler and Wallace[15, 107, 16] demonstrated its application and validity to the analysis and performance prediction of shaded-pole type of single-phase motors.

Desai and Matthew[29] carried out the transient analysis of the shaded pole motor. An analysis of the reluctance augmented shaded-pole motor, and the distribution of flux, current and torque operating under locked rotor conditions was carried out by Ooka[85, 86]. Eastham and Williamson[33] developed and verified a simple design technique of step-phase modulation based on a numerical-optimisation routine used to obtain a two-speed shaded-pole induction motor.

Saturation of the magnetic circuit[82] is an important factor in shaded-pole induction motors[88], and it varies widely when slip varies from 1 to 0. According to Williamson and Breese[109], high levels of saturation present in shaded-pole motors make the determination of leakage reactances and saturation factors extremely difficult. The authors also examined the reluctance-augmentation principle in shaded-pole motors[111]. Williamson and Ostojic' developed a new type of bi-directional shaded-pole motor which retains use of single-turn copper shading rings with full reversing capabilities rather than simply reversible[110].

Nondahl[81] presented an equivalent circuit model for a shaded pole induction motor – one shading coil with a stepped air gap. Lock[62, 61] carried out an analysis of the steady-

state performance of the reluctance-augmented shaded-pole motor and transient analysis of the shaded-pole motor by numerical solution of the basic performance equations. Hoang-Minh Dao[22, 21] worked on the calculation of the starting behaviour of shaded pole motors at standstill by stretching the contour of the machine. Dao also presented characteristic graphs for starting force, shaded pole current and eddy current losses in dependence of constriction parameters.

Computer-aided design using finite element method was used by Matsubara[67] in analysing the distribution of magnetic flux in the shaded-pole induction motor at various slips. Akbaba and Fakhro[3, 2] carried out a detailed field distribution in a reluctance augmented shaded-pole motor using finite element method, and improved technique for calculating inductance parameters. The result showed the effect of shading coil on the spatial distribution of the air-gap flux density, and it was found that the demagnetising effect of the shading rings helps towards more uniform distribution of the air-gap flux.

The single-phase single-sided shaded-pole linear induction motor with rotating disc under investigation is one of the simplest electric motors. The first physical model was jointly constructed at the University of Cape Town and Cape Technikon in 1991, and the first experimental results were published in 1992[49]. It is a rather simple, reliable and cheap electric motor. As the author is aware, no theoretical analysis has been published so far except for the author's paper[26, 27, 25]

Chapter 2

Construction

2.1 General Assembly

The general assembly of the single-phase single-sided shaded-pole LIM is shown in Figure 2.1. The physical model has been earlier constructed [49].

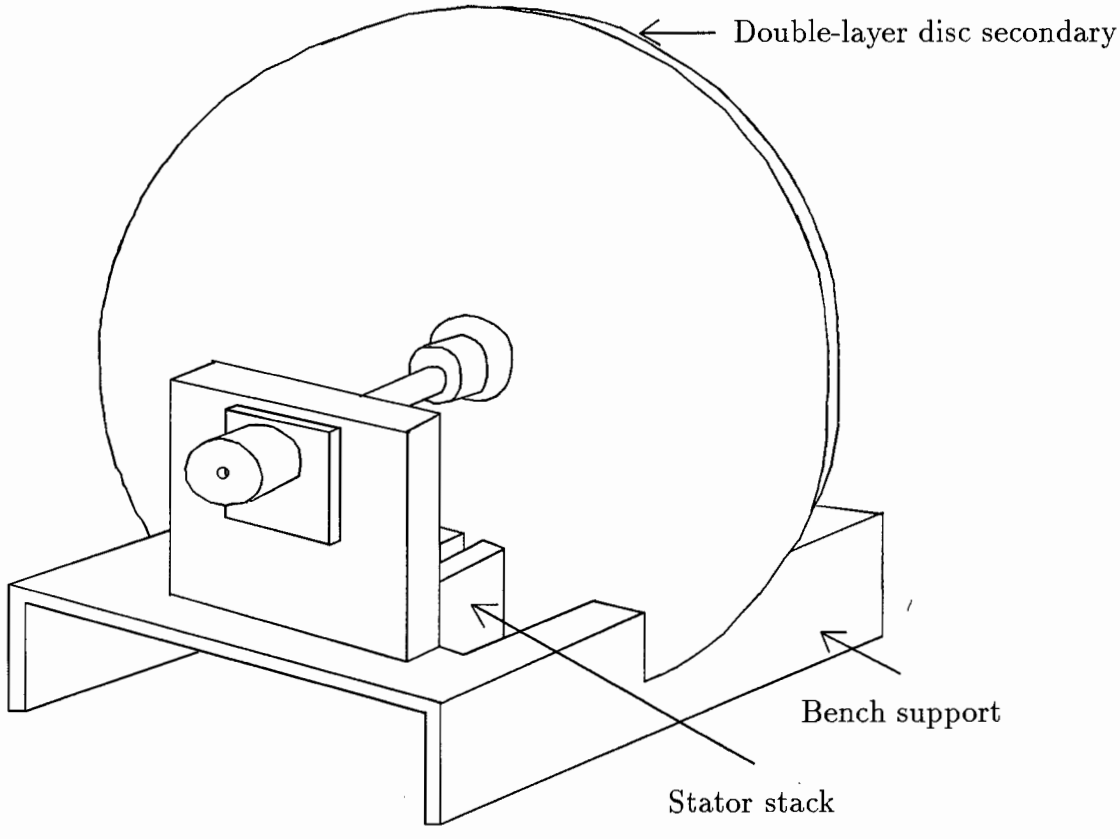

Figure 2.1: General Assembly of the 4-pole Shaded-Pole LIM

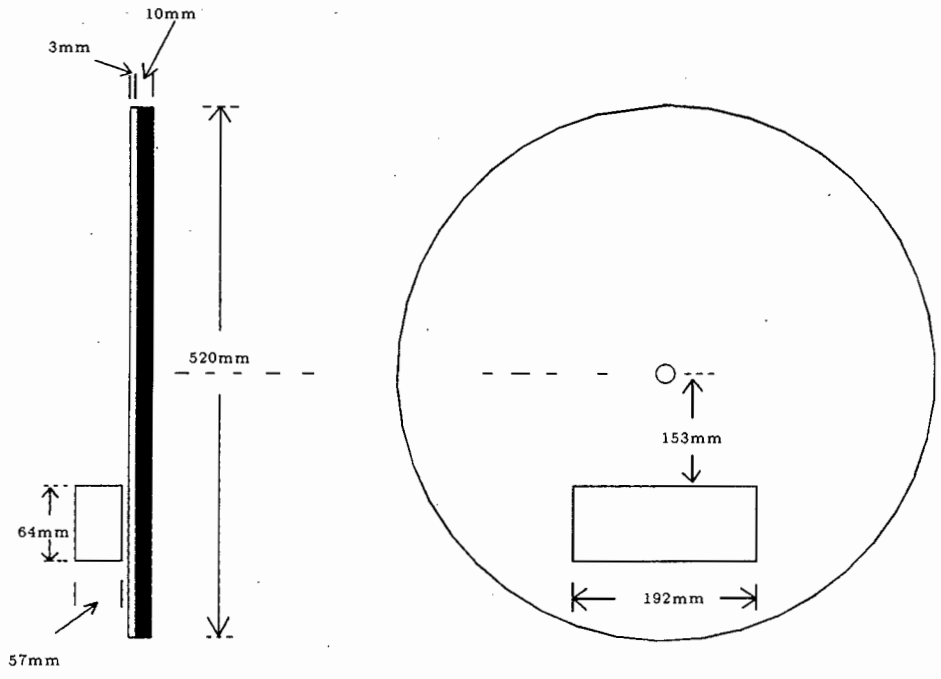

Figure 2.2: Sectional View of the Shaded-Pole LIM

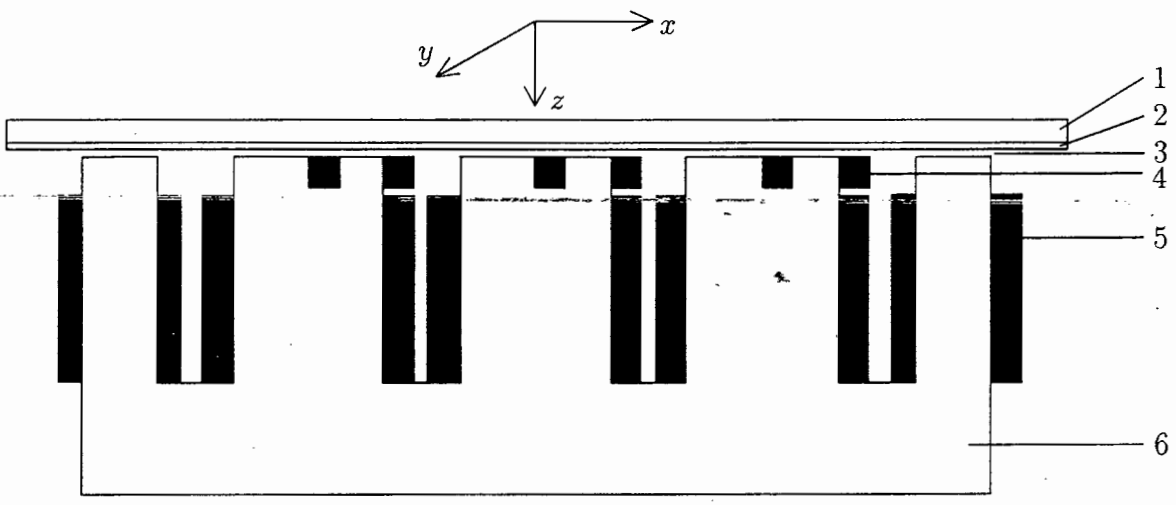

Figure 2.3: Structure of the 4-pole Shaded-Pole LIM: 1 - secondary back iron, 2 - aluminium cap, 3 - airgap, 4 - short-circuited coil, 5 - main winding, 6 - primary stack

Figure 2.2 shows the sectional view of both the primary stack and secondary disc of the shaded-pole LIM. Figure 2.3 shows the detailed structure of the single-phase shaded-pole LIM. The basic construction consists of two parts: a flat magnetic core(6) and a round conductive disc(1,2).

The stationary primary stack has salient poles with a main multi-turn winding with concentrated parameters, and slots accommodating an auxiliary single-turn shorted coil[49]. The construction of the shaded-pole LIM is similar to that of a rotary shaded-pole motor[102, 19]. The laminated core is made of a standard 0.5mm, non-oriented silicon steel transformer laminations. The slots have to be open as this makes it possible to design a simple winding, and reduces the leakage fluxes of the main and auxiliary windings.

Shaded-pole copper rings fit tightly into the slots. The copper rings have been soldered in a very clean environment with a silver solder. It is important to solder the seams with material that has a high melting point to prevent disintegration during extreme operating conditions. The main winding is then wound, and the complete primary stack is then placed into an oven and heated to $160°C$, so as to obtain a homogenous temperature throughout the core. Then the core is impregnated, i.e. dipped in a special transformer resin until all air bubbles disappeared[49].

The high temperature of the core ensures that the resin in the vicinity becomes thinner and is therefore able to fill every air gap that exists between the laminations and the windings. Finally the primary stack is baked dry in order to harden the resin. The disc is made of a 10mm mild steel plate to which a 3mm aluminium cap is laminated. The primary and the disc are mounted on a supportive structure in such a way that the airgap and the distance of the core, from the centre of the disc to the edge of the disc, can be varied. In the tested shaded-pole LIM, the rotor (secondary) is a double-layer disc made of aluminium and back-iron plates.

2.2 Design Data for shaded-pole motor

Table 2.1 shows the specification data of the LIM and the materials used for its construction, while Table 2.2 shows the design data for the single-phase shaded-pole single-sided linear induction motor.

At rated mains supply voltage of 220V and 50Hz, the current drawn by the shaded-pole LIM is 11.6A. But at this voltage, the performance is poor. At 160V and 75Hz for example, the current drawn is 6.6A, and the efficiency is much better since the winding losses I^2R are reduced. In general, the performance of the LIM was found to improve as the voltage decreases and frequency increases.

Table 2.1: Specification data of the tested shaded-pole LIM

Quantity	Value	Unit
Number of phases	1	
Frequency	50	Hz
Rated Current	11.6	A
Rated Voltage	220	V
Resistance	12.8	Ω
Number of pole pairs	$p = 2$	
Number of turns per main phase	$N_a = 520$	
Resistance of main winding for dc current	$R_{dc} = 12.813$	Ω
Primary winding factor	$k_{w1a} = 1$	
Linear Speed at 50Hz	84	rpm
Weight of Stator Core	4.26	kg
Weight of Al. and Mild Steel Disk	9.5	kg
Machine Primary(Stator)	Single-phase, Shaded-Pole	
Stator Core	Laminated (H18, 0.5mm, Non-Orientated Silicon Steel)	
Motor Secondary(Rotor disk)	Al. cap laminated to mild steel disk	
Slot Insulation	DMD-Mitron (6510)	
Shaded-Pole	Copper soldered with silver solder	

Table 2.2: Design Data of LIM

Quantity	Value	Unit
Length of primary stack	$L_\tau = 0.192$	m
Width of primary stack	$L_i = 0.09$	m
Pole pitch	$\tau = 0.048$	m
Air gap	$g = 0.0015$	m
Height of pole	$h_P = 0.048$	m
Width of pole	$w_p = 0.016$	m
Diameter of wire with insulation	$d_w = 0.00125$	m
Cross section of copper Wire	1.227×10^{-6}	m^2
Thickness of insulation paper between windings	$t_p = 0.0006$	m
Height of Shading Ring Slot	$h_s = 0.005$	m
Width of Shading Pole Slot	$w_s = 0.005$	m
Thickness of ferromagnetic core	$H_{sec} = 0.010$	m
Thickness of Al (Disc) Layer	$d = 0.003$	m
Diameter of Disc Secondary	$d_{sec} = 0.52$	m
Diameter of Secondary (Al. & Mild Steel Rotor Disk)	0.52	m
Air Gap	1.5	mm
Thickness of Mild Steel Disk	12	mm
Thickness of Aluminium Cap	3	mm
Length of Primary (Stator Core)	0.09	m
Height of Stator Core	0.064	m
Width of Stator Core	0.192	m
Cross section of Shaded-Pole Ring	0.0024	m^2

2.3 Main Dimension and Electromagnetic Loading

Fig. 2.4 shows the schematic circuit diagram of the single-phase shaded-pole LIM, where R_a, X_a - resistance, inductance of main phase winding; R_s, X_s - resistance, inductance of secondary; X_m - mutual inductance between primary and secondary; R_{Fe} - resistance representing core loss; Z_b - impedance of auxiliary winding.

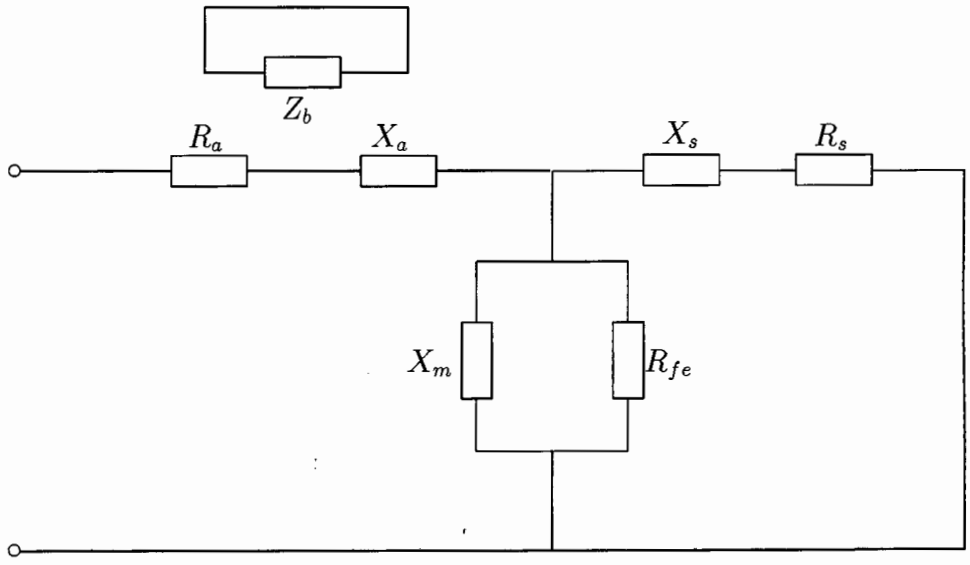

Figure 2.4: Schematic diagram of shaded-pole LIM parameters

2.3.1 Transformation Factor, k_{tr}

The transformation factor, k_{tr}, that is, the turns ratio between the primary and secondary system for the resistance and leakage reactances, is [43]:

$$k_{tr} = \frac{4(N_a k_{w1a})^2}{p} \tag{2.1}$$

where N_a is the number of turns of the main phase, k_{w1a} is the winding factor of phase a for fundamental space harmonic, and p is the number of pole pairs.

2.3.2 Carter's Coefficient

Carter's coefficient is calculated according to the following formula[45]:

$$k_{C1} = \frac{t_1}{t_1 - \gamma_1 g_t} \tag{2.2}$$

where,

$$\gamma_1 = \frac{4}{\pi}\{\frac{b_{14}}{2g_t}\arctan\frac{b_{14}}{2g_t} - \ln\sqrt{[1+(\frac{b_{14}}{2g_t})^2]}\}$$

t_1 is the primary slot pitch and b_{14} is the primary slot opening. For the single-sided LIM with an aluminium cap, the modified Carter's coefficient is given as[45];

$$k_{C_g} = \frac{k_C(g+d)g + d^2 - gd}{g^2 + d^2} \tag{2.3}$$

The effective airgap is therefore $k_{C_g}g$. For the shaded-pole LIM, the Carter coefficient is calculated for the shading ring slot on the main poles.

2.3.3 Resistance of Primary Winding, R_{1a}

The resistance of the main phase winding is:

$$R_{1a} = \frac{N_a l_{av}}{\sigma_{cu} A_{cu}} \tag{2.4}$$

where the electric conductivity σ_{Cu} of copper should be calculated for $75°C$, l_{av} is the average length of a turn, and A_{Cu} is the cross sectional area of conductor.

2.3.4 Winding Impedances

Since the MMFs of the two phases are equal:

$$I_b N_b k_{w1b} = I_a N_a k_{w1a} \tag{2.5}$$

k_{w1a}, k_{w1b} are winding factors, and N_a, N_b are the number of turns per main and auxiliary phase windings. Referring the auxiliary winding to the main stator winding side:

$$I'_b = I_b / k_{ab} \tag{2.6}$$

where,

$$k_{ab} = \frac{N_a k_{w1a}}{N_b k_{w1b}} \tag{2.7}$$

The winding impedances for the main and auxiliary phases are:

$$Z_{1a} = R_{1a} + jX_{1a} \tag{2.8}$$

$$Z_{1b} = R_{1b} + jX_{1b} \tag{2.9}$$

where R_{1a}, X_{1a} are the resistance and leakage reactance of the main stator winding respectively, and R_{1b}, X_{1b} are the resistance and leakage reactance of auxiliary winding.

2.3.5 Mutual(Magnetising) Reactance

The mutual reactance for a single-phase motor is [34, 44]:

$$X_m = \frac{8}{\pi} f \frac{\mu_0 (N_a k_{w1a})^2}{p(g + d_{Al}) k_{sat}} \tau L_i \tag{2.10}$$

where g is the airgap (mechanical clearance), d_{Al} is the thickness of the aluminium layer, k_{sat} is the saturation factor of magnetic circuit, and L_i is the effective width of the primary stack.

2.3.6 Stator Leakage Reactance as seen from the Main Phase

For main stator phase a and auxiliary phase b, the leakage reactances are [34]:

$$X_{1a} \approx \gamma(\sigma_1 - 1) X_m \tag{2.11}$$

where linkage factor, $\gamma = 0.6 - 0.9$, and the leakage factor of main winding, $\sigma_1 = 1.1 - 1.16$. For auxiliary phase b [34]:

$$X_{1b} = 0.5 \mu_0 f \lambda_{1b} L_i \tag{2.12}$$

$$\lambda_{1b} = 0.4\pi \frac{h}{b} + 0.3 \left(\frac{l_{Bav}}{L_i} - 1 \right) \tag{2.13}$$

where the first component caters for the slot leakage and the second is the end connection leakage.

2.3.7 Auxiliary Phase Leakage Reactance

The impedance of the auxiliary phase referred to the main phase is:

$$X'_{1b} = \left(\frac{k_{w1a}}{k_{w1b}} N_a \right)^2 X_{1b} \tag{2.14}$$

where, $k_{w1a} = 1$, $\qquad k_{w1b} = sin(\frac{b_{sh}}{\tau} \frac{\pi}{2})$

and b_{sh} is width of shading ring edge.

2.3.8 Impedance of Vertical Branch for Series Connection

It is convenient to replace the parallel connection of R_{Fe} and X_m by series connection as in Figs. 3.13 – 3.16, i.e.

$$Z_o = R_o + jX_o$$

$$= \frac{R_{Fe}X_m^2}{R_{Fe}^2 + X_m^2} + j\frac{R_{Fe}^2 X_m}{R_{Fe}^2 + X_m^2}$$

where,

$$R_o = \frac{R_{Fe}X_m^2}{R_{Fe}^2 + X_m^2}$$

$$X_o = \frac{R_{Fe}^2 X_m}{R_{Fe}^2 + X_m^2}$$

The resistance R_{Fe} represents the core losses.

2.3.9 Mutual Reactance Between Main and Auxiliary Phases

The mutual reactance is:

$$Z_{ab} = jX_{ab} = j\omega M_{ab} \tag{2.15}$$

where X_{ab} is the mutual reactance between main phase a and auxiliary phase b[34].

$$X_{ab} \approx \frac{\alpha_{ik}}{\alpha}\frac{X_0}{2p} = \frac{\alpha_{ik}\tau}{b_p}\frac{X_0}{2p} \tag{2.16}$$

where $\alpha = b_p/\tau = 0.6 - -0.9$, $\alpha_{ik} \approx \frac{1}{3}\alpha$ and X_0 is the reactance of main winding of stator.

2.3.10 Rotor Impedance

The impedances of aluminium cap and solid back iron for the fundamental space harmonic $\nu = 1$ are [45]:

$$Z'_{Al}(s) = \frac{js\omega\mu_0}{k_{Al}}\frac{1}{tanh(k_{Al}d)}k_{tr}\frac{L_i}{\tau} \tag{2.17}$$

$$Z'_{Fe}(s) = \frac{js\omega\mu_{Fe}}{k_{Fe}}\frac{1}{tanh(k_{Fe}h_{sec})}k_{tr}k_z\frac{L_i}{\tau} \tag{2.18}$$

where the propagation constant for aluminium is:

$$k_{Al} = \sqrt{js\omega\mu_0\sigma'_{Al} + \left(\frac{\pi}{\tau}\right)^2} \tag{2.19}$$

and the propagation constant for iron is:

$$k_{Fe} = \sqrt{js\omega\mu_{Fe}\sigma_{Fe} + \left(\frac{\pi}{\tau}\right)^2} \tag{2.20}$$

The transverse edge effect coefficient for the back iron is [93, 43]:

$$k_z = 1 - \frac{g}{L_i} + \frac{2}{\pi}\frac{\tau}{w}[1 - exp(-\frac{\pi}{2}\frac{w}{L_i})] \tag{2.21}$$

This applies to the forward sequence slip s. For the backward sequence slip $(2 - s)$:

$$Z'_{Al}(2-s) = \frac{j(2-s)\omega\mu_0}{k_{Al}} \frac{1}{tanh(k_{Al}d)} k_{tr}\frac{L_i}{\tau} \tag{2.22}$$

$$Z'_{Fe}(2-s) = \frac{j(2-s)\omega\mu_{Fe}}{k_{Fe}} \frac{1}{tanh(k_{Fe}h_{sec})} k_{tr}k_z\frac{L_i}{\tau} \tag{2.23}$$

where:

$$k_{Al} = \sqrt{j(2-s)\omega\mu_0\sigma'_{Al} + (\frac{\pi}{\tau})^2} \tag{2.24}$$

$$k_{Fe} = \sqrt{j(2-s)\omega\mu_{Fe}\sigma_{Fe} + (\frac{\pi}{\tau})^2} \tag{2.25}$$

The coefficient k_{tr} is given by (2.1). σ'_{Al} is the equivalent electric conductivity of aluminium cap given by:

$$\sigma'_{Al} = k_{rn} \times \sigma_{Al} \tag{2.26}$$

where σ_{Al} is the electric conductivity of aluminium, ω is angular frequency for fundamental harmonic ($\omega = 2\pi f$) and μ_{Fe} is the magnetic permeability of iron.

2.3.11 Coefficient including Transverse Edge Effect, k_{rn}

The coefficient including transverse edge effect in aluminium layer, k_{rn}, for fundamental is[46]:

$$k_{rn} = 1 - \frac{\tanh(\beta\frac{w}{2})}{\beta\frac{w}{2}(1 + \tanh(\beta\frac{w}{2})\tanh(\beta h_{ov}))} \tag{2.27}$$

where $\beta = \pi/\tau$, the effective width of the secondary ferromagnetic core $w = \tau + L_i$. L_i is the effective width of the primary core, and the secondary winding overhang $h_{ov} = 0$.

2.3.12 Linear Speed of LIM

Since speed is independent of the number of poles pairs, the synchronous linear speed of the stator travelling field for the shaded-pole LIM is given by[45]:

$$v_s = 2f\tau \tag{2.28}$$

where f is the input frequency, and τ is the pole pitch.

The rotor linear speed is:

$$v = v_s(1 - s) \tag{2.29}$$

2.3.13 Slip

The rotor slip relative to the positive sequence field is:

$$s^+ = \frac{\omega_1 - \omega_2}{\omega_1} = 1 - \frac{\omega_2}{\omega_1} \tag{2.30}$$

and for the negative sequence field:

$$s^- = \frac{-\omega_1 - \omega_2}{-\omega_1} = \frac{\omega_1 + \omega_2}{\omega_1} = 1 + \frac{\omega_2}{\omega_1} \tag{2.31}$$

where ω_1 is the angular synchronous speed (stator supply frequency) for fundamental harmonic, ω_2 is the angular rotor frequency, and s is rotor slip relative to $+ve$ sequence slip.

But,

$$\frac{\omega_2}{\omega_1} = 1 - s^+$$

$$s^- = 1 + (1 - s^+) = 2 - s^+$$

$$s^- = 2 - s^+$$

Thus,

$$s = s^+, \qquad s^- = 2 - s^+ \tag{2.32}$$

2.3.14 Electromagnetic field equations

The shaded-pole LIM has a solid ferromagnetic core, and a multi-layer secondary made up of the airgap, aluminium cap and back iron.

$$\frac{\partial^2 \mathbf{A}_{x\nu i}}{\partial x^2} + \frac{\partial^2 \mathbf{A}_{x\nu i}}{\partial y^2} + \frac{\partial^2 \mathbf{A}_{x\nu i}}{\partial z^2} = \alpha_{\nu i}^2 \mathbf{A}_{x\nu i} \tag{2.33}$$

$$\frac{\partial^2 \mathbf{A}_{y\nu i}}{\partial x^2} + \frac{\partial^2 \mathbf{A}_{y\nu i}}{\partial y^2} + \frac{\partial^2 \mathbf{A}_{y\nu i}}{\partial z^2} = \alpha_{\nu i}^2 \mathbf{A}_{y\nu i} \tag{2.34}$$

where $\mathbf{A}_{x\nu i}$, $\mathbf{A}_{y\nu i}$ are components of the magnetic vector potential $\mathbf{A}$ of the eddy current field in the secondary. These currents flow only in the x, y directions. Therefore, $E_{z\nu i} = 0$ (electric field strength) and $A_{z\nu i} = 0$.

For the 2-D analysis, $\beta = \pi/2$ and,

$$\chi_i = (\alpha_i^2 + \beta^2)^{1/2} = (a_{Ri} + ja_{Xi})k_i \tag{2.35}$$

The complex propagation constant, $\alpha_{\nu i}$, is a function of slip s. For the forward travelling magnetic field[41, 42]:

$$\alpha_{\nu i} = \alpha_{\nu i}^{+} = \sqrt{j\omega_{\nu i}^{+}\mu_i\sigma_i}$$

$$= (a_{Ri} + ja_{Xi})\sqrt{1 - \nu(1-s)}k_i \tag{2.36}$$

For the backward travelling magnetic field[41, 42]:

$$\alpha_{\nu i} = \alpha_{\nu i}^{-} = \sqrt{j\omega_{\nu i}^{-}\mu_i\sigma_i}$$

$$= (a_{Ri} + ja_{Xi})\sqrt{1 + \nu(1-s)}k_i \tag{2.37}$$

where s and $2 - s$ are according to (2.30, 2.31).

The attenuation factor for the fundamental space harmonic in the i^{th} layer at $s = 1$ is[45]:

$$k_i = \sqrt{0.5\omega\mu_0\mu_{ri}\sigma_i} \tag{2.38}$$

and σ_i is conductivity of the medium.

2.3.15 Magnetic Permeability, μ_i

The magnetic permeability of a non-ferromagnetic layer is a real quantity:

$$\mu_i = \mu_0\mu_{ri} \tag{2.39}$$

where $\alpha_{Ri} = \alpha_{Xi} = 1$. μ_{ri} is the relative permeability of the i^{th} layer, and $\mu_{ri} \approx 1$. For air, $\alpha = 0$, and $\sigma \to 0$. For aluminium (which is paramagnetic), $\mu_{ri} \approx 1$, and for back iron $\mu_{ri} > 1$.

The magnetic permeability of a ferromagnetic layer is a complex quantity[40, 48]:

$$\mu_i = \mu_0\mu_{rsi}(\mu' - j\mu'') \tag{2.40}$$

where μ_{rsi} is surface relative permeability of a ferromagnetic layer, and μ^i, μ'' are coefficients of the complex magnetic permeability taking into account the non-linearity of the ferromagnetic medium and hysteresis losses.

2.3.16 Magnetic Flux Density Components, B_{mz_1}

The peak value of the ν-th space harmonic of the MMF (for fundamental harmonic) is[45]:

$$\Theta_{m\nu} = \frac{2\sqrt{2}m_1}{\pi}\frac{1}{p}\frac{1}{\nu}N_1 k_{wa\nu} I_1 = m_1[\Theta_{m\nu}]_{m_1=1} \tag{2.41}$$

and the peak value of the ν-th space harmonic of the magnetic flux density is:

$$B_{mz\nu} = \Theta_{m\nu}\frac{\mu_0}{2g_t k_C k_{sat}} \tag{2.42}$$

The amplitude of the MMF is:

$$\Theta^+_{m\nu} = 0.5\Theta_{m\nu}e^{[j(\nu-1)\frac{m_1-1}{m_1}\pi]} \qquad \Theta^-_{m\nu} = 0.5\Theta_{m\nu}e^{[j(\nu+1)\frac{m_1-1}{m_1}\pi]} \tag{2.43}$$

For the single-phase LIM, and using the fundamental harmonic, $\nu = 1$:

$$\Theta_{m_1} = \frac{2\sqrt{2}}{m_1}\pi\frac{1}{p}N_1 k_{wa} I_1 = \frac{2\sqrt{2}}{p}\pi N_1 k_{wa} I_1 \tag{2.44}$$

and the magnetic flux density is:

$$B_{mz_1} = \frac{\sqrt{2}}{\pi p}N_1 k_{wa} I_1 \frac{\mu_0}{g_t k_C k_{sat}} \tag{2.45}$$

where $k_{wa\nu}$ is the winding factor for the νth space harmonic, g_t is the total airgap between ferromagnetic cores, i.e., $(g + d)$, k_C is Carter's coefficient, k_{sat} is saturation factor of the magnetic circuit, I_1 is the line current (or armature current), and m_1 is number of machine phases.

The amplitude of the magnetic flux density is:

$$B^+_{mz\nu} = 0.5B_{mz\nu}e^{[j(\nu-1)\frac{m_1-1}{m_1}\pi]} \qquad B^-_{mz\nu} = 0.5B_{mz\nu}e^{[j(\nu+1)\frac{m_1-1}{m_1}\pi]} \tag{2.46}$$

For fundamental space harmonic $\nu = 1$ for the single-phase LIM:

$$B^+_{mz\nu} = B^-_{mz\nu} = 0.5B_{mz\nu} = \frac{\sqrt{2}}{\pi p}N_1 k_{w1} I_1 \frac{\mu_0}{2g_t k_C k_{sat}} \tag{2.47}$$

The instantaneous magnetic field density, b, is estimated from the normal component of the magnetic field density:

$$b = B_{mg} = \frac{E_1}{2\sqrt{2}fN_1 k_{w1}\tau L_i} \tag{2.48}$$

where E_1 is the EMF. $E_1 = k_E.V_1$ where $k_E < 1$ for motors.

2.4 Effect of reaction rail curvature

The reaction rail is a disc while the primary stack is a cube. There are braking forces arising from the disc curvature in comparison with an arc LIM. The normal attractive force F_y between the stator stack and disc secondary is determined by the FEM using Maxwell's stress tensor method. The forces acting on the secondary are given by (eqns. 5.29,5.30):

$$F_x = -\frac{1}{2\mu_0}\Re[\mathbf{B}_y\mathbf{B}_x^*](2p\tau L_i)$$

$$F_z = \frac{1}{2\mu_0}\Re[\frac{1}{2}\mathbf{B}_{mz}\mathbf{B}_{mz}^* - \frac{1}{2}\mathbf{B}_{mx}\mathbf{B}_{mx}^*](2p\tau L_i)$$

where μ_0 is the magnetic permeability of free space, $\mathbf{B}_z$, $\mathbf{B}_x$ are the normal and tangential components of magnetic flux density in the airgap, and L_i is the effective length of the primary stack (in the y-direction). The shaft torque is obtained from the expression, $T = F_x r$, where r is the radius of disc.

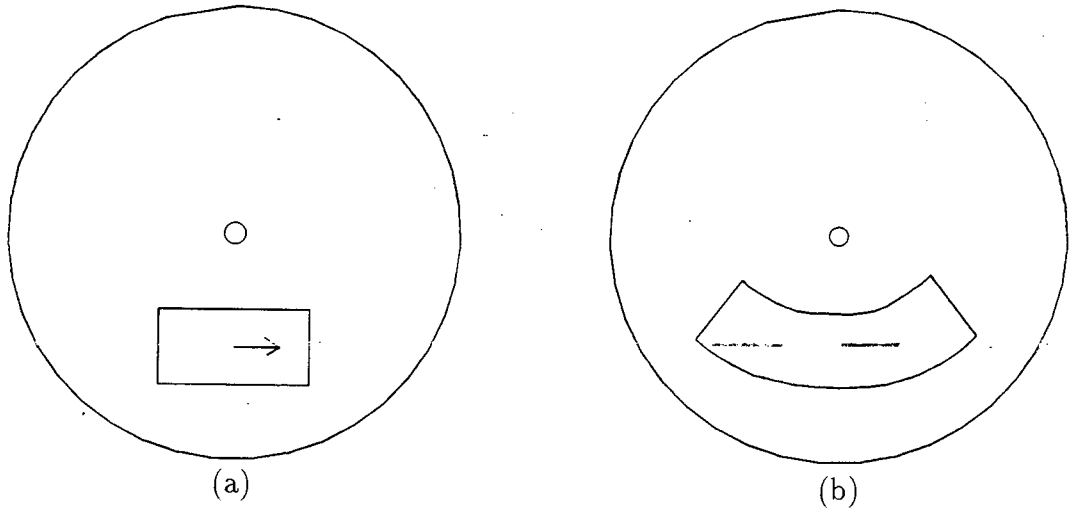

Figure 2.5: LIM Topology (a) shaded-pole primary stack (b) arc-shaped primary

Due to the topology of the shaded-pole LIM under investigation, there are errors introduced by these braking forces. The parameters affecting this error invariably include the pole pitch τ, diameter of the disc D, and the number of pole pairs p.

Chapter 3

Performance Calculation Using Symmetrical Components

In the circuital approach to the analysis of single-phase or two-phase motors, symmetrical components[36] for a two-phase system are usually used[100, 102, 103, 19, 55, 15, 16, 5]. This method can be used in both the analysis of motors with windings shifted by 90° (electrical) and less than 90° (shaded-pole motors).

3.1 Stator Magnetic Field

The stator travelling magnetic field is created by the MMFs of the main excitation winding a and shaded pole winding b, provided there is a space shift between them and a time shift between the voltages applied to these windings. The magnetic field vector remains constant in magnitude, that is, the field remains circular under the following conditions:

(a) the stator windings are spaced apart through an angle $\alpha = 90$ electrical degrees

(b) the currents through the stator windings are shifted in time by an angle $\beta = 90°$

(c) the stator windings have equal MMFs

Since the currents in the main and auxiliary windings are shifted by an angle less than 90° and the space angle between the two windings is also less than 90°, an elliptical travelling magnetic field is produced in the airgap[5].

The normal component of the magnetic flux density distribution in the airgap can be described by the following equation[41]:

$$b(x,t) = \sum_{\nu=1}^{\infty} [B^{+}_{m\nu} e^{j(\omega^{+}_{s\nu} t - \beta_\nu x)} + B^{-}_{m\nu} e^{j(\omega^{-}_{s\nu} t + \beta_\nu x)}] \tag{3.1}$$

where $B^{+}_{m\nu}$ and $B^{-}_{m\nu}$ are the peak values of the ν^{th} space harmonic waves travelling in the x-direction (along the pole pitch), $\nu = 1, 3, 5...$ are the higher space harmonics, $\omega^{+}_{s\nu}$ is

the angular frequency for the forward travelling field, $\omega_{s\nu}^{-}$ is the angular frequency for the backward travelling field, $\beta_\nu = \nu\pi/\tau$, and τ is the primary pole pitch.

The peak values of magnetic flux densities in (3.1) are[26]:

$$B_{m\nu}^{+} = 0.5[B_a b_{\nu a} + B_b b_{\nu b} e^{-j(\beta-\nu\alpha)}]$$

$$B_{m\nu}^{-} = 0.5[B_a b_{\nu a} + B_b b_{\nu b} e^{-j(\beta+\nu\alpha)}]$$

where B_a and B_b are the normal components of the magnetic flux density (rectangular distribution) in the symmetry axis of the phase a and b, respectively, $b_{\nu a}$ and $b_{\nu b}$ are the Fourier's coefficients, $\beta < 90°$ is the phase angle between the currents in phase a and b, and α is the space angle between symmetry axes of phase a and b.

This is a two-phase machine, therefore, the higher harmonics ν= 3, 9, 15, ... exist. They are only eliminated in three-phase circuits.

For $\nu = 1$ the angular frequencies are:

$$\omega_{s\nu=1}^{+} = 2\pi f s$$

$$\omega_{s\nu=1}^{-} = 2\pi f(2 - s)$$

where s is the slip for fundamental.

For further analysis, the fundamental space harmonic $\nu = 1$ will be assumed. Assuming equal MMFs in the main and auxiliary windings according to (2.4), the auxiliary winding current I_b' is (2.5).

3.2 Symmetrical Components of Two-Phase System

The two-phase asymmetric system of vectors of currents $\dot{I}_a$ and $\dot{I}_b$ having unequal magnitudes and spaced apart by an arbitrary angle can be resolved into two symmetrical systems each composed of two vectors equal in magnitude and spaced 90° apart[5].

The forward-sequence system of vectors is $\dot{I}_a^{+}$ and $\dot{I}_b^{+}$. It has the same phase sequence as the original system. The backward-sequence system of vectors is $\dot{I}_a^{-}$ and $\dot{I}_b^{-}$. It has a backward phase sequence.

Thus, for $\alpha = 90°$,

$$\dot{I}_b^+ = -j\dot{I}_a^+, \qquad \dot{I}_b^- = j\dot{I}_a^-$$

For an angle $\alpha = 90°$, the original and derived systems are equivalent hence:

$$\dot{I}_a^+ + \dot{I}_a^- = I_a \tag{3.2}$$

$$\dot{I}_b^+ + \dot{I}_b^- = I_b \tag{3.3}$$

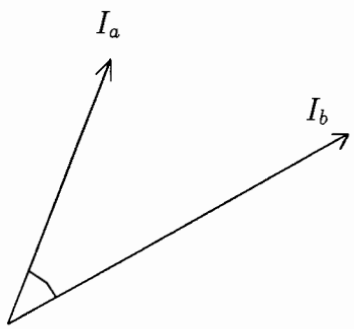

Figure 3.1: Asymmetric system of current vectors

Since the symmetry conditions are not satisfied in the shaded-pole LIM, as spacing between a and b is not 90°, [$\alpha < 90°$]

$$I_b \neq I_a$$

hence the magnetic flux vector describes an ellipse and not a circle. The resultant phasor flux $\dot{\Phi}$ does not therefore remain constant while rotating and varies in magnitude. Thus symmetrical components for a two-phase system must be used.

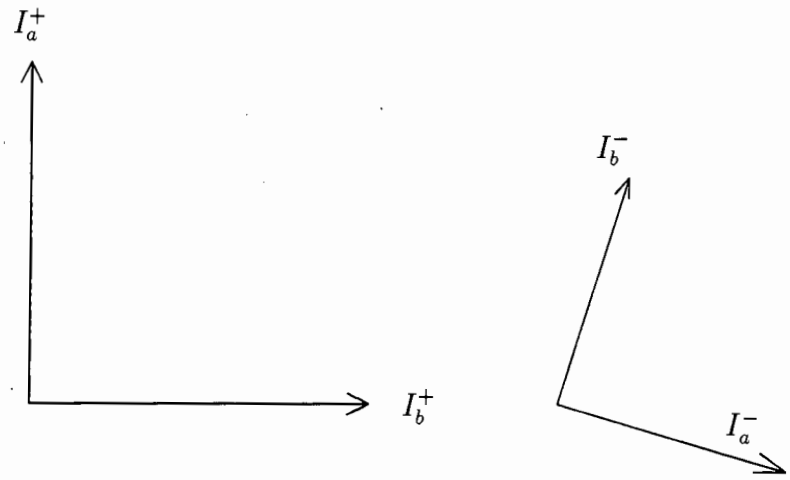

Figure 3.2: Symmetrical components of asymmetric system of current vectors

3.3 Equations for Phase Currents I_a and I_b

For an angle α between phases a and b, where $\alpha \neq 90°$, the positive and negative sequence components are defined as [92]:

$$I_a^+ = \frac{I_a}{2} + \frac{I_b e^{-j\alpha}}{2} \tag{3.4}$$

$$I_a^- = \frac{I_a}{2} + \frac{I_b e^{j\alpha}}{2} \tag{3.5}$$

$$I_b^+ = I_a^+ e^{j\alpha} \tag{3.6}$$

$$I_b^- = I_a^- e^{-j\alpha} \tag{3.7}$$

To find a system of equations defining the performance characteristics of the LIM in which $\alpha < 90°$, it is necessary to obtain expressions for I_a and I_b.

$$I_a^+ - I_a^- = \frac{I_b}{2}(e^{-j\alpha} - e^{j\alpha}) \tag{3.8}$$

Since $e^{-j\alpha} = cos\alpha - j \cdot sin\alpha$, and $e^{j\alpha} = cos\alpha + j \cdot sin\alpha$, the above equation gives the current in the short-circuited coil as:

$$I_b = j(\frac{I_a^+}{sin\alpha} - \frac{I_a^-}{sin\alpha}) \tag{3.9}$$

For the main phase, the current components are:

$$I_a^+ = \frac{I_a - jI_b'}{2}$$

$$I_a^- = \frac{I_a + jI_b'}{2}$$

Resolving,

$$I_a^+ e^{j\alpha} = \frac{I_a}{2} e^{j\alpha} + \frac{I_b}{2}$$

This gives the input current in the main phase as:

$$I_a = -j(\frac{I_a^+}{sin\alpha} e^{j\alpha} - \frac{I_a^-}{sin\alpha} e^{-j\alpha}) \tag{3.10}$$

For angle $\alpha = 90°$,

$$I_b^+ = j \cdot I_a^+ \tag{3.11}$$

$$I_b^- = -j \cdot I_a^- \tag{3.12}$$

Also eqns (3.9) and (3.10) become, for a:

$$I_a = I_a^+ + I_a^- \tag{3.13}$$

for b:

$$I_b = jI_a^+ - jI_a^- \tag{3.14}$$

The equivalent circuit for the two-phase system, with main stator windings a and auxiliary (shorted windings) b, can be represented by phasor diagrams. Tables 3.1 – 3.9 show the simulation results of currents (in complex notation). Figs. 3.3 – 3.11 show the diagrams of the current phasors for phases a and b, and their positive and negative sequence components, for the shaded pole LIM for specific operating conditions of voltage, speed and frequency. The results also show the variation of circuit parameters with change in space angle α for the single-phase shaded-pole LIM.

The space between winding phases a and b is given by:

$$\alpha = \frac{d_{ik}}{d_k} \times \frac{\pi}{2} \tag{3.15}$$

in radians where $d_{ik} = 0.014m$ is the width of shading ring, and $d_k = 0.043m$ is the width of pole. For the tested shaded pole LIM, α is 29.3° (or ratio 0.3256:1).

Table 3.1: Simulation data of shaded-pole LIM at 90V, 50Hz and $\alpha = 90°$

N	I_a^+	I_a^-	I_a	I_b^+	I_b^-	I_b
rpm	A	A	A	A	A	A
2.5	1.414 -3.446	-.00624 -.00680	1.408 -3.453	3.446 1.414	-.00680 .00624	3.439 1.420
5.0	1.437 -3.488	-.00632 -.00702	1.430 -3.495	3.488 1.437	-.00702 .00632	3.481 1.443
7.5	1.435 -3.489	-.00632 -.00702	1.429 -3.496	3.489 1.436	-.00702 .00632	3.482 1.442
10.0	1.434 -3.490	-.00632 -.00702	1.427 -3.497	3.490 1.434	-.00702 .00632	3.483 1.440
12.5	1.434 -3.500	-.00635 -.00704	1.428 -3.507	3.500 1.435	-.00704 .00635	3.493 1.441
15.0	1.433 -3.501	-.00635 -.00704	1.426 -3.508	3.501 1.433	-.00704 .00635	3.494 1.439
17.5	1.431 -3.503	-.00635 -.00705	1.425 -3.511	3.504 1.431	-.00705 .00635	3.496 1.438
20.0	1.429 -3.504	-.00635 -.00704	1.423 -3.511	3.504 1.429	-.00704 .00635	3.497 1.436
22.5	1.430 -3.515	-.00638 -.00707	1.424 -3.522	3.515 1.430	-.00707 .00638	3.508 1.436
25.0	1.428 -3.515	-.00638 -.00707	1.422 -3.523	3.516 1.428	-.00707 .00638	3.508 1.434
27.5	1.426 -3.516	-.00638 -.00707	1.420 -3.523	3.516 1.426	-.00707 .00638	3.509 1.432
30.0	1.424 -3.516	-.00638 -.00706	1.417 -3.523	3.516 1.424	-.00706 .00638	3.509 1.430
32.5	1.422 -3.517	-.00638 -.00706	1.415 -3.524	3.517 1.422	-.00706 .00638	3.510 1.428
35.0	1.422 -3.528	-.00641 -.00709	1.416 -3.535	3.528 1.422	-.00709 .00641	3.521 1.429
37.5	1.420 -3.528	-.00641 -.00708	1.414 -3.535	3.528 1.420	-.00708 .00641	3.521 1.427
40.0	1.418 -3.529	-.00641 -.00708	1.412 -3.536	3.529 1.418	-.00708 .00641	3.522 1.424
42.5	1.416 -3.529	-.00641 -.00708	1.409 -3.536	3.529 1.416	-.00708 .00641	3.522 1.422
45.0	1.413 -3.530	-.00641 -.00707	1.407 -3.537	3.530 1.413	-.00707 .00641	3.522 1.420
47.5	1.414 -3.541	-.00644 -.00710	1.408 -3.548	3.541 1.414	-.00710 .00644	3.534 1.421
50.0	1.412 -3.542	-.00644 -.00710	1.405 -3.549	3.542 1.412	-.00710 .00644	3.535 1.418
52.5	1.409 -3.542	-.00644 -.00709	1.403 -3.549	3.542 1.409	-.00709 .00644	3.535 1.416
55.0	1.407 -3.543	-.00644 -.00709	1.400 -3.550	3.543 1.407	-.00709 .00644	3.536 1.413
57.5	1.408 -3.554	-.00647 -.00712	1.401 -3.562	3.555 1.408	-.00712 .00647	3.547 1.414
60.0	1.405 -3.555	-.00647 -.00711	1.399 -3.562	3.555 1.405	-.00711 .00647	3.548 1.412
62.5	1.403 -3.556	-.00648 -.00711	1.396 -3.563	3.556 1.403	-.00711 .00648	3.549 1.409
65.0	1.401 -3.559	-.00648 -.00711	1.394 -3.566	3.559 1.401	-.00711 .00648	3.552 1.407
67.5	1.398 -3.559	-.00649 -.00711	1.392 -3.566	3.559 1.398	-.00711 .00649	3.552 1.405
70.0	1.399 -3.572	-.00652 -.00713	1.393 -3.579	3.572 1.399	-.00713 .00652	3.564 1.406
72.5	1.397 -3.572	-.00652 -.00713	1.390 -3.579	3.572 1.397	-.00713 .00652	3.565 1.403
75.0	1.394 -3.573	-.00652 -.00712	1.387 -3.580	3.573 1.394	-.00712 .00652	3.566 1.401

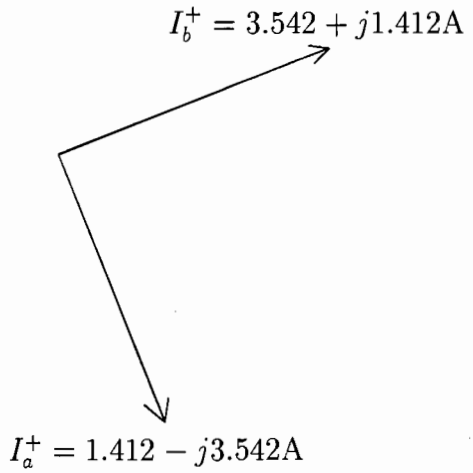

Figure 3.3: Phasor diagram of stator phase currents I_a^+ and I_b^+, $\alpha = 90°$

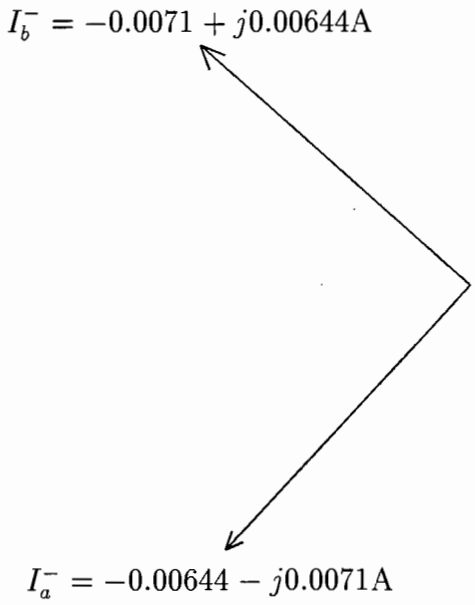

Figure 3.4: Phasor diagram of stator phase currents I_a^- and I_b^-, $\alpha = 90°$

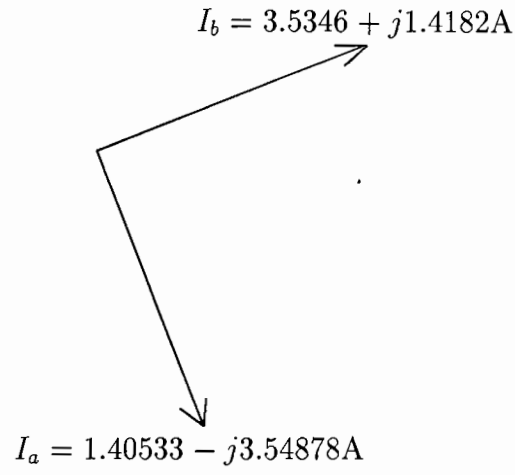

Figure 3.5: Phasor diagram of stator phase currents I_a and I_b, $\alpha = 90°$

Table 3.2: Phase current I_a and symmetrical components at 90V, 50Hz, $\alpha = 90°$

N	I_a^+	I_a^-	I_a
rpm	A	A	A
50.0	1.41177 - j3.54169	-0.00644 - j0.00710	1.40533 - j3.54878

Table 3.3: Phase current I_b and symmetrical components at 90V, 50Hz, $\alpha = 90°$

N	I_b^+	I_b^-	I_b
rpm	A	A	A
50.0	3.542 + j1.412	-0.00710 + j0.00644	3.5346 + j1.4182

Table 3.4: Simulation data of shaded-pole LIM at 90V, 50Hz and $\alpha = 75°$

N	I_a^+	I_a^-	I_a	I_b^+	I_b^-	I_b
rpm	A	A	A	A	A	A
2.5	1.574 -3.671	-.00495 -.00608	.587 -4.100	3.953 .570	-.00715 .00321	3.794 1.635
5.0	1.599 -3.714	-.00501 -.00625	.600 -4.150	4.001 .583	-.00733 .00322	3.839 1.660
7.5	1.598 -3.716	-.00501 -.00625	.599 -4.151	4.003 .581	-.00734 .00322	3.840 1.659
10.0	1.596 -3.716	-.00501 -.00625	.597 -4.151	4.003 .580	-.00734 .00322	3.841 1.657
12.5	1.597 -3.729	-.00503 -.00627	.595 -4.164	4.015 .578	-.00736 .00324	3.854 1.659
15.0	1.596 -3.729	-.00503 -.00627	.593 -4.164	4.015 .576	-.00736 .00324	3.854 1.657
17.5	1.594 -3.732	-.00504 -.00627	.591 -4.166	4.017 .574	-.00736 .00324	3.857 1.656
20.0	1.592 -3.733	-.00504 -.00627	.589 -4.167	4.018 .572	-.00736 .00325	3.858 1.654
22.5	1.594 -3.745	-.00506 -.00629	.587 -4.180	4.030 .570	-.00739 .00326	3.871 1.655
25.0	1.592 -3.746	-.00507 -.00629	.585 -4.180	4.030 .568	-.00739 .00326	3.871 1.653
27.5	1.590 -3.746	-.00507 -.00629	.583 -4.180	4.030 .566	-.00738 .00327	3.872 1.651
30.0	1.588 -3.747	-.00507 -.00628	.580 -4.180	4.030 .564	-.00738 .00327	3.873 1.649
32.5	1.586 -3.747	-.00507 -.00628	.578 -4.180	4.030 .562	-.00738 .00327	3.873 1.647
35.0	1.587 -3.760	-.00509 -.00630	.576 -4.193	4.043 .560	-.00741 .00329	3.886 1.648
37.5	1.585 -3.761	-.00509 -.00630	.574 -4.193	4.043 .557	-.00740 .00329	3.887 1.646
40.0	1.583 -3.761	-.00510 -.00630	.571 -4.193	4.043 .555	-.00740 .00329	3.888 1.644
42.5	1.580 -3.762	-.00510 -.00629	.569 -4.193	4.043 .553	-.00740 .00330	3.888 1.641
45.0	1.578 -3.763	-.00510 -.00629	.566 -4.193	4.043 .550	-.00740 .00330	3.889 1.639
47.5	1.579 -3.776	-.00513 -.00631	.564 -4.207	4.056 .548	-.00742 .00332	3.902 1.640
50.0	1.577 -3.776	-.00513 -.00631	.562 -4.207	4.056 .546	-.00742 .00332	3.903 1.638
52.5	1.574 -3.777	-.00513 -.00630	.559 -4.207	4.056 .543	-.00742 .00332	3.904 1.635
55.0	1.572 -3.777	-.00513 -.00630	.556 -4.206	4.056 .541	-.00741 .00333	3.904 1.633
57.5	1.573 -3.791	-.00516 -.00632	.554 -4.220	4.069 .539	-.00744 .00334	3.918 1.634
60.0	1.571 -3.792	-.00516 -.00632	.551 -4.220	4.069 .536	-.00744 .00335	3.919 1.632
62.5	1.568 -3.793	-.00516 -.00632	.549 -4.221	4.069 .533	-.00744 .00335	3.920 1.629
65.0	1.567 -3.796	-.00517 -.00632	.546 -4.224	4.072 .531	-.00744 .00336	3.923 1.627
67.5	1.564 -3.797	-.00517 -.00631	.543 -4.224	4.072 .528	-.00744 .00336	3.924 1.625
70.0	1.565 -3.811	-.00520 -.00634	.541 -4.238	4.086 .526	-.00747 .00338	3.939 1.626
72.5	1.563 -3.812	-.00520 -.00633	.538 -4.238	4.086 .523	-.00746 .00339	3.940 1.623
75.0	1.560 -3.812	-.00520 -.00633	.535 -4.238	4.086 .520	-.00746 .00339	3.940 1.621

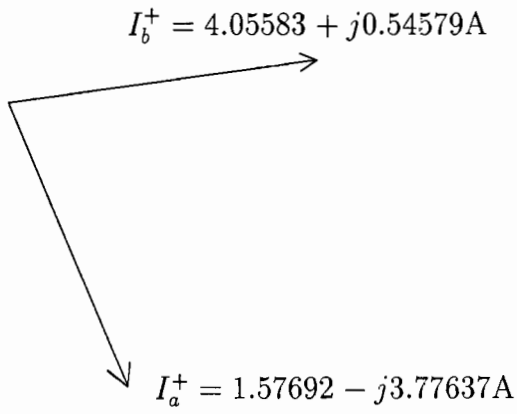

Figure 3.6: Phasor diagram of stator phase currents I_a^+ and I_b^+, $\alpha = 75°$

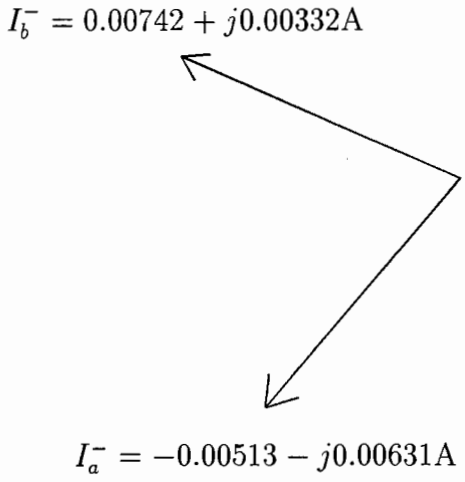

Figure 3.7: Phasor diagram of stator phase currents I_a^- and I_b^-, $\alpha = 75°$

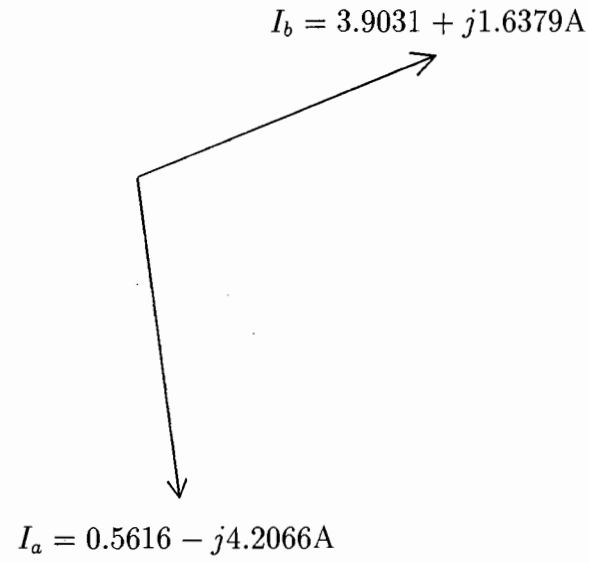

Figure 3.8: Phasor diagram of stator phase currents I_a and I_b, $\alpha = 75°$

Table 3.5: Phase current I_a and symmetrical components at 90V, 50Hz, $\alpha = 75°$

N	I_a^+	I_a^-	I_a
rpm	A	A	A
50.0	1.57692 - j3.77637	-0.00513 - j0.00631	0 .5616 - j4.2066

Table 3.6: Phase current I_b and symmetrical components at 90V, 50Hz, $\alpha = 75°$

N	I_b^+	I_b^-	I_b
rpm	A	A	A
50.0	4.05583 + j0.54579	-0.00742 + j0.00332	3.9031 + j1.6379

Table 3.7: Simulation data of shaded-pole LIM at 90V, 50Hz and $\alpha = 45°$

N	I_a^+	I_a^-	I_a	I_b^+	I_b^-	I_b
rpm	A	A	A	A	A	A
2.5	2.507 -5.418	-.00277 -.00413	-2.910 -7.932	5.604 -2.059	-.00488 -.00096	7.657 3.549
5.0	2.545 -5.477	-.00280 -.00424	-2.931 -8.028	5.672 -2.073	-.00498 -.00101	7.739 3.603
7.5	2.543 -5.479	-.00280 -.00424	-2.934 -8.029	5.673 -2.076	-.00498 -.00101	7.742 3.601
10.0	2.541 -5.479	-.00280 -.00423	-2.937 -8.027	5.671 -2.078	-.00498 -.00101	7.743 3.598
12.5	2.545 -5.498	-.00282 -.00425	-2.951 -8.051	5.688 -2.088	-.00500 -.00101	7.770 3.604
15.0	2.543 -5.499	-.00282 -.00425	-2.954 -8.049	5.687 -2.090	-.00500 -.00101	7.771 3.600
17.5	2.542 -5.504	-.00283 -.00425	-2.960 -8.053	5.689 -2.094	-.00500 -.00100	7.777 3.599
20.0	2.540 -5.504	-.00283 -.00425	-2.963 -8.051	5.688 -2.096	-.00500 -.00100	7.778 3.596
22.5	2.544 -5.524	-.00285 -.00426	-2.979 -8.075	5.705 -2.107	-.00503 -.00100	7.806 3.602
25.0	2.541 -5.524	-.00285 -.00426	-2.982 -8.073	5.703 -2.109	-.00503 -.00100	7.807 3.598
27.5	2.538 -5.525	-.00285 -.00426	-2.985 -8.071	5.702 -2.112	-.00503 -.00099	7.808 3.594
30.0	2.536 -5.526	-.00285 -.00425	-2.989 -8.069	5.700 -2.114	-.00503 -.00099	7.809 3.590
32.5	2.533 -5.526	-.00286 -.00425	-2.992 -8.066	5.699 -2.117	-.00502 -.00099	7.809 3.586
35.0	2.537 -5.546	-.00288 -.00426	-3.008 -8.090	5.716 -2.128	-.00505 -.00098	7.838 3.592
37.5	2.534 -5.547	-.00288 -.00426	-3.012 -8.088	5.714 -2.131	-.00505 -.00098	7.839 3.588
40.0	2.531 -5.548	-.00288 -.00426	-3.015 -8.086	5.713 -2.133	-.00505 -.00098	7.840 3.583
42.5	2.528 -5.548	-.00288 -.00426	-3.019 -8.084	5.711 -2.136	-.00505 -.00097	7.841 3.579
45.0	2.525 -5.549	-.00288 -.00425	-3.023 -8.081	5.709 -2.139	-.00505 -.00097	7.842 3.575
47.5	2.529 -5.570	-.00290 -.00427	-3.040 -8.106	5.727 -2.150	-.00507 -.00097	7.871 3.580
50.0	2.525 -5.571	-.00290 -.00426	-3.044 -8.103	5.725 -2.153	-.00507 -.00096	7.872 3.576
52.5	2.522 -5.571	-.00291 -.00426	-3.048 -8.101	5.723 -2.156	-.00507 -.00096	7.873 3.571
55.0	2.519 -5.572	-.00291 -.00426	-3.052 -8.098	5.721 -2.159	-.00507 -.00095	7.874 3.566
57.5	2.523 -5.594	-.00293 -.00427	-3.069 -8.124	5.739 -2.171	-.00509 -.00095	7.905 3.572
60.0	2.519 -5.594	-.00293 -.00427	-3.074 -8.121	5.737 -2.174	-.00509 -.00095	7.906 3.567
62.5	2.516 -5.595	-.00293 -.00427	-3.078 -8.118	5.736 -2.177	-.00509 -.00094	7.907 3.562
65.0	2.514 -5.601	-.00294 -.00427	-3.085 -8.122	5.738 -2.183	-.00510 -.00094	7.915 3.560
67.5	2.511 -5.602	-.00294 -.00426	-3.090 -8.120	5.736 -2.186	-.00510 -.00093	7.916 3.555
70.0	2.515 -5.624	-.00297 -.00428	-3.108 -8.146	5.755 -2.199	-.00512 -.00093	7.948 3.560
72.5	2.511 -5.625	-.00297 -.00428	-3.113 -8.143	5.753 -2.202	-.00512 -.00092	7.949 3.555
75.0	2.507 -5.626	-.00297 -.00427	-3.118 -8.141	5.751 -2.205	-.00512 -.00092	7.951 3.550

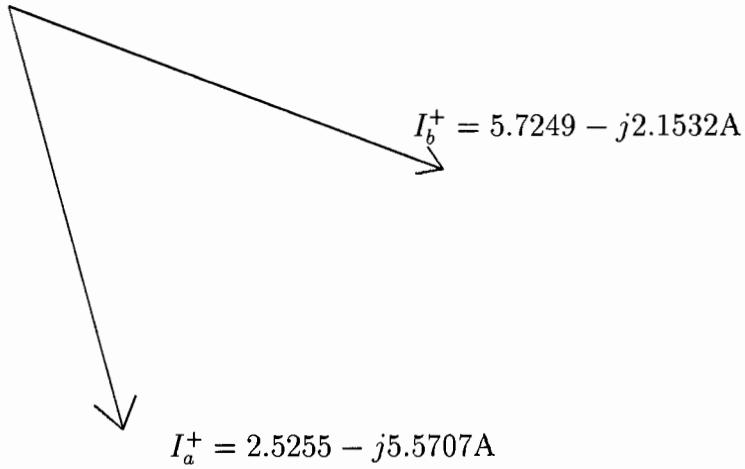

Figure 3.9: Phasor diagram of stator phase currents I_a^+ and I_b^+, $\alpha = 45°$

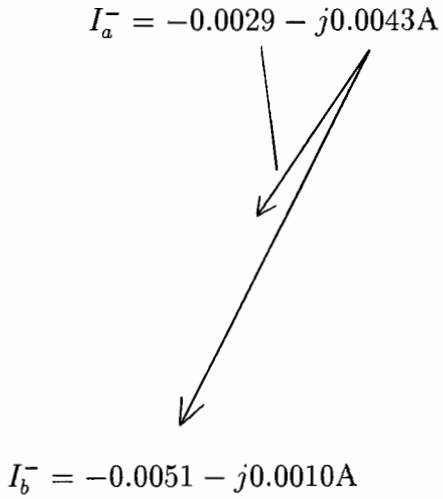

Figure 3.10: Phasor diagram of stator phase currents I_a^- and I_b^-, $\alpha = 45°$

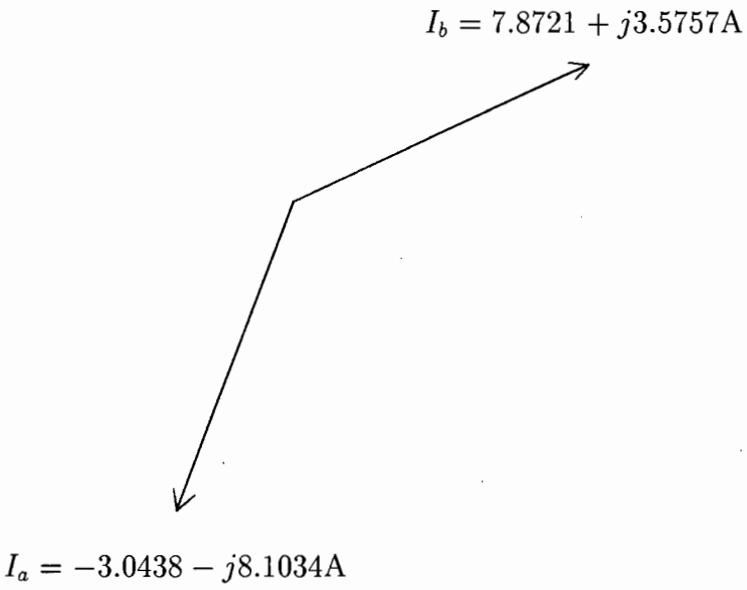

Figure 3.11: Phasor diagram of stator phase currents I_a and I_b, $\alpha = 45°$

Table 3.8: Phase current I_a and symmetrical components at 90V, 50Hz, $\alpha = 45°$

N	I_a^+	I_a^-	I_a
rpm	A	A	A
50.0	2.5255 - j5.5707	-0.0029 - j0.0043	-3.0438 - j8.1034

Table 3.9: Phase current I_b and symmetrical components at 90V, 50Hz, $\alpha = 45°$

N	I_b^+	I_b^-	I_b
rpm	A	A	A
50.0	5.7249 - j2.1532	-0.0051 - j0.0010	7.8721 + j3.5757

3.4 Circuital Analysis

This section contains results of the circuital approach to the single-sided shaded-pole linear induction motor. The equivalent circuit for each phase is set up to determine currents flowing in the stator and rotor windings. The procedure is:

(a) Set up separate circuits for forward and backward sequences

(b) The positive and negative sequence fields revolve at a different speed with respect to the rotor.

This determines the expression for slip and impedances of the equivalent circuit.

3.4.1 Voltage Equations for Main and Auxiliary Phases

The input voltage across the main phase terminals, including the mutual reactance between stator windings a and b, is given by the expression:

$$V_a = I_a Z_{1a} + I_a^+ Z^+ + I_a^- Z^- + (I_a + I_b) Z_{ab} \tag{3.16}$$

A similar equation can be written for the auxiliary phase:

$$V_b = 0 = I_b Z_{1b} + I_b^+ Z^+ + I_b^- Z^- + (I_a + I_b) Z_{ab} \tag{3.17}$$

or

$$V_b = 0 = I_b Z_{1b} + I_a^+ Z^+ e^{j\alpha} + I_a^- Z^- e^{-j\alpha} + (I_a + I_b) Z_{ab}$$

where Z^+ and Z^- are the positive and negative sequence impedances of the vertical branch and secondary branch, as seen from the input terminals. These are explained in subsequent sections.

3.4.2 Voltage and Current Equations for Angle $\alpha \leq 90°$

The equations for the equivalent circuit for phases a and b at $\alpha \neq 90°$ is derived as follows:

From symmetrical components the equation relating currents in phases a and b are:

$$I_b^+ = I_a^+ \cdot e^{j\alpha},$$

$$I_b^- = I_a^- \cdot e^{-j\alpha}$$

or

$$I_a^+ = I_b^+ \cdot e^{-j\alpha},$$

$$I_a^- = I_b^- \cdot e^{j\alpha}$$

The current in phase a is given by:

$$I_a = -j(\frac{I_a^+}{sin\alpha}e^{j\alpha} - \frac{I_a^-}{sin\alpha}e^{-j\alpha}) \tag{3.18}$$

For phase b:

$$I_b = j(\frac{I_a^+}{sin\alpha} - \frac{I_a^-}{sin\alpha}) \tag{3.19}$$

or

$$I_b = j(\frac{I_b^+}{sin\alpha}e^{-j\alpha} - \frac{I_b^-}{sin\alpha}e^{j\alpha}) \tag{3.20}$$

Also, for $\alpha \neq 90°$:

$$I_a + I_b = -j(\frac{I_a^+}{sin\alpha}e^{j\alpha} - \frac{I_a^-}{sin\alpha}e^{-j\alpha}) + j(\frac{I_a^+}{sin\alpha} - \frac{I_a^-}{sin\alpha})$$

$$I_a + I_b = j\frac{I_a^+}{sin\alpha} - j\frac{I_a^+}{sin\alpha}e^{j\alpha} + j\frac{I_a^-}{sin\alpha}e^{-j\alpha} - j\frac{I_a^-}{sin\alpha}$$

$$(I_a + I_b) = j(\frac{1 - e^{j\alpha}}{sin\alpha})I_a^+ - j(\frac{1 - e^{-j\alpha}}{sin\alpha})I_a^- \tag{3.21}$$

In terms of phase b sequence parameters, substitute (3.6,3.7) in (3.20):

$$I_a + I_b = j(\frac{1 - e^{j\alpha}}{sin\alpha})I_b^+ \cdot e^{-j\alpha} - j(\frac{1 - e^{-j\alpha}}{sin\alpha})I_b^- \cdot e^{j\alpha}$$

$$(I_a + I_b) = -j(\frac{1 - e^{-j\alpha}}{sin\alpha})I_b^+ + j(\frac{1 - e^{j\alpha}}{sin\alpha})I_b^- \tag{3.22}$$

3.4.3 Main Phase

Substituting (3.17, 3.21) in (3.16) as seen below,

$$V_a = I_a Z_{1a} + I_a^+ Z^+ + I_a^- Z^- + (I_a + I_b)Z_{ab}$$

This gives:

$$V_a = Z_{1a}[-j(\frac{I_a^+}{sin\alpha}e^{j\alpha} - \frac{I_a^-}{sin\alpha}e^{-j\alpha})] + I_a^+ Z^+ + I_a^- Z^- + [j(\frac{1 - e^{j\alpha}}{sin\alpha})I_a^+ - j(\frac{1 - e^{-j\alpha}}{sin\alpha})I_a^-]Z_{ab}$$

$$V_a = -jZ_{1a}\frac{I_a^+}{sin\alpha}e^{j\alpha} + jZ_{1a}\frac{I_a^-}{sin\alpha}e^{-j\alpha} + I_a^+Z^+ + I_a^-Z^- + jZ_{ab}(\frac{1-e^{j\alpha}}{sin\alpha})I_a^+ - jZ_{ab}(\frac{1-e^{-j\alpha}}{sin\alpha})I_a^-$$

Thus:

$$V_a = I_a^+[-j\frac{Z_{1a}\cdot e^{j\alpha}}{sin\alpha} + Z^+] + I_a^+[j\frac{Z_{ab}(1-e^{j\alpha})}{sin\alpha}] + I_a^-[j\frac{Z_{1a}\cdot e^{-j\alpha}}{sin\alpha} + Z^-] + I_a^-[-j\frac{Z_{ab}(1-e^{-j\alpha})}{sin\alpha}] \tag{3.23}$$

This expression determines the equivalent circuit for phase a. For $\alpha = 90°$, we have the simplified expression:

$$V_a = I_a^+(Z_{1a} + Z^+) + I_a^+[Z_{ab}(1+j)] + I_a^-(Z_{1a} + Z^-) + I_a^-[Z_{ab}(1-j)]$$

Denoting,

$$Z_a^+ = Z_{1a} + Z^+$$

$$Z_a^- = Z_{1a} + Z^-$$

then

$$V_a = I_a^+Z_a^+ + I_a^+[Z_{ab}(1+j)] + I_a^-Z_a^- + I_a^-[Z_{ab}(1-j)]$$

where Z_{1a} is the impedance of the main windings. Thus, Z_a^+ and Z_a^- are the resultant impedances of the main phase winding for positive and negative sequence currents, respectively, as seen from the input terminals.

3.4.4 Auxiliary Phase

Similarly, for phase b, substituting (3.20, 3.22) in (3.17) below:

$$V_b = 0 = I_bZ_{1b} + I_b^+Z^+ + I_b^-Z^- + (I_a + I_b)Z_{ab}$$

$$0 = Z_{1b}[j(\frac{I_b^+}{sin\alpha}e^{-j\alpha} - \frac{I_b^-}{sin\alpha}e^{j\alpha})] + I_b^+Z^+ + I_b^-Z^- + Z_{ab}[-j(\frac{1-e^{-j\alpha}}{sin\alpha})I_b^+ + j(\frac{1-e^{j\alpha}}{sin\alpha})I_b^-]$$

This gives:

$$0 = j(\frac{Z_{1b}\cdot e^{-j\alpha}}{sin\alpha})I_b^+ - j(\frac{Z_{1b}\cdot e^{j\alpha}}{sin\alpha})I_b^- + I_b^+Z^+ + I_b^-Z^- - j\frac{Z_{ab}(1-e^{-j\alpha})}{sin\alpha}I_b^+ + j\frac{Z_{ab}(1-e^{j\alpha})}{sin\alpha}I_b^-$$

Thus:

$$0 = I_b^+[j\frac{Z_{1b}\cdot e^{-j\alpha}}{sin\alpha} + Z^+] + I_b^+[-j\frac{Z_{ab}(1-e^{-j\alpha})}{sin\alpha}] + I_b^-[-j\frac{Z_{1b}\cdot e^{j\alpha}}{sin\alpha} + Z^-] + I_b^-[j\frac{Z_{ab}(1-e^{j\alpha})}{sin\alpha}] \tag{3.24}$$

This expression determines the equivalent circuit for phase b.

For $\alpha = 90°$:

$$V_b = 0 = I_b^+(Z_{1b} + Z^+) + I_b^+[Z_{ab}(1-j)] + I_b^-(Z_{1b} + Z^-) + I_b^-[Z_{ab}(1+j)]$$

Similarly if

$$Z_b^+ = Z_{1b} + Z^+$$

$$Z_b^- = Z_{1b} + Z^-$$

then

$$V_b = 0 = I_b^+ Z_a^+ + I_b^+[Z_{ab}(1-j)] + I_b^- Z_a^- + I_b^-[Z_{ab}(1+j)]$$

where Z_{1b} is the impedance of the short-circuited coil (auxiliary phase). Thus, Z_b^+ and Z_b^- represents the resultant impedance of the motor together with the stator auxiliary winding.

3.4.5 Verification of Equations

For angle $\alpha = 90°$:

$$I_a = I_a^+ + I_a^-$$

$$I_b = I_b^+ + I_b^-$$

The equation

$$V_a = I_a Z_{1a} + I_a^+ Z^+ + I_a^- Z^- + (I_a + I_b)Z_{ab}$$

becomes:

$$V_a = I_a^+ Z_{1a} + I_a^- Z_{1a} + I_a^+ Z^+ + I_a^- Z^- + (I_a + I_b)Z_{ab}$$

which gives:

$$V_a = I_a^+ Z_a^+ + I_a^- Z_a^- + (I_a + I_b) Z_{ab} \tag{3.25}$$

Similarly:

$$V_b = 0 = I_b Z_{1b} + I_b^+ Z^+ + I_b^- Z^- + (I_a + I_b) Z_{ab}$$

becomes:

$$V_b = 0 = I_b^+ Z_{1b} + I_b^- Z_{1b} + I_b^+ Z^+ + I_b^- Z^- + (I_a + I_b) Z_{ab}$$

which gives:

$$V_b = 0 = I_b^+ Z_b^+ + I_b^- Z_b^- + (I_a + I_b) Z_{ab} \tag{3.26}$$

or

$$V_b = 0 = jI_a^+ Z_b^+ - jI_a^- Z_b^- + (I_a + I_b) Z_{ab}$$

It should be noted that the following expressions:

$$Z_a^+ = Z_{1a} + Z^+ \tag{3.27}$$

$$Z_a^- = Z_{1a} + Z^- \tag{3.28}$$

$$Z_b^+ = Z_{1b} + Z^+ \tag{3.29}$$

$$Z_b^- = Z_{1b} + Z^- \tag{3.30}$$

are only valid on the condition that angle $\alpha = 90°$. However, if angle $\alpha \neq 90°$, equations (3.27 - 3.30) become,

$$Z_a^+ = -j \frac{Z_{1a} \cdot e^{j\alpha}}{sin\alpha} + Z^+ \tag{3.31}$$

$$Z_a^- = j \frac{Z_{1a} \cdot e^{-j\alpha}}{sin\alpha} + Z^- \tag{3.32}$$

$$Z_b^+ = j \frac{Z_{1b} \cdot e^{-j\alpha}}{sin\alpha} + Z^+ \tag{3.33}$$

$$Z_b^- = -j \frac{Z_{1b} \cdot e^{j\alpha}}{sin\alpha} + Z^- \tag{3.34}$$

where according to (3.16, 3.17):

$$Z^+ = \frac{Z_0 \cdot Z_2'^+}{Z_0 + Z_2'^+} \tag{3.35}$$

$$Z^- = \frac{Z_0 \cdot Z_2'^-}{Z_0 + Z_2'^-} \tag{3.36}$$

3.4.6 Equations for Currents I_a^+ and I_a^-

For the positive and negative sequence main phase currents in terms of V, α, Z_{1a}, Z_{1b}, Z^+ and Z^-, including the mutual reactance of main stator and auxiliary windings, the positive and negative sequence stator currents are:

$$I_a^+ = \frac{V(Z_{1b} + Z_{ab}(1 - e^{-j\alpha}) + jZ^- e^{-j\alpha} sin\alpha)}{sin\alpha[(Z_{1a} + Z_{1b})(Z^+ + Z^- + 2Z_{ab}) + 2(Z_{1a}Z_{1b} + Z^+Z^- sin^2\alpha + Z_{ab}(Z^+ + Z^-)(1 - cos\alpha))]} \tag{3.37}$$

and

$$I_a^- = \frac{V(Z_{1b} + Z_{ab}(1 - e^{j\alpha}) - jZ^+ e^{j\alpha} sin\alpha)}{sin\alpha[(Z_{1a} + Z_{1b})(Z^+ + Z^- + 2Z_{ab}) + 2(Z_{1a}Z_{1b} + Z^+Z^- sin^2\alpha + Z_{ab}(Z^+ + Z^-)(1 - cos\alpha))]} \tag{3.38}$$

which is simplified as:

$$I_a^+ = \frac{V_a(Z_{1b} + Z_{ab}(1 - e^{-j\alpha}) + jZ^- e^{-j\alpha} sin\alpha)}{sin\alpha[G1 + G2]} \tag{3.39}$$

and

$$I_a^- = \frac{V_a(Z_{1b} + Z_{ab}(1 - e^{j\alpha}) - jZ^+ e^{j\alpha} sin\alpha)}{sin\alpha[G1 + G2]} \tag{3.40}$$

where

$$G1 = (Z_{1a} + Z_{1b})(Z^+ + Z^- + 2Z_{ab})$$

$$G2 = 2(Z_{1a}Z_{1b} + Z^+Z^- sin^2\alpha + Z_{ab}(Z^+ + Z^-)(1 - cos\alpha))$$

where, as mentioned before, Z_{1a} is the impedance of the main stator winding, Z_{1b} is the impedance of the auxiliary winding, Z^+ is the positive sequence impedance of the vertical branch in parallel with the secondary, and Z^- is the negative sequence impedance of the vertical branch in parallel with the secondary. For the forward-travelling field $s = s^+$, and for the backward travelling $s^- = 2 - s^+$.

To obtain expressions for I_b^+ and I_b^-, recall the following equations relating currents in phases a and b, namely:

$$I_b^+ = I_a^+ \cdot e^{j\alpha} \tag{3.41}$$

$$I_b^- = I_a^- \cdot e^{-j\alpha} \tag{3.42}$$

Since the positive and negative sequence currents in phase a are:

$$I_a^+ = \frac{V_a(Z_{1b} + Z_{ab}(1 - e^{-j\alpha}) + jZ^- e^{-j\alpha} sin\alpha)}{sin\alpha[G1 + G2]} \tag{3.43}$$

and

$$I_a^- = \frac{V_a(Z_{1b} + Z_{ab}(1 - e^{j\alpha}) - jZ^+ e^{j\alpha} sin\alpha)}{sin\alpha[G1 + G2]} \tag{3.44}$$

where

$$G1 = (Z_{1a} + Z_{1b})(Z^+ + Z^- + 2Z_{ab})$$

$$G2 = 2(Z_{1a}Z_{1b} + Z^+Z^- sin^2\alpha + Z_{ab}(Z^+ + Z^-)(1 - cos\alpha))$$

For phase b, the positive and negative sequence currents are:

$$I_b^+ = I_a^+ \cdot e^{j\alpha} = \frac{V_a(Z_{1b} + Z_{ab}(1 - e^{-j\alpha}) + jZ^- e^{-j\alpha} sin\alpha)}{sin\alpha[G1 + G2]} \times e^{j\alpha}$$

which gives:

$$I_b^+ = \frac{V_a(Z_{1b} \cdot e^{j\alpha} - Z_{ab}(1 - e^{j\alpha}) + jZ^- sin\alpha)}{sin\alpha[G1 + G2]} \tag{3.45}$$

likewise for I_b^-:

$$I_b^- = I_a^- \cdot e^{-j\alpha} = \frac{V_a(Z_{1b} + Z_{ab}(1 - e^{j\alpha}) - jZ^+ e^{j\alpha} sin\alpha)}{sin\alpha[G1 + G2]} \times e^{-j\alpha} \tag{3.46}$$

which gives:

$$I_b^- = \frac{V_a(Z_{1b} \cdot e^{-j\alpha} - Z_{ab}(1 - e^{-j\alpha}) - jZ^+ sin\alpha)}{sin\alpha[G1 + G2]} \tag{3.47}$$

Figs. 3.12 – 3.14 show the current phasors for phases a and b, and their positive and negative sequence components, for the shaded pole LIM for the tested motor with angle $\alpha = 29.3°$.

Table 3.10: Simulation data of shaded-pole LIM at 90V, 50Hz and $\alpha = 29.3°$

N	I_a^+	I_a^-	I_a	I_b^+	I_b^-	I_b
rpm	A	A	A	A	A	A
2.5	3.323 -7.568	-.00621 -.00885	-10.152 -13.509	6.602 -4.973	-.00975 -.00468	15.445 6.802
5.0	3.375 -7.652	-.00627 -.00907	-10.250 -13.687	6.689 -5.021	-.00991 -.00484	15.617 6.909
7.5	3.374 -7.655	-.00628 -.00908	-10.256 -13.687	6.689 -5.024	-.00992 -.00484	15.622 6.906
10.0	3.371 -7.656	-.00628 -.00907	-10.260 -13.682	6.686 -5.026	-.00992 -.00484	15.624 6.900
12.5	3.376 -7.681	-.00632 -.00910	-10.301 -13.717	6.703 -5.046	-.00997 -.00484	15.677 6.911
15.0	3.373 -7.682	-.00632 -.00910	-10.306 -13.713	6.701 -5.049	-.00997 -.00484	15.679 6.904
17.5	3.371 -7.689	-.00633 -.00910	-10.319 -13.717	6.703 -5.055	-.00998 -.00484	15.692 6.902
20.0	3.368 -7.670	-.00634 -.00909	-10.324 -13.711	6.701 -5.057	-.00998 -.00483	15.694 6.895
22.5	3.373 -7.716	-.00638 -.00912	-10.366 -13.747	6.718 -5.078	-.01003 -.00483	15.748 6.905
25.0	3.369 -7.717	-.00638 -.00912	-10.371 -13.741	6.715 -5.081	-.01003 -.00483	15.749 6.898
27.5	3.366 -7.718	-.00638 -.00911	-10.376 -13.736	6.712 -5.083	-.01003 -.00482	15.751 6.890
30.0	3.362 -7.719	-.00639 -.00911	-10.381 -13.730	6.710 -5.086	-.01003 -.00482	15.752 6.883
32.5	3.358 -7.719	-.00639 -.00910	-10.386 -13.724	6.707 -5.088	-.01003 -.00481	15.754 6.875
35.0	3.363 -7.747	-.00643 -.00913	-10.430 -13.760	6.724 -5.110	-.01008 -.00481	15.810 6.885
37.5	3.359 -7.748	-.00643 -.00912	-10.436 -13.754	6.721 -5.112	-.01008 -.00481	15.812 6.877
40.0	3.355 -7.748	-.00644 -.00912	-10.441 -13.747	6.718 -5.115	-.01008 -.00480	15.813 6.869
42.5	3.351 -7.749	-.00644 -.00911	-10.447 -13.741	6.715 -5.118	-.01008 -.00479	15.815 6.860
45.0	3.347 -7.750	-.00645 -.00911	-10.453 -13.735	6.712 -5.121	-.01008 -.00479	15.817 6.852
47.5	3.351 -7.778	-.00649 -.00913	-10.498 -13.771	6.730 -5.143	-.01013 -.00479	15.875 6.861
50.0	3.347 -7.779	-.00649 -.00913	-10.504 -13.764	6.726 -5.146	-.01013 -.00478	15.877 6.852
52.5	3.343 -7.780	-.00650 -.00912	-10.511 -13.757	6.723 -5.149	-.01013 -.00477	15.879 6.844
55.0	3.338 -7.781	-.00650 -.00912	-10.517 -13.751	6.720 -5.152	-.01013 -.00477	15.881 6.835
57.5	3.343 -7.810	-.00655 -.00914	-10.564 -13.787	6.738 -5.175	-.01018 -.00477	15.939 6.844
60.0	3.338 -7.811	-.00655 -.00914	-10.570 -13.780	6.734 -5.178	-.01018 -.00476	15.942 6.834
62.5	3.334 -7.813	-.00655 -.00913	-10.577 -13.773	6.731 -5.181	-.01018 -.00475	15.944 6.825
65.0	3.331 -7.820	-.00657 -.00913	-10.593 -13.776	6.732 -5.189	-.01020 -.00475	15.960 6.820
67.5	3.326 -7.821	-.00657 -.00912	-10.600 -13.769	6.729 -5.193	-.01020 -.00474	15.962 6.810
70.0	3.331 -7.851	-.00662 -.00915	-10.649 -13.807	6.747 -5.217	-.01025 -.00474	16.024 6.819
72.5	3.326 -7.853	-.00663 -.00915	-10.657 -13.780	6.744 -5.220	-.01025 -.00473	16.027 6.809
75.0	3.321 -7.854	-.00663 -.00914	-10.664 -13.792	6.740 -5.224	-.01026 -.00473	16.029 6.799

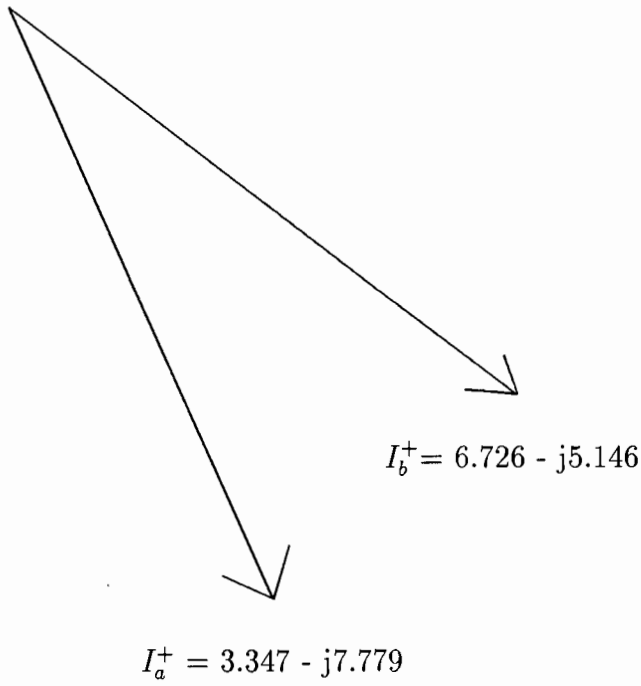

Figure 3.12: Phasor diagram of stator phase currents I_a^+ and I_b^+, $\alpha = 29.3°$

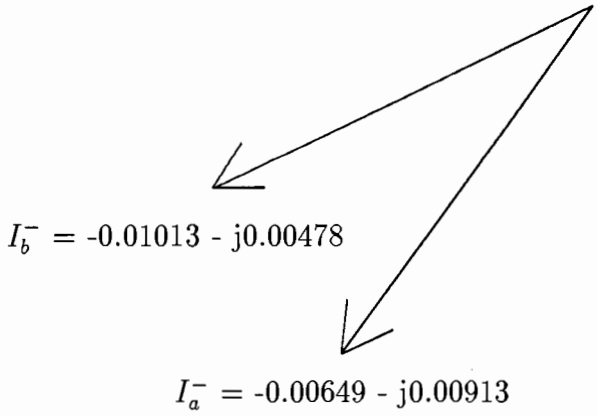

Figure 3.13: Phasor diagram of stator phase currents I_a^- and I_b^-, $\alpha = 29.3°$

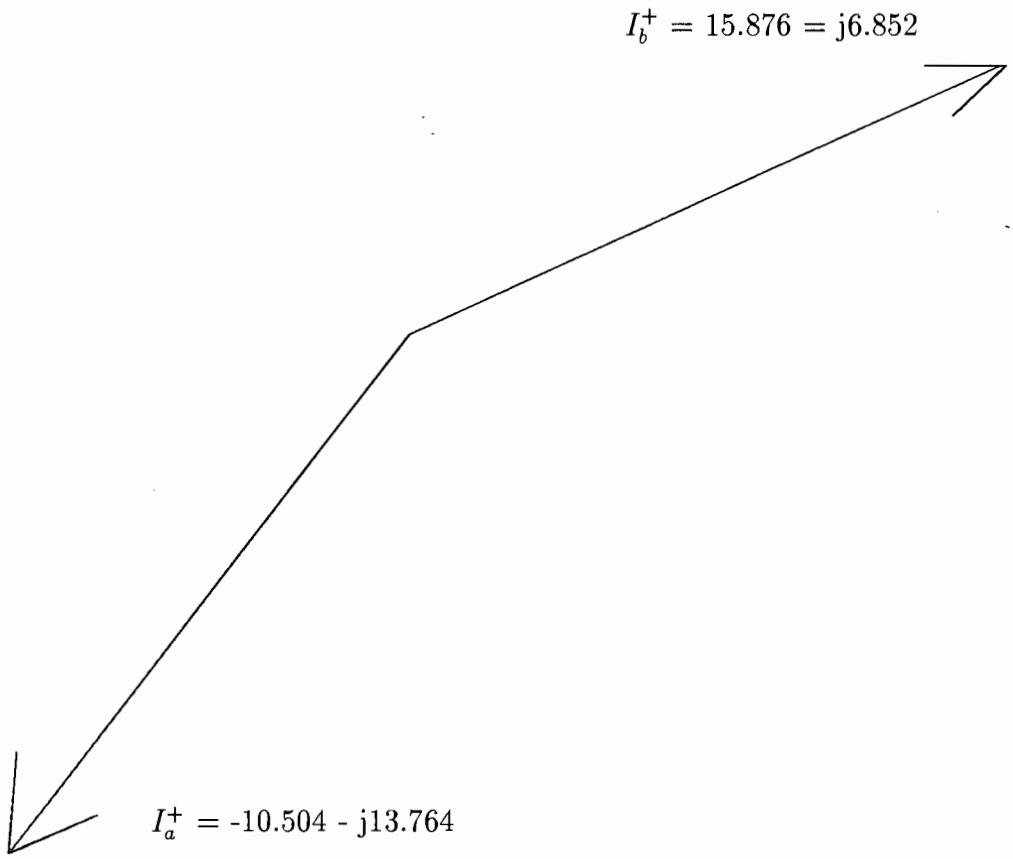

Figure 3.14: Phasor diagram of stator phase currents I_a and I_b, $\alpha = 29.3°$

Table 3.11: Phase current I_a and symmetrical components at 90V, 50Hz, $\alpha = 29.3°$

N	I_a^+	I_a^-	I_a
rpm	A	A	A
50.0	3.3472 - j7.7794	-0.0065 - j0.0091	-10.5044 - j13.7642

Table 3.12: Phase current I_b and symmetrical components at 90V, 50Hz, $\alpha = 29.3°$

N	I_b^+	I_b^-	I_b
rpm	A	A	A
50.0	6.726 - j5.146	-0.0101 - j0.0048	15.8766 + j6.8525

3.5 Resistances and reactances of the equivalent circuit of LIM

The equivalent circuit of each phase and sequence can then be separately drawn as represented as shown in Figs. 3.15 - 3.18.

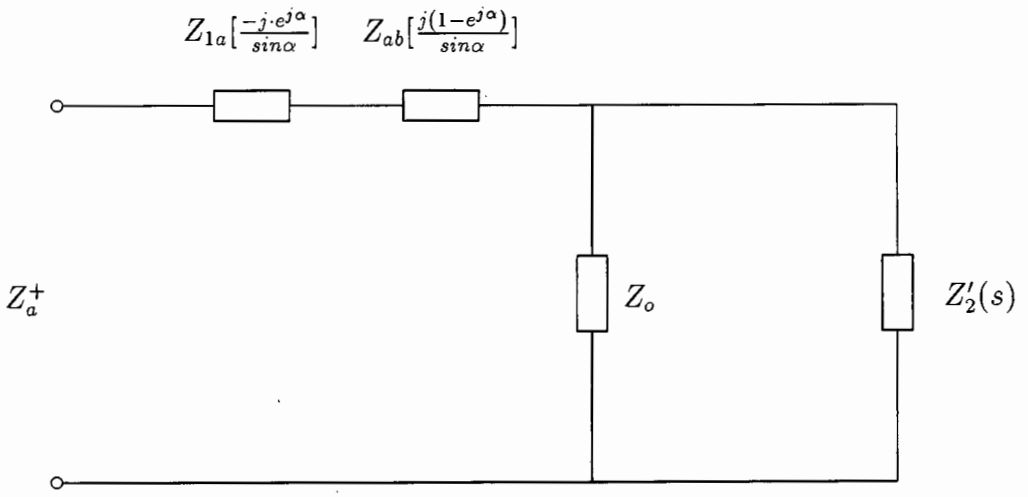

Figure 3.15: Equivalent circuit of a shaded pole induction motor, Phase a positive sequence

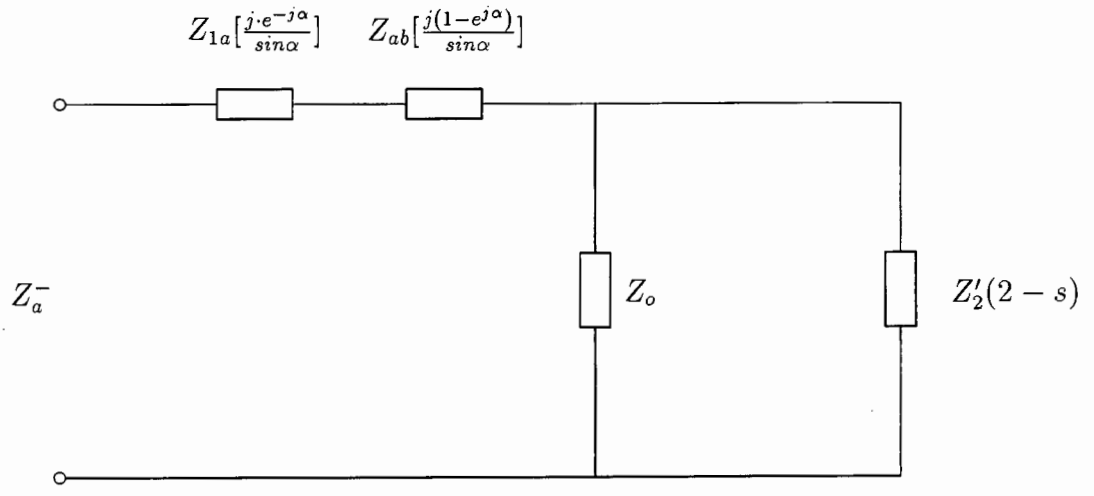

Figure 3.16: Equivalent circuit of a shaded pole induction motor, Phase a negative sequence

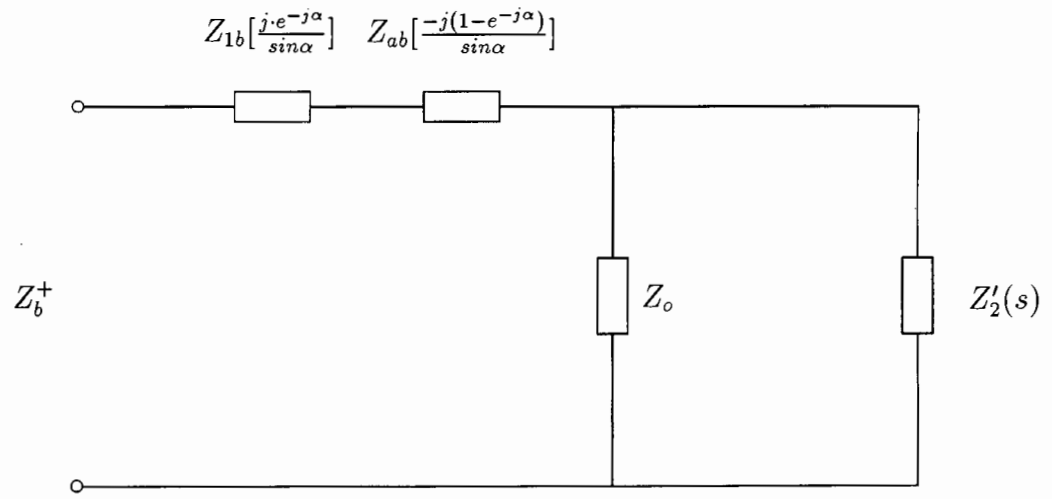

Figure 3.17: Equivalent circuit of a shaded pole induction motor, Phase b positive sequence

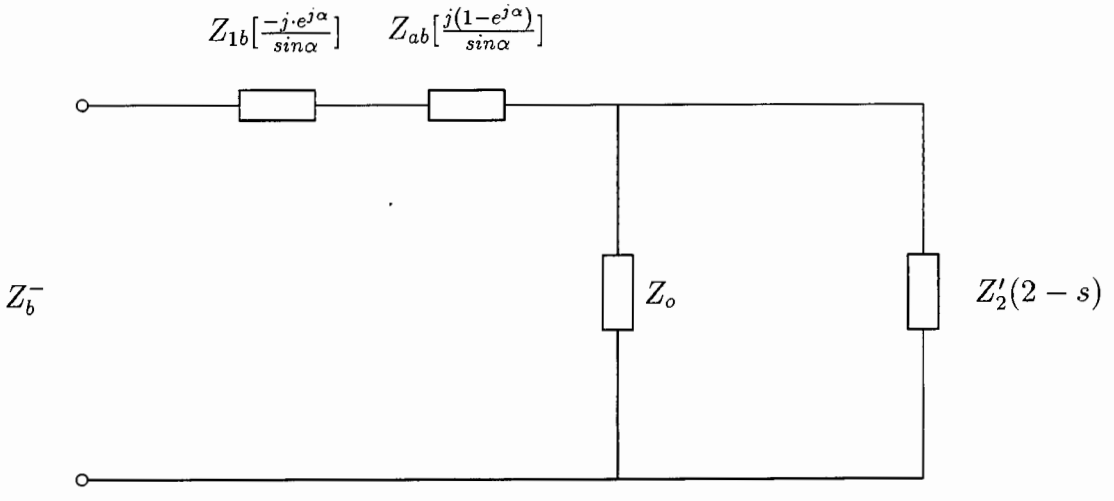

Figure 3.18: Equivalent circuit of a shaded pole induction motor, Phase b negative sequence

3.6 Resultant Secondary Impedance

The secondary circuit impedances referred to the primary system for the fundamental harmonic is:

$$Z_2'^{+} = Z_2'(s) = \frac{Z'_{Al}(s)Z'_{Fe}(s)}{Z'_{Al}(s) + Z'_{Fe}(s)}\frac{1}{s} \tag{3.48}$$

and

$$Z_2'^{-} = Z_2'(2-s) = \frac{Z'_{Al}(2-s)Z'_{Fe}(2-s)}{Z'_{Al}(2-s) + Z'_{Fe}(2-s)}\frac{1}{2-s} \tag{3.49}$$

where $Z_2'^{+} = Z_2'(s)$ and $Z_2'^{-} = Z_2'(2-s)$. Note that Z^+ is a parallel connection of $Z_2'^{+}$ and Z_o, and Z^- is a parallel connection of $Z_2'^{-}$ and Z_o.

3.7 Total Impedance of Motor

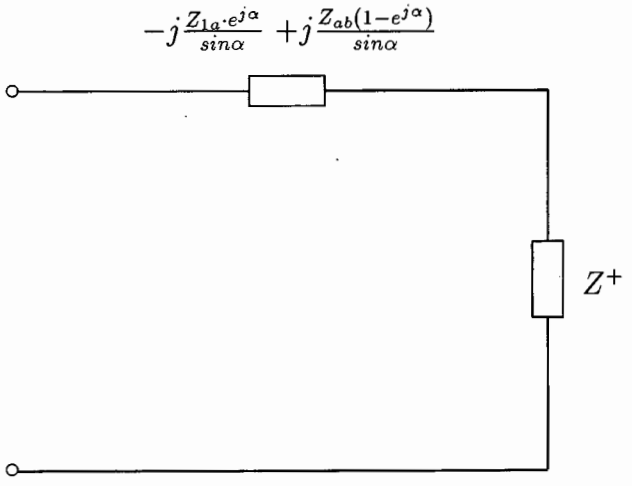

Figure 3.19: Equivalent circuit of a shaded-pole induction motor, positive sequence

The total impedance as seen from the input terminals of the equivalent circuit are:

$$Z_t^+ = -j\frac{Z_{1a}\cdot e^{j\alpha}}{sin\alpha} + j\frac{Z_{ab}(1-e^{j\alpha})}{sin\alpha} + Z^+ \tag{3.50}$$

$$Z_t^- = j\frac{Z_{1a}\cdot e^{-j\alpha}}{sin\alpha} - j\frac{Z_{ab}(1-e^{-j\alpha})}{sin\alpha} + Z^- \tag{3.51}$$

Total impedance of motor for phase a for both positive and negative sequences at $\alpha = 90°$ are,

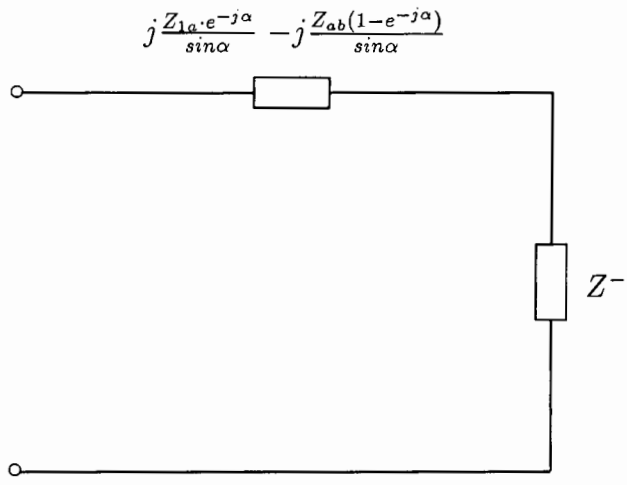

Figure 3.20: Equivalent circuit of a shaded-pole induction motor, negative sequence

$$Z_t^+ = Z_{1a} + Z_{ab}(1+j) + Z^+ \tag{3.52}$$

$$Z_t^- = Z_{1a} + Z_{ab}(1-j) + Z^- \tag{3.53}$$

The impedances of the vertical and secondary branch are:

$$Z^+ = \frac{Z_0 \cdot Z_2'^+}{Z_0 + Z_2'^+} \tag{3.54}$$

$$Z^- = \frac{Z_0 \cdot Z_2'^-}{Z_0 + Z_2'^-} \tag{3.55}$$

Neglecting R_{Fe}, since core losses are small, results in

$$Z^+ \approx \frac{jX_m Z_2'^+}{Z_2'^+ + jX_m} \tag{3.56}$$

$$Z^- \approx \frac{jX_m Z_2'^-}{Z_2'^- + jX_m} \tag{3.57}$$

3.8 Rotor Currents

The symmetrical components of the rotor current can be obtained from the equivalent circuits (Figs 3.15 to 3.20), i.e.:

$$I_2'^+ = I_a^+ \frac{|Z_o|}{|Z_o + Z_2'^+|} \tag{3.58}$$

$$I_2'^- = I_a^- \frac{|Z_o|}{|Z_o + Z_2'^-|} \tag{3.59}$$

where, $Z_2'^+$ and $Z_2'^-$ are forward and backward impedances of the secondary referred to the main stator winding turns.

3.9 Electromagnetic Torque

For the motor primary the magnetic field is of an elliptical form due to an unbalance of the MMFs of the windings a and b since the windings are spaced at an angle $\alpha < 90°$. The time shift angle β of vectors $\dot{I}_a$ and $\dot{I}_b$ is other than 90°. The electromagnetic torque in a multiphase symmetrical motor is developed by:

$$T = \frac{m_1 (I_2')^2 R_2'}{\omega_1 s} \tag{3.60}$$

where m_1 is the number of stator phases, I_2' is the rotor current referred to the number of phases and stator winding turns, and R_2' is the rotor resistance referred to the number of phases and stator winding turns.

The equations for the forward and backward sequence of a two-phase motor electromagnetic torque are therefore[5]:

$$T^+ = \frac{2(I_2'^+)^2 R_2'(s)}{\omega_1 s} \tag{3.61}$$

$$T^- = \frac{2(I_2'^-)^2 R_2'(2-s)}{\omega_1 (2-s)} \tag{3.62}$$

The resultant torque is the difference between the positive and negative sequence torques given by:

$$T = T^+ - T^-$$

3.10 Software Program

A software program was developed for analyzing the performance of the single-phase single-sided shaded-pole linear induction motor using the Fortran Language. Fig 3.21 shows the flow chart of the program. The program was based on classical circuit theory with field approach used in the calculation of the impedance of the secondary (double-layer disc rotor)[45, 10, 9, 87]. Results obtained from simulation were compared with measurements.

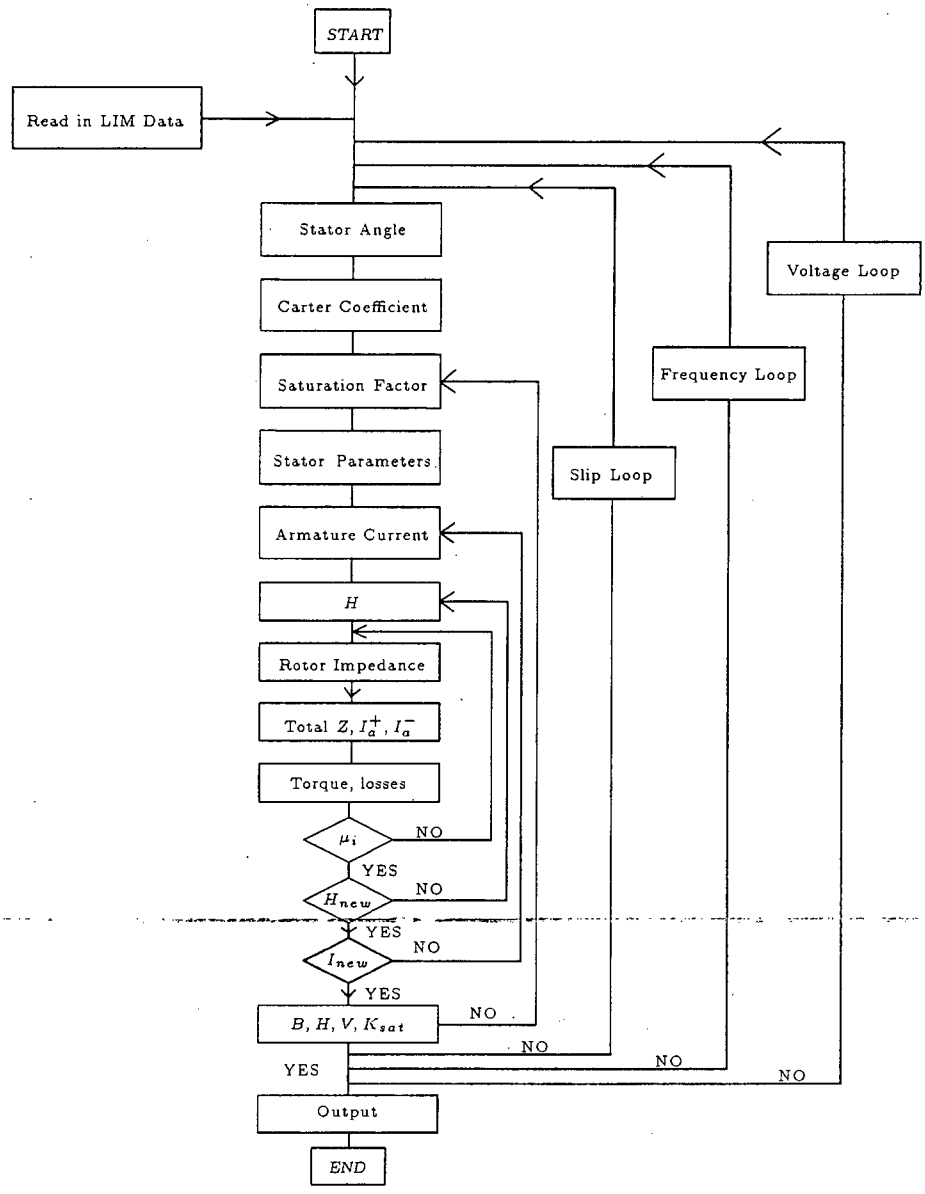

Figure 3.21: Flow-Chart of Shaded-pole Motor Computer Program

3.11 Conclusions

Figs 3.22-3.25 show the result of torque against speed for varying frequency. The voltages and frequencies used are: 90V at 50Hz, 110V at 60Hz and 160V at 75Hz. A comparison of the analytical approach with measurements shows a good correlation for the operating region of the LIM, taking into account the formulation of the analysis method, mechanical design constraints including materials and construction, vibrations at power frequencies and asymmetricity of the disc secondary. These parameters do introduce some errors into the measurements.

The estimation of machine design parameters such as linkage and leakage factors of main windings for the computation of stator leakage reactance do also contribute to the error between analytical results and measurements. The influence of edge effects is minimal in low speed LIMs. However saturation effects and the presence of 3rd time harmonics in the voltage and current waveforms contribute to erros in calculations. Mechanical losses and stray load losses which have not been estimated nor included here also contribute to the differences between the results of computation and experimental test.

For small machines, errors in calculations are usually higher than in high performance machines. An accurate estimation of these losses and influences will reduce the errors in calculations. Machine parameters such as linkage and leakage factors of main windings were assumed constant.

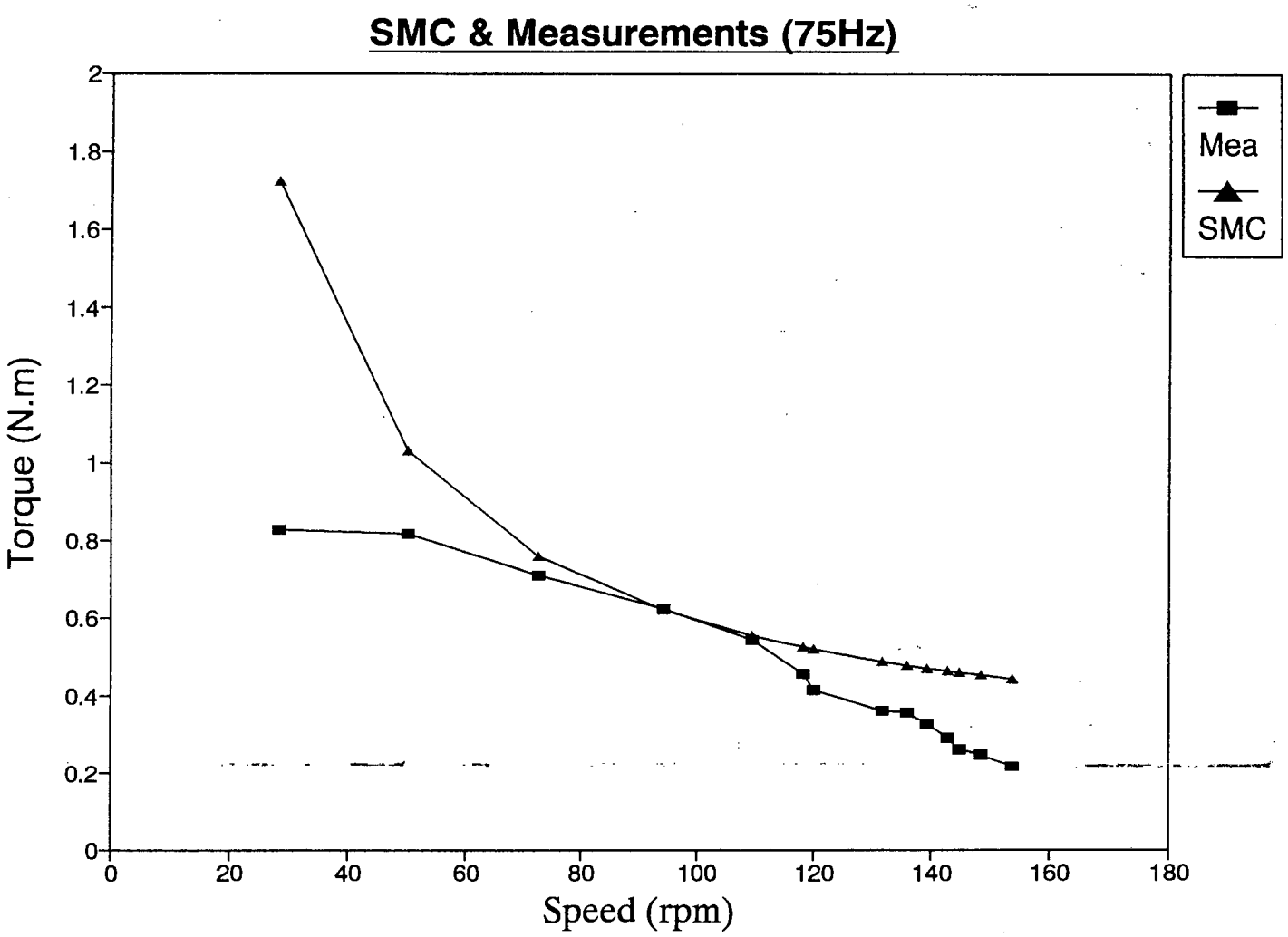

Figure 3.22: Torque against speed at $f = 75Hz$

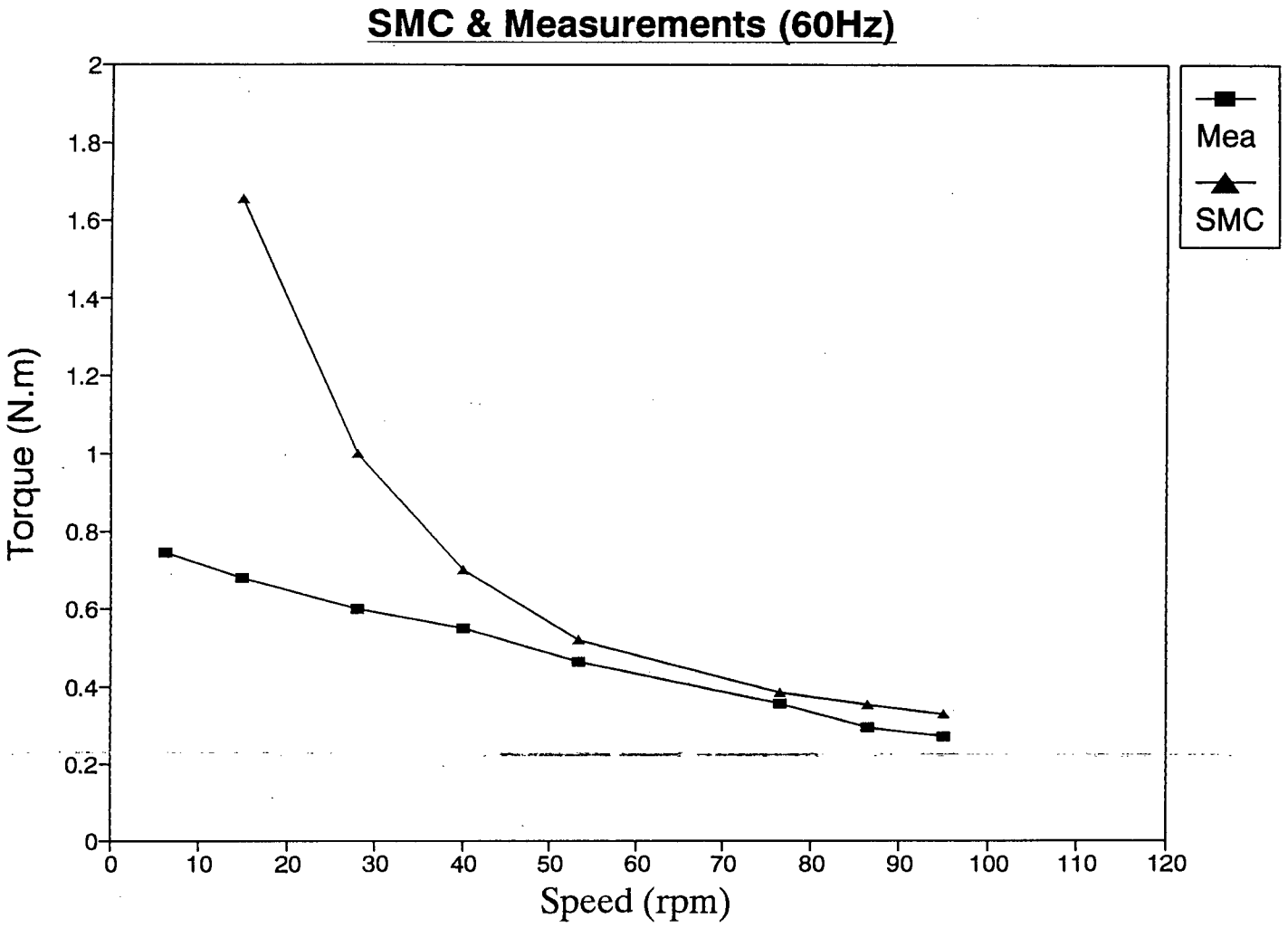

Figure 3.23: Torque against speed at $f = 60Hz$

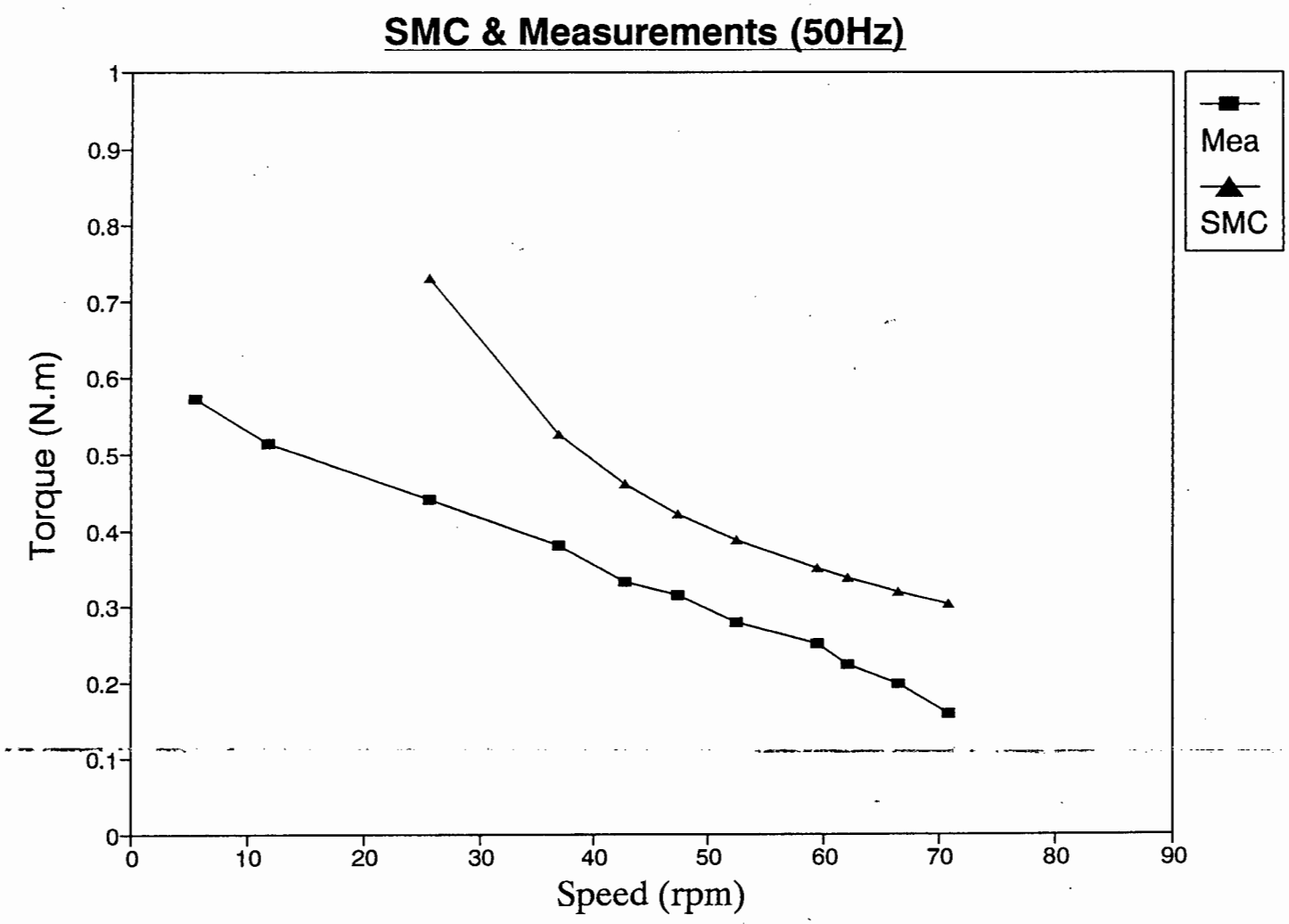

Figure 3.24: Torque against speed at $f = 50Hz$

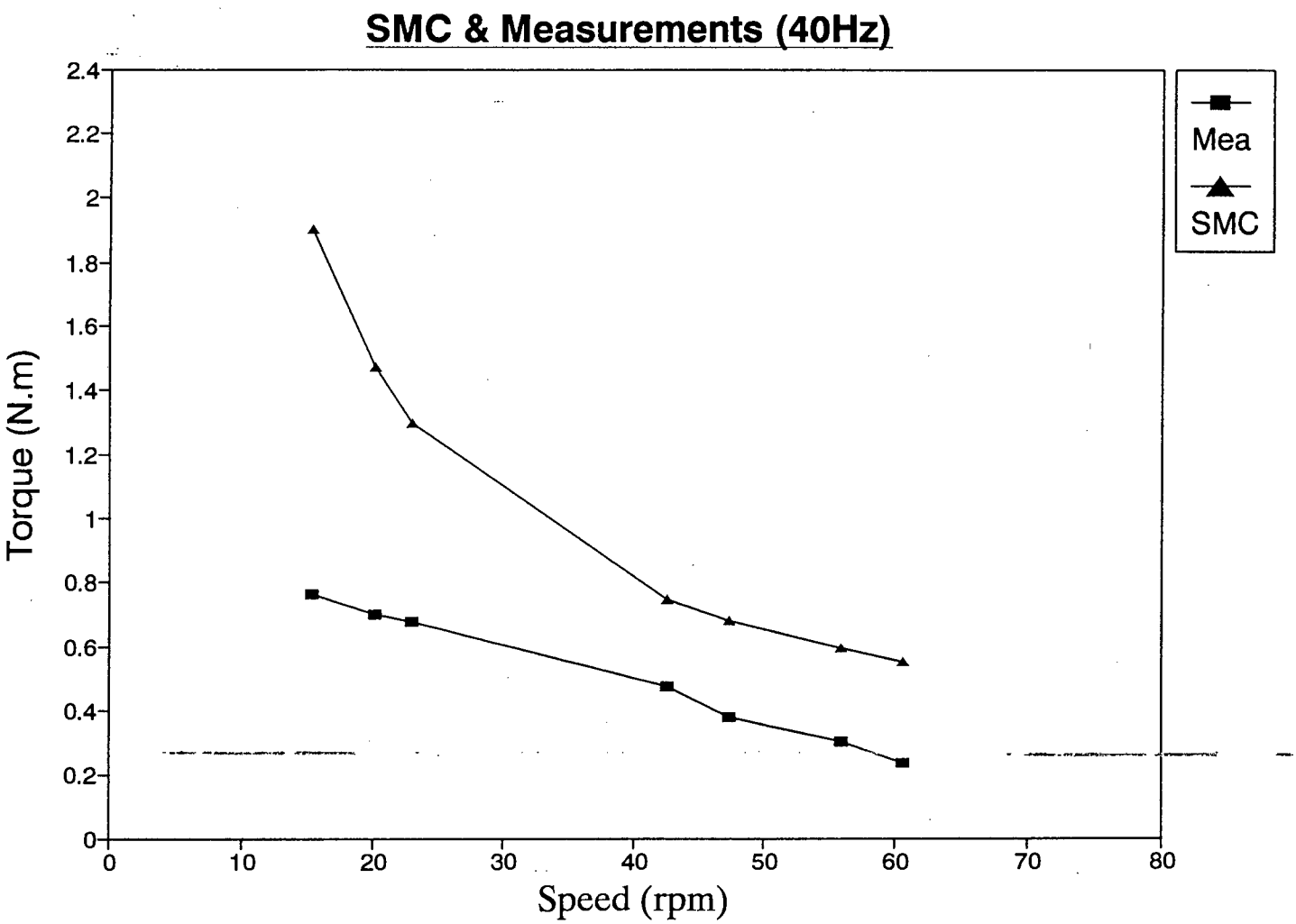

Figure 3.25: Torque against speed at $f = 40Hz$

Chapter 4

Performance Calculation Using Finite Element Analysis

In designing and analysing electromagnetic devices such as linear motors or launchers with higher power density, the effect of eddy-currents is important. Eddy-currents do appear in non-linear ferromagnetic media as well as in moving media, hence numerical solutions, such as the finite element method are used in the determination of eddy-currents in the shaded-pole LIM configuration.

Since the LIM armature (or secondary) is a solid disc consisting of back iron and aluminium, currents would be induced in it by its motion across the magnetic field. By Lenz's law, eddy-currents always tend to oppose the motion of a solid conductor in a magnetic field, and this force can be estimated.

4.1 Fundamental electromagnetic field equations

To develop a mathematical model for analysing the shaded-pole LIM, a set of mathematical relations and equivalent circuit(s) governed by fundamental and constitutive laws of elctromagnetic phenomena must be developed in a unique, coherent and stable way. Maxwell's equations[6, 12, 20] are used in LIM analysis, i.e.

$$curl\ \mathbf{H} = \mathbf{J} + \frac{\partial \mathbf{D}}{\partial t} \tag{4.1}$$

$$curl\ \mathbf{E} = -\frac{\partial \mathbf{B}}{\partial t} - curl\ (\mathbf{B} \times \mathbf{v}) \tag{4.2}$$

$$div\mathbf{B} = 0 \tag{4.3}$$

Eqn (4.1) states that the integral of the magnetic field intensity $\mathbf{H}$, along any closed contour is equal to the total current $\mathbf{J}$ plus the displacement current (non-stationary) or $\mathbf{H}$ is produced by varying current $\mathbf{J}$. The permeability μ, may not be a linear proportionality except for ferromagnctic and isotropic materials which at low frequencies and direct current

depends on **B**. Eqn (4.3) is the law of conservation of magnetic flux, i.e. no sources of **B** or no magnetic charges exist on which lines of magnetic flux can terminate.

The three equations above summarize the magneto-dynamics of quasi-stationary fields where **H**, **B** and **J** have three space components, i.e. they are not defined with respect to any particular co-ordinate system. For completeness, we add the following;

$$\mathbf{B} = \mu\mathbf{H} \tag{4.4}$$

$$\mathbf{D} = \epsilon\mathbf{E} \tag{4.5}$$

$$\mathbf{J} = \sigma\mathbf{E} \tag{4.6}$$

The constituent relations ϵ and σ are the permittivity and conductivity of the medium.

From (4.3), it is possible to derive a vector potential **A**, such that;

$$\mathbf{B} = curl\ \mathbf{A} \tag{4.7}$$

We can thence derive the complete field equations from the above. Assuming an infinitely long primary and secondary, the solutions to equations of electromagnetic field distribution for LIMs are the same as those for rotary motors with solid rotors, hence this generalized analysis takes into account linear or rotational displacement of the machine rotor.

For $\frac{\partial \mathbf{D}}{\partial t} = 0$, Maxwell equation (4.1) and (4.7) becomes;

$$curl\left(\frac{1}{\mu} curl\mathbf{A}\right) = \mathbf{J} \tag{4.8}$$

or

$$\nabla \times \left(\frac{1}{\mu}\nabla \times \mathbf{A}\right) = \mathbf{J} \tag{4.9}$$

From (4.2) and (4.6) we obtain

$$\mathbf{J} = \sigma\left(-\frac{\partial \mathbf{A}}{\partial t} - grad\omega + \mathbf{v} \times curl\mathbf{A}\right) \tag{4.10}$$

or

$$\mathbf{J} = \sigma\left(-\frac{\partial \mathbf{A}}{\partial t} - \nabla\omega + \mathbf{v} \times (\nabla \times \mathbf{A})\right) \tag{4.11}$$

Thus, from (4.9) and(4.11)

$$\nabla \times \left(\frac{1}{\mu}\nabla \times \mathbf{A}\right) = \sigma\left(-\frac{\partial \mathbf{A}}{\partial t} - \nabla\omega + \mathbf{v} \times (\nabla \times \mathbf{A})\right) \tag{4.12}$$

If μ is constant, i.e. $\mu \neq \mu(x, y, z)$, and $\nabla \cdot \mathbf{A}$ $(div\mathbf{A} = 0)$ then

$$\nabla^2 \mathbf{A} = -\mu\sigma\left(-\frac{\partial \mathbf{A}}{\partial t} - \nabla\omega + \mathbf{v} \times (\nabla \times \mathbf{A})\right) \tag{4.13}$$

For 2-D field

$$\mathbf{A} = \mathbf{1}_z A, \quad \mathbf{J} = \mathbf{1}_z J, \quad \nabla\omega = \mathbf{I}_z \frac{\partial \omega}{\partial z}, \quad \mathbf{v} \times curl\mathbf{A} = -v_x \frac{\partial A}{\partial x} - v_y \frac{\partial A}{\partial y}$$

and equation (4.12) becomes

$$\frac{\partial}{\partial x}\left(\frac{1}{\mu}\frac{\partial A}{\partial x}\right) + \frac{\partial}{\partial y}\left(\frac{1}{\mu}\frac{\partial A}{\partial y}\right) = -J_{mo} - J_{tr} - J_{out}, \tag{4.14}$$

where J_{mo} is the current density caused by motional electromotice force,

$$J_{mo} = -\sigma\left(v_x \frac{\partial A}{\partial x} + v_y \frac{\partial A}{\partial y}\right), \tag{4.15}$$

where J_{tr} is the current density caused by transformer electromotice force,

$$J_{tr} = -\sigma \frac{\partial A}{\partial t},$$

and J_{out} is the current density caused by the "outside" sources , i.e. voltage U across the conductor,

$$J_{out} = -\sigma \frac{\partial \omega}{\partial z} = \sigma \frac{U}{L}.$$

For the stator windings region, $J_{mo} = 0$ and $J = J_{tr} + J_{out}$. For the rotor region, $J_{out} = 0$ and $J = J_{tr} + J_{mo}$. Using complex variables, $v_y = 0$, $v_x = v$. In the rotor region, equation 4.14 can be replaced by

$$\frac{\partial}{\partial x}(\frac{1}{\mu}\frac{\partial \mathbf{A}}{\partial x}) + \frac{\partial}{\partial y}(\frac{1}{\mu}\frac{\partial \mathbf{A}}{\partial y}) - js\omega\sigma\mathbf{A} = 0 \tag{4.16}$$

where the over-bars indicate complex quantities and ω is the supply angular frequency.

Modifying these equations for a 2-D electromagnetic field analysis and for the shaded-pole single-sided LIM, the above equations can be simplified based on the following assumptions:

(a) LIM has finite dimensions along x, y directions but infinitely long in the z direction

(b) the relative motion of LIM components is assumed to be in the x-direction only

(c) all currents are constrained to flow in the z-direction only

Since the accuracy of a FEM depends both on the type of approximation functions used in each element[54, 108], and on the number of elements used to make up the device geometry, a high number of finite elements and high-order approximation functions were employed.

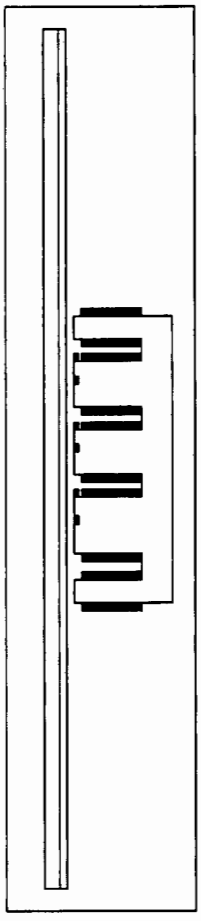

Figure 4.1: Geometric Model of shaded-pole LIM

4.2 Modelling the shade-pole LIM

Fig 4.1 shows the outline of the geometric model of the shaded-pole LIM with boundaries, using Infolytica MagNet 5 finite element analysis package[37]. The model was designed and scaled to the physical machine dimensions following the general procedure in electromagnetic field simulation, namely[54, 63];

(a) modelling

(b) selection of materials and sources

(c) mesh generation

(d) solving for field values, and

(e) using these values for other calculations, such as force, torque.

The boundary conditions are expressed by the magnetic vector potential itself. The constraints for the finite element analysis of the LIM problem is determined by Dirichlet's condition (if constant) means that the boundary is given by the highly conducting material, and Neumann's condition (if homogenous) which implies that the boundary represents a highly permeable material.

4.3 Magnetostatic Analysis

This involved measuring the magnetic flux density, B. Fig 4.2 shows the magnetic flux density distribution in the shaded-pole LIM. Practical measurements were carried out using an electronic fluxmeter and a search coil utilized for comparison and verification of the results obtained. Fig 4.3 shows the normal component of the magnetic flux density in the airgap over a pole pitch for the shaded-pole LIM, d.c. excitation ($f = 0Hz$). A comparison of results obtained from the FEM simulation and practical measurements shows a reasonable correlation.

4.4 Eddy Current (Time-harmonic) Analysis of LIM

To carry out the time harmonic field analysis of the LIM, it is important to estimate the depth of penetration and thus ascertain eddy-currents and power losses in the machine. Following[50, 99] one can distinguish

- resistance-limited state
- inductance-limited state

In the first case, eddy-currents do not affect the magnetic field and thus limited by the resistance of the LIM, while the second case is applied when eddy-currents develop in

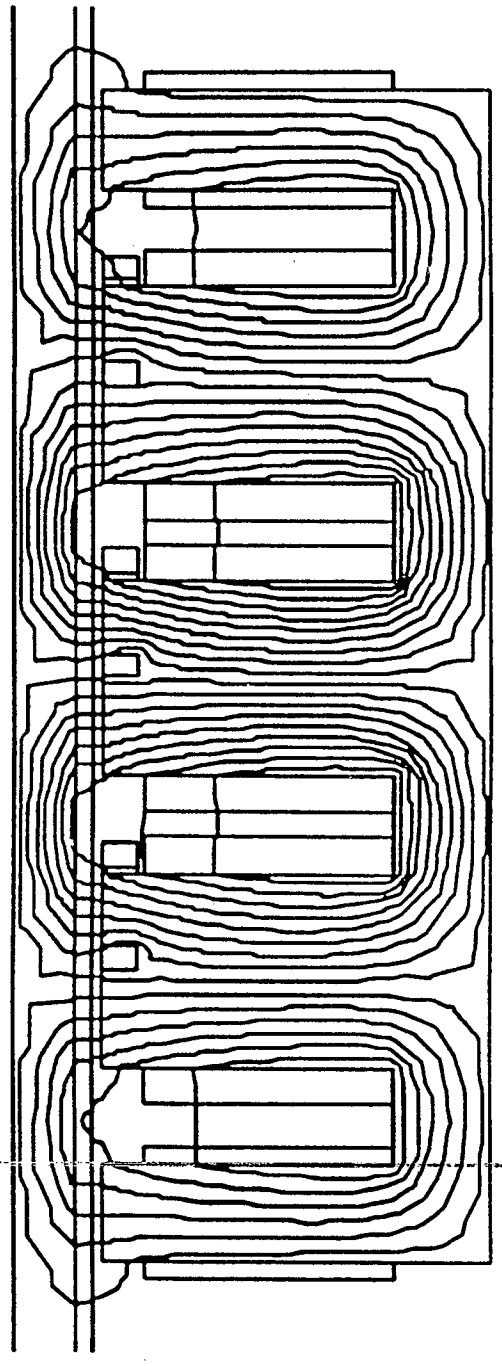

Figure 4.2: Magnetic field distribution of shaded-pole LIM

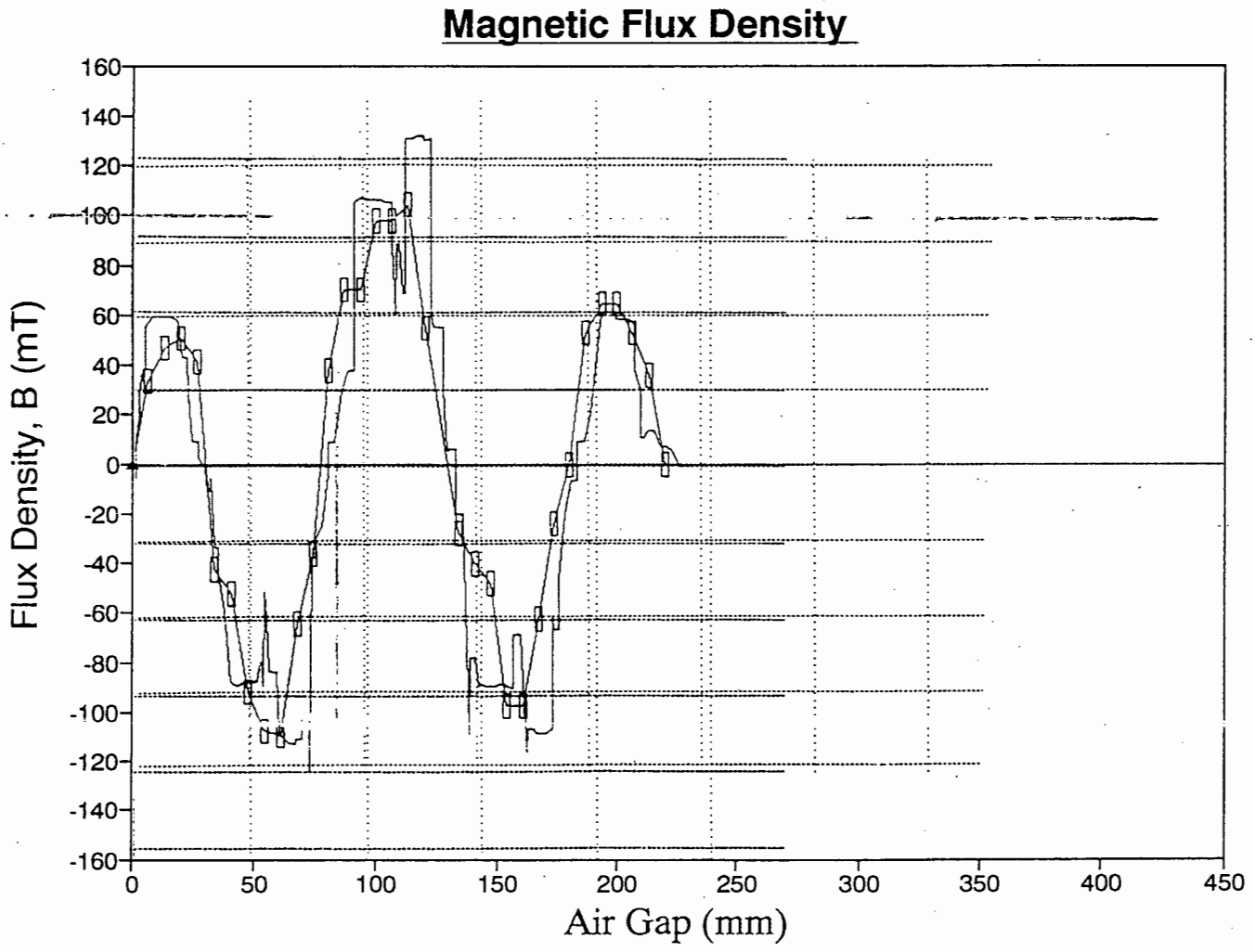

Figure 4.3: Normal component of airgap magnetic flux density at stand-still,(Magnetostatic), $V_1 = 220V$ and $f = 0Hz$: 1 - FEM computation, 2 - measurements.

the LIM until they vanish. Then the inductance limits them. The use of both states is determined by geometry of the body and parameters of the exciting field. The skin depth, δ, for quasi-stationary state is,

$$\delta = \sqrt{\frac{2}{\omega \mu \gamma s}} \tag{4.17}$$

In the resistance-limited case eddy currents do not influence the magnetic field inside the plate, thus power losses[99],

$$P_e = \frac{|\hat{H}_s|^2}{\gamma \delta} \frac{4}{3} \frac{b^3}{\delta^3} \tag{4.18}$$

for the condition $b/\delta << 1$.

In the inductance-limited case, one can assume that the magnetic field inside the plate is determined by eddy currents, hence,

$$P_e = \frac{|\hat{H}_s|^2}{\gamma \delta} \tag{4.19}$$

for the condition $b/\delta >> 1$.

If neither condition is fulfilled, then[99],

$$P_e = \frac{|\hat{H}_s|^2}{\gamma \delta} \frac{sinh(b/\delta) - sin(b/\delta)}{cosh(b/\delta) + cos(b/\delta)} \tag{4.20}$$

Since the LIM problem can be analysed as an eddy current problem[54], the steady-state characteristics, where computed, using an appropriate method for considering movement[24, 74, 23, 90] in field equations and the accuracy of the results obtained.

4.5 Comparison of FEM calculation and measurement

The steady-state characteristics, that is thrust and normal force versus speed were carried out for the shaded-pole LIM for various power frequencies from 75Hz to 40Hz. Figures 4.4-4.8 show the plot of torque against speed for various supply frequencies. For a 2-D electromagnetic field analysis, the performance calculation for the shaded-pole single-sided LIM was carried out using the FEM software package based on the Maxwell Stress method. The force in the x-direction acting on the rotating disc has been calculated using the FEM and Maxwell's stress tensor method. The forces acting on the secondary are given by the following equations:

$$F_x = \frac{y}{\mu_0} \int B_z B_x dl \tag{4.21}$$

$$F_z = \frac{y}{2\mu_0} \int [{B_z}^2 - {B_x}^2] dl \qquad (4.22)$$

where F_x, F_x are force components for an axial length y, μ_0 is the magnetic permeability of free space, B_z, B_x are the normal and tangential components of magnetic flux density in the airgap, and L_i is the effective length of the primary stack (in the z-direction). These equations are obtained by integrating the stresses over a closed surface which is entirely air. The integration over a closed surface reduces to an integral around a closed path which is around the LIM airgap region. The normal and tangential force components are thus calculated and shaft torque obtained from the expression, $T = F_x r$, where r is the radius of disc.

A comparison of measurements of magnetic flux density distribution and FEM analysis shows a very good correlation. This high accuracy in the results shows the reliability of magnetostatic analysis for static conditions using the FEM. The results of torque calculations from analytical approach (using symmetrical components) and the FEM with measurements are presented also.

4.6 Conclusions

The estimation of some machine design parameters have contributed to the deviation in the results of the analytical approach compared to measurements. The FEM results also have errors due to the limitation of using eddy current analysis for each machine condition of position, current and frequency.

This is a limitation of the Magnet 5 Finite Element package used for this analysis. More accurate results could be expected and obtained for eddy current analysis using an FEM motion-solver, since it solves for dynamic conditions, and not the step by step static solution approach inwhich some parameters are varied for each solution to the problem.

The results of steady-state characteristics shown in figs 4.4-4.7 also show the effect of asymmetricity in the analytical method when compared with measurements. Owing to the asymmetry of the magnetic circuit and elliptical rotating magnetic field, errors are introduced into the analytical solution. The results from computation do show an agreement when compared with measurements.

The application of FEM appears well justified in order to obtain not only the performance characteristics, but also to analyse and optimise the magnetic circuit of the LIM[11, 30, 3, 2]. FEM computation for standstill conditions and magnetostatic problems are generally more accurate. This will make it very useful as well in analysing linear induction machines for standstill applications[78].

Figs 4.8-4.11 shows the comparison of the classical approach, FEM and measurememts.

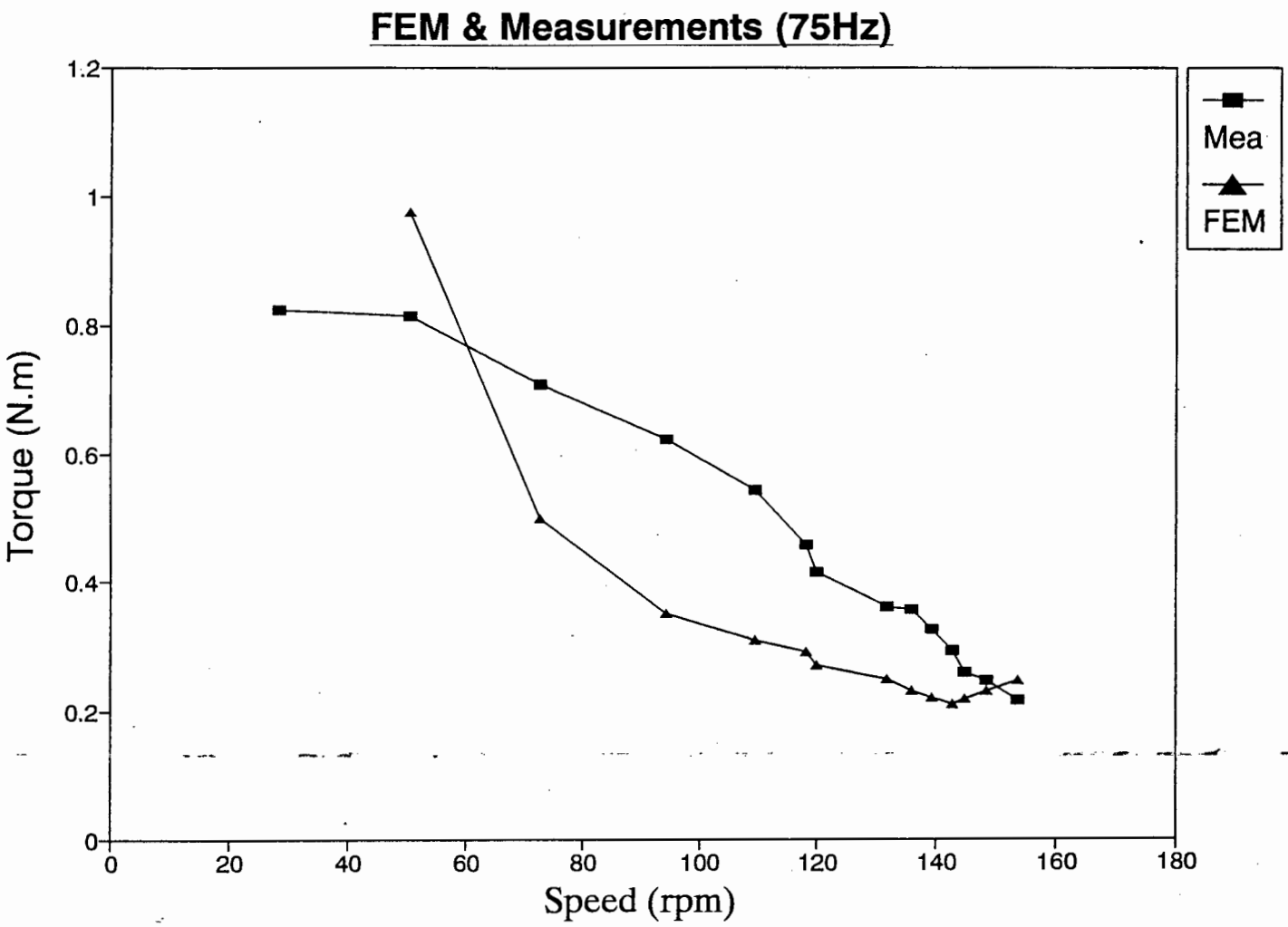

Figure 4.4: Torque against speed at $f = 75Hz$

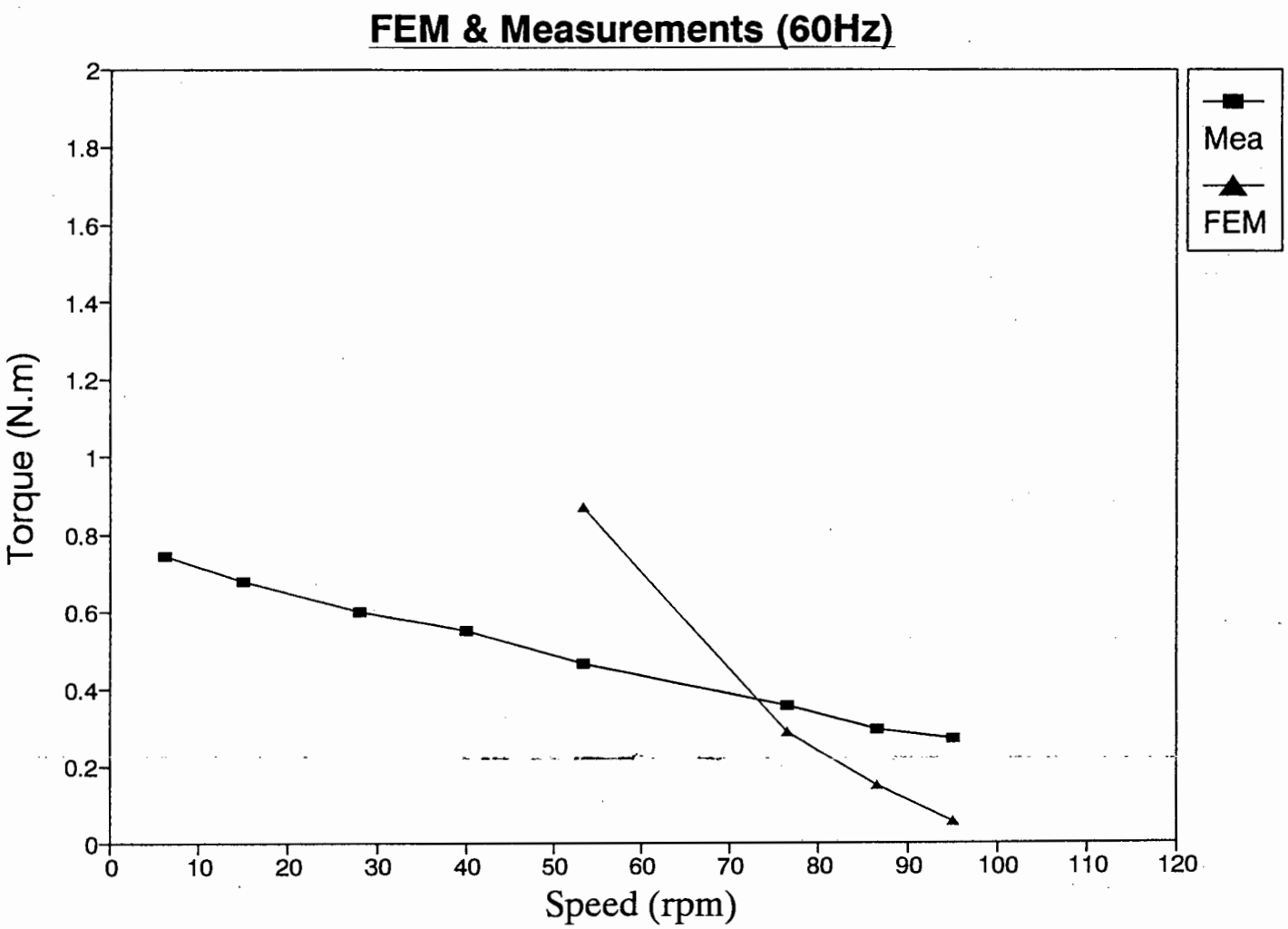

Figure 4.5: Torque against speed at $f = 60Hz$

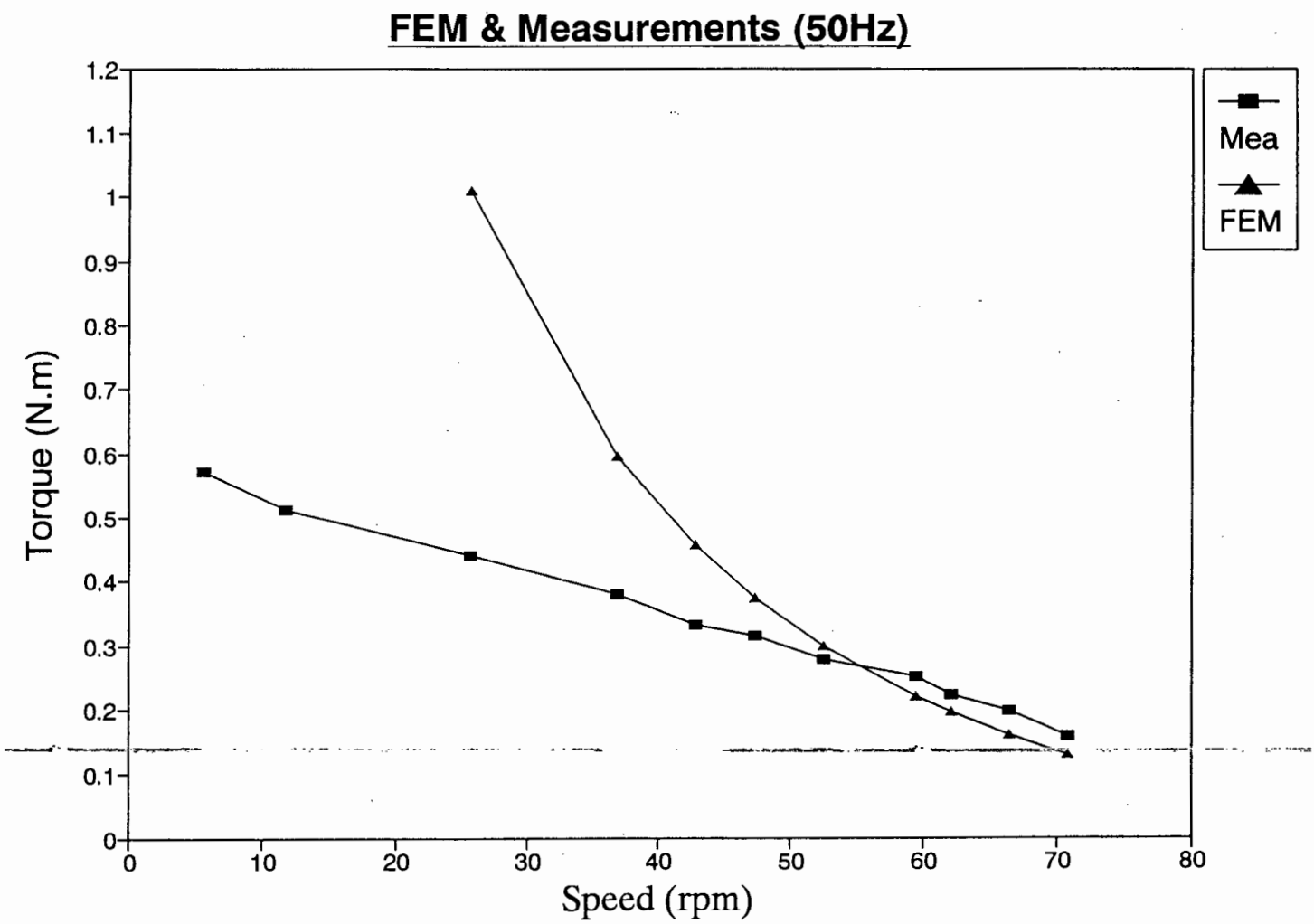

Figure 4.6: Torque against speed at $f = 50Hz$

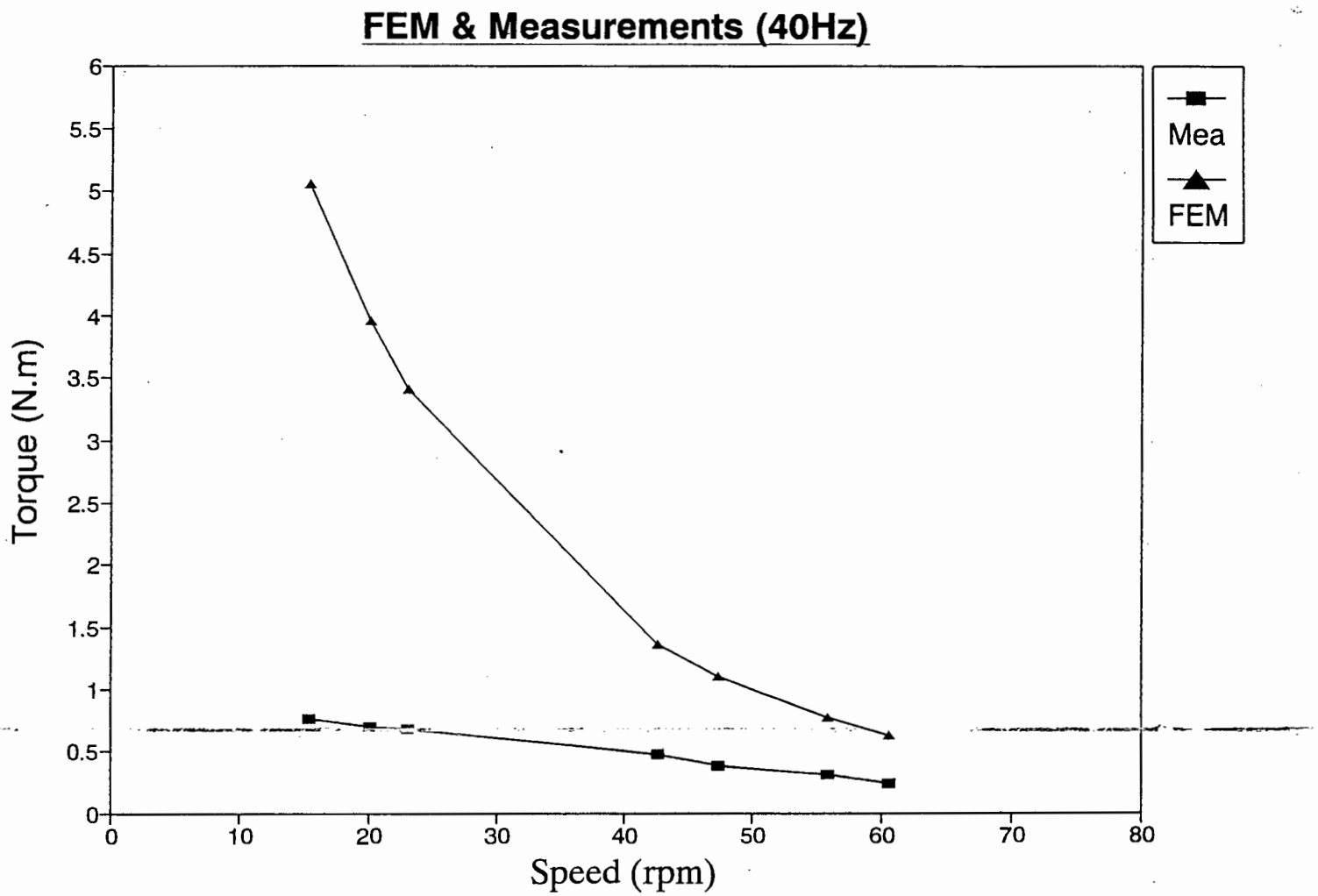

Figure 4.7: Torque against speed at $f = 40Hz$

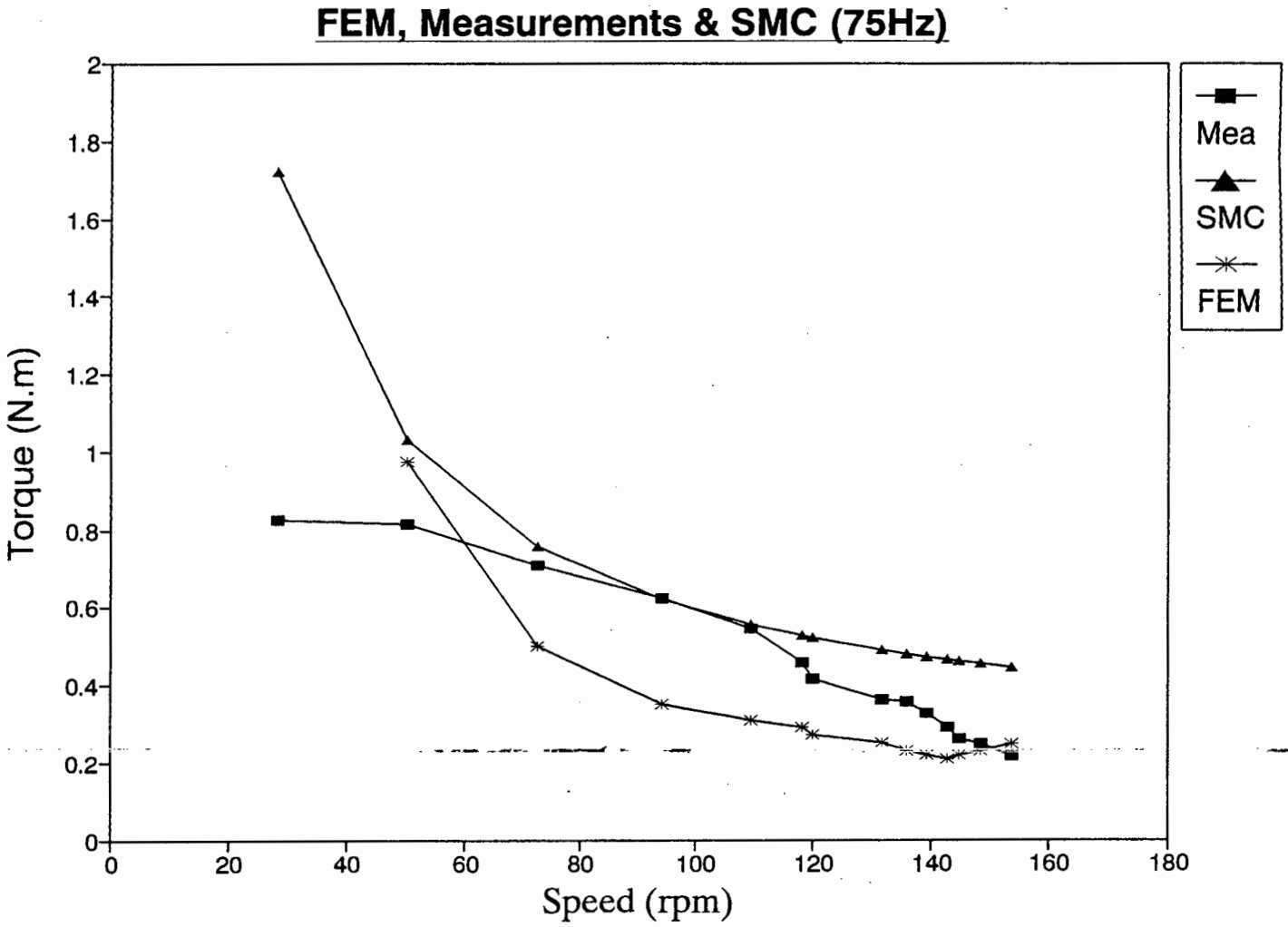

Figure 4.8: Torque against speed at $f = 75Hz$

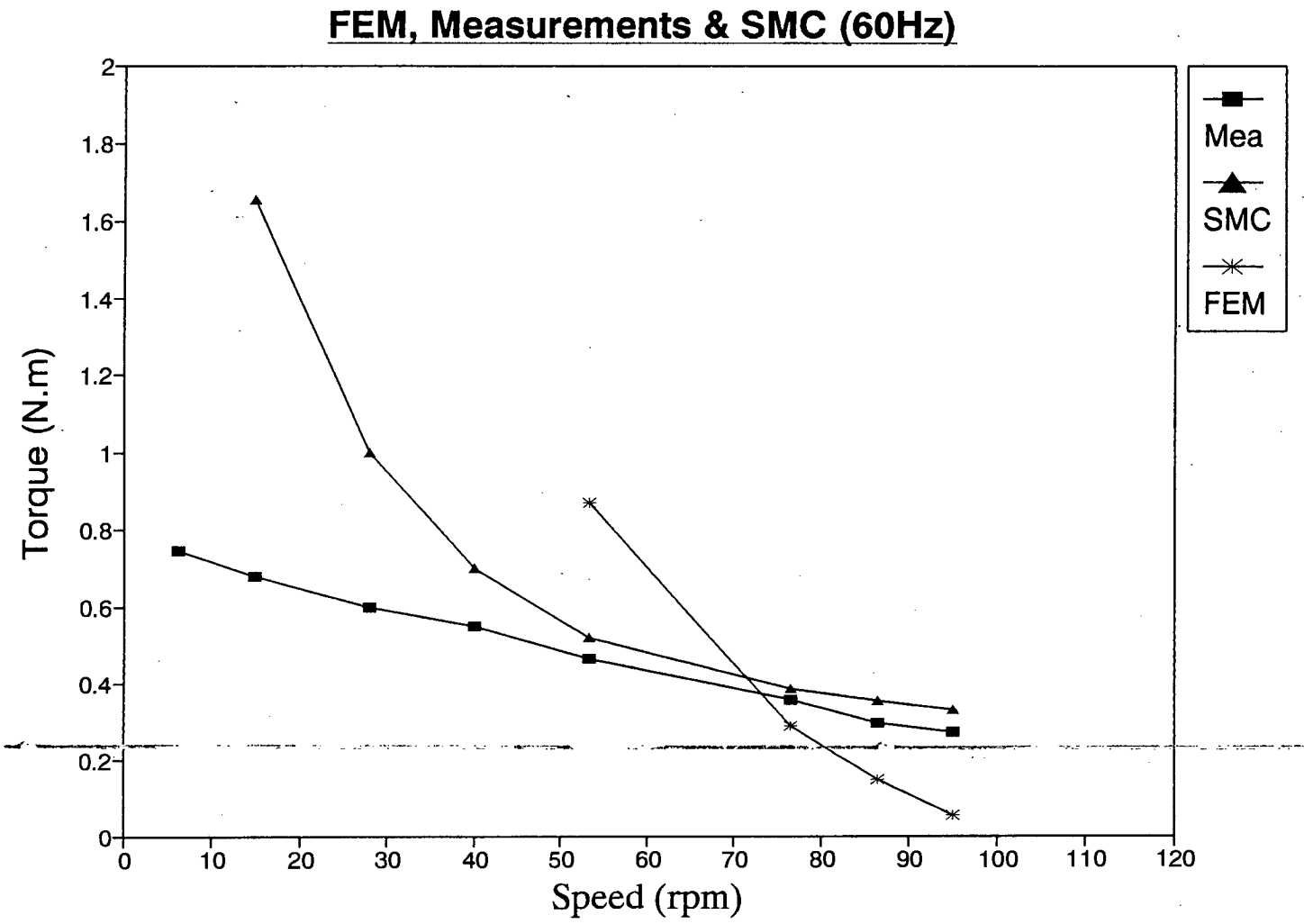

Figure 4.9: Torque against speed at $f = 60Hz$

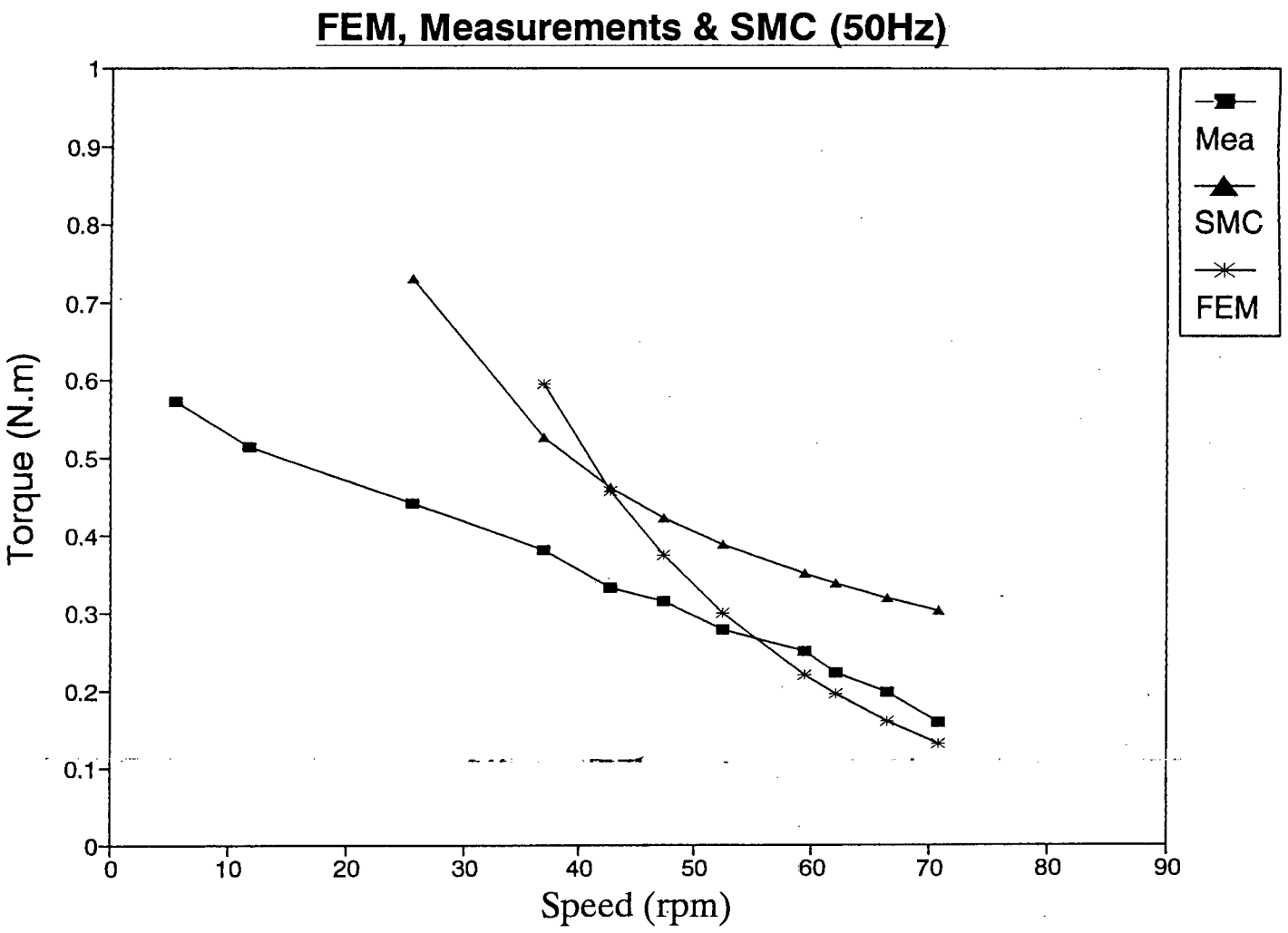

Figure 4.10: Torque against speed at $f = 50Hz$

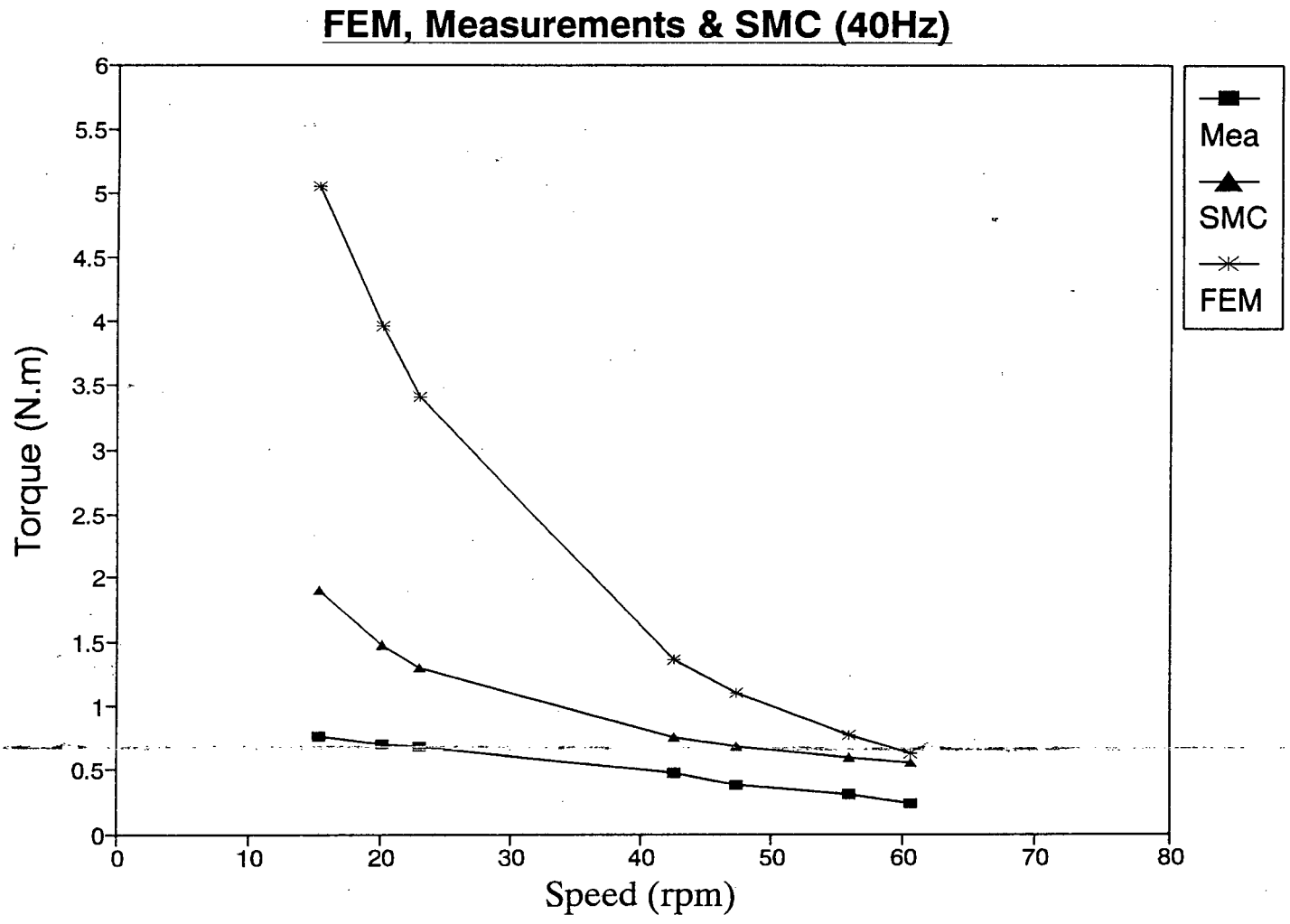

Figure 4.11: Torque against speed at $f = 40Hz$

Chapter 5

Performance Calculation Using Field Theory Approach

The electromagnetic field in the cross-section of an electric motor may be described by the non-linear Poisson equation [63, 6, 66]:

$$\frac{\partial}{\partial x}(\frac{1}{\mu}\frac{\partial \mathbf{A}}{\partial x}) + \frac{\partial}{\partial y}(\frac{1}{\mu}\frac{\partial \mathbf{A}}{\partial y}) = -\mathbf{J}(x,y) \tag{5.1}$$

5.1 Defining the LIM problem

For the single-sided LIM, assuming that all currents are constrained to flow in the z-direction only, recall equation 4.16, the 2-D electrodynamic field distribution is described by the equation[7, 8]:

$$\frac{\partial}{\partial x}(\frac{1}{\mu}\frac{\partial \mathbf{A}}{\partial x}) + \frac{\partial}{\partial y}(\frac{1}{\mu}\frac{\partial \mathbf{A}}{\partial y}) - \sigma v\frac{\partial \mathbf{A}}{\partial x} = j\omega\sigma\mathbf{A} \tag{5.2}$$

where $\mathbf{A}$ is a vector potential, $\mathbf{J}$ is the current density in the y-direction, σ is the electric conductivity, v is the speed of rotor, and $\mu = \mu_0\mu_r$ is the magnetic permeability. The x-coordinate is in the direction of motion, the y-coordinate is perpendicular to the active surfaces, and the z-coordinate is in the radial direction.

The following assumptions have been made:

(a) LIM has finite dimensions along x (pole pitch), y (normal) directions, but infinitely long in the z direction (end effects are neglected),

(b) the relative motion of the LIM secondary is assumed to be in the x-direction only,

(c) the magnetic permeability of the primary stack and secondary back iron is a non-linear function of the magnetic field intensity.

5.2 Solution of field equations

For a three-dimensional analysis of induction machine such as the single-phase single-sided shaded-pole LIM, with multilayer secondary and distributed parameters, the magnetic vector potential is used. The distribution of magnetic vector potential in an i^{th} layer is described by the equation [87, 41],

$$\nabla^2 \mathbf{A} = j\omega\mu\epsilon\mathbf{A} - \mu\epsilon v \times (\nabla \times \mathbf{A}) \tag{5.3}$$

where $\mathbf{A}$ is the magnetic vector potentiaL defined as

$$\mathbf{B} = \nabla \times \mathbf{A} \tag{5.4}$$

ϵ is the electric conductivity, v is linear velocity, and μ is magnetic permeability.

For the solution of the LIM field analysis problem using the x, y, z coordinate system, and the LIM secondary (rotor) travelling with a velocity v, (5.1) has the form,

$$\nabla^2 \mathbf{A} = j\omega s\mu\epsilon\mathbf{A} \tag{5.5}$$

where s is the slip for fundamental harmonic.

The scalar differential equations for ν^{th} space harmonics of three-dimensional distribution of the electromagnetic field in the i^{th} isotropic layer are:

$$\frac{\partial^2 \mathbf{F}_{x\nu i}}{\partial x^2} + \frac{\partial^2 \mathbf{F}_{x\nu i}}{\partial y^2} + \frac{\partial^2 \mathbf{F}_{x\nu i}}{\partial z^2} = \alpha_{\nu i}^2 \mathbf{F}_{x\nu i} \tag{5.6}$$

$$\frac{\partial^2 \mathbf{F}_{y\nu i}}{\partial x^2} + \frac{\partial^2 \mathbf{F}_{y\nu i}}{\partial y^2} + \frac{\partial^2 \mathbf{F}_{y\nu i}}{\partial z^2} = \alpha_{\nu i}^2 \mathbf{F}_{y\nu i} \tag{5.7}$$

$\mathbf{F}_{m\nu i}$ is a general symbol for the x y, or z components of the magnitudes of the νth space harmonics of the magnetic field intensity $\mathbf{H}_{m\nu i}$, electric field intensity $\mathbf{E}_{m\nu i}$, or magnetic vector potential $\mathbf{A}_{m\nu i}$ in an i^{th} layer.

5.3 Electromagnetic field equations

The general solutions of equations for electromagnetic field distribution in an induction machine with salient poles, gives the following recurrence relations[41, 10, 40, 9, 46, 42]:

For $0 \leq z \leq d_k$,

$$H_{xk}^{(k)} = \sum_{\nu=1}^{\infty} \sum_{n=1}^{\infty} \frac{1}{M_k^{(k)}} [\frac{1}{\chi_k} H_{xk-1}^{(k-1)}(x, y, 0) \cosh \chi_k (z - d_k) +$$

$$\frac{1}{j\omega_{k-1}\mu_{k-1}}\frac{\mu_{k-1}}{\mu_k}E_{yk-1}^{k-1}(x,y,0)\sinh\chi_k(z-d_k)]\times\frac{\mu_1}{\mu_k}\frac{\chi_k}{\chi_1}H_{x1}^{(1)} \tag{5.8}$$

$$H_{zk}^{(k)}=\sum_{\nu=1}^{\infty}\sum_{n=1}^{\infty}\frac{1}{M_k^{(k)}}\{\frac{1}{\chi_k}[-H_{xk-1}^{(k-1)}(x,y,0)]\sinh\chi_k(z-d_k)+$$

$$\frac{1}{j\omega_k\mu_{k-1}}\frac{\mu_{k-1}}{\mu_k}[-E_{yk-1}^{k-1}(x,y,0)]\cosh\chi_k(z-d_k)\}\times\frac{\mu_1}{\mu_k}H_{z1}^{(1)} \tag{5.9}$$

$$E_{yk}^{(k)}=\sum_{\nu=1}^{\infty}\sum_{n=1}^{\infty}\frac{1}{M_k^{(k)}}\{\frac{1}{\chi_k}[-H_{xk-1}^{(k-1)}(x,y,0)]\sinh\chi_k(z-d_k)+$$

$$\frac{1}{j\omega_{k-1}\mu_{k-1}}\frac{\mu_{k-1}}{\mu_k}[-E_{yk-1}^{k-1}(x,y,0)]\cosh\chi_k(z-d_k)\}\times\frac{\omega_k}{\omega_1}E_{y1}^{(1)} \tag{5.10}$$

For the fundamental harmonic, $\nu=1$, the equations for the respective layers for i=1,2,3 and 4, where 1 is air halfspace, 2 is back iron, 3 is aluminium, and 4 is the airgap, are given as,

for air halfspace, $i=1$, $-\infty\le z\le 0$,

$$H_{z1}^{(1)-}=\frac{1}{\mu_0}\mathbf{B}^{-}\mathbf{b}_\nu e^{j\beta x}e^{-\chi_1^{-}z} \tag{5.11}$$

$$H_{z1}^{(1)+}=\frac{1}{\mu_0}\mathbf{B}^{+}\mathbf{b}_\nu e^{-j\beta x}e^{-\chi_1^{+}z} \tag{5.12}$$

$$H_{x1}^{(1)-}=-j\frac{\beta}{\alpha_p^2}\frac{1}{\mu_0}\chi_1^{-}\mathbf{B}^{-}\mathbf{b}_\nu e^{j\beta x}e^{-\chi_1^{-}z} \tag{5.13}$$

$$H_{x1}^{(1)+}=j\frac{\beta}{\alpha_p^2}\frac{1}{\mu_0}\chi_1^{+}\mathbf{B}^{+}\mathbf{b}_\nu e^{-j\beta x}e^{-\chi_1^{+}z} \tag{5.14}$$

$$E_{y1}^{(1)-}=(j\omega_1^{-})j\frac{\beta}{\alpha_p^2}\mathbf{B}^{-}\mathbf{b}_\nu e^{j\beta x}e^{-\chi_1^{-}z} \tag{5.15}$$

$$E_{y1}^{(1)+}=(-j\omega_1^{+})j\frac{\beta}{\alpha_p^2}\mathbf{B}^{+}\mathbf{b}_\nu e^{-j\beta x}e^{-\chi_1^{+}z} \tag{5.16}$$

where $\beta=\pi/\tau$, $\omega=\omega_{s\nu=1}^{+}=2\pi fs$, and $\omega_{s\nu=1}^{-}=2\pi f(2-s)$, that is, $\omega_1=\omega_2=\omega_3=\omega_4$.

for back iron layer, $i=2$, $0\le z\le H_{sec}$,

$$H_{x2}^{(2)}=\sum_{\nu=1}^{\infty}\sum_{n=1}^{\infty}\frac{1}{M_2^{(2)}}[\frac{1}{\chi_2}H_{x1}^{(1)}(x,y,0)\cosh\chi_2(z-d_2)+$$

$$\frac{1}{j\omega_1\mu_1}\frac{\mu_1}{\mu_2}E^1_{y1}(x,y,0)\sinh\chi_2(z-d_2)] \times \frac{\mu_1}{\mu_2}\frac{\chi_2}{\chi_1}H^{(1)}_{x1} \tag{5.17}$$

$$H^{(2)}_{z2} = \sum_{\nu=1}^{\infty}\sum_{n=1}^{\infty}\frac{1}{M^{(2)}_2}\{\frac{1}{\chi_2}[-H^{(1)}_{x1}(x,y,0)]\sinh\chi_2(z-d_2) +$$

$$\frac{1}{j\omega_2\mu_1}\frac{\mu_1}{\mu_2}[-E^1_{y1}(x,y,0)]\cosh\chi_2(z-d_2)\} \times \frac{\mu_1}{\mu_2}H^{(1)}_{z1} \tag{5.18}$$

$$E^{(2)}_{y2} = \sum_{\nu=1}^{\infty}\sum_{n=1}^{\infty}\frac{1}{M^{(2)}_2}\{\frac{1}{\chi_2}[-H^{(1)}_{x1}(x,y,0)]\sinh\chi_2(z-d_2) +$$

$$\frac{1}{j\omega_1\mu_1}\frac{\mu_1}{\mu_2}[-E^1_{y1}(x,y,0)]\cosh\chi_2(z-d_2)\} \times \frac{\omega_2}{\omega_1}E^{(1)}_{y1} \tag{5.19}$$

$$M^{(2)}_2 = \frac{1}{\chi_2}H^{(1)}_{x1}\sinh(\chi_2 d_2) + \frac{1}{j\omega_1\mu_1}\frac{\mu_1}{\mu_2} \times E^{(1)}_{y1}\cosh(\chi_2 d_2) \tag{5.20}$$

for aluminium cap layer, $i = 3$, $H_{sec} \le z \le H_{sec} + d$,

$$H^{(3)}_{x3} = \sum_{\nu=1}^{\infty}\sum_{n=1}^{\infty}\frac{1}{M^{(3)}_3}[\frac{1}{\chi_3}H^{(2)}_{x2}(x,y,0)\cosh\chi_k(z-d_3) +$$

$$\frac{1}{j\omega_2\mu_2}\frac{\mu_2}{\mu_3}E^2_{y2}(x,y,0)\sinh\chi_3(z-d_3)] \times \frac{\mu_1}{\mu_3}\frac{\chi_3}{\chi_1}H^{(1)}_{x1} \tag{5.21}$$

$$H^{(3)}_{z3} = \sum_{\nu=1}^{\infty}\sum_{n=1}^{\infty}\frac{1}{M^{(3)}_3}\{\frac{1}{\chi_3}[-H^{(2)}_{x2}(x,y,0)]\sinh\chi_3(z-d_3) +$$

$$\frac{1}{j\omega_3\mu_2}\frac{\mu_2}{\mu_3}[-E^2_{y2}(x,y,0)]\cosh\chi_3(z-d_3)\} \times \frac{\mu_1}{\mu_3}H^{(1)}_{z1} \tag{5.22}$$

$$E^{(3)}_{y3} = \sum_{\nu=1}^{\infty}\sum_{n=1}^{\infty}\frac{1}{M^{(3)}_3}\{\frac{1}{\chi_3}[-H^{(2)}_{x2}(x,y,0)]\sinh\chi_3(z-d_3) +$$

$$\frac{1}{j\omega_2\mu_2}\frac{\mu_2}{\mu_3}[-E^2_{y2}(x,y,0)]\cosh\chi_3(z-d_3)\} \times \frac{\omega_3}{\omega_1}E^{(1)}_{y1} \tag{5.23}$$

$$M^{(3)}_3 = \frac{1}{\chi_3}H^{(2)}_{x2}\sinh(\chi_3 d_3) + \frac{1}{j\omega_2\mu_2}\frac{\mu_2}{\mu_3} \times E^{(2)}_{y2}\cosh(\chi_3 d_3) \tag{5.24}$$

for airgap, $i = 4$, $H_{sec} + d \le z \le H_{sec} + d + g$,

$$H_{x4}^{(4)} = \sum_{\nu=1}^{\infty}\sum_{n=1}^{\infty}\frac{1}{M_4^{(4)}}[\frac{1}{\chi_4}H_{x3}^{(3)}(x,y,0)\cosh\chi_4(z-d_4) +$$

$$\frac{1}{j\omega_3\mu_3}\frac{\mu_3}{\mu_4}E_{y3}^{3}(x,y,0)\sinh\chi_4(z-d_4)] \times \frac{\mu_1}{\mu_4}\frac{\chi_4}{\chi_1}H_{x1}^{(1)} \tag{5.25}$$

$$H_{z4}^{(4)} = \sum_{\nu=1}^{\infty}\sum_{n=1}^{\infty}\frac{1}{M_4^{(4)}}\{\frac{1}{\chi_4}[-H_{x3}^{(3)}(x,y,0)]\sinh\chi_4(z-d_4) +$$

$$\frac{1}{j\omega_4\mu_3}\frac{\mu_3}{\mu_4}[-E_{y3}^{3}(x,y,0)]\cosh\chi_4(z-d_4)\} \times \frac{\mu_1}{\mu_4}H_{z1}^{(1)} \tag{5.26}$$

$$E_{y4}^{(4)} = \sum_{\nu=1}^{\infty}\sum_{n=1}^{\infty}\frac{1}{M_4^{(4)}}\{\frac{1}{\chi_4}[-H_{x3}^{(3)}(x,y,0)]\sinh\chi_k(z-d_4) +$$

$$\frac{1}{j\omega_3\mu_3}\frac{\mu_3}{\mu_4}[-E_{y3}^{3}(x,y,0)]\cosh\chi_4(z-d_4)\} \times \frac{\omega_4}{\omega_1}E_{y1}^{(1)} \tag{5.27}$$

$$M_4^{(4)} = \frac{1}{\chi_4}H_{x3}^{(3)}\sinh(\chi_4 d_4) + \frac{1}{j\omega_3\mu_3}\frac{\mu_3}{\mu_4} \times E_{y3}^{(3)}\cosh(\chi_4 d_4) \tag{5.28}$$

5.4 Calculation of forces using Maxwell's stress tensor method

Using the definition of Maxwell's stress tensor, the total electromagnetic force or torque can be determined by the line integral along a closed path l. An expression can be derived for the force in the x-direction acting on the rotating disc using the Maxwell's stress tensor method. The forces acting on the secondary are given by:

$$F_x = -\frac{1}{2\mu_0}\Re[\mathbf{B}_z\mathbf{B}_x^*](2p\tau L_i) \tag{5.29}$$

$$F_z = \frac{1}{2\mu_0}\Re[\frac{1}{2}\mathbf{B}_{mz}\mathbf{B}_{mz}^* - \frac{1}{2}\mathbf{B}_{mx}\mathbf{B}_{mx}^*](2p\tau L_i) \tag{5.30}$$

where μ_0 is the magnetic peameability of free space, $\mathbf{B}_y$, $\mathbf{B}_x$ are the normal and tangential components of magnetic flux density in the airgap, and L_i is the effective length of the primary stack (in the z-direction). The shaft torque is obtained from the expression, $T = F_x r$, where r is the radius of disc.

In three dimension, the approach is to calculate the force per unit area of the secondary active surface using Maxwell's stress tensor. For a flat LIM the final equations expressing unit forces in N/m^2 are given as[45],

in the x direction:

$$f_x = -0.5\mu_0 \sum_{\nu=1}^{\infty} \Re e[\mathbf{H}_{mz\nu i}\mathbf{H}^*_{mx\nu i}] \tag{5.31}$$

in the y direction:

$$f_y = 0.5\mu_0 \sum_{\nu=1}^{\infty} \Re e[\mathbf{H}_{mz\nu i}\mathbf{H}^*_{my\nu i}] \tag{5.32}$$

in the z direction:

$$f_z = 0.5\mu_0 \sum_{\nu=1}^{\infty} \Re e[0.5\mathbf{H}_{mz\nu i}\mathbf{H}^*_{mz\nu i} - 0.5\mathbf{H}_{mx\nu i}\mathbf{H}^*_{mx\nu i} - 0.5\mathbf{H}_{my\nu i}\mathbf{H}^*_{my\nu i}] \tag{5.33}$$

where $\mathbf{H}_{mx\nu i}$, $\mathbf{H}_{my\nu i}$, $\mathbf{H}_{mz\nu i}$ are magnetic components of the field distribution at the secondary active surface and $\mathbf{H}^*_{mx\nu i}$, $\mathbf{H}^*_{my\nu i}$, $\mathbf{H}^*_{mz\nu i}$ are their conjugates.

5.5 Field analysis software program

A software program was developed for the field analysis of the single-phase single-sided shaded-pole linear induction motor using the Fortran Language. Fig 5.1 shows the flow chart of the software program. The field approach was used in the calculation of the normal and tangential forces. The torque was then calculated for the shaded-pole LIM. Results obtained from similation were also compared with measurements.

5.6 Comparison of analytical approach with FEM

Figs 5.2-5.5 show results of torque against linear velocity for some power frequencies using the field approach. The steady-state characteristics, that is thrust and normal force versus speed were carried out for the shaded-pole LIM for similar power frequencies from 75Hz to 40Hz. For the flat LIM the unit forces given in N/m^2 and acting on the secondary are given by equations 5.31-5.33. These were computed using the field theory program.

5.7 Conclusions

A comparison of the of the field theory approach for the salient pole machine with the FEM and the classical method is shown in figs 7.1-7.4. The solution of Maxwell's equations for air gap which produces a three-dimensional solution is applicable to all machines with an open airgap. The analytical solution obtained in the X-, Y- and Z- components using the Laplace transformation, ordinary differential equation method and Fourier transformation

respectively[112, 41] provides general solutions. These solutions are limited in their flexibilibility in being adapted to special electromagnetic and electromechanical devices. For simplicity, the two dimensional solution was applied in the field theory approach here for calculating the thrust of the LIM (both normal and tangential forces) and consequently the torque. The two-dimensional solution takes into account the field variation of the air gap both in the direction of the motor motion and the direction perpendicular to it.

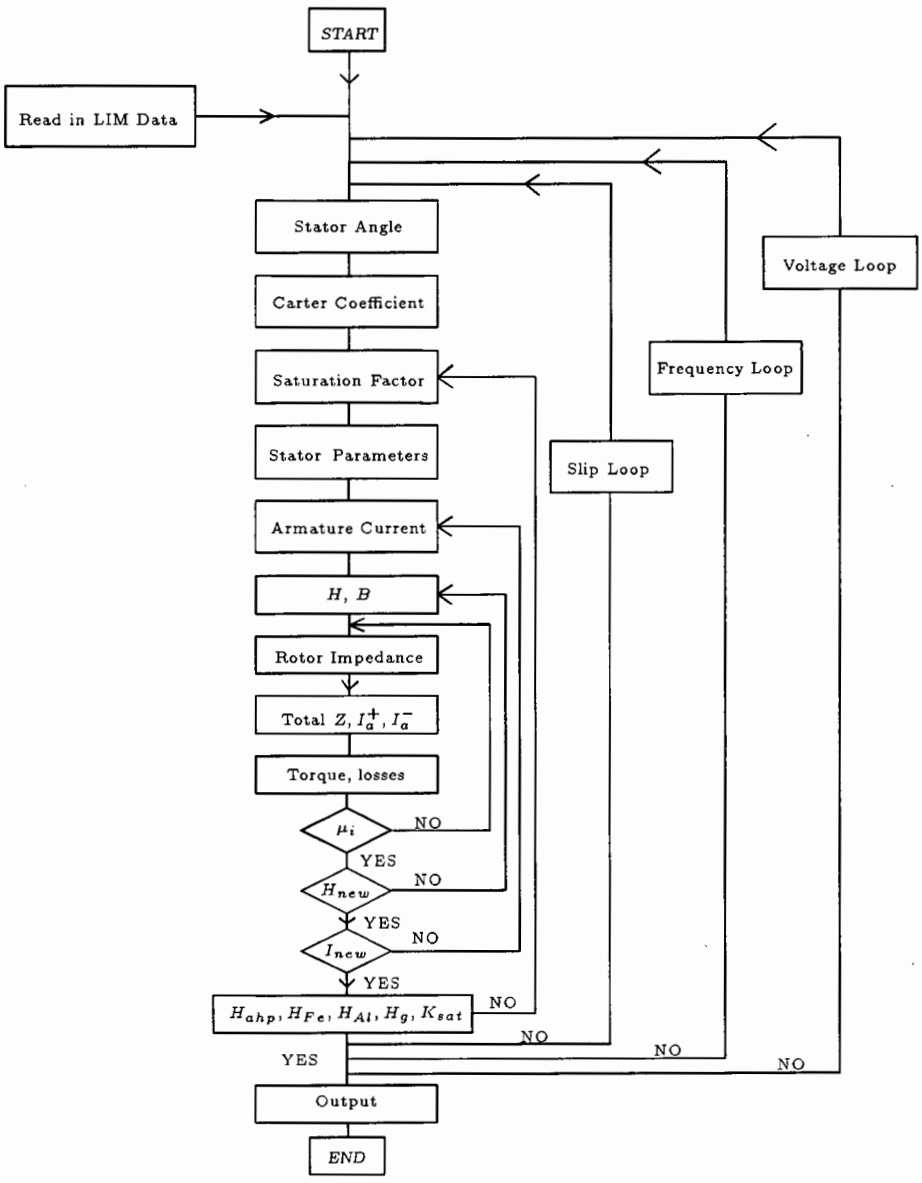

Figure 5.1: Flow-Chart of Shaded-pole LIM using Field Theory

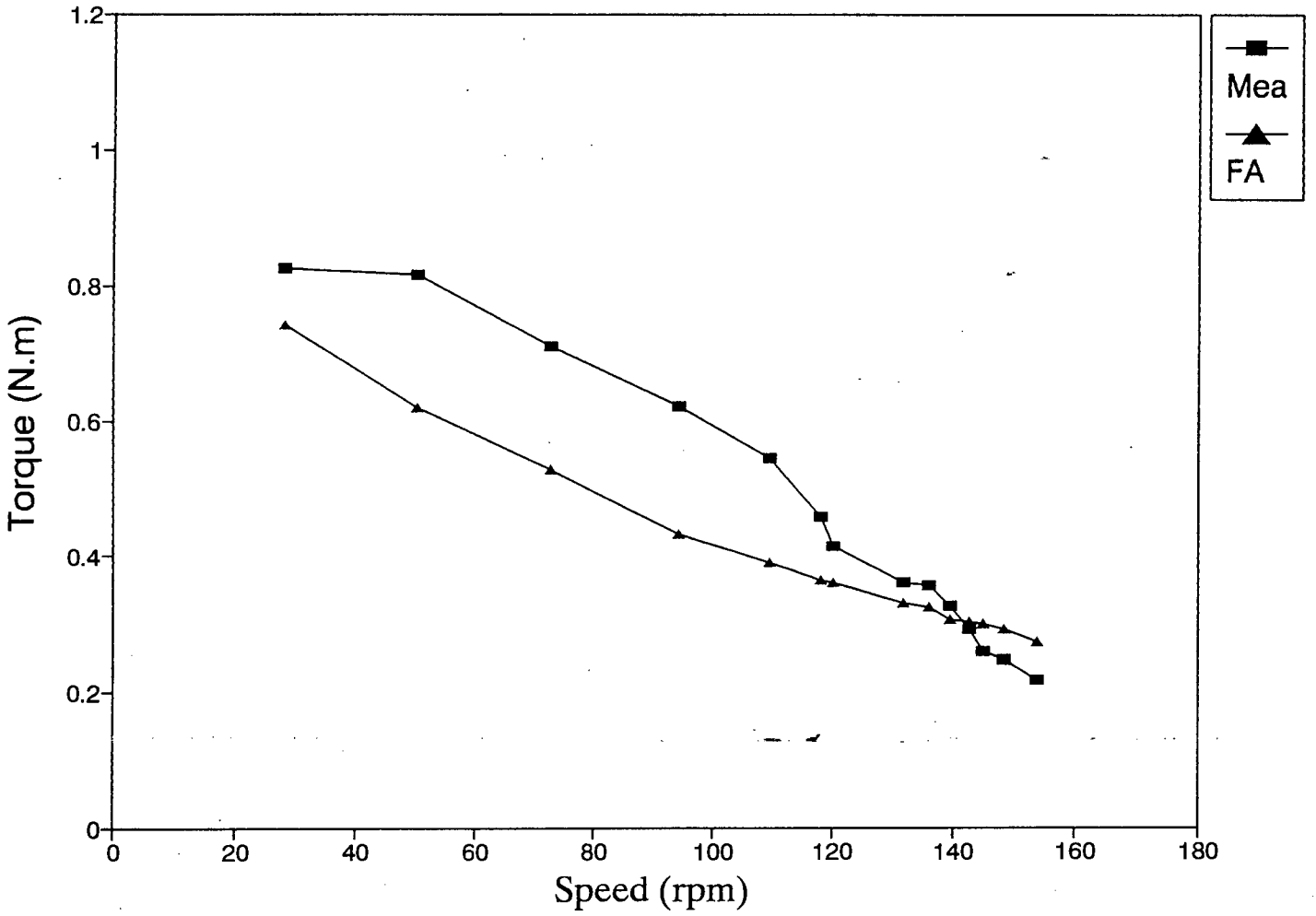

Figure 5.2: Torque against speed at $f = 75Hz$

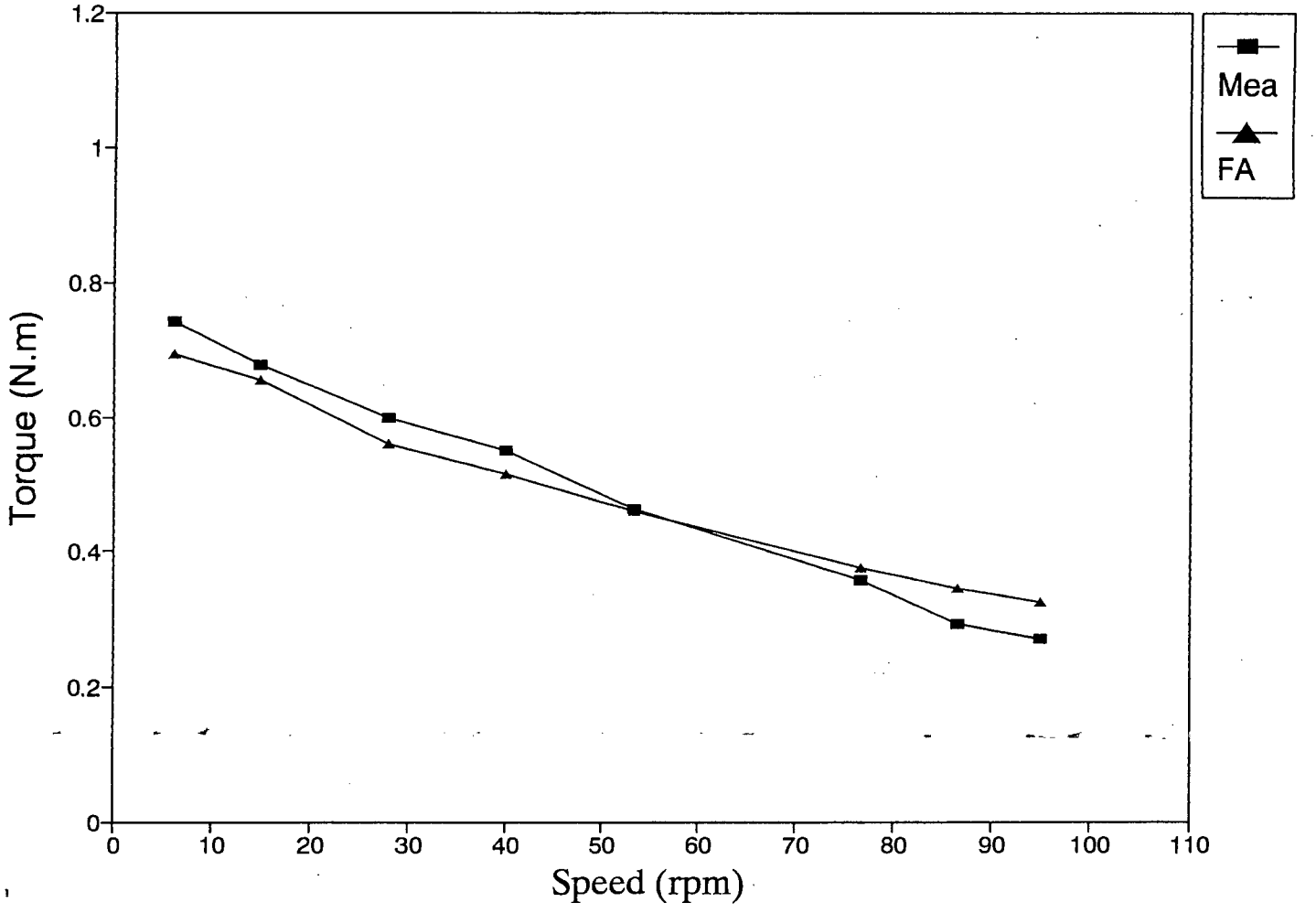

Figure 5.3: Torque against speed at $f = 60Hz$

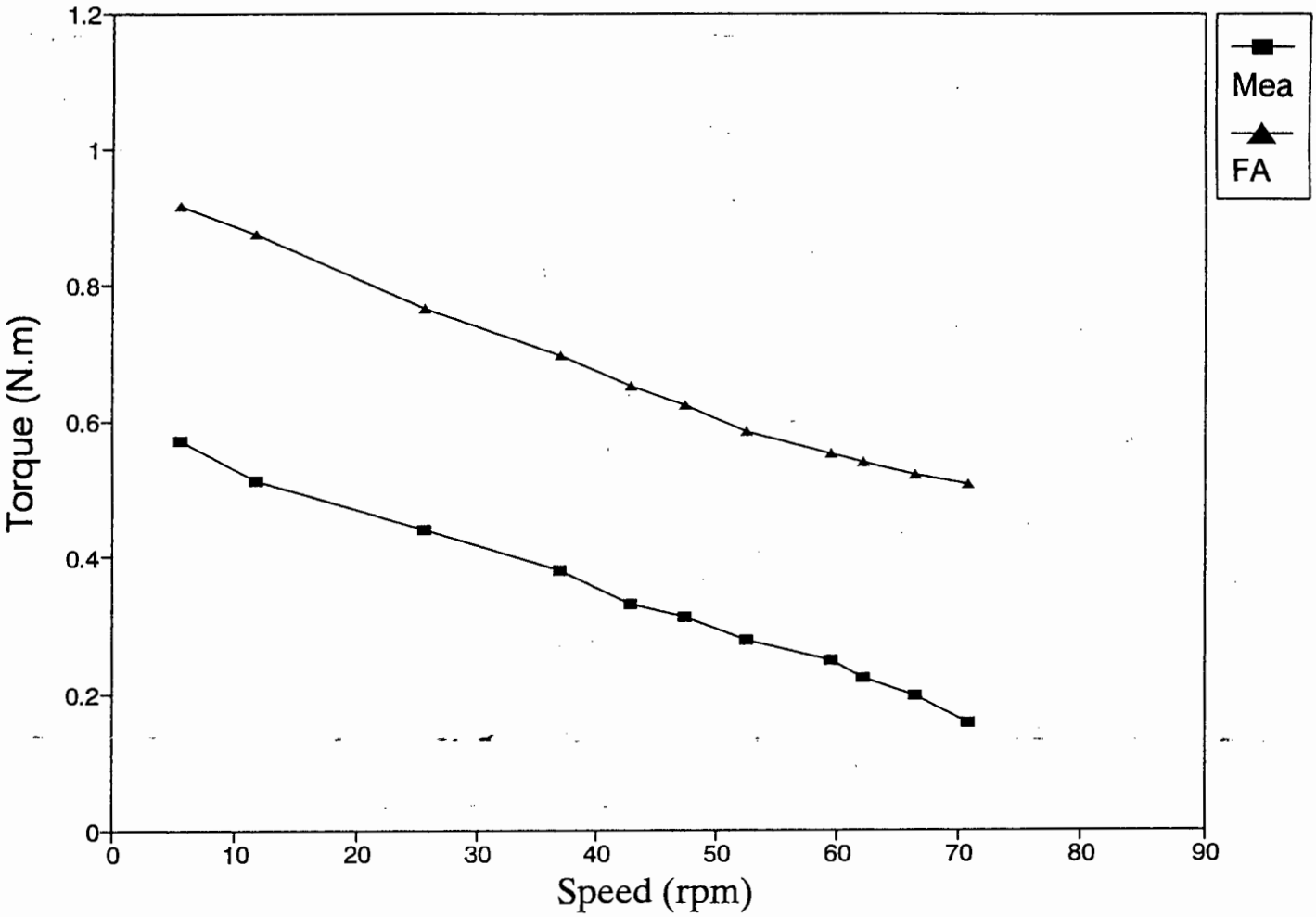

Figure 5.4: Torque against speed at $f = 50Hz$

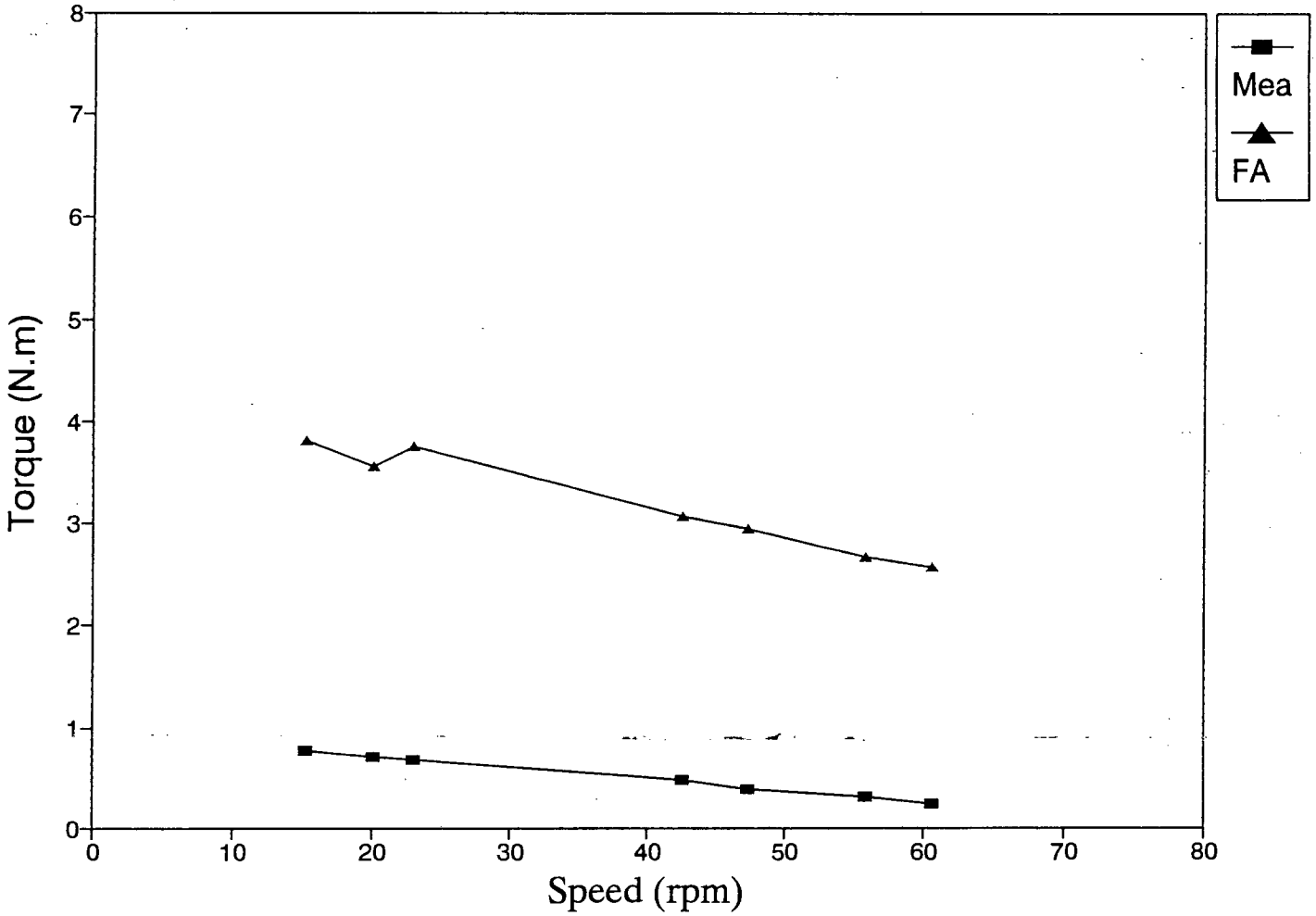

Figure 5.5: Torque against speed at $f = 40Hz$

Chapter 6

Experimental Tests Using Sinusoidal Excitation

Experimental tests were carried out on the shaded-pole LIM under three categories of investigation. Sinusoidal excitation was used for all these measurements.

(a) - Testing at rated voltage and frequency.
   i. No-Load Test
   ii. Load Test
   iii. Short Circuit (Locked-rotor) Test

(b) - Testing for optimum performance (V/f $\approx$ constant).
   i. No-Load
   ii. Load Test

6.1 Testing at rated voltage and frequency

The first set of experimental tests were carried out on the shaded-pole LIM using sinusoidal excitation at rated voltage of 220V taken from the mains terminal at a supply frequency of 50Hz. Results for the no-load test, load test and locked rotor tests are presented.

6.1.1 No-Load Test of LIM at rated voltage and frequency

The no-load characteristics, that is, the input current, input power and power factor were obtained for the LIM at these frequencies. Results obtained from measurements were plotted to show the trend for increasing supply frequency.

Figs 6.1-6.3 show the curves for no-load test results for input current, power factor and input power against input voltage. These curves show graphically the performance of the LIM at no-load.

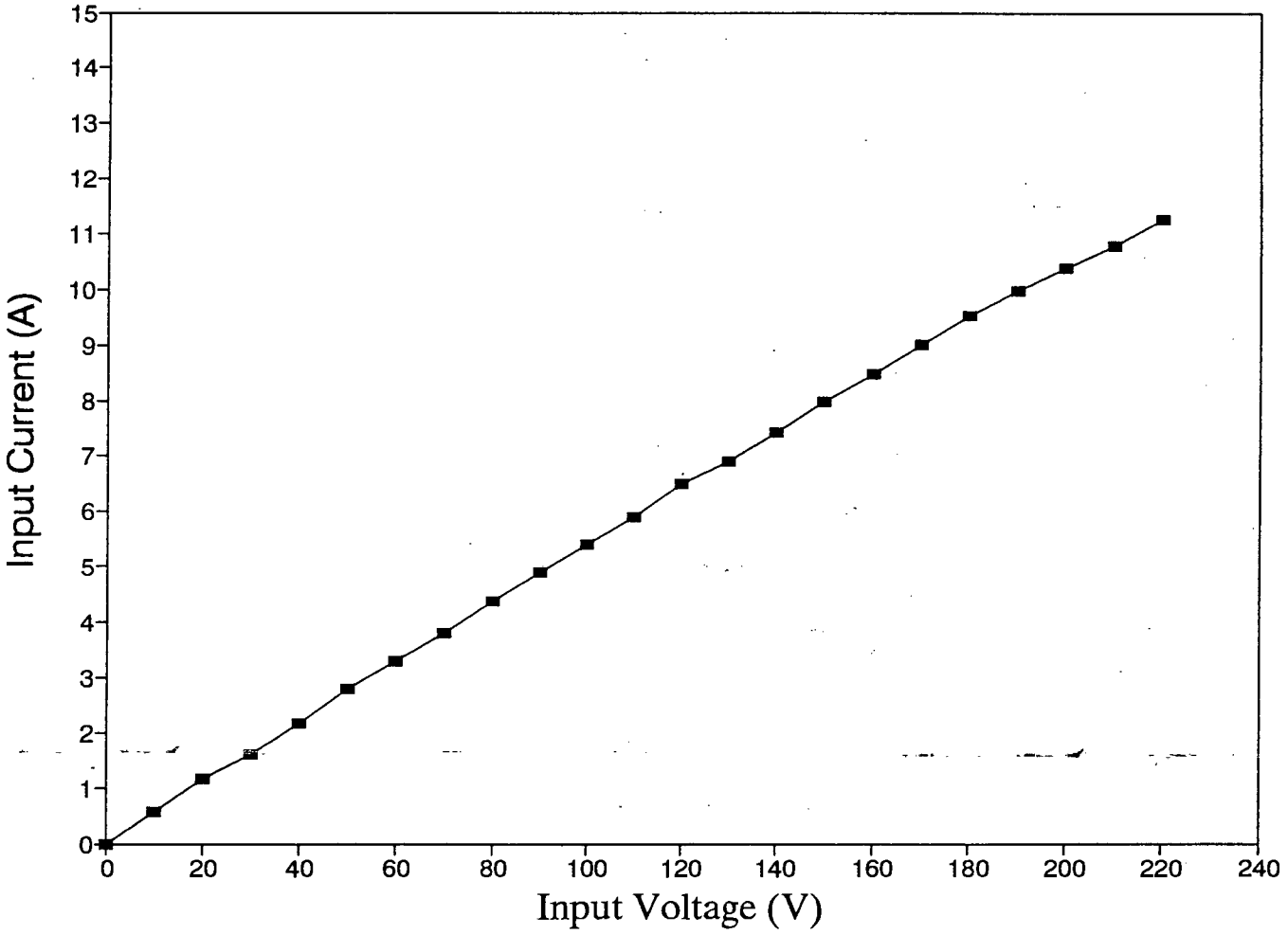

Figure 6.1: Shaded-pole LIM, Voltage Vs Input Current.

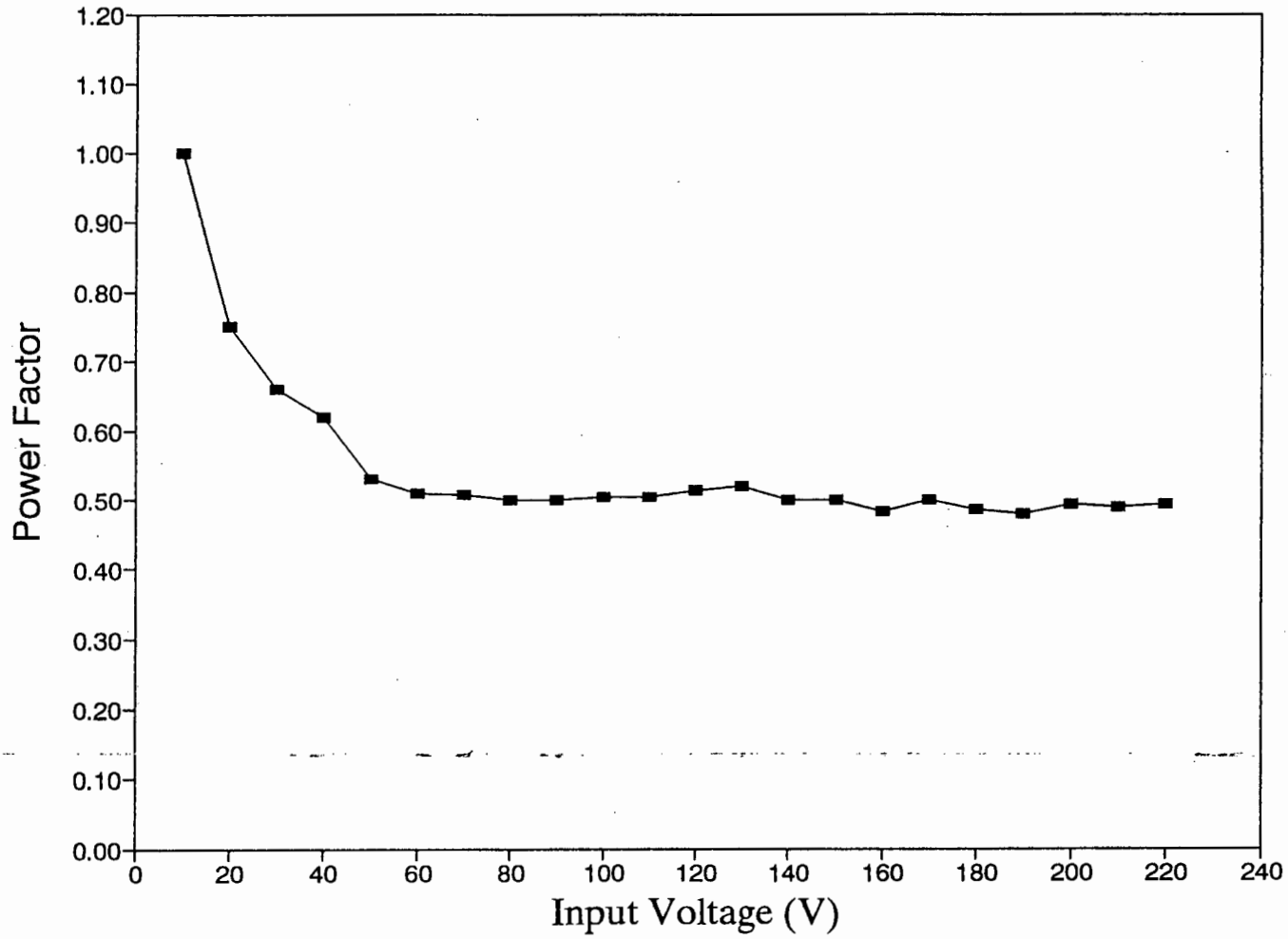

Figure 6.2: Shaded-pole LIM, Voltage Vs Power Factor.

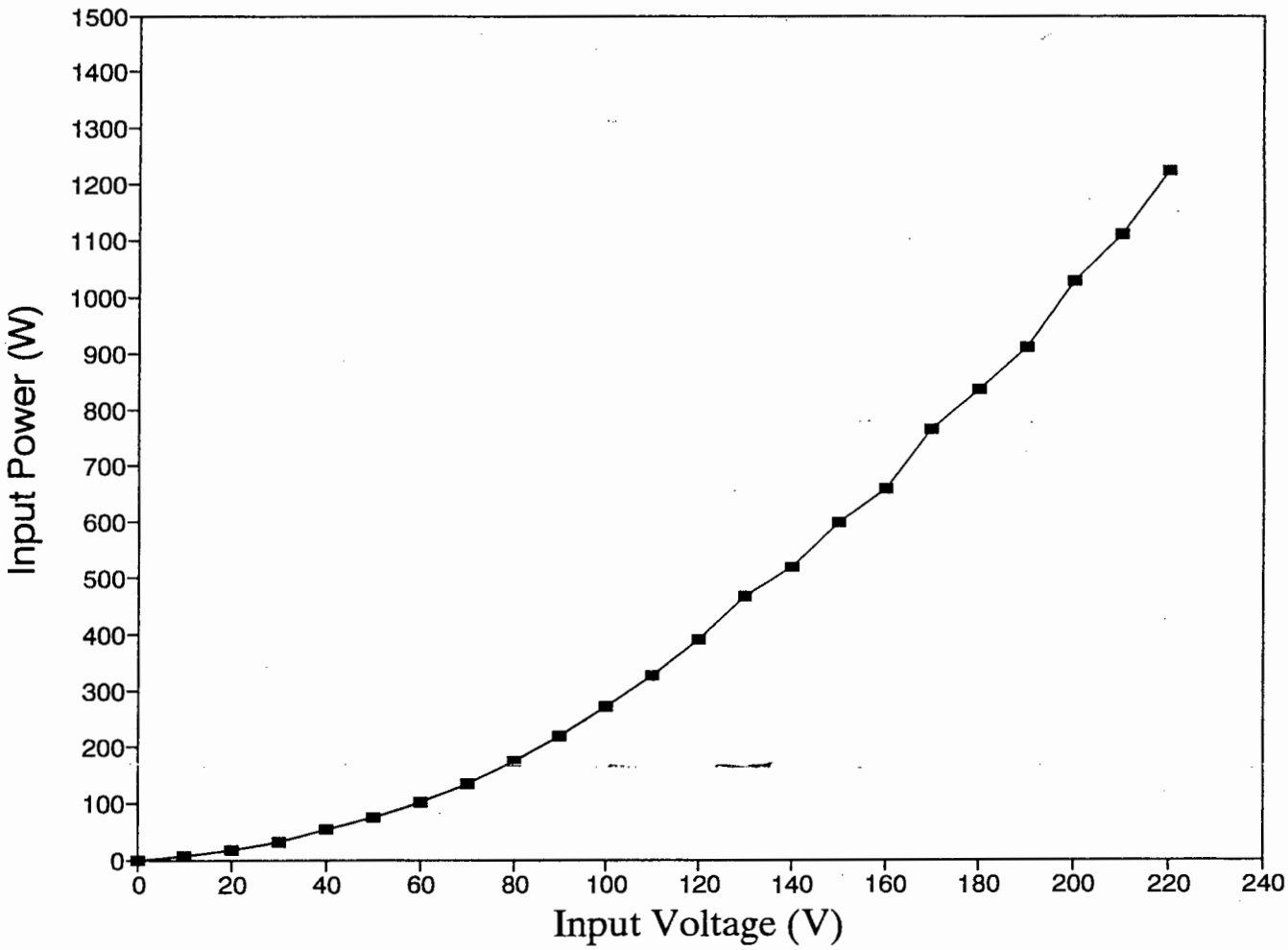

Figure 6.3: Shaded-pole LIM, Voltage Vs Input Power.

6.1.2 Load Test of LIM at rated voltage and frequency

The load test was carried out to determine other machine parameters such as power output, efficiency,torque, power factor, input current versus speed. Using a Prony's brake method shown in fig 6.4, with involves using a spring balance, weights for loading and a cord wound around the secondary disc shaft to produce friction on the rotating shaft, the resistant force is measured on the scale, and torque computed using appropriate mathematical relations. Figs 6.5-6.10 show the curves for the load test of torque, efficiency, input power, output power and power factor against speed. These curves show graphically the performance of the LIM under load conditions.

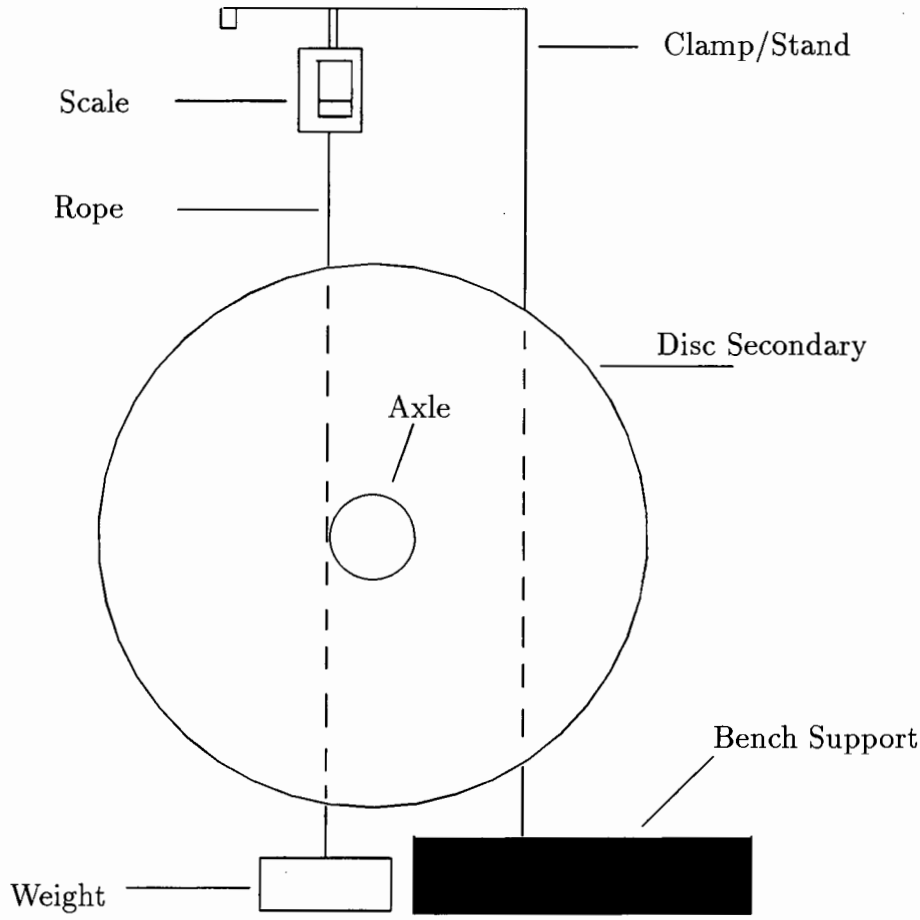

Figure 6.4: Torque Measurement Using the Prony's Brake Method.

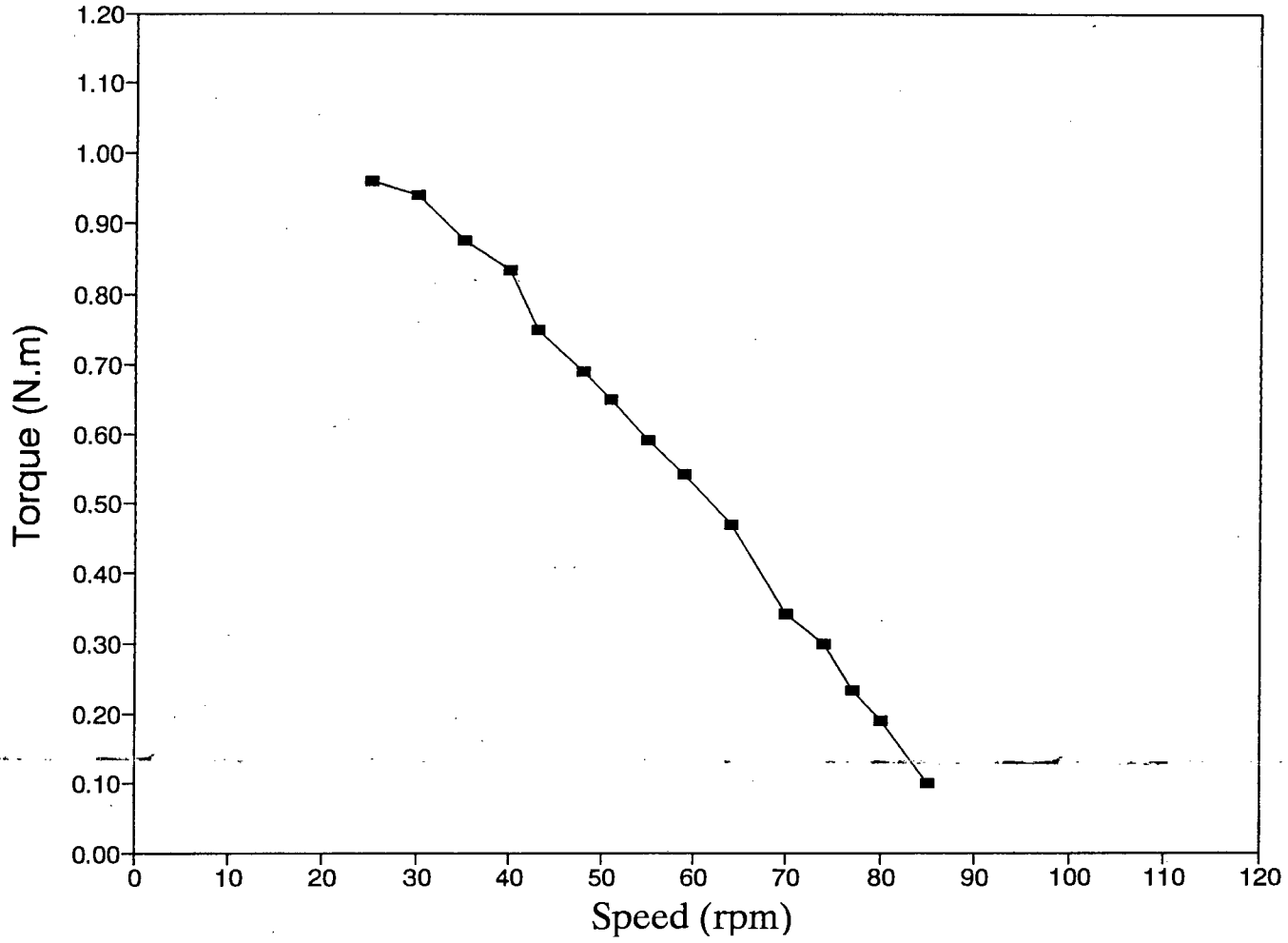

Figure 6.5: Shaded-pole LIM, Torque Vs Speed.

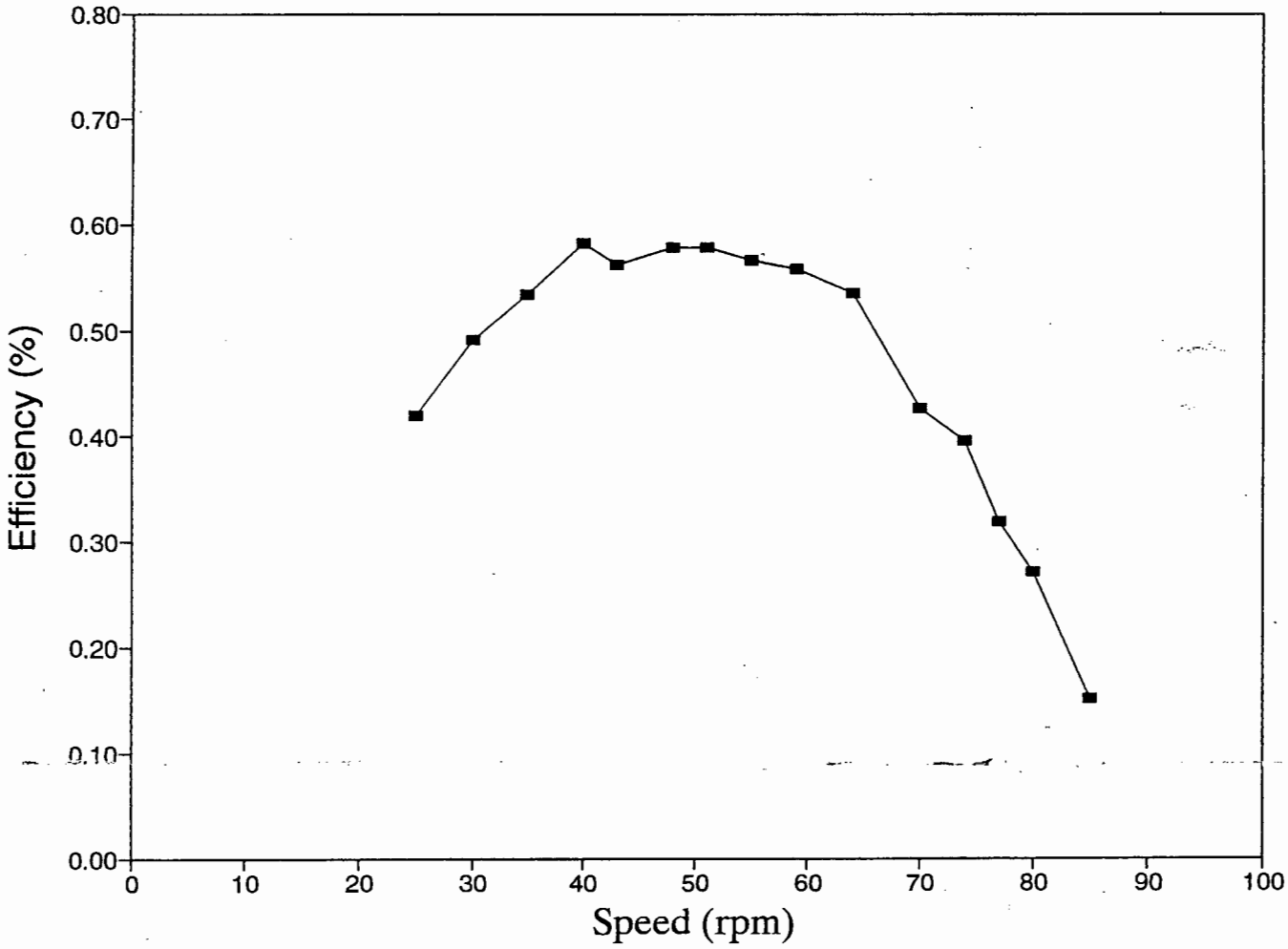

Figure 6.6: Shaded-pole LIM, Efficiency Vs Speed.

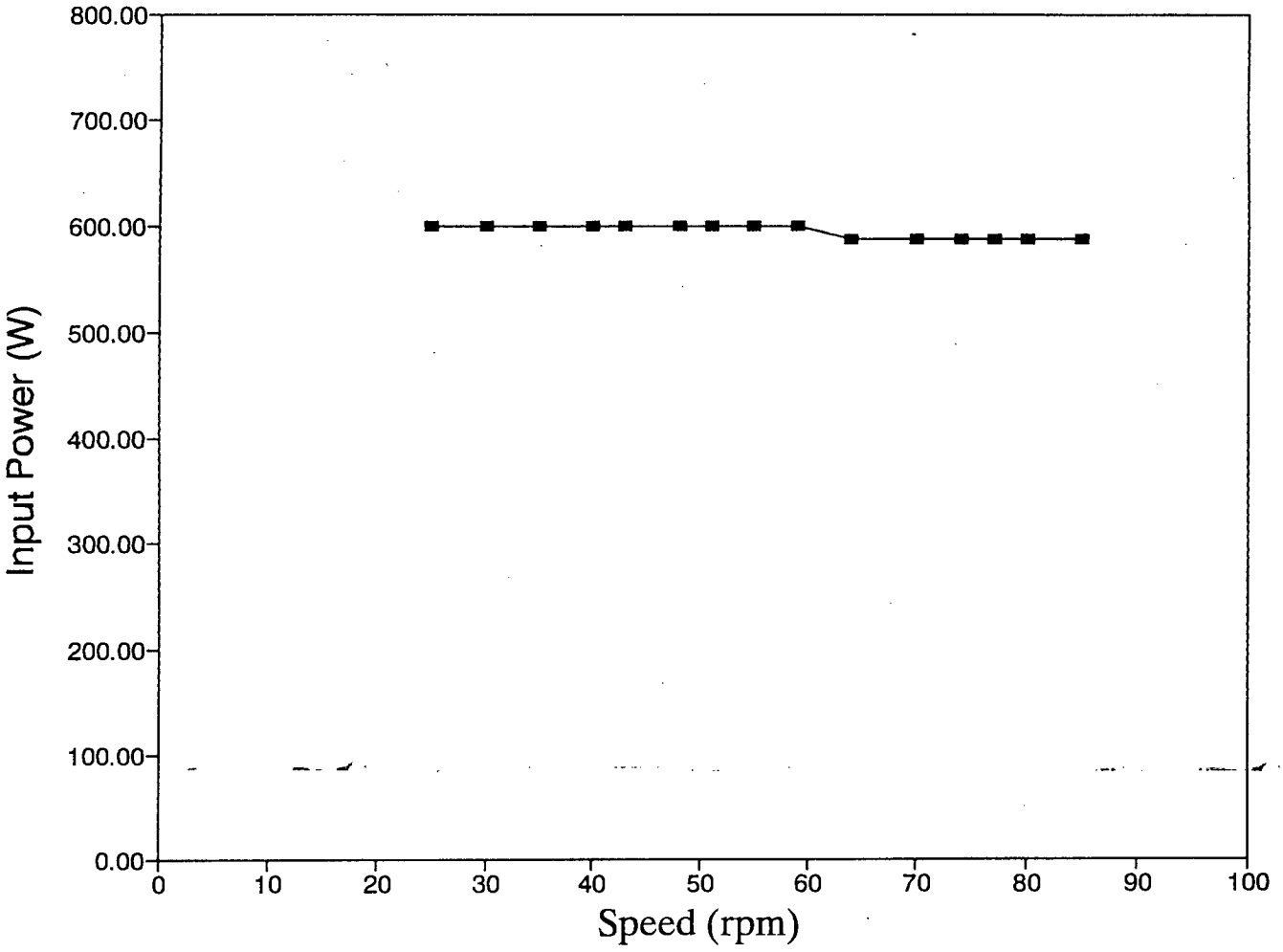

Figure 6.7: Shaded-pole LIM, Input Power Vs Speed.

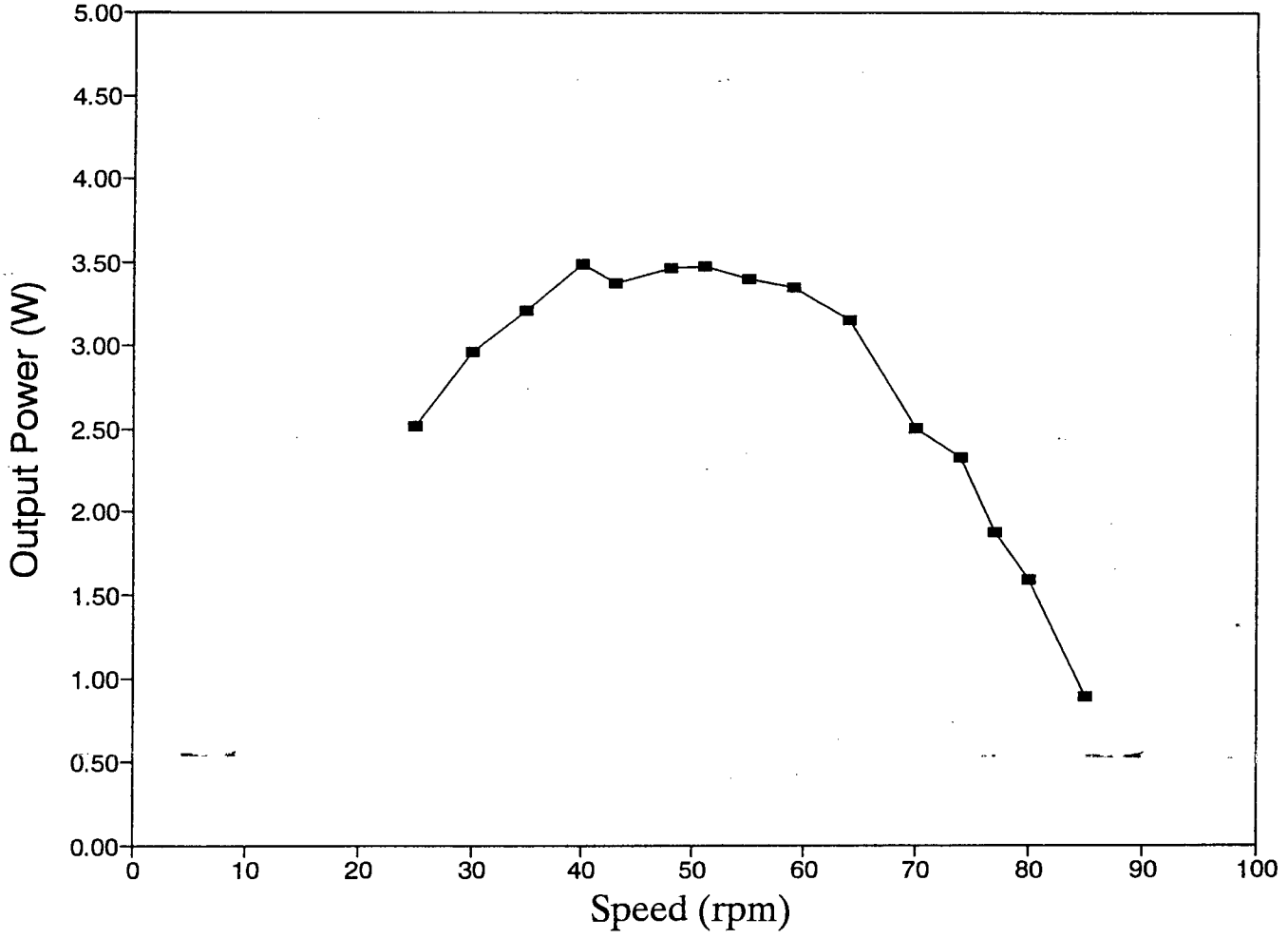

Figure 6.8: Shaded-pole LIM, Output Power Vs Speed.

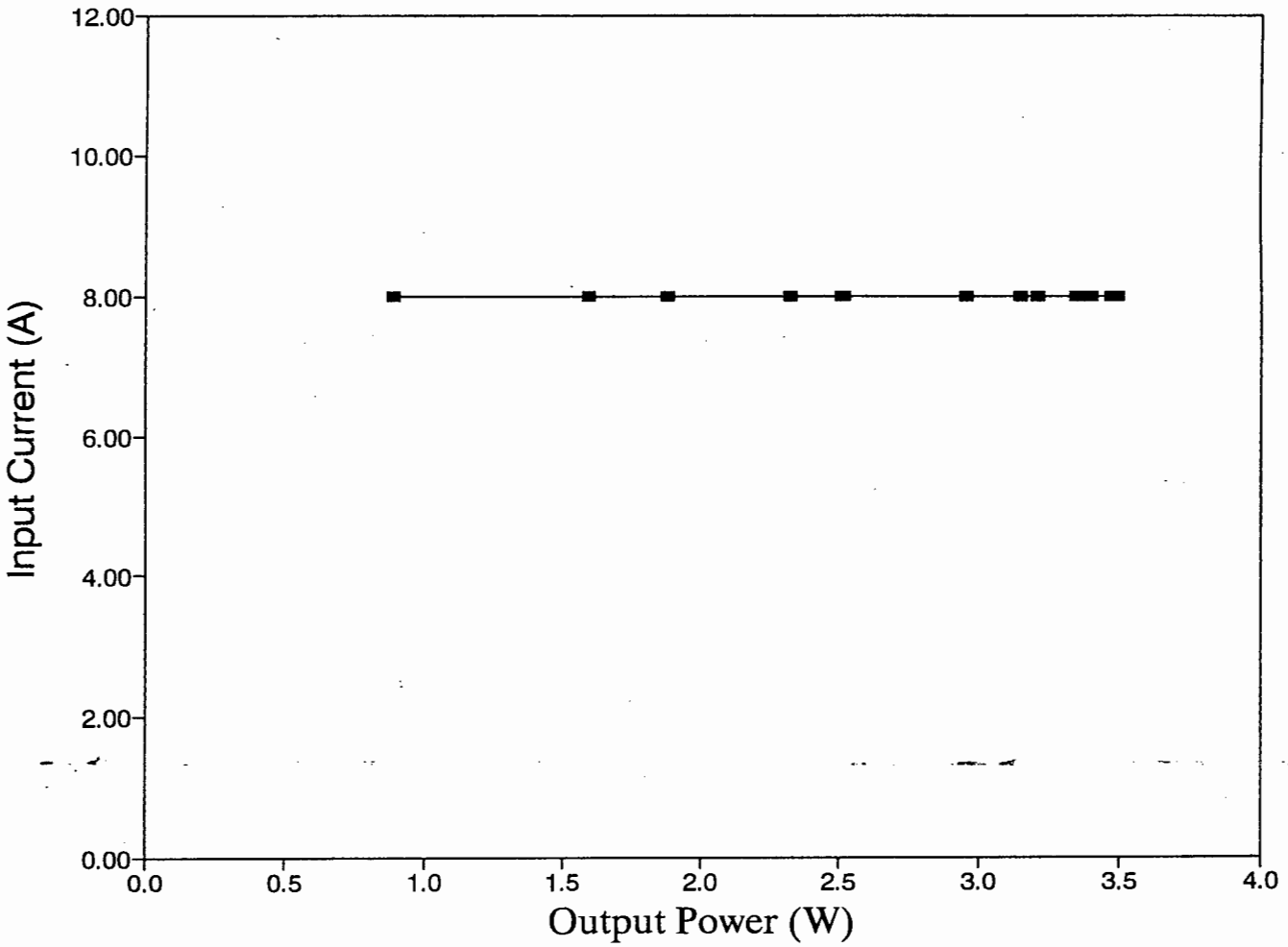

Figure 6.9: Shaded-pole LIM, Input Current Vs Output Power.

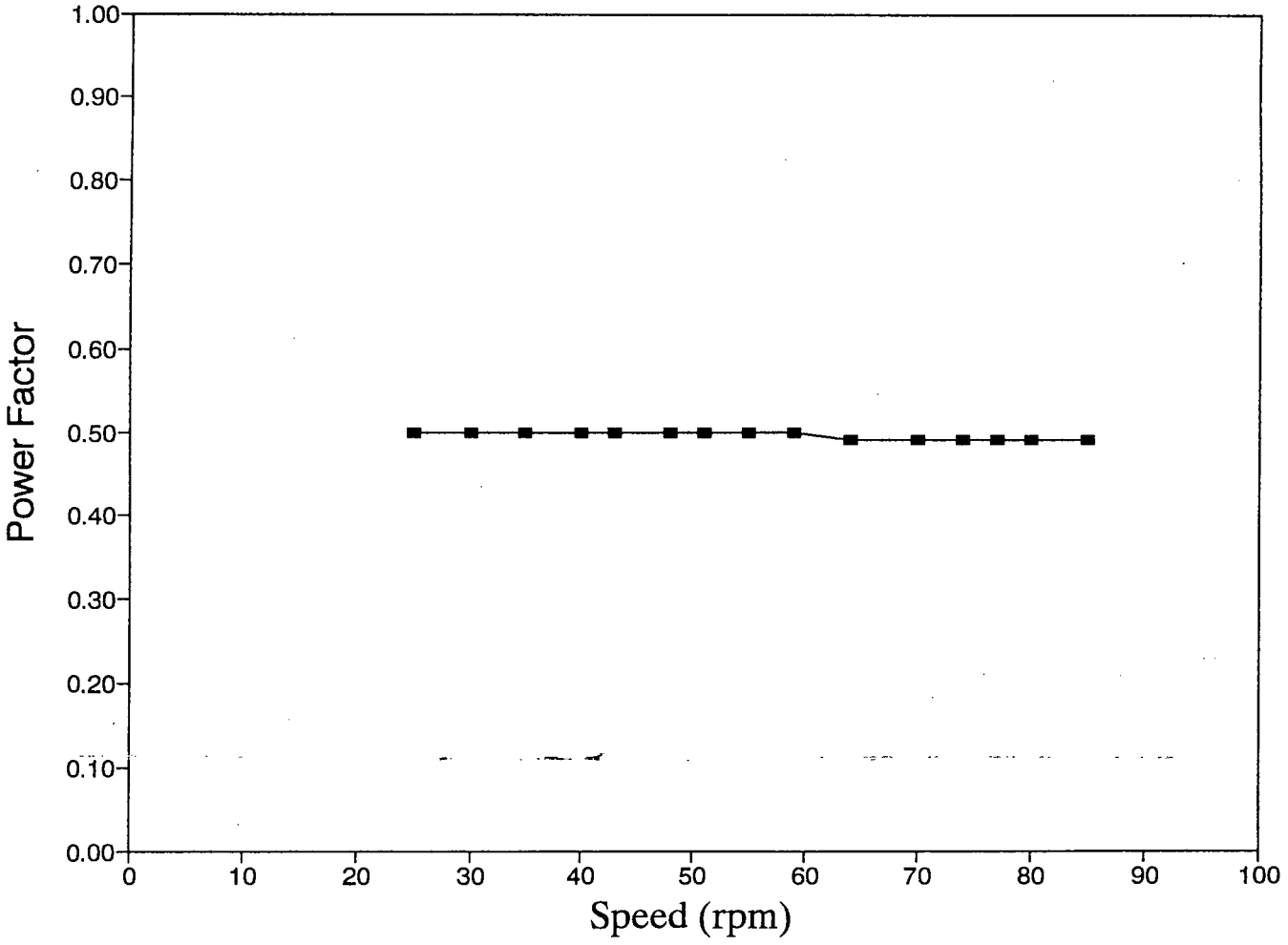

Figure 6.10: Shaded-pole LIM, Power Factor Vs Speed.

6.1.3 Short Circuit Test of LIM

The short circuit test, a string is wound around the secondary disc, and connected to a scale which is perpendicular to the centre of the disk. The supply voltage is increased in small increments and readings of voltage, input current, power factor and torque were taken. Figs 6.11-6.14 show the curves for short-circuit test results for input current, power factor, input power and torque against the input voltage. These curves show graphically the performance of the LIM under short-circuit conditions.

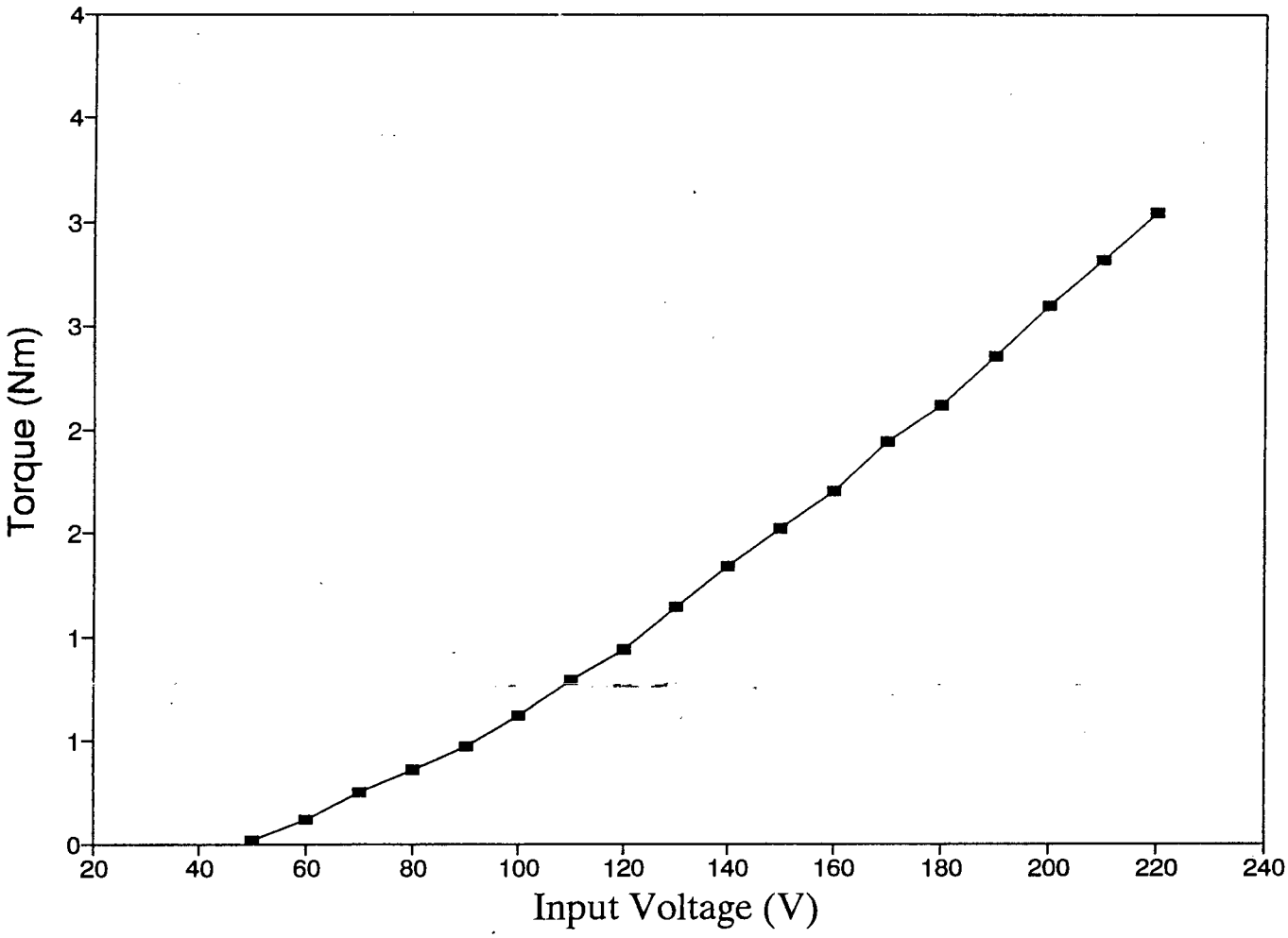

Figure 6.11: Shaded-pole LIM, Torque Vs Input Voltage.

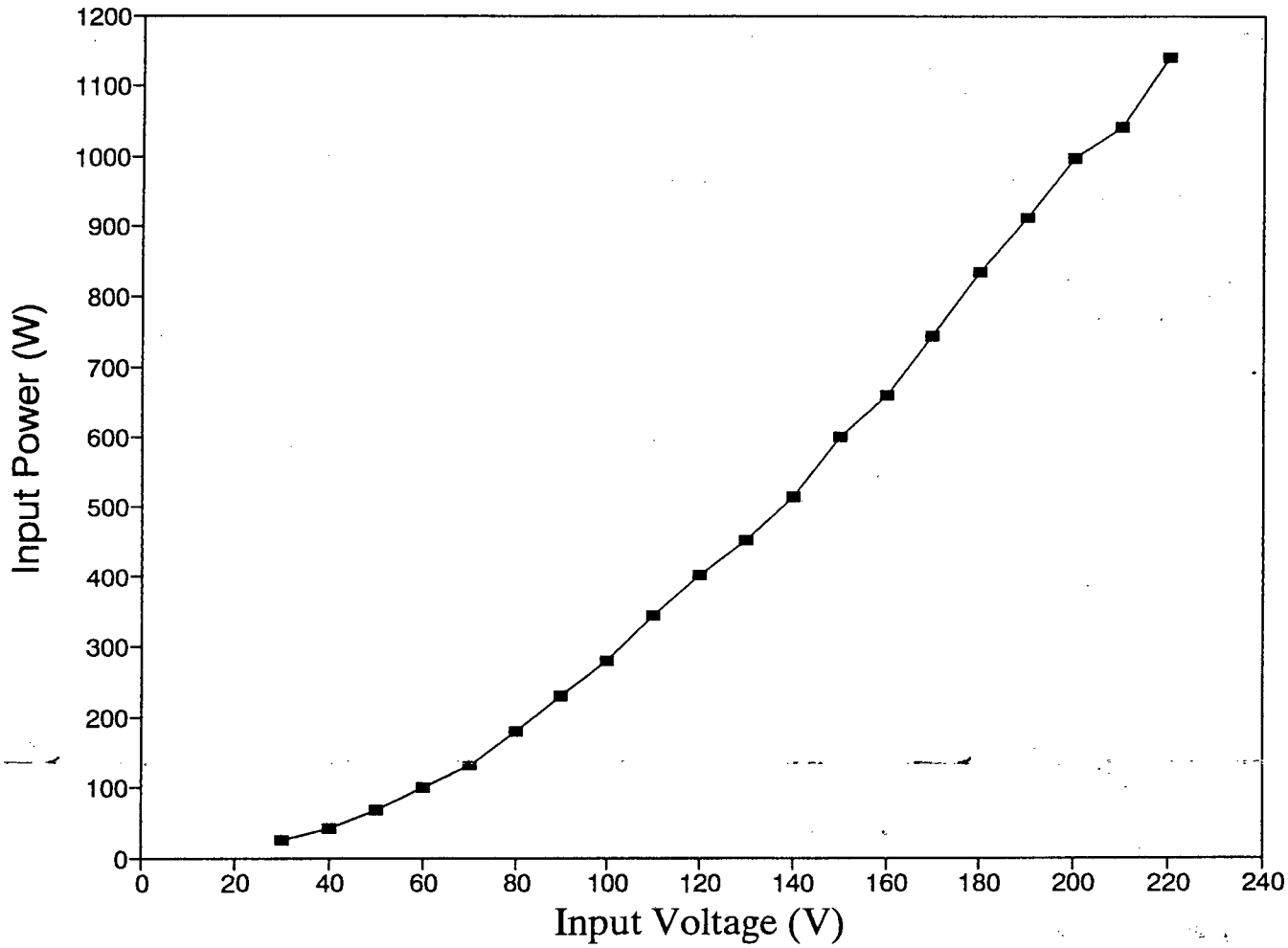

Figure 6.12: Shaded-pole LIM, Input Power Vs Input Voltage.

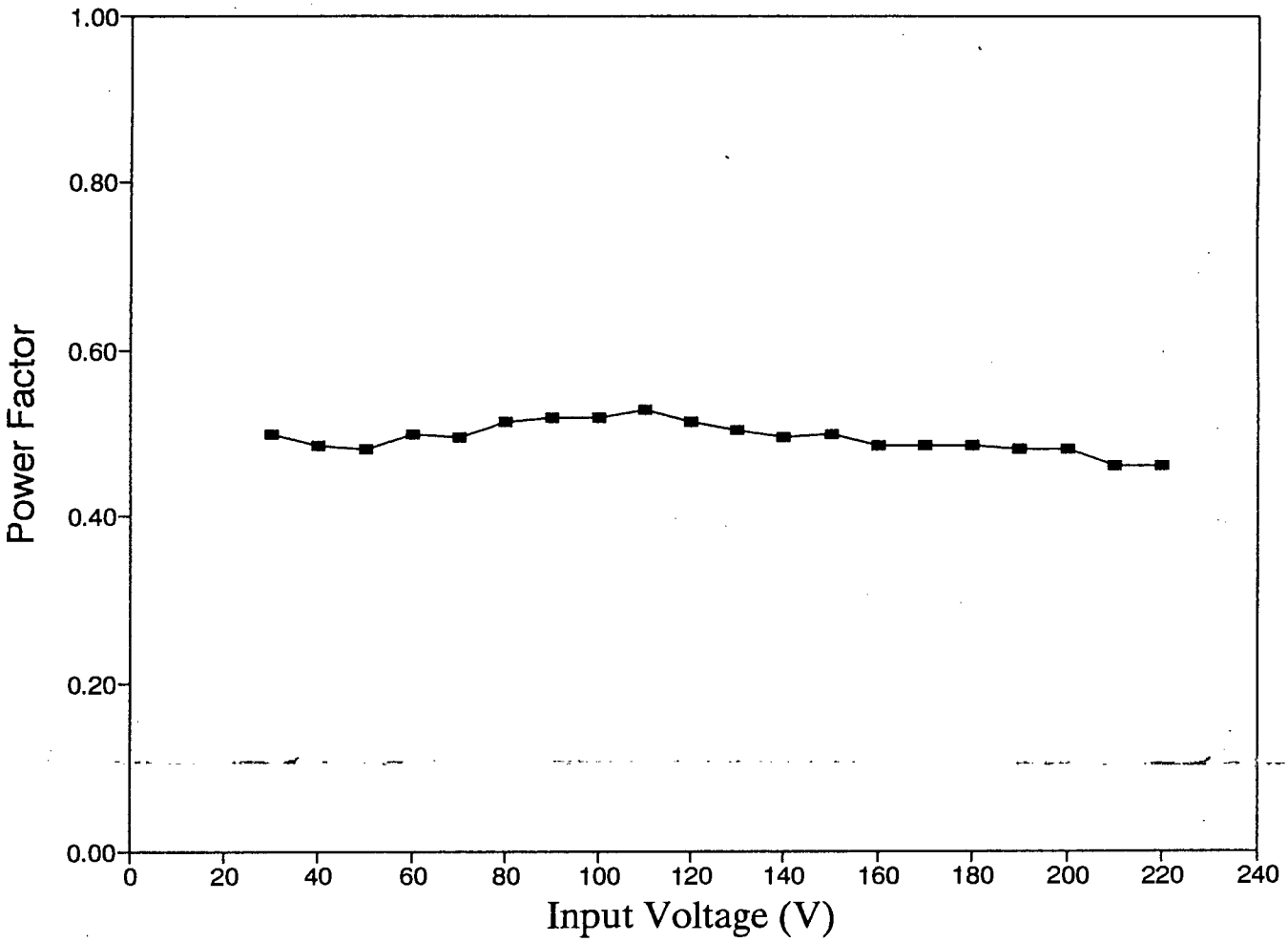

Figure 6.13: Shaded-pole LIM, Power Factor Vs Input Voltage.

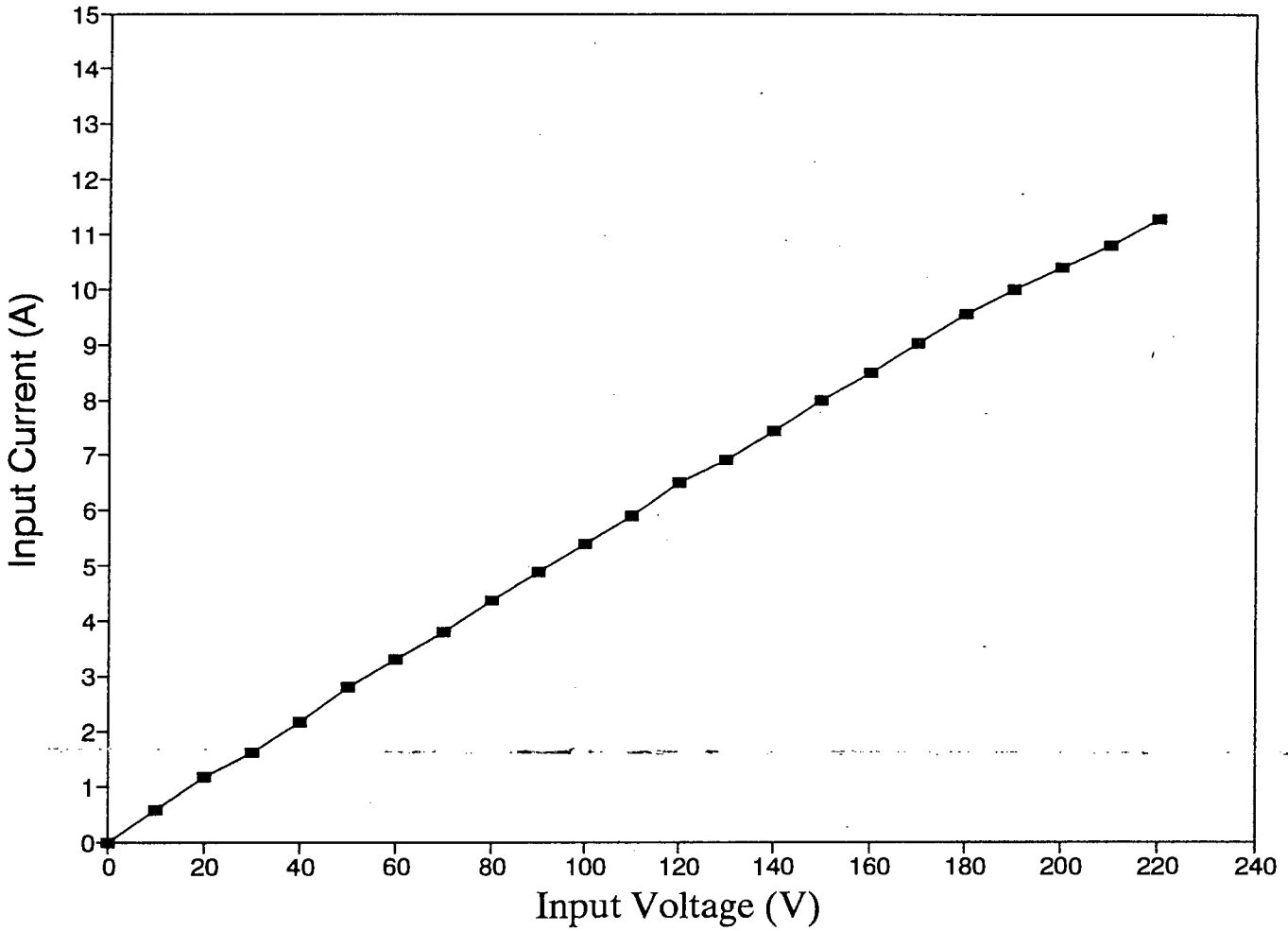

Figure 6.14: Shaded-pole LIM, Input Current Vs Input Voltage.

6.2 Testing for optimum performance of LIM

The second set of experimental tests were carried out on the shaded-pole LIM using sinusoidal excitation at various power frequencies - 40, 50, 60 and 75Hz respectively. The supply voltage to frequency ratio being kept approximately constant, V/f $\approx$ 2.0. This ensures the field parameter Φ is approximately constant throughout the tests.

6.2.1 No-Load Test of LIM with V/f $\approx$ 2.0

The no-load characteristics, that is, the input current, input power and power factor were obtained for the LIM at these frequencies. Results obtained from measurements were plotted to show the trend for increasing supply frequency. Figs 6.15-6.17 show the curves for no-load test results for input current, power factor, input power and input voltage, for various supply frequencies. These curves show graphically the performance of the LIM at no-load.

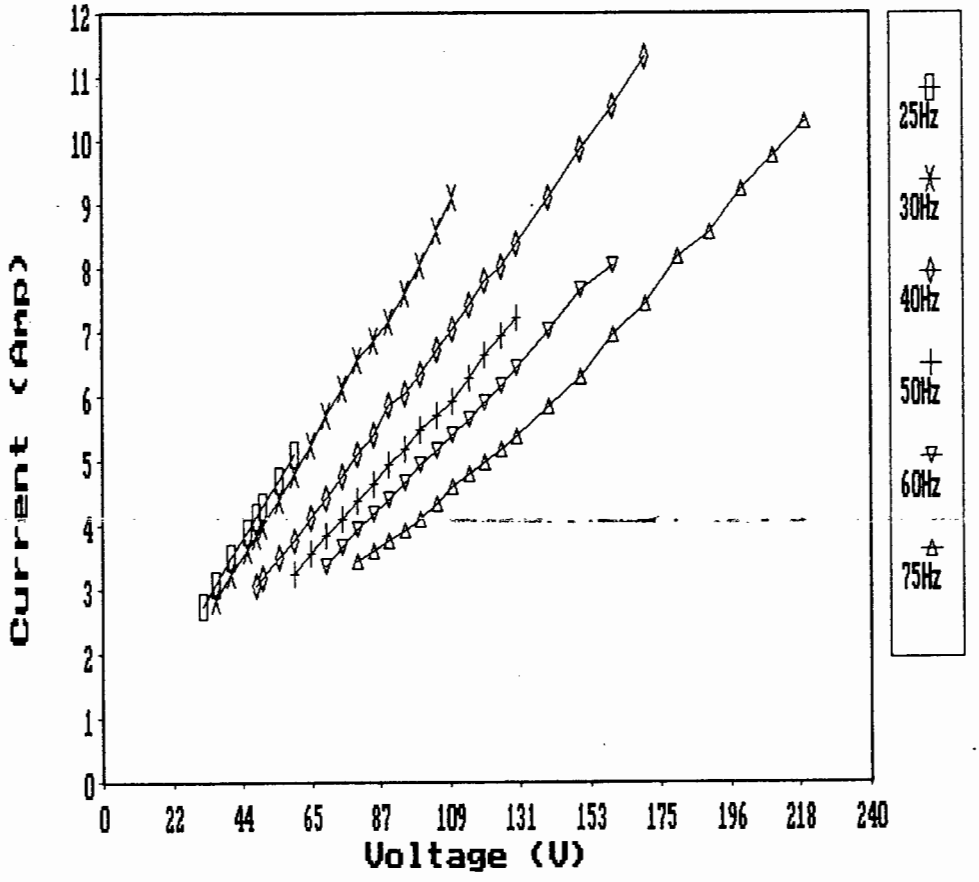

Figure 6.15: Shaded-pole LIM, Voltage Vs Input Current

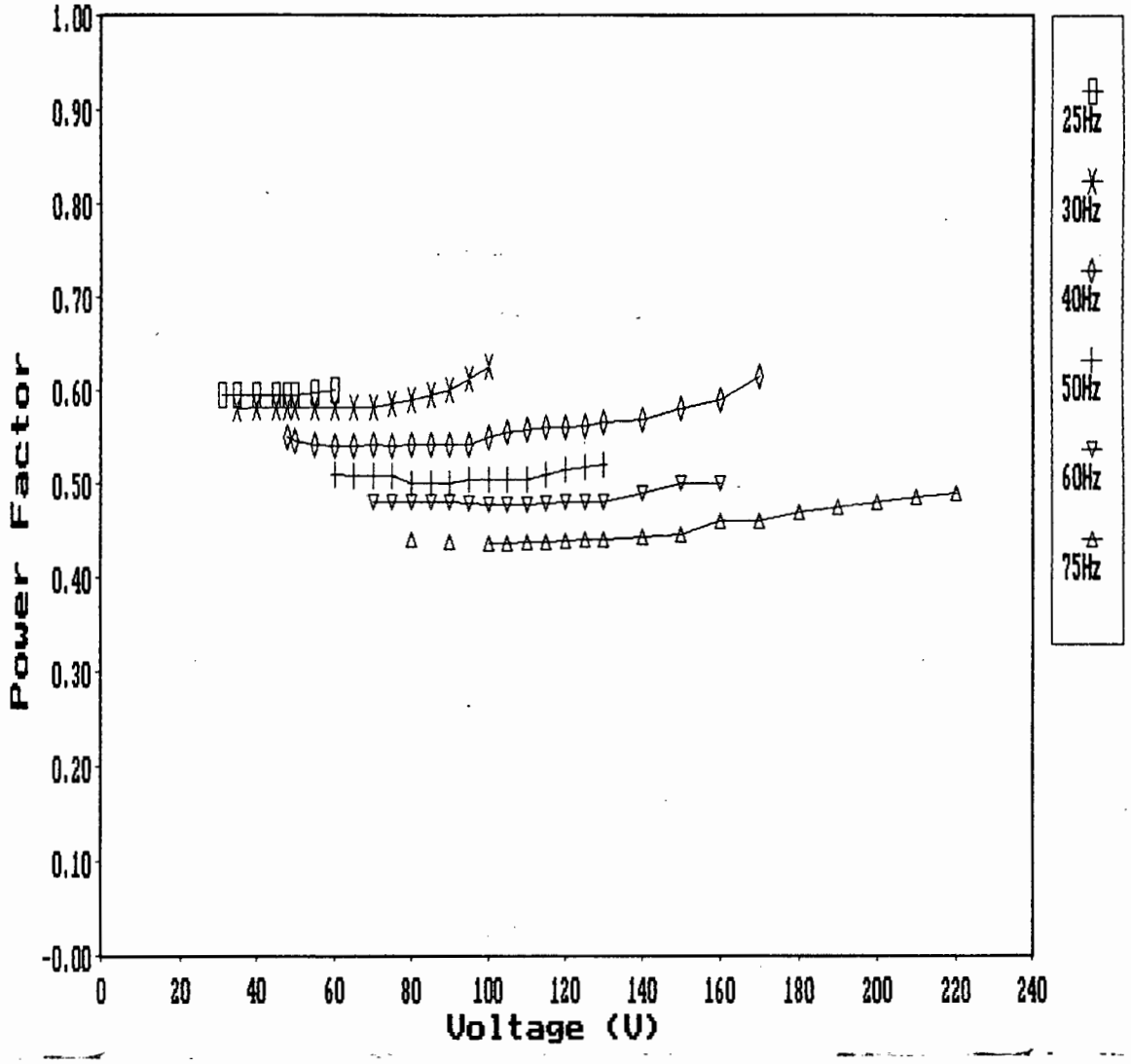

Figure 6.16: Shaded-pole LIM, Voltage Vs Power Factor

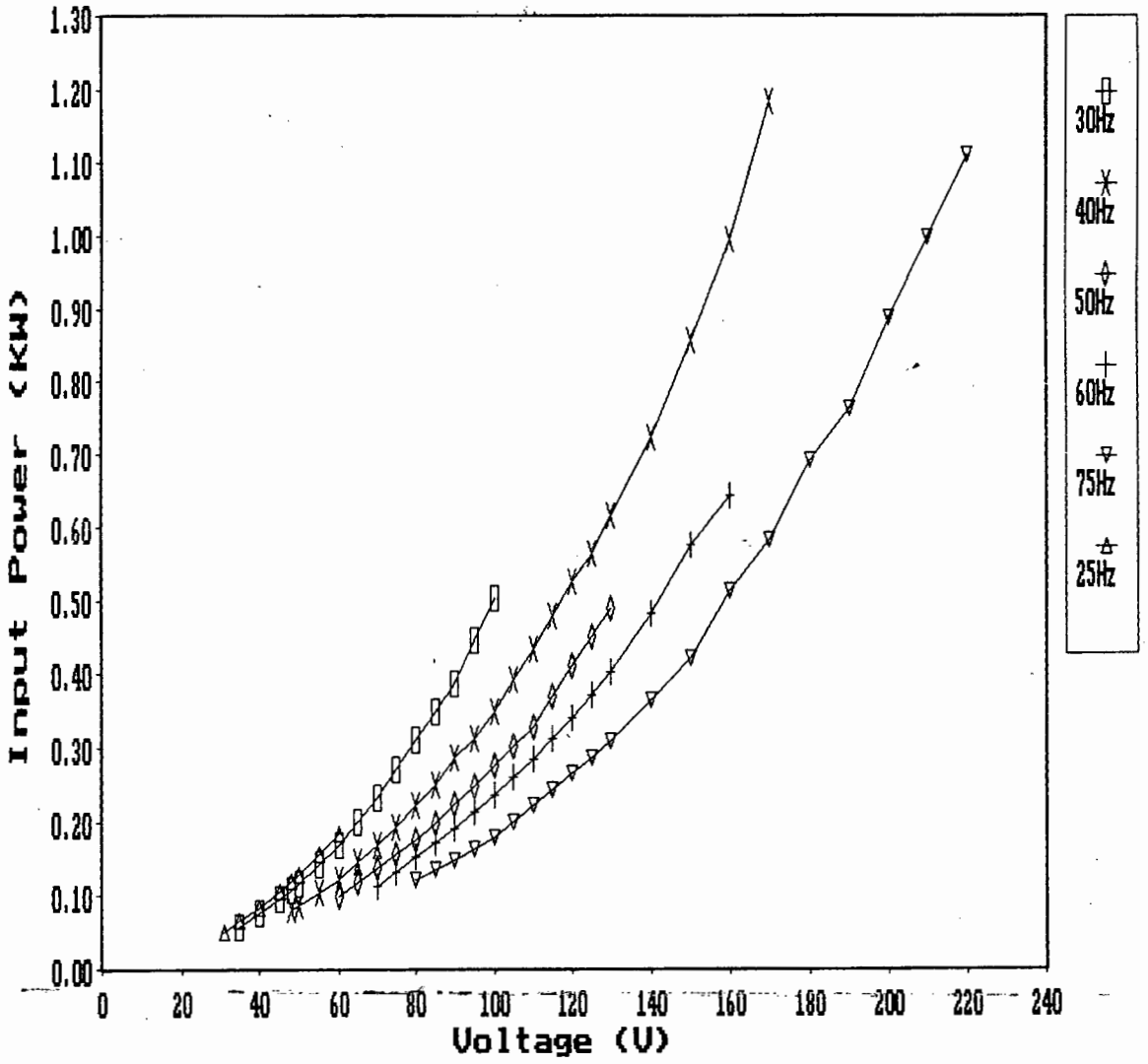

Figure 6.17: Shaded-pole LIM, Voltage Vs Input Power

6.2.2 Load Test of LIM with V/f $\approx$ 2.0

The load test was carried out to determine other machine parameters such as power output, efficiency, torque, power factor, input current versus speed, and how these vary with varying frquency. Results obtained from measurements were plotted to show the variation of efficiency with increasing supply frequency. Figs 6.18-6.21 show the curves for load test of torque, efficiency, output power and power factor against speed. These curves show graphically the performance of the LIM under load conditions with V/f $\approx$ constant.

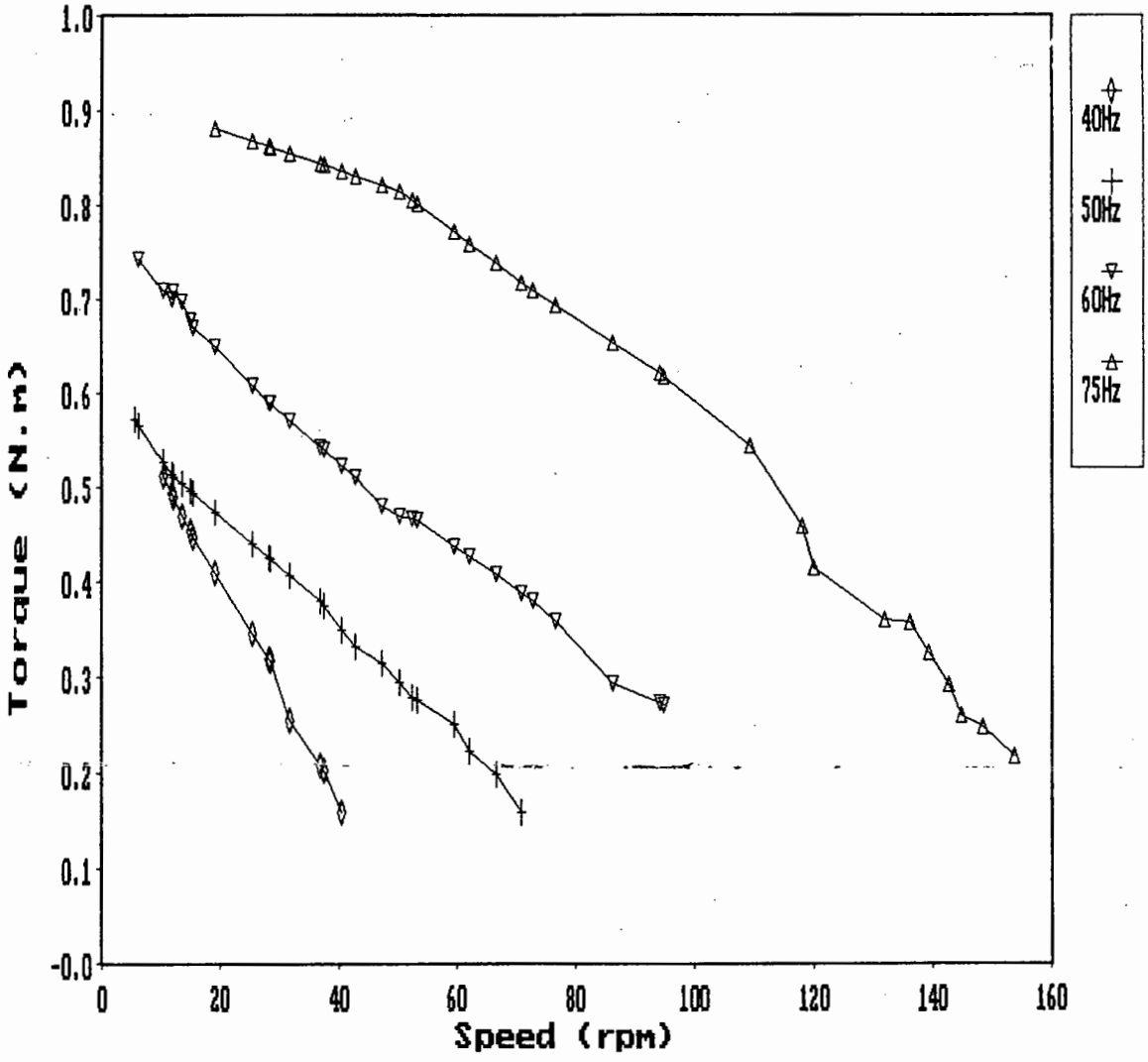

Figure 6.18: Torque Vs Speed for Varying Frequency

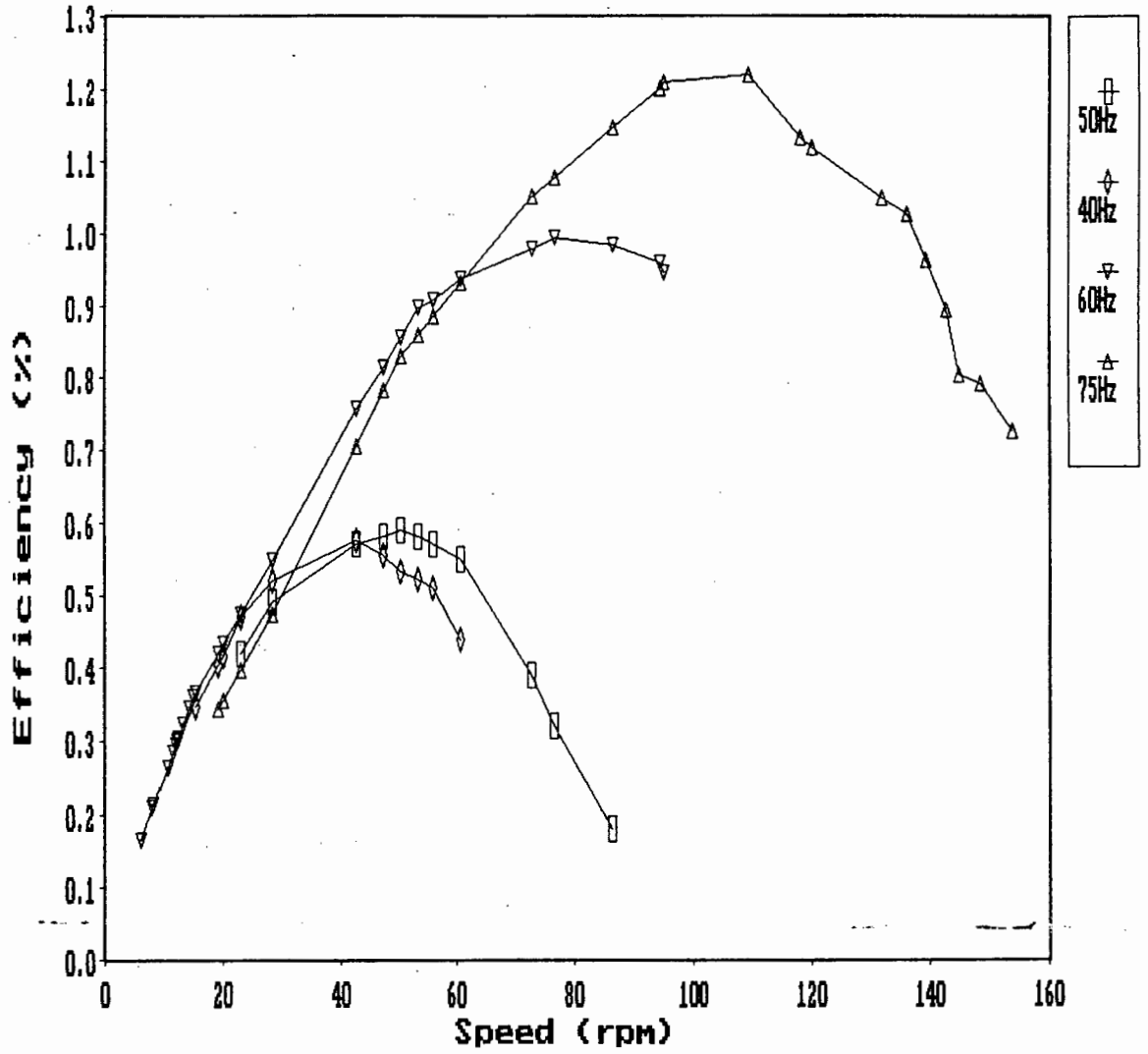

Figure 6.19: Efficiency Vs Speed for Varying Frequency

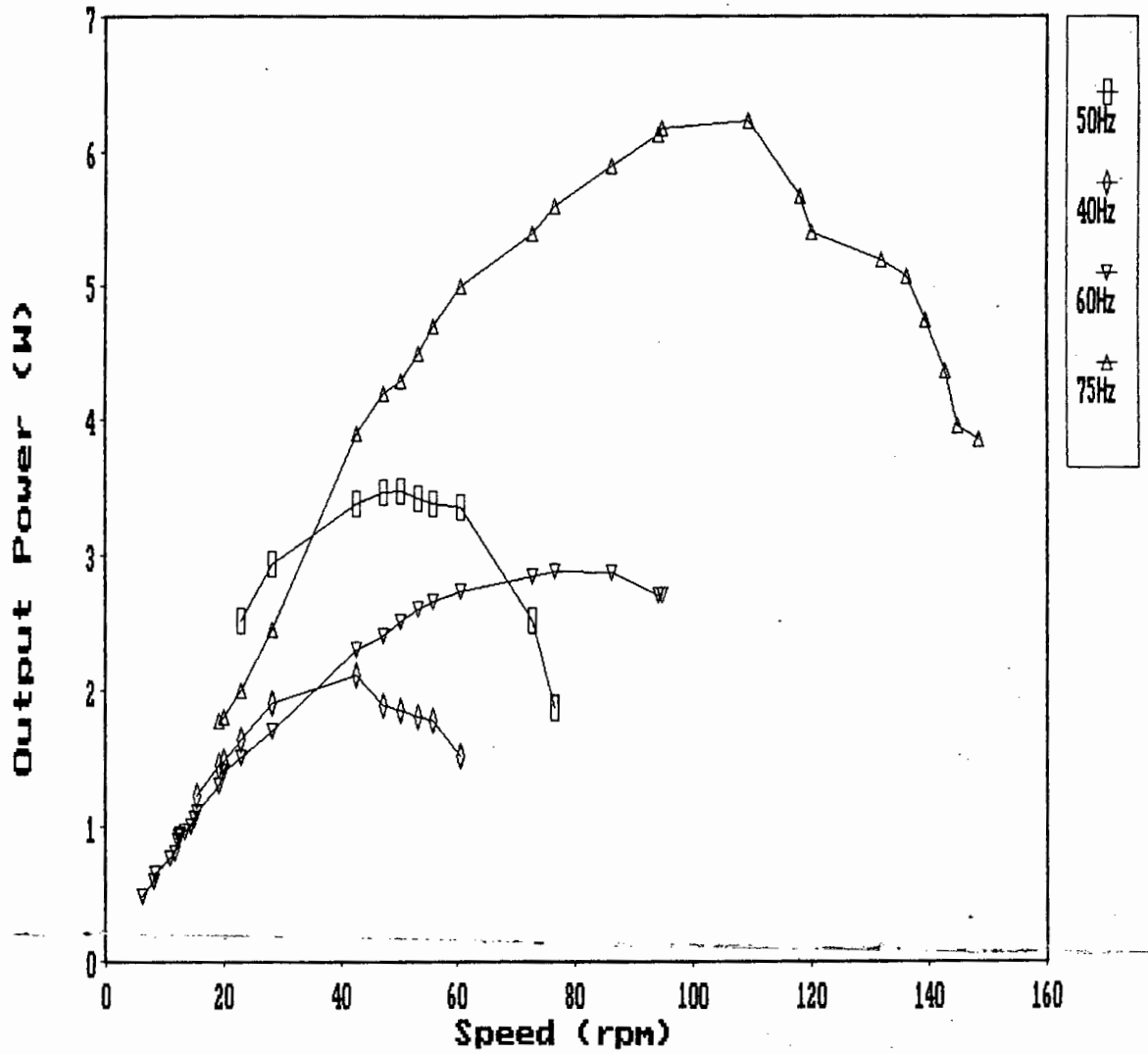

Figure 6.20: Output Power Vs Speed for Varying Frequency

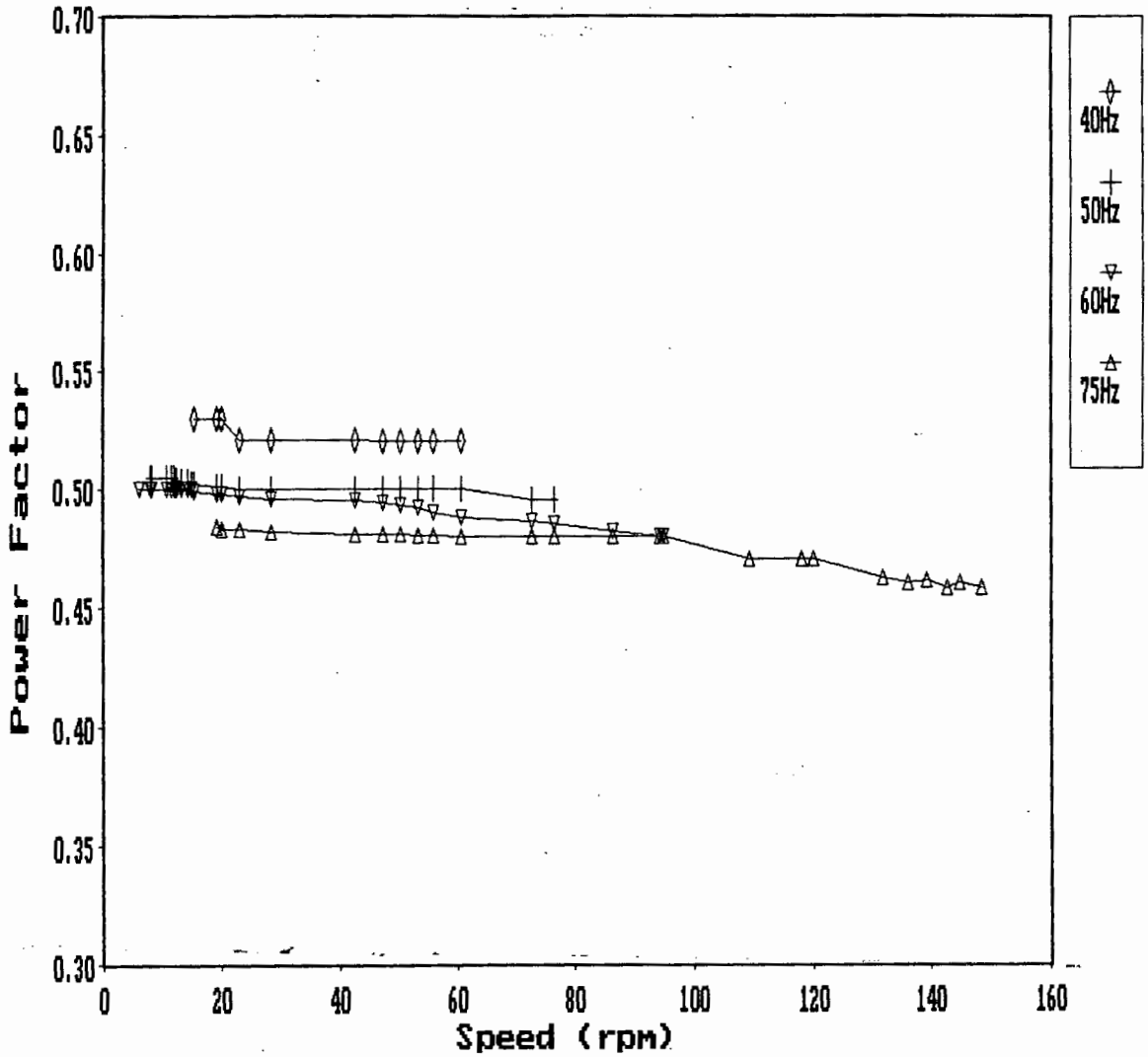

Figure 6.21: Power Factor Vs Speed for Varying Frequency

6.2.3 Analysis of Results

From the measurements obtained, the machine characteristics, that is, the output power, torque, efficiency, input current, and power factor were calculated for the LIM at each power frequency. Figs 6.22-6.26 show graphs of power factor, shaft torque, output power, efficiency and speed against input frequency with $V/f \approx$ constant.

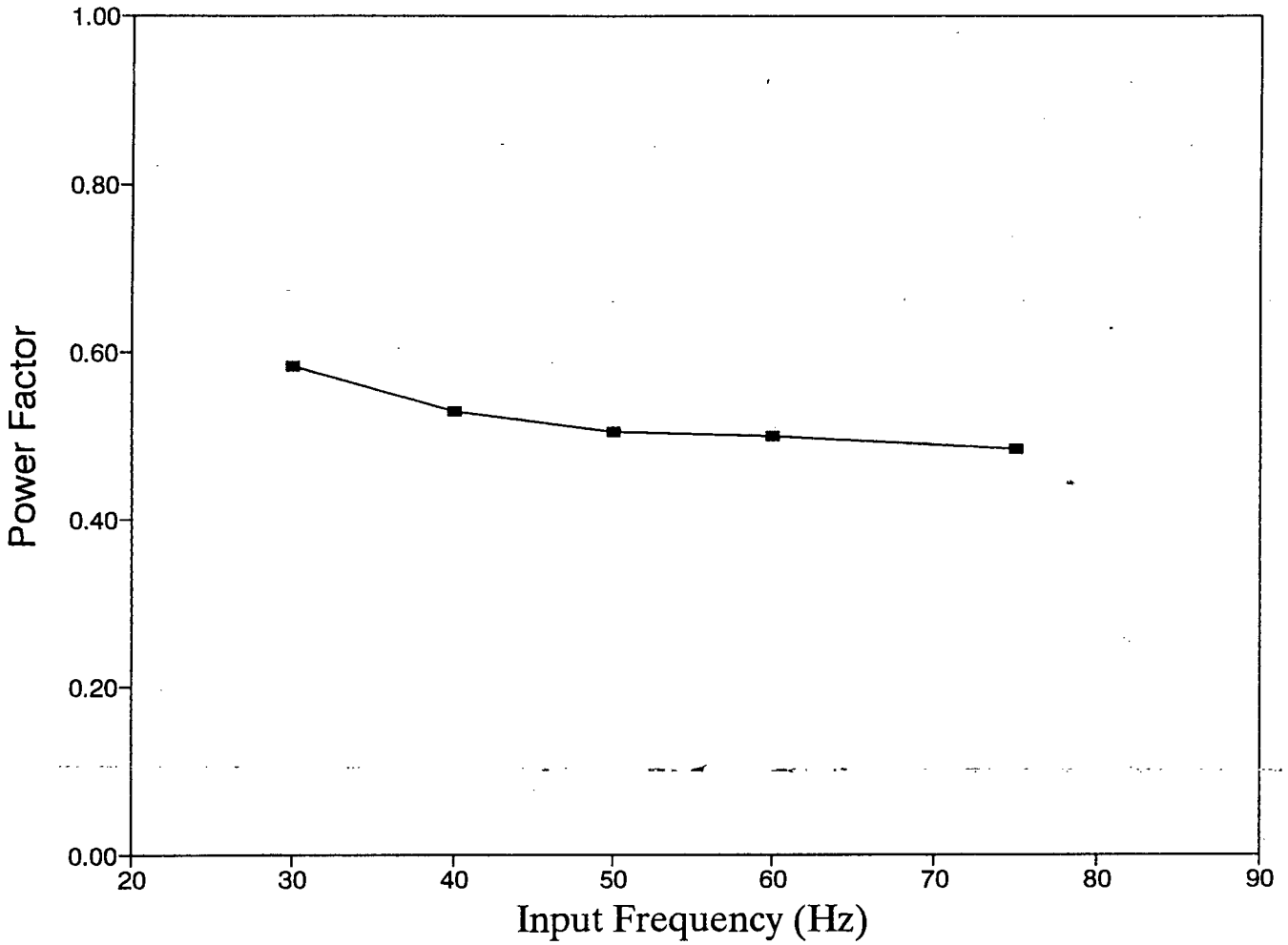

Figure 6.22: Power Factor Vs Input Frequency ($V/f \approx 2.0$)

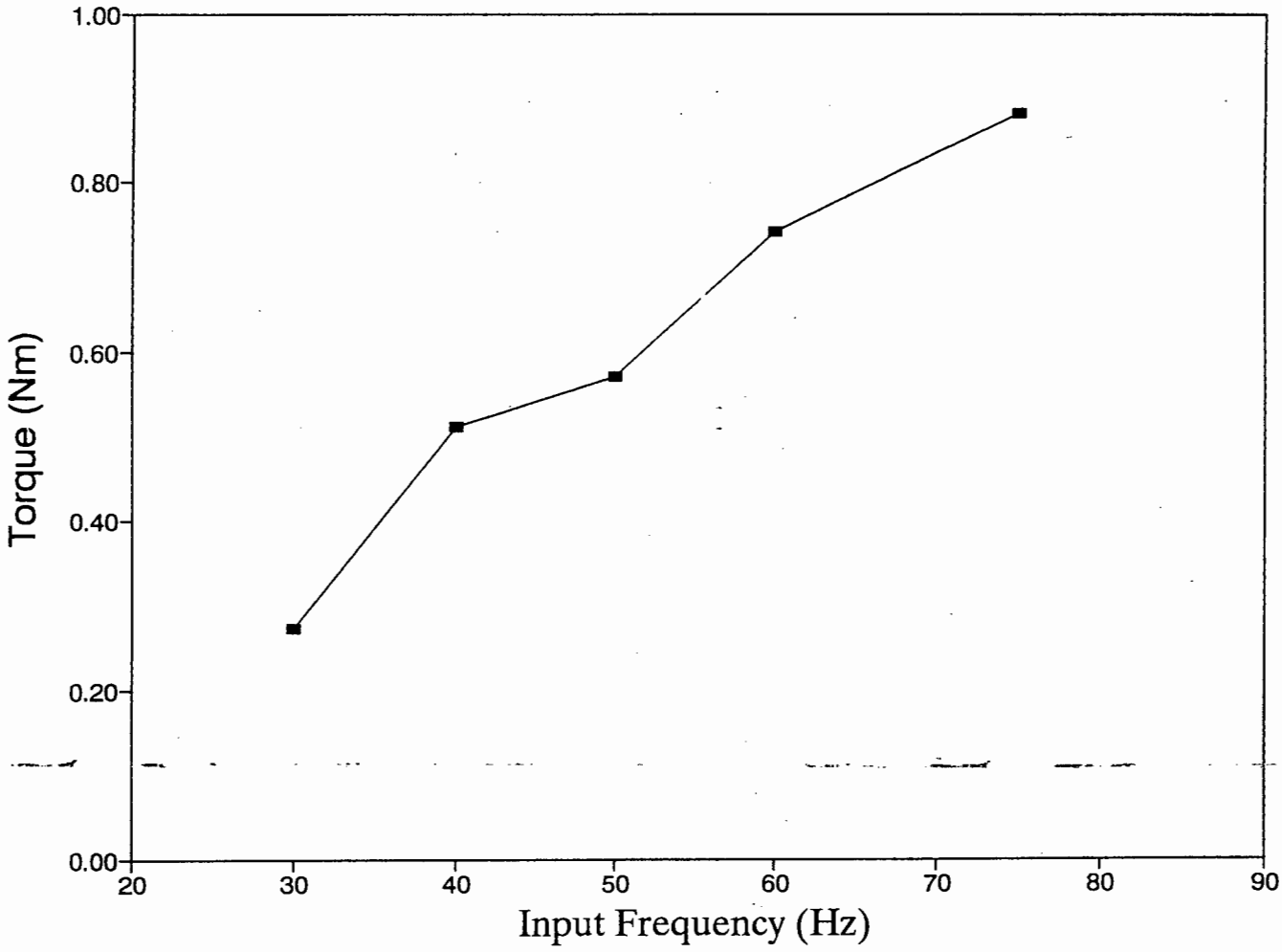

Figure 6.23: Shaft Torque Vs Input Frequency ($V/f \approx 2.0$)

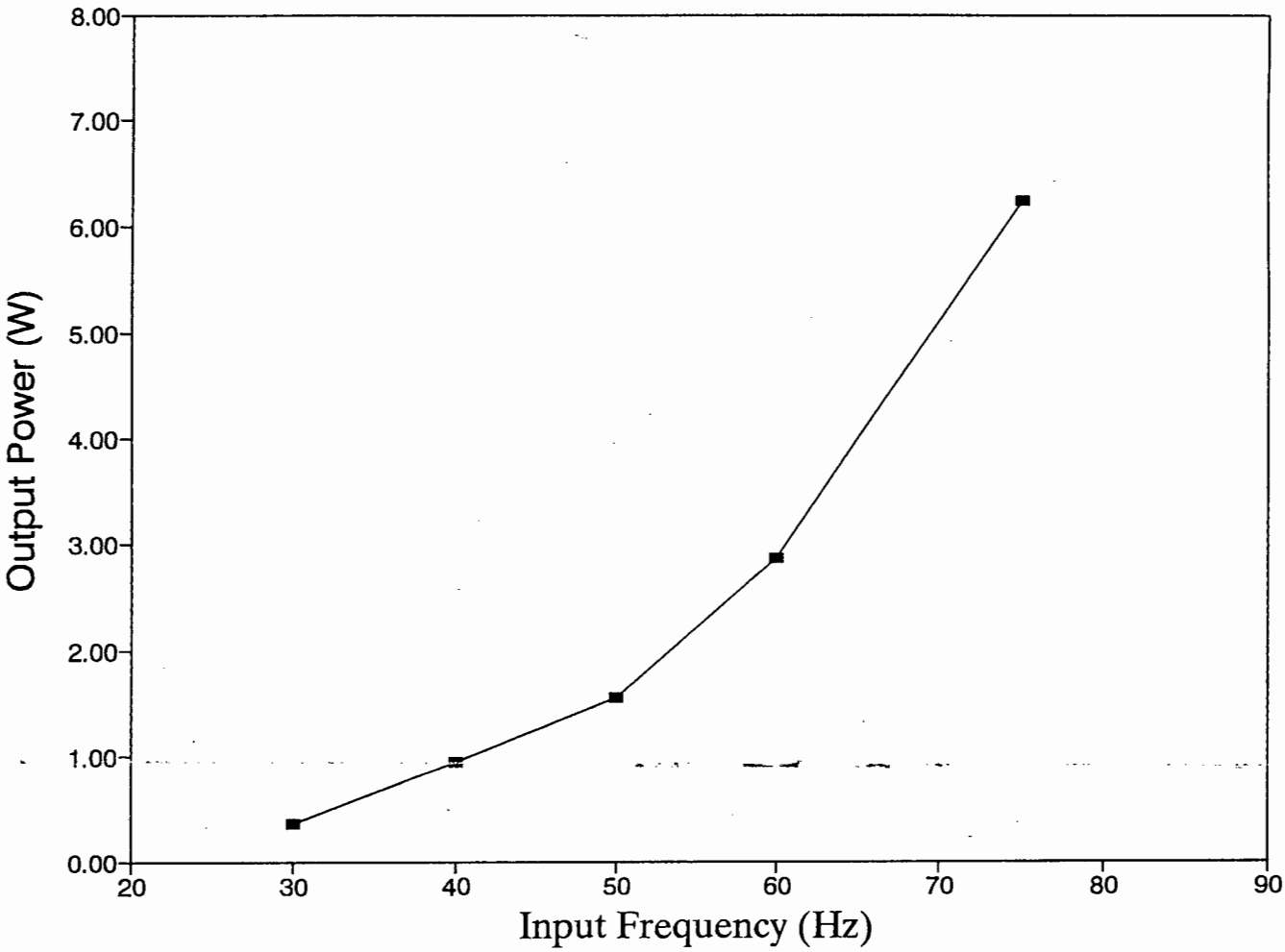

Figure 6.24: Output Power Vs Input Frequency ($V/f \approx 2.0$)

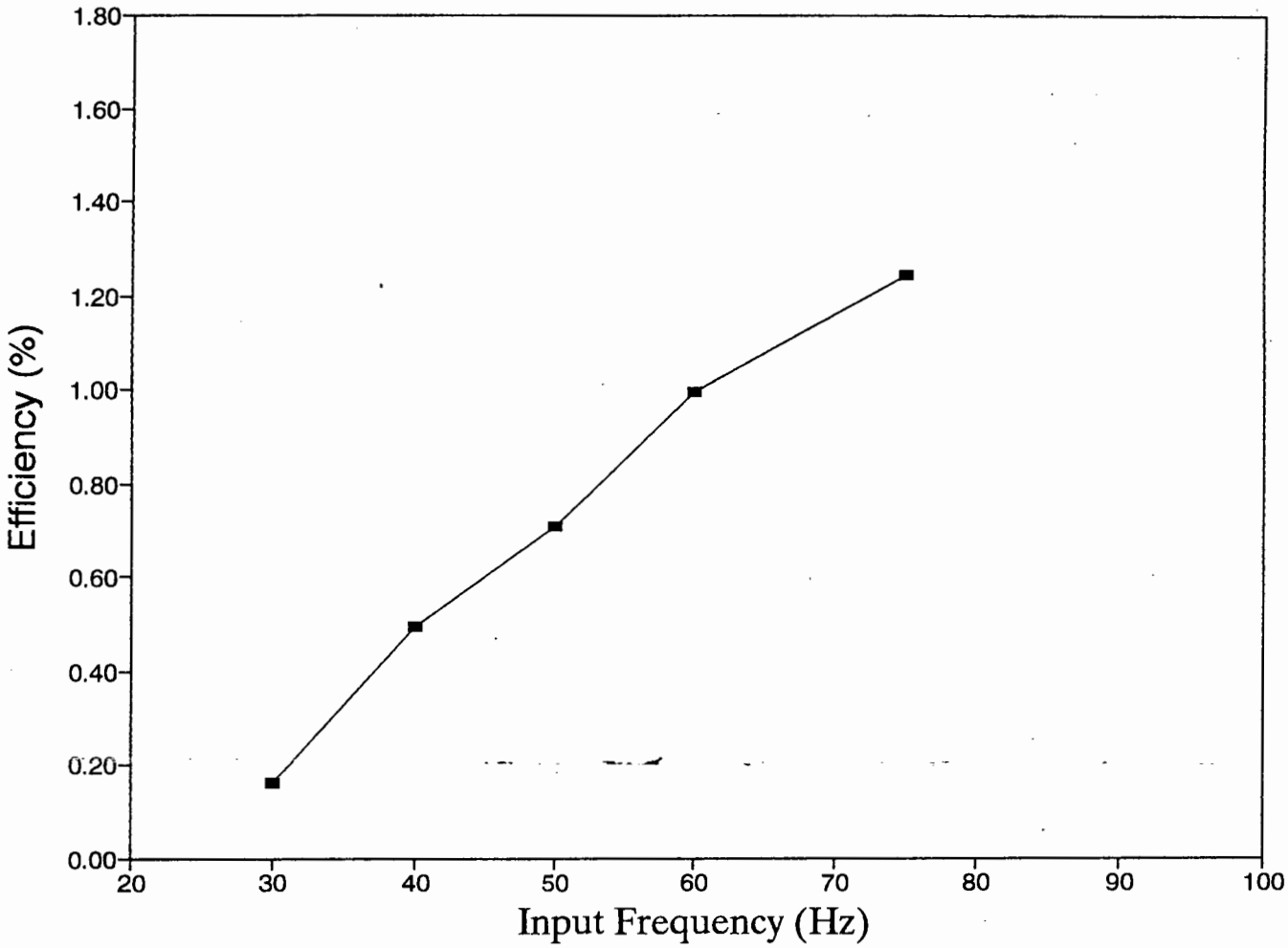

Figure 6.25: Efficiency Vs Input Frequency ($V/f \approx 2.0$)

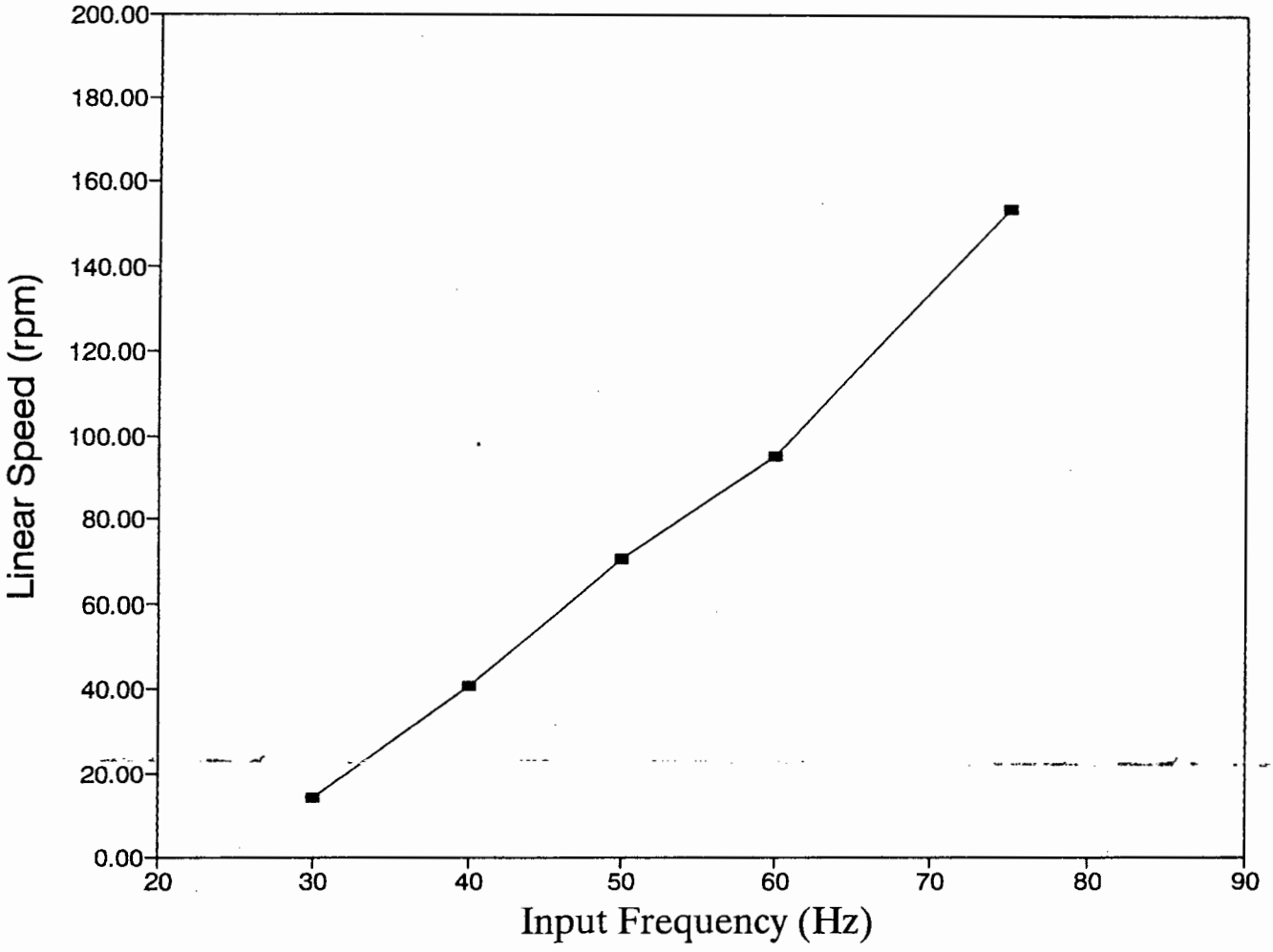

Figure 6.26: Speed Vs Input Frequency ($V/f \approx 2.0$)

The efficiency was found to increase with increasing supply frequency. For example, testing with a mains supply voltage of 220V, 50Hz frequency gave an efficiency of 0.59%. With a decrease in the input voltage to 90V, the efficiency of the LIM increased to 0.71%. Table 6.1 shows the variation of efficiency with frequency, with $V/f \approx 2.0$.

Table 6.1: Variation of LIM efficiency with Frequency $V/f \approx$ constant

Frequency (Hz)	Voltage (V)	Efficiency (%)
40	90	0.496
50	90	0.708
60	110	0.995
75	160	1.244

Table 6.2 shows the result of further tests carried out[47] for higher power frequencies up to 130Hz at 220V. Figs 6.27-6.31 show the plot of these parameters at 220V. These results are complimentary and show the influence of reduced voltage and increasing frequency to the overall performance of the shaded-pole LIM.

Table 6.2: Variation of LIM efficiency with Frequency, V = 220 volts

Frequency	Power Factor	Speed	Torque	Output Power	Efficiency
Hz		rpm	Nm	W	%
50	0.4856	088	0.1444	1.1764	0.0940
60	0.4851	100	0.1512	1.8209	0.1434
70	0.4776	140	0.1581	2.4838	0.2473
80	0.4737	170	0.1657	3.4624	0.4007
90	0.4280	220	0.1732	4.0265	0.5060
100	0.4143	278.3	0.1856	5.4097	0.8070
110	0.4115	303	0.1925	6.1161	0.9420
120	0.3947	334	0.2063	7.2052	1.2870
125	0.3899	350.7	0.2338	8.5845	1.5810
130	0.3801	401	0.2613	9.8144	1.8650

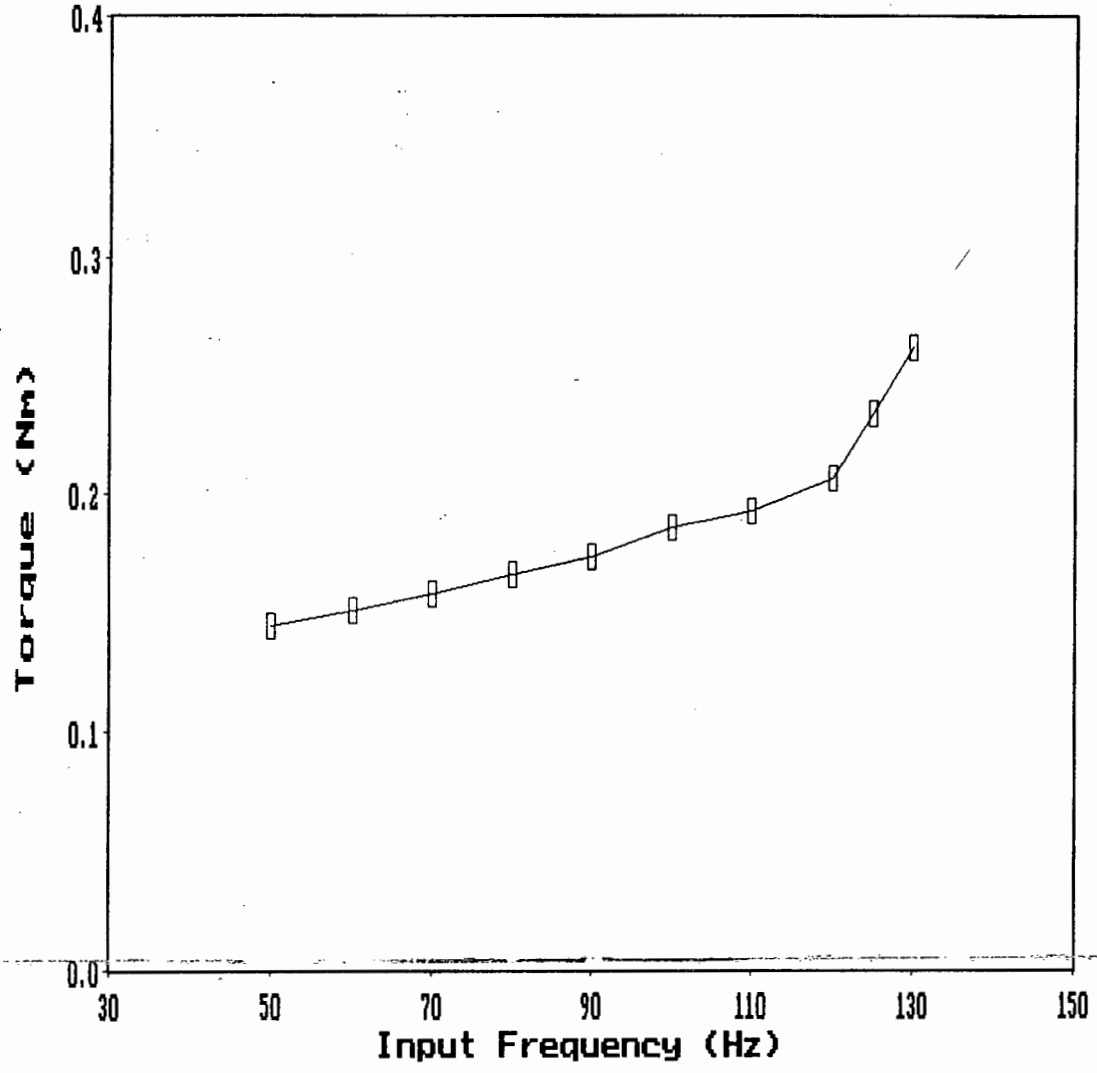

Figure 6.27: Shaft Torque Vs Input Frequency at 220V and rated load

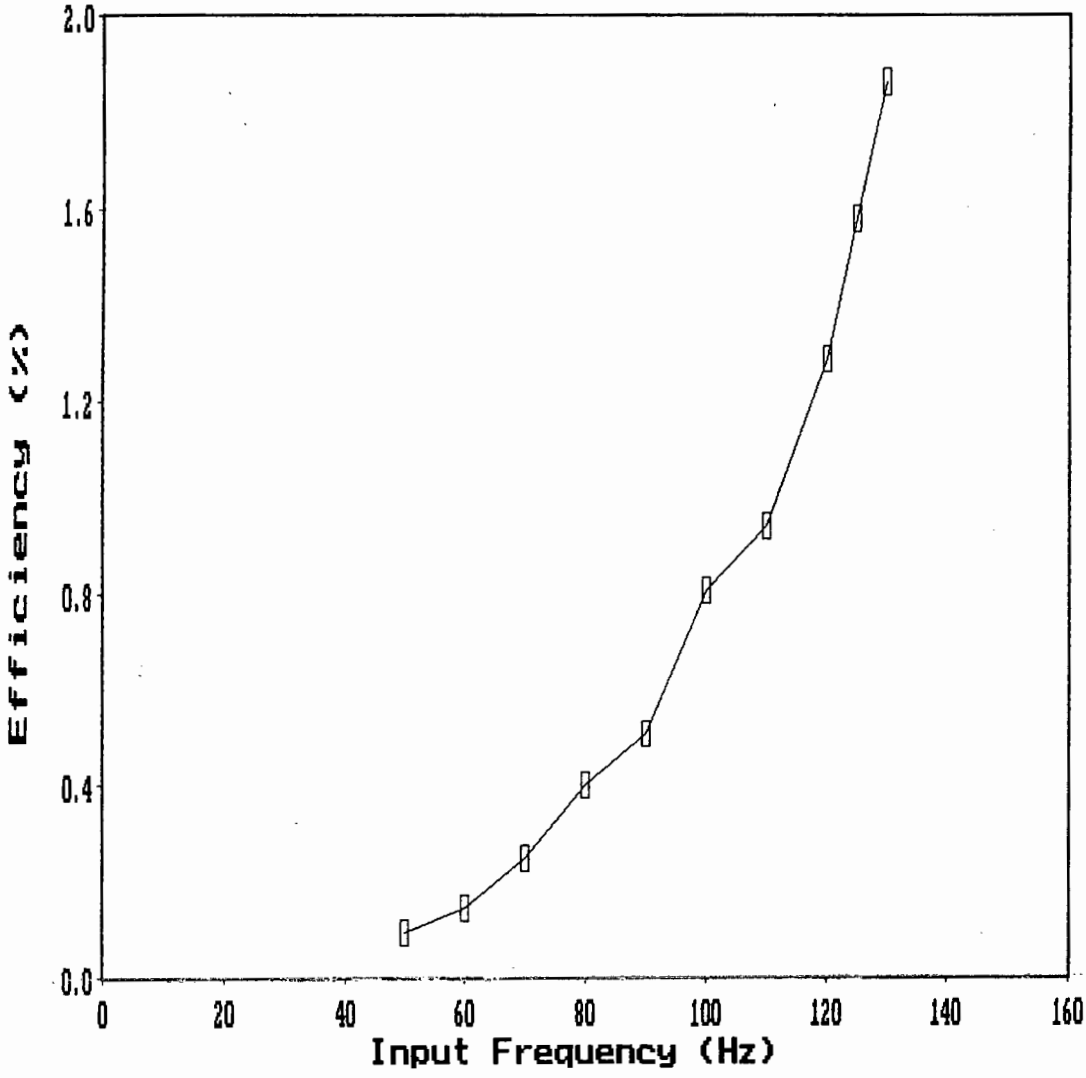

Figure 6.28: Efficiency Vs Input Frequency at 220V and rated load

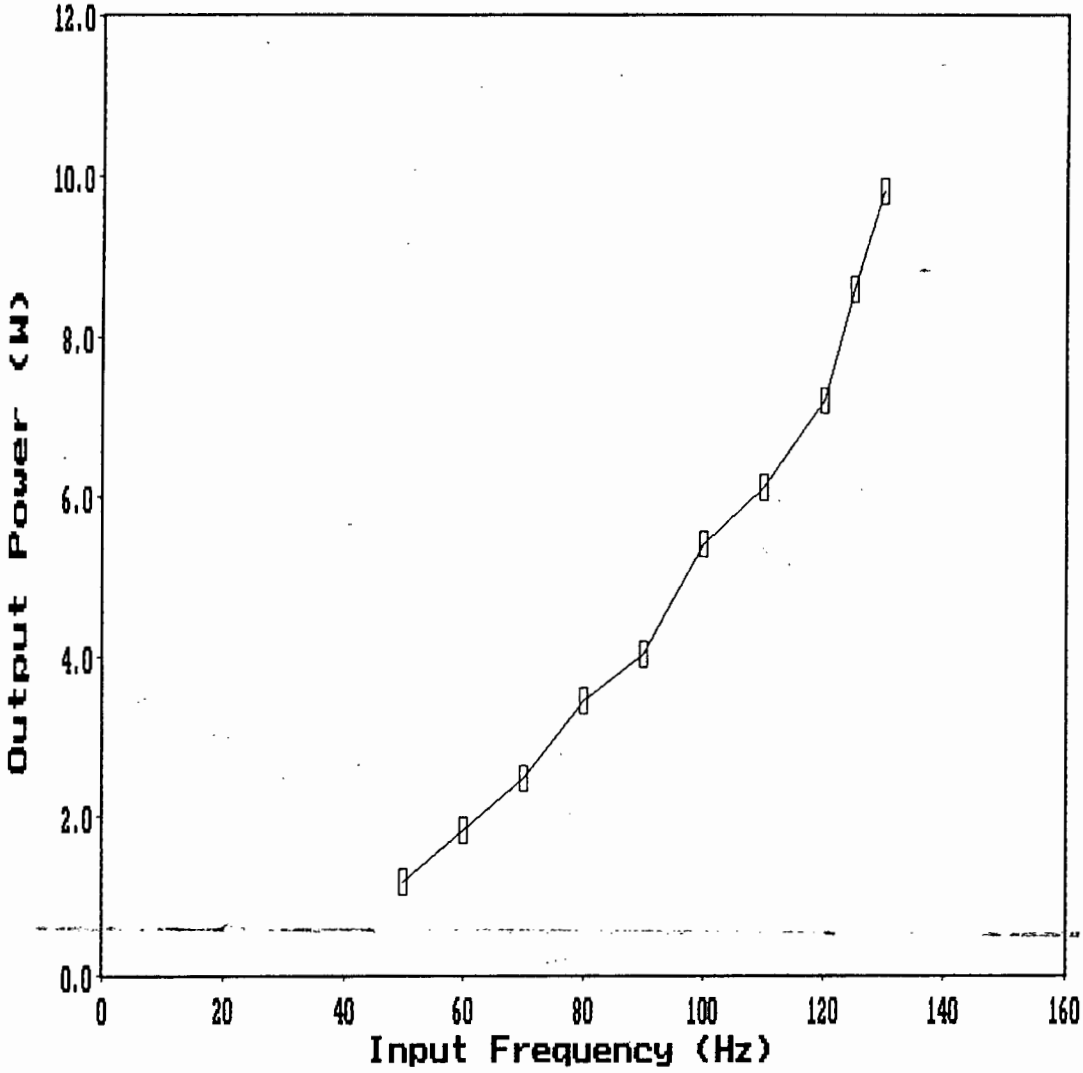

Figure 6.29: Output Power Vs Input Frequency at 220V and rated load

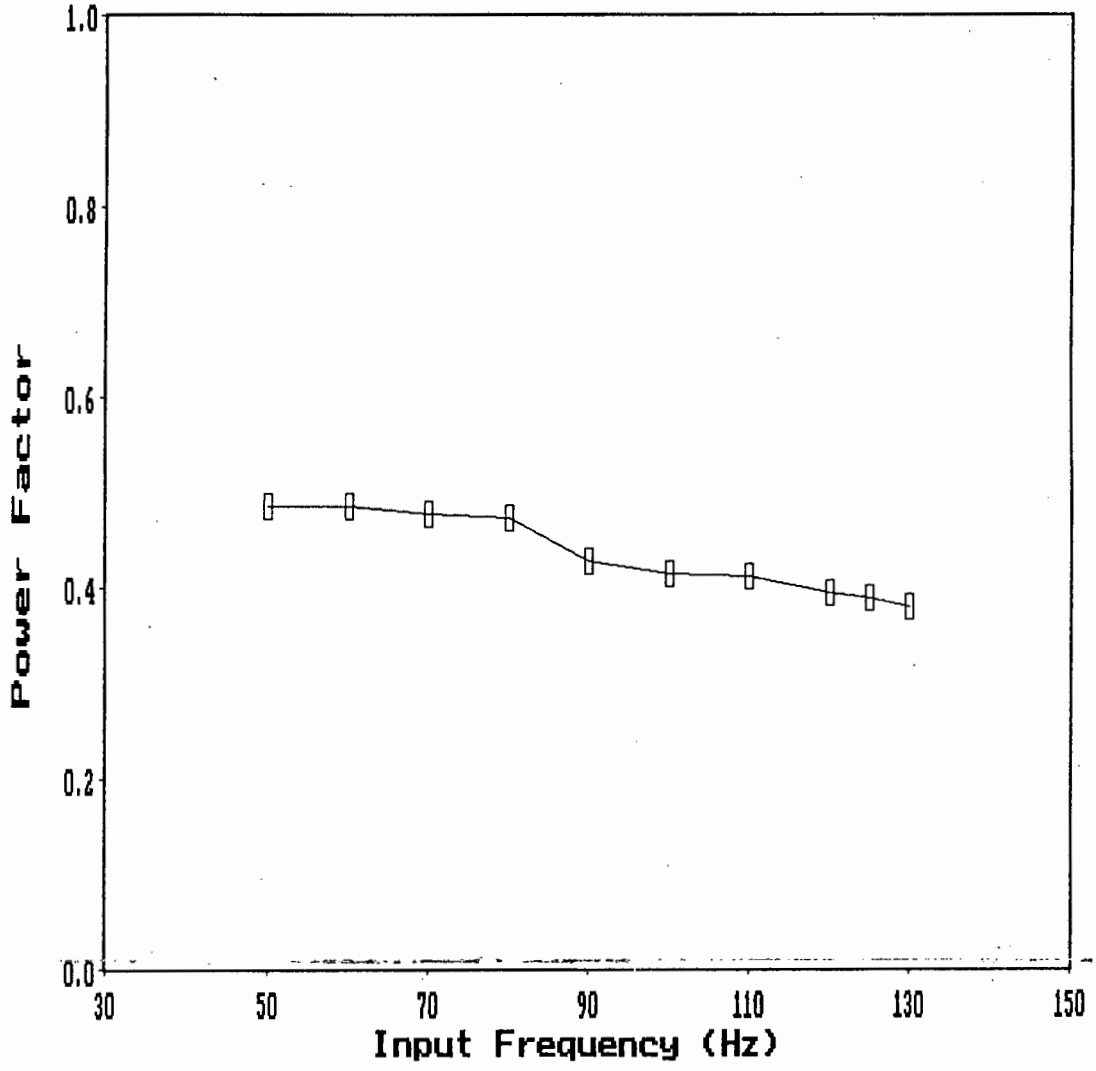

Figure 6.30: Power Factor Vs Input Frequency at 220V and rated load

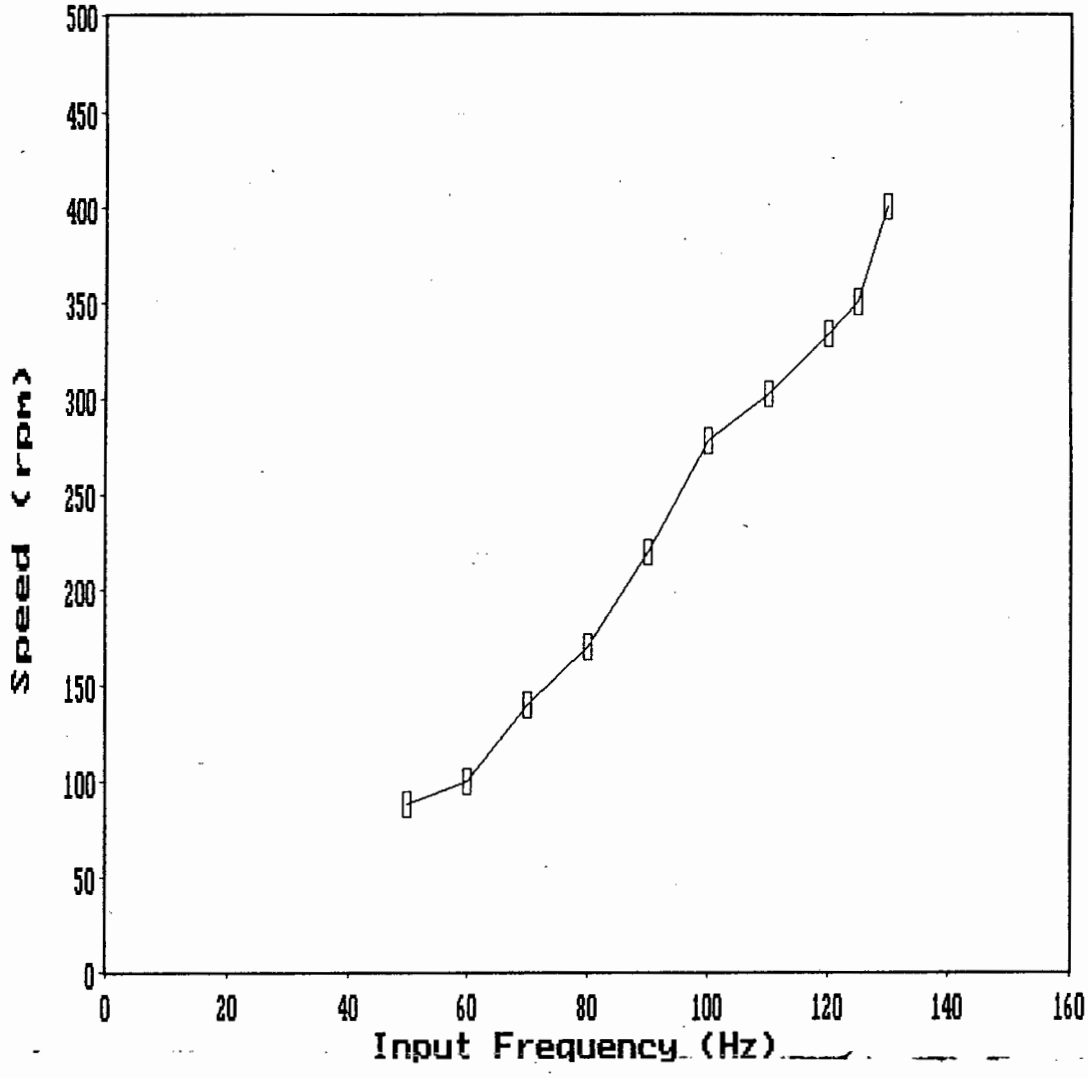

Figure 6.31: Speed Vs Input Frequency at 220V and rated load

6.3 Comments on Measurements and Analytical Results

The deviations between measurements and analytical results for various operating conditions can be attributed to several factors, which are further discussed in Chapter 7.4. The no-load test characteristics provide information for the estimation of mechanical losses in the shaded-pole LIM.

In the classical approaches, the mechanical loss is assumed to be independent of the value of supply voltage. The magnetic tension (normal force) in the direction perpendicular to the disc causes the additional mechanical loss in the shaded-pole LIM, producing braking effects. The magnetic tension incidentally depends on the value of stator voltage. Therefore, the additional mechanical loss also depends on the supply voltage. The analysis of mechanical losses can help to explain the difference between results of computation and experimental test.

Another consideration is the influence of estimated machine parameters such as the stator linkage factor γ and stator leakage factor σ_1 (equation 2.11) which is quite significant. For example, calculating the motor performance at two specific supply voltages of 90V, 160V at a frequency of 50Hz, 75Hz respectively, with these two parameters γ and σ_1 varied, the results obtained are shown in figures 6.32 and 6.33.

Table 6.3: Variation of LIM torque with γ and σ_1

	Stator linkage factor γ	Stator linkage factor σ_1
SMC1	0.85	1.16
SMC2	0.80	1.16
SMC3	0.75	1.10

From the graphs, at 50Hz and 90V, there is a better correlation between measurements and SMC3 where stator linkage and leakage factors are minimised, when compared with results for higher values. However at 75Hz and 160V, there is poorer colleration with measurements, indicating a significant frequency dependency. This implies that optimizing these machine parameters may improve on the results obtained from calculations.

Figure 6.34 shows the graph of the short-circuit charactersitics of the shaded-pole LIM from calculations using symmetrical components compared with measurements. The excellent correlation shows the reliability of this analysis technique for estimating motor parameters and losses from this data.

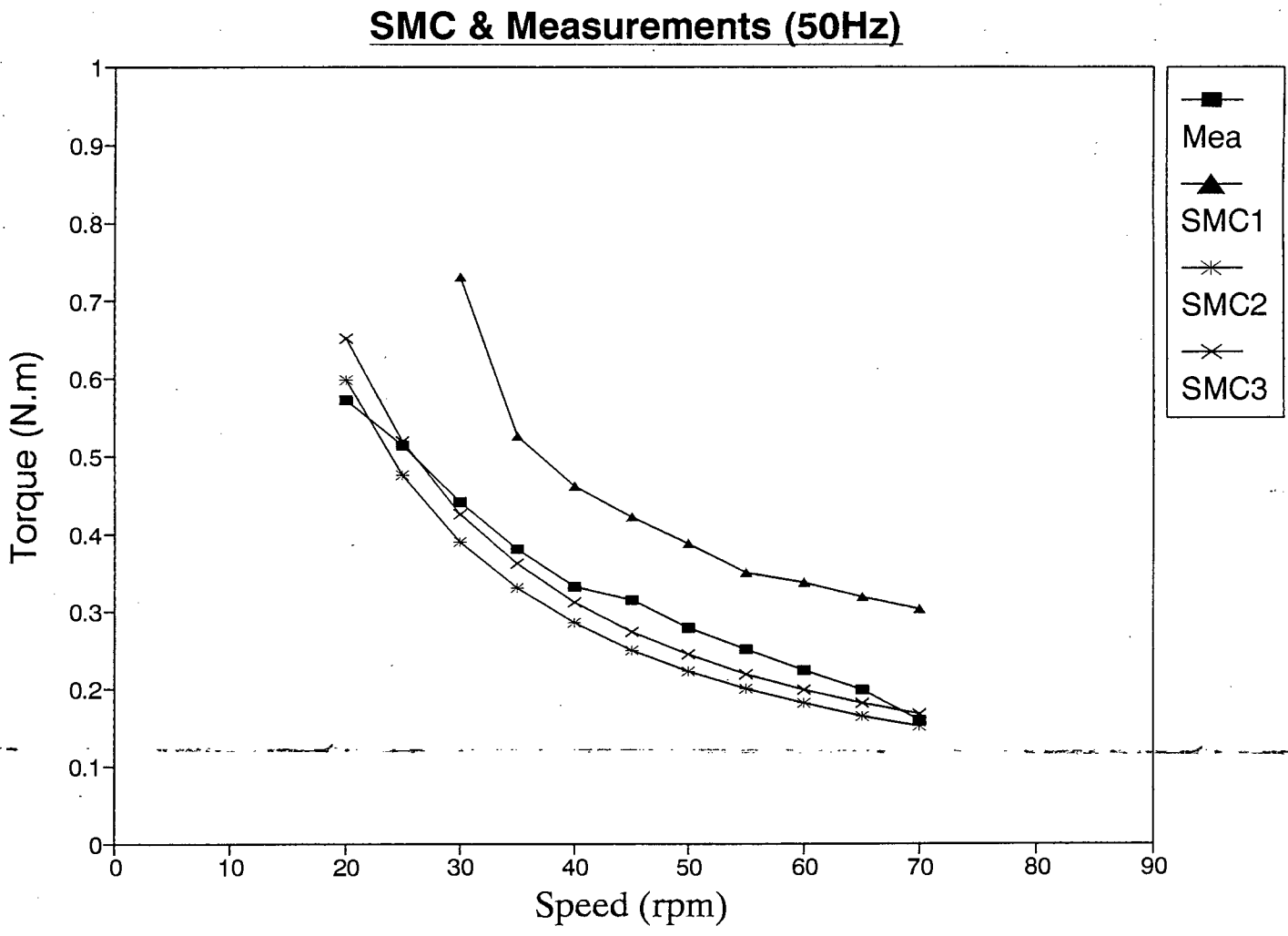

Figure 6.32: Torque Vs Speed for varying γ and σ_1, f=50Hz, V=90V

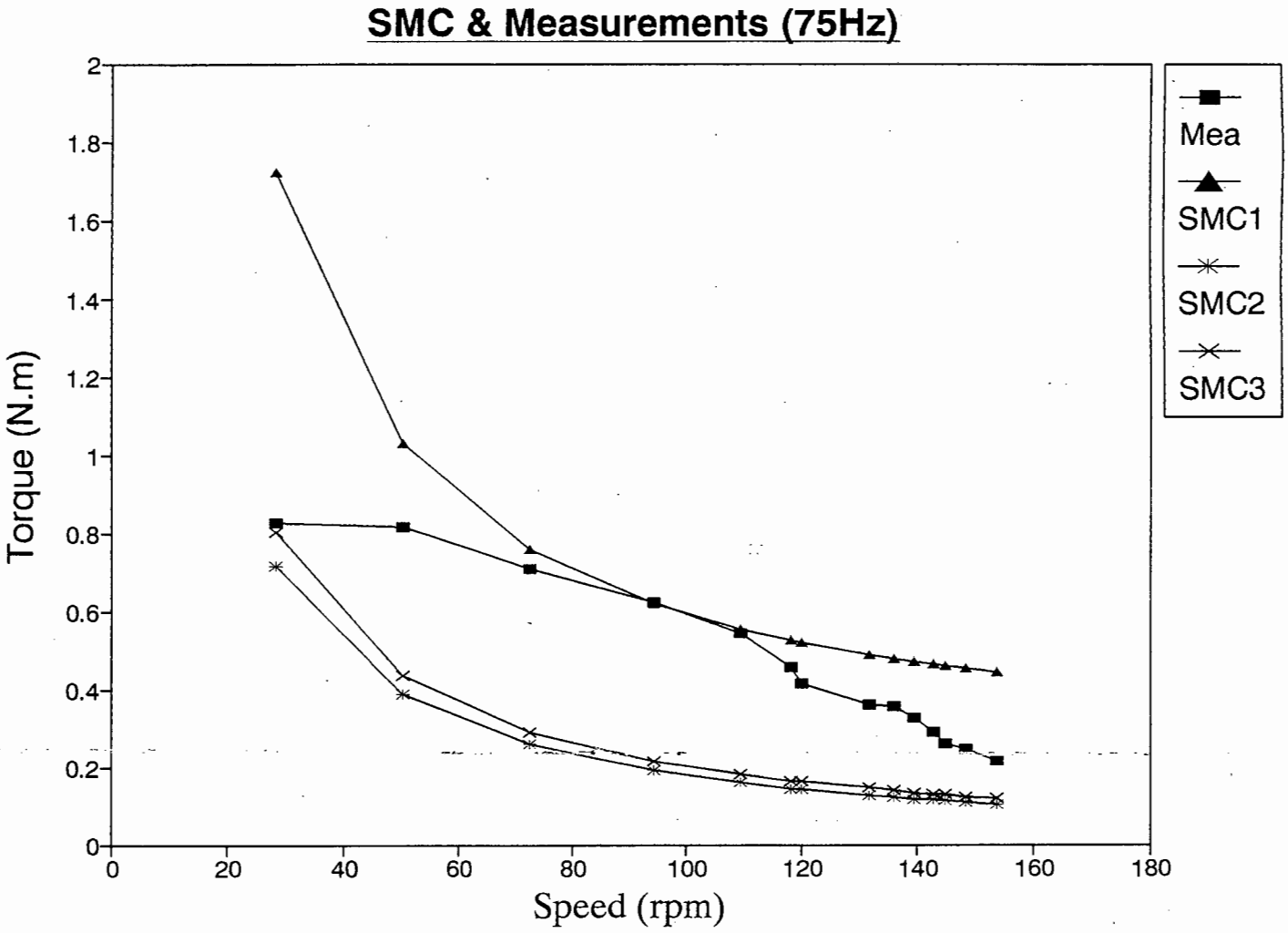

Figure 6.33: Torque Vs Speed for varying γ and σ_1, f=75Hz, V=160Hz

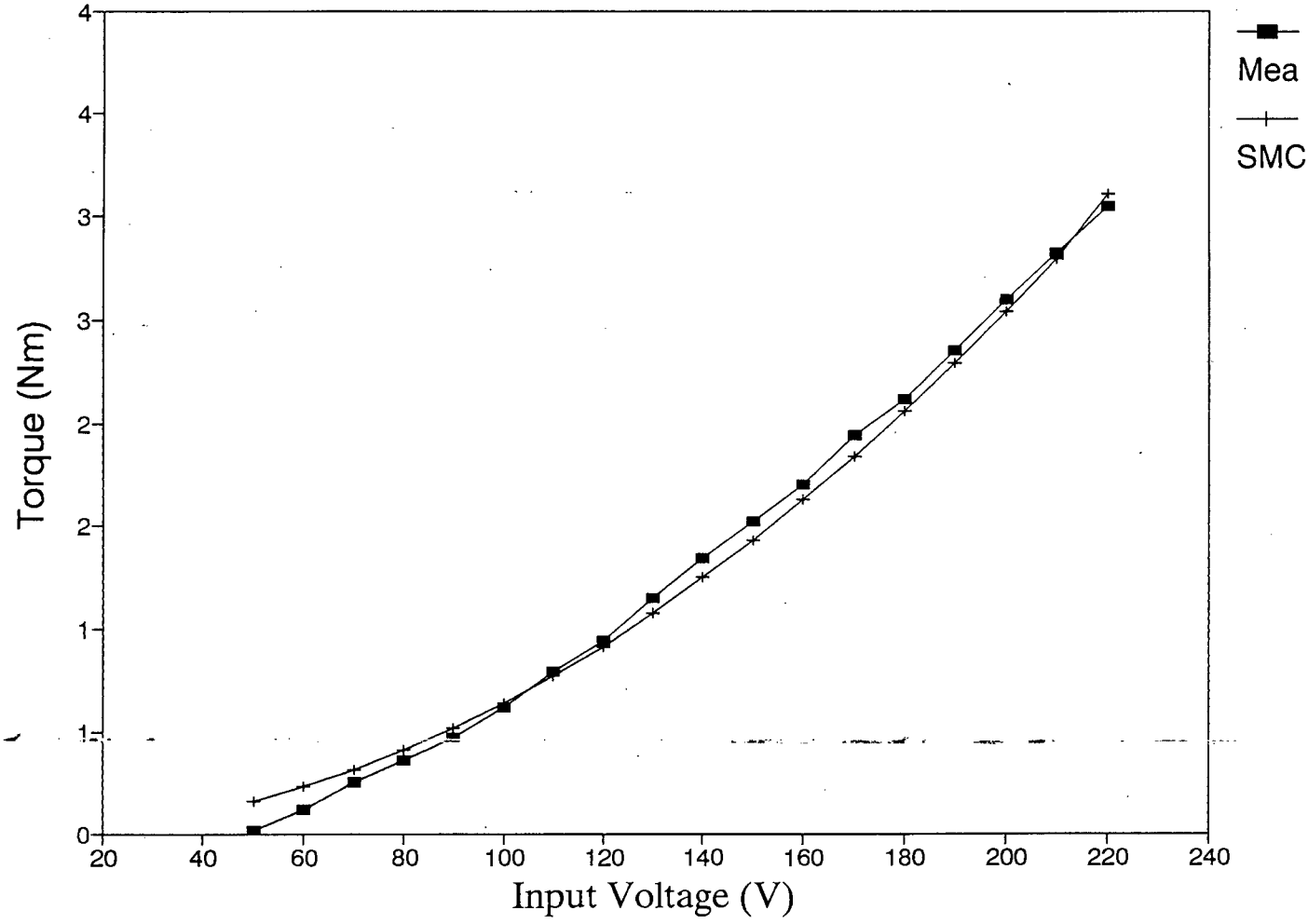

Figure 6.34: Short-circuit Test: Torque Vs Input Voltage

Chapter 7

Conclusion

7.1 Optimisation

Current trends in the design of electrical machines require optimising the construction while minimising the cost of manufacturing[80, 79, 83, 94, 1]. The induction motor remains the cheapest and most reliable electrical machine. The single-phase single-sided shaded-pole LIM under investigation is cheap to manufacture when compared to other motors. In the past, the norm has been to carry out the construction of a machine and then test. Discrepancies may then require further modifications to the design to improve its performance, hence the sequence: $\longrightarrow$ *build–test–modify* design cycle[84]. However, modern design methods for electrical machines require optimising the construction and minimising the use of materials while enhancing performance[83].

The utilisation of finite element tools for machine analysis, increasingly demand predicting the machine's performance by ascertaining an optimal design based on standard specifications, before building and testing. This certainly requires accurate design parameter estimation for the practical machine for specific industrial application, as well as creative thinking and requires extensive simulation for several operating conditions. Hence, designing, constructing and adaptation of special machines to specialised practical applications, which satisfy required specifications has become the trend also in linear machines. The application of FEM to calculate the performance is simpler than using the symmetrical components of two phase systems.

7.2 Error Estimation in Measurement and Analysis

From the experimental point of view, a few limitations were encountered during the testing. The M-G set used for variable frequency supply is a synchronous generator driven by a separately excited d.c. motor. This machine set has difficulty in varying voltage and frequency independently, a task which can be easily achieved in inverter supplies. This accounts for the slight variation in the V/f ratio for optimum LIM performance tests. Furthermore, the operating point of the synchronous machine is limited for each voltage

and frequency, beside severe vibrations and noise level. The voltage and current waveforms are very close to sinusoids with some content of the 3rd time harmonic (7-10% and 4-4.5% respectively).

7.3 Comparison of Measurements and Calculated Parameters

Figs 7.1 - 7.4 shows results for calculated characteristics and measurements. At different frequencies and machine operating conditions, each technique produced a measure of correlation with measurements than the other. The influence of a low power rating of the shaded-pole LIM further adds to this error.

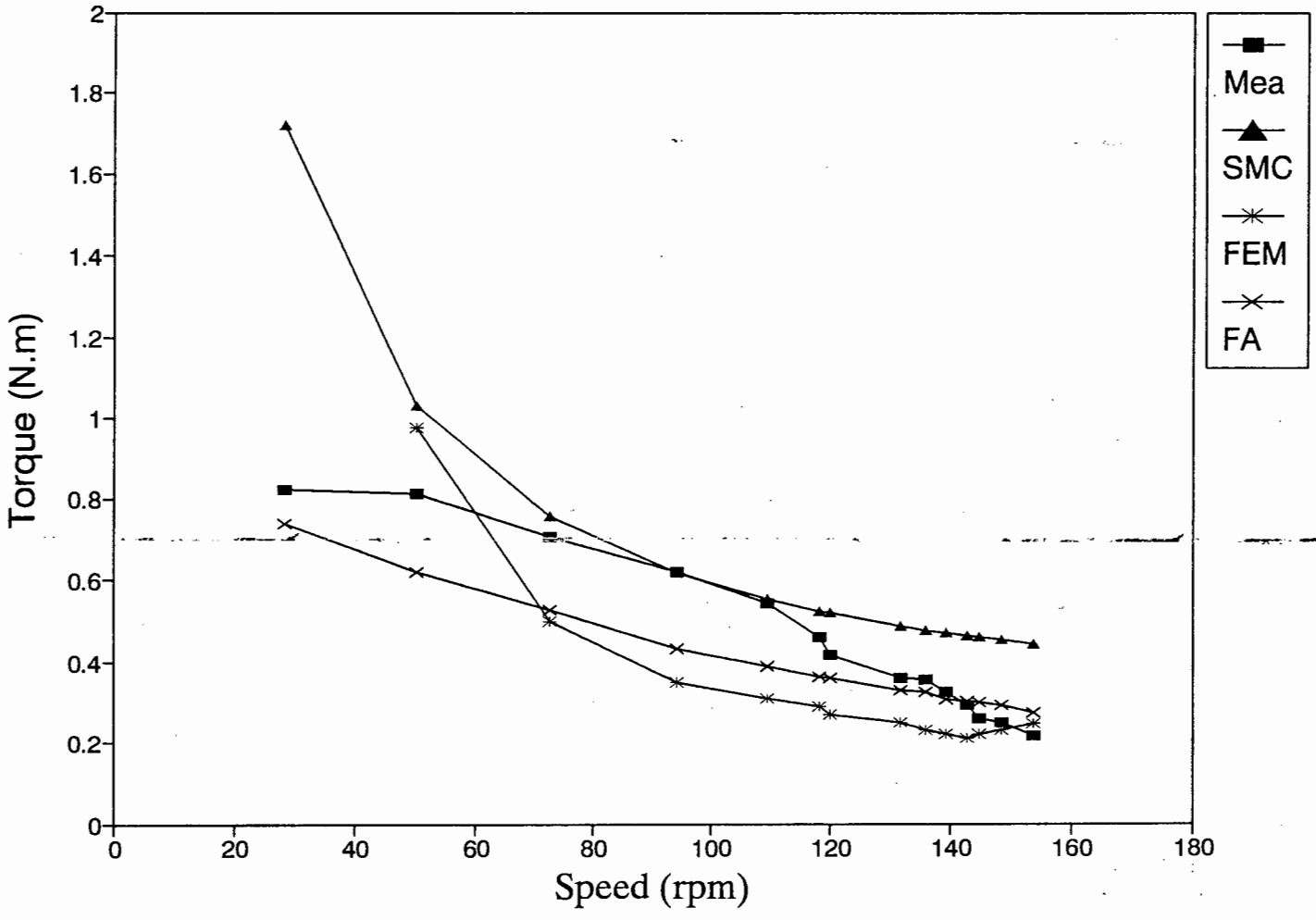

Figure 7.1: Torque against speed at $f = 75Hz$

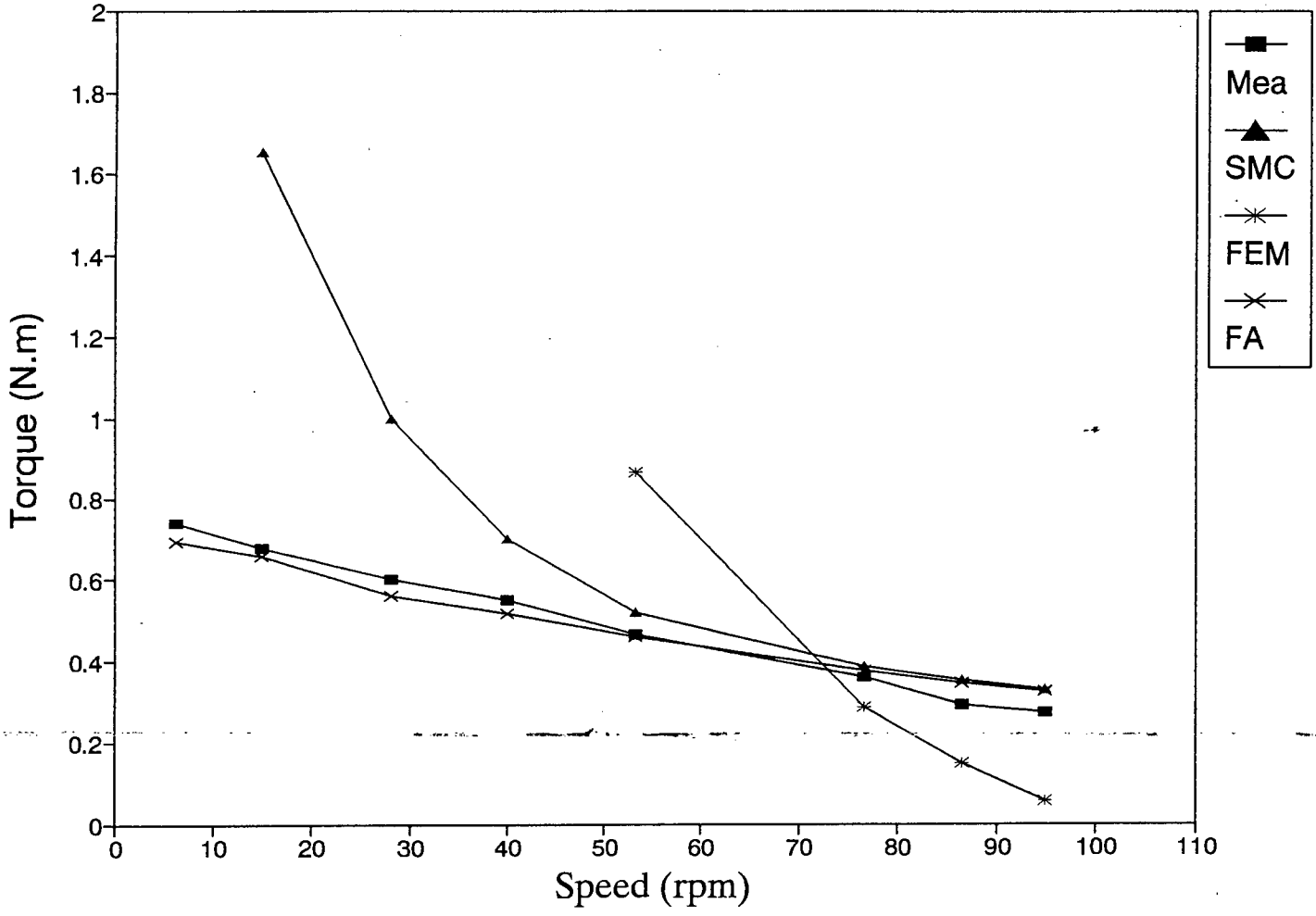

Figure 7.2: Torque against speed at $f = 60Hz$

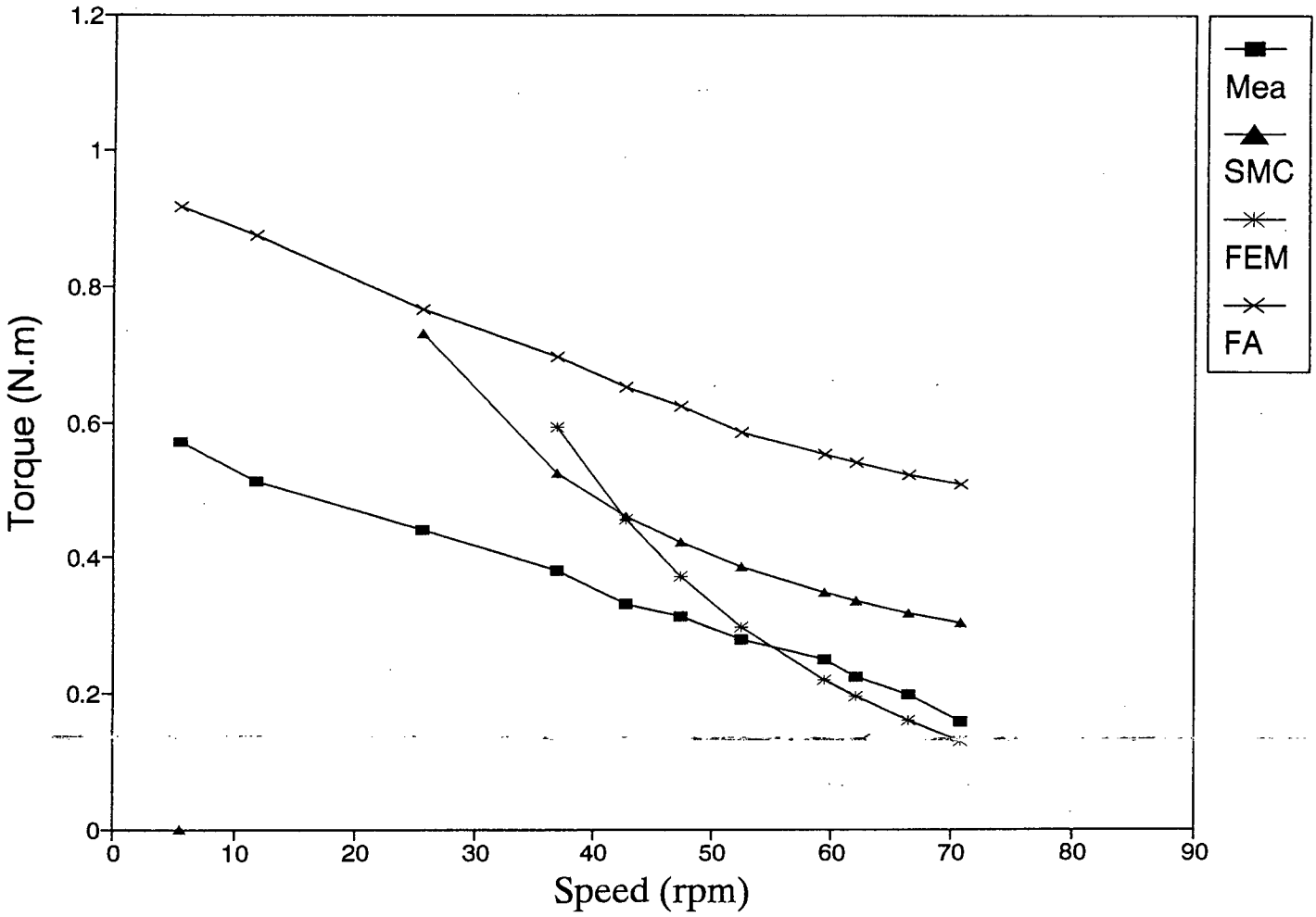

Figure 7.3: Torque against speed at $f = 50Hz$

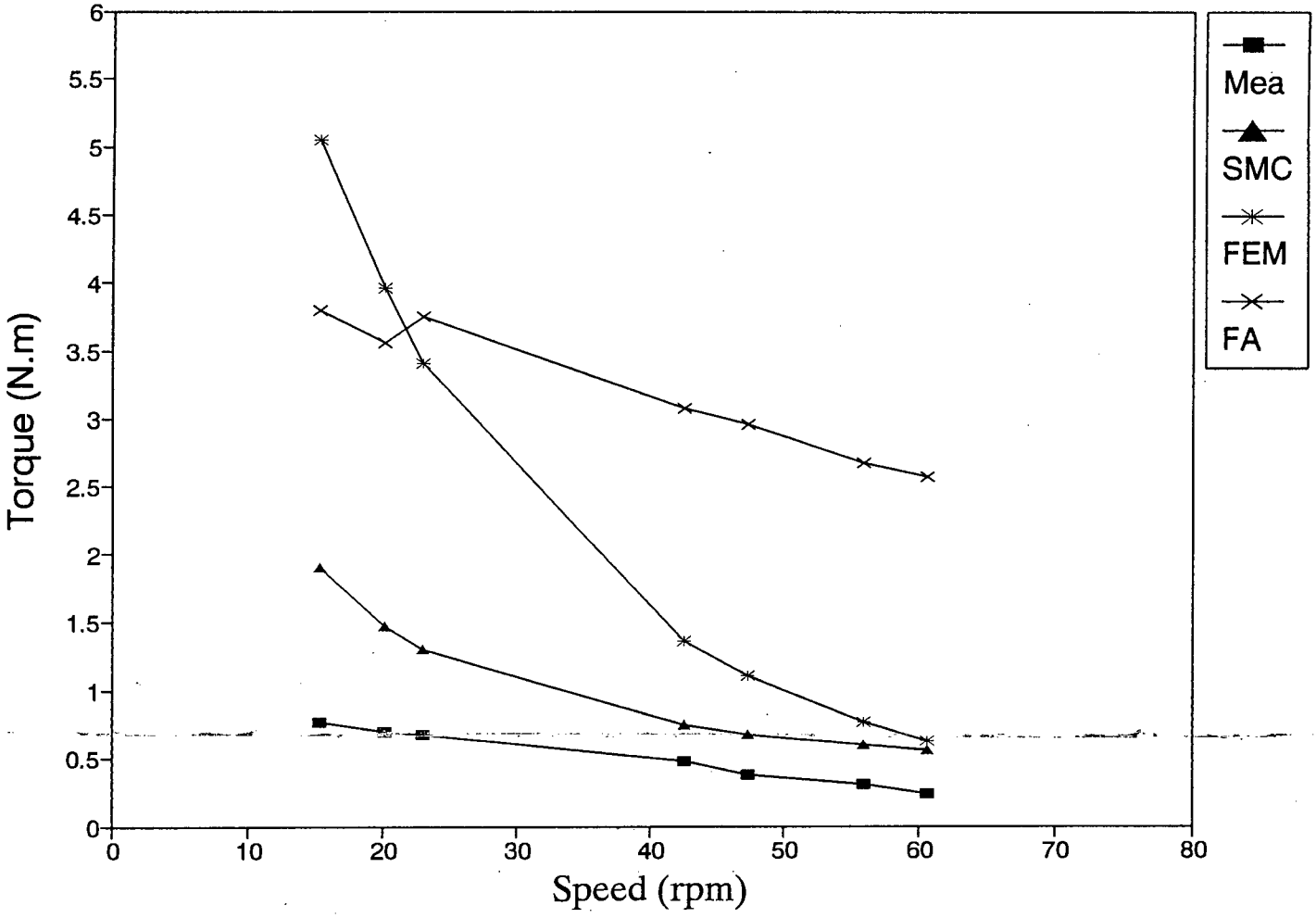

Figure 7.4: Torque against speed at $f = 40Hz$

7.4 Comparison of Analytical Techniques

The steady-state load characteristics, i.e. thrust and normal force versus speed at different power frequencies have been calculated using the symmetrical components, field theory approach and FEM. These calculated results were compared with experimental tests performed on the shaded-pole LIM using sinusoidal excitation at varying power frequencies from 50 to 75 Hz. Symmetrical components gave the best performance prediction. It is a reliable and proven method as applied to rotary motors, but also proven to yield good results as applied to the linear machines with non-symmetrical supply.

Finite element method is the trend in the modern technical world. It is a very reliable tool in design and optimization of electric motors, but requires skilled use to get proper conclusions. The 2-D FEM is versatile in the computation of field parameters especially for magnetostatic analysis. It also lends itself to the ease of optimizing the magnetic circuit. The field approach based on the multi-layer theory of a.c. machines is not flexible in modelling the LIM. The results obtained here show much deviation with varying frequency, and the curves tend to be more linear than hyperbolic. At higher frequencies, 60 and 75 Hz, the field approach correlates well with measurements, while at lower frequencies, (50 or 40 Hz) the diferences are significant.

The application of symmetrical components of two phase systems to calculate the performance of the shaded-pole LIM has been presented, and the results compared with measurements are satisfactory. Additional conclusions can be made from a comparison of results obtained from symmetrical components, FEM, field analysis with measurements. For small machines, errors in calculations are usually higher than in high performance machines. The efficiency of the low power single-phase LIMs in general is low, so that error in calculations are higher than those in high performance machines. The performance of the shaded-pole single-sided LIM is poor when compared to three-phase LIMs. However, the agreement between computation and measurements is satisfactory. These results provide information on the performance characteristics of the shaded-pole LIM, and hence make significant contributions to the understanding of the operation of this motor.

Finite-element analysis offer several advantages in addition to providing detailed field maps. By lending itself to easy digital computations, the area of computer-aided-design is advancing more than ever before. By studying electromagnetic field contour, we gain understanding of how a device works and how design modifications will affect its performance. For example, by varying the vital dimensions and/or the materials of a the LIM, its performance and sensitivity to these parameters can be observed readily. Adapting a package to suit a particular problem or vice versa requires extensive checking and modifications to obtain meaningful results. As an example, when representing supply frequency for a specific LIM test, the speed of the rotating disc is used to obtain the slip frequency which is used in the analysis.

Recall that for an LIM, speed is independent of the number of poles pairs, that is;

$$v = v_s(1 - s) = 2f\tau(1 - s) \tag{7.1}$$

where f is the input frequency, and τ is the pole pitch.

Thus, the speed of a linear induction motor can be controlled by a simple variable voltage variable frequency (VVVF) converter.

A 4-pole shaded-pole LIM with 0.52m double layer disc has been analysed and tested. The efficiency of the shaded-pole LIM is very small at power frequency. It has also been found that the efficiency increases with the input frequency. With a large air gap of 1.5mm, the magnetizing current increases significantly and consequently, stator I^2R loss in the shading coil (auxiliary winding), thereby reducing the efficiency and power factor $\cos\varphi$. From tests, it was observed that increasing frequency of supply gives better mechanical performance such as: less vibrations, improved torque and efficiency for the shaded-pole flat linear induction motor. From $50Hz$ to $75Hz$, efficiency increased by 120% of its nominal value at $50Hz$.

The influence of edge effects is minimal in low speed LIMs. However saturation effects and the presence of 3rd time harmonics in the voltage and current waveforms contribute to errors in calculations. Mechanical losses and stray load losses which have not been estimated nor included here also contribute to the differences between the results of computation and experimental test. An accurate estimation of these losses and influences will reduce the errors in calculations. Machine parameters such as linkage and leakage factors of main windings were assumed constant.

7.5 Efficiency of Shaded-pole LIM

Reference data tables show that LIMs generally have low efficiencies due to their open airgap. It is necessary to mention that the maximum efficiency of rotary shaded-pole induction motors with cage rotors rated at 10W usually does not exceed 20%. The efficiencies of LIMs and the rotary shaded-pole induction motor give the impression that hybrid forms of these machines will have a relationship in their optimal performance and efficiency. For a three-phase LIMs, rotary induction motors, rotary shaded-pole motors, etc, their efficiencies are well known. The large airgap of LIM (aluminium cap) further deteriorates the performance as compared with a rotary cage motor.

From tests performed (fig.6.9), the I^2R losses and overall performance of the shaded-pole LIM was found to be better at lower voltages and current than the rated voltage of 220V and 11.6A current. Thus, it has been found that the efficiency can be improved by reducing voltage and increasing the input frequency. Experimental tests have provided lots of information on how to improve the design techniques of shaded-pole LIMs. The optimum frequency has not been reached as the maximum frequency of 130 Hz was limited by the capability of the synchronous generator. To provide higher power supply frequencies required for better LIM performance, it is recommended to design a cheap single phase

inverter or frequency tripler to provide power supply at 150Hz. Since it is not practicable to use frequency converters in cheap drives, it is recommended that other single-phase LIMs, e.g. with auxiliary winding with capacitors be considered and investigated.

7.6 Applications

The shaded-pole LIM is simple to build, cheap to manufacture but it's mathematical model is more complicated than the model of classical induction motor. It finds use in specialised applications in industry, especially where short-time duty is only required. In the case of short-time duty, the efficiency is not as important as functional requirement. The shaded-pole LIM can find applications in turntables used in industry or in small mechanisms where a three-phase power supply is not available, and low torque is acceptable or where the price and simplicity of the drive is important. In such mechanisms like roller-conveyor system, it is often necessary to divert the load at certain points in the system to one or more tracks, for selection purposes, and the inclusion of a turntable is necessary. In these cases, the provision of one or more fixed linear motors beneath the turntable plate, which is faced with 3mm aluminium plate, provides the rotating motion, eliminating a circular motor and gearing. Position control enables the turntable to be rotated through 90° if required, with accurate stopping to within 3mm, and complete operation with reversing capabilities. Furthermore, a spare stator can be switched in if needed, either as a replacement or to increase the load capacity of the turntable under certain conditions.

In agro-allied industries, the shaded-pole LIM will find ready application of it's linear stator to the rotation of horizontal circular plates which is useful for the production of dried milk, potters' wheels, automatic cow-milking equipment, and bottle manufacture, together with lens-rotation drives for lighthouses. In each case, duty cycles are important in determining the rating of the stator required, but heat losses in the secondary are readily dissipated within its volume. The absence of a gearbox not only produces an initial saving in cost but also gives a greatly reduced maintenance cost. In some instances where more than one stator is used, it is practicable that should a stator develop a fault in service, it can be changed in a few minutes without shutting down the whole drive[95]. To achieve reduced cost of electrification, large remote rural areas in Southern Africa have only single phase power supply systems. These motors can be used in such rural areas with simple recticulation systems.

Bibliography

[1] K. Adamiak. "A method of optimization of winding in linear induction motor". *Archiv fur Elektrotechnik*, 69:83–91, Springer-Verlag 1986.

[2] M. Akbaba and S. Q. Fakhro. "An Improved Computational Technique of the Inductance Parameters of Reluctance Augmented Shaded-Pole Motors Using Finite Element Method". *IEEE Transactions on Energy Conversion*, 7(2):308–314, 1992.

[3] M. Akbaba and S. Q. Fakhro. "Field Distribution and Iron Loss Computation in Reluctance Augmented Shaded-Pole Motors Using Finite Element Method". *IEEE Transactions on Energy Conversion*, 7(2):302–307, 1992.

[4] P. L. Alger. "The dilemma of single-phase induction motor theory". *AIEE Transactions*, 77(Pt III):1045, 1958.

[5] E. V. Armensky and G. B. Falk. *Fractional-Horsepower Electrical Machines.* Mir Publishers, Moscow, Russia, 1978.

[6] K. J. Binns, P. J. Lawrenson, and C. W. Trowbridge. *The Analytical and Numerical Solution of Electric and Magnetic Fields.* Wiley, Chicester, England, 1992.

[7] J. Bohmann. "Untersuchung Uber das Verhalten von Drehstrommotoren in der Kurzschuss Sanftanhauf (Kusa) Schaltung". *Arch. Electrotech.*, 28:759–770, 1934.

[8] H. L. Bojer. "Pre-determination of shaded-pole induction-motor performance". *Det Kongelige Norske Videnskabers Seleskabs Skrifters (Trondheim, Norway)*, .(5):1–120, 1941.

[9] I. Boldea and M. Babescu. "Multilayer Theory of D.C Linear Brakes with Solid-Iron Secondary". In *Proceedings of IEE*, volume 123(3), pages 220–222, March 1976.

[10] I. Boldea and M. Babescu. "Multilayer approach to the analysis of single-sided linear induction motors". In *Proc. IEE*, volume 125(4), pages 283–287, Apr. 1978.

[11] J. R. Brauer. "Saturated Magnetic Energy Functional for Finite Element Analysis of Electric Machines". *IEEE (P.E.S.), New York*, January 1975.

[12] J. R. Brauer. *What Every Engineer Should Know About Finite Element Analysis.* Marcel Dekker, New York, 1988.

[13] J. Breimanns. "A Single-Phase Induction Motor (in German)". *Arch. fur Elek.*, 17(5):519–533, 1926.

[14] K. Burian. "Analysis of Unsymmetrical Machines". *AIEE Transactions*, 67:643–646, 1948.

[15] O. I. Butler and A. K. Wallace. "Generalized Theory of Induction Motors with Asymmetrical Primary Windings and its Application to the Analysis and Performance Prediction of Shaded Pole Motors". In *Proc. IEE*, volume 115(5), pages 685–694, May 1968.

[16] O. I. Butler and A. K. Wallace. "Effect of parameter changes on the performance of shaded-pole motors". In *Proc. IEE*, volume 116(5), pages 732–736, May 1969.

[17] C. J. Carpenter. "Surface-Integral Methods of Calculating Forces on Magnetized Iron Parts". In *The Institution of Electrical Engineers Monograph*, volume No.342, pages 19–28, August 1959.

[18] S. S. L. Chang. "The Equivalent Circuit of the Capacitor Motor". In *AIEE Proceedings*, volume 66, pages 631–640, 1947.

[19] S. S. L. Chang. "Equivalent Circuits and Their Applications in Designing Shaded Pole Motors". *AIEE Transactions*, 70:690–699, 1951.

[20] M. V. K. Chari and P. P. Silvester. *Finite Elements in Electrical and Magnetic Field Problems.* John Wiley & Sons Ltd, New York, 1980.

[21] Hoang-Minh. Dao. *Feldberechung eines spaltolmotors mit anwendung auf das anlaufverhalten.* PhD thesis, Technischen Universitat Berlin, Berlin, 1987.

[22] Hoang-Minh. Dao. "Anlaufverhalten eines Spaltpolmotors". *Archiv fur Electrotechnik*, 71:357–367, 1988.

[23] B. Davat, M. Lajoie, and J. Hector. "Magnetic Structure and Feeding Circuit Modelling". *IEEE Transactions on Magnetics*, MAG-19(6):2471–2473, November 1983.

[24] B. Davat, Z. Ren, and M. Lajoie-Mazenc. "The Movement in Field Modelling". *IEEE Transactions on Magnetics*, MAG-21(6):2296–2294, 1985.

[25] I. E. Davidson. "Performance calculation of a single-sided, single-phase shaded-pole linear induction motor using symmetrical components and finite-element method". *Electromotion*, 4(4), 1997.

[26] I. E. Davidson and J. F. Gieras. "Performance Calculation for a Shaded-pole Single-sided Linear Induction Motor Using Finite-Element Method". In *Proc. of 1st Int. Conf. on Linear Drives for Industry Applications, Nagasaki, Japan*, volume LDIA '95, pages 377–380, 1995.

[27] I. E. Davidson and J. F. Gieras. "New Shaded-pole Linear Induction Motor: Computation Using Classical and Field Theory Approach". In *Proc. of Int. Conf. on Electrical Machines, ICEM '96, Vigo, Spain*, volume II, pages 283–288, 1996.

[28] G. E. Dawson and A. R. Eastham. "The Comparative performance of single-sided linear induction motors with squirrel-cage, solid steel and aluminium-capped reaction rails". In *Proc. 16th Ann. IEEE Ind. Applications Soc. Mtg.(Philadelphia, PA)*, volume IEEE Conf. Rec.81CH 1678-2, pages 323–329, 1981.

[29] B. G. Desai and M. A. Matthew. "Transient Analysis of Shaded Pole Motor". *IEEE Transactions*, PAS-90(2):484–494, 1971.

[30] J. Donea, S. Giuliani, and A. Philippe. "Finite Elements in the Solution of Electromagnetic Induction Problems". *International Journal for Numerical Methods in Engineering*, 8, 1974.

[31] N. A. Duffie, R. D. Lorenz, and J. L. Sanders. "High-Performance LIM-Based Material Transfer". In *Proc. NSF Design and Manufacturing Systems Conf., Atlanta, GA*, volume January 8-10, 1992.

[32] J. F. Eastham. "Novel Synchronous Machines: Linear and Disc". In *Proc. IEE*, volume 137, Pt.B., No.1, pages 49–58, January 1990.

[33] J. F. Eastham and S. Williamson. "Design and analysis of close-ratio two-speed shaded-pole induction motors". In *Proc. IEE*, volume 120, pages 1243–1249, October 1973.

[34] N. R. Ermolin. *Small Power Electrical Machines (in Russian).* Energia, Moscow, 1962.

[35] A. E Fitzgerald, D. E. Higginbotham, and A. Grabel. *Basic Electrical Engineering.* McGrawHill, Singapore, 5th edition, 1981.

[36] C. L. Fortescue. "Method of Symmetrical Co-ordinates Applied to the Solution of Polyphase Networks". *AIEE Transactions*, 37(part 2):1027–1115, 1918.

[37] E. M. Freeman. *MagNet 5 User Guide - Using the MagNet Version 5 Package from Infolytica.* Infolytica, Montreal, 1993.

[38] T. Fujii. "Performance analysis of the shaded-pole motor". *Hitachi Rev.*, pages 79–86, 1953.

[39] A. Gibbon and J. H. Parker. "Operational experience with a LIM-driven transit system". In *Proc. Int. Conf. Maglev and Linear Drives*, volume May, pages 135–140, 1986.

[40] J. F. Gieras. "Analytical Method of Calculating the Electromagnetic Field and Power Losses in Ferromagnetic Half-space, taking into account Saturation and Hyteresis". In *Proc. IEE*, volume 124(11), pages 1098–1104, 1977.

[41] J. F. Gieras. *Elements of electromagnetic theory of induction machines. D.Sc Thesis.* Zeszyty Naukowe ATR 'Elektrotechnika' 70, Bydgoszcz, 1979.

[42] J. F. Gieras. "Analysis of multilayer rotor induction motor with higher space harmonics taken into account". In *Proc. IEE*, volume Pt.B, 138, pages 32–6, 1991.

[43] J. F. Gieras. "Calculation of Resistances and Reactances of a Single-Sided Linear Induction Motor". *European Transaction on Electric Power Engineering*, 2(6):383–388, 1992.

[44] J. F. Gieras. "Experimental Tests on Linear Induction Motors". In *Proc. Int. Conf. SpeedUp Technology for Railway and Maglev Vehicles, Yokohama, Japan*, volume November 22-26, 1993.

[45] J. F. Gieras. *Linear Induction Drives.* Clarendon Press, Oxford, 1994.

[46] J. F. Gieras, G. E. Dawson, and A. R. Eastham. "Performance Calculation for Single-sided Linear Induction Motors with a Double-Layer Reaction Rail Under Constant Current Excitation". *IEEE Trans. on Magnetics*, MAG-22(1):54–62, 1986.

[47] J. F. Gieras, P. K. Diale, and P. R. M. Munyay. "Linear Induction Motor for Single Phase Reticulation Systems". In *Proc. of 2nd Int. Conf. on Linear Drives for Industry Applications, Tokyo, Japan*, volume LDIA '98, 1998.

[48] J. F. Gieras, A. R. Eastham, and G.E Dawson. "Performance calculation for single-sided linear induction motors with a solid steel reaction plate under constant current excitation". In *Proc. IEE*, volume 132(4), pages 185–194, 1985.

[49] J. F. Gieras, P. Kleinhans, M. L. Manchen, and E. Voss. "Experimental Investigations of a Shaded-Pole Flat Linear Induction Motor". In *Africon'92 Int. Conf. IEEE (SA Section), Swaziland*, pages 404 – 408, 1992.

[50] P. Hammond. *Applied Electromagnetism.* Pergamon Press, Oxford, 1971.

[51] P. L. Jansen, L. J. Li, B. Werner, and R. D. Lorenz. "An Integrated Vehicle and Electromagnetic Propulsion Unit for a High-Speed Material Transport System". In *Proc. IEEE-IAS Annual Meeting, Houston, TX*, volume October, pages 274–281, 1992.

[52] A. L. Kimball Jr. and P. L. Alger. "Single-Phase Motor Torque Pulsations". *AIEE Transactions*, 43:730–739, 1924.

[53] E. E. Kimberly. "The Field Fluxes of the Shaded-Pole Motor". *AIEE Transactions*, 68:273–277, 1949.

[54] A. Krawcyzk and J. A. Tegopoulos. *Numerical Modelling of Eddy Currents.* Clarendon Press, Oxford, 1st edition, 1993.

[55] G. Kron. "Equivalent Circuits of the Shaded-Pole Motor with Space Harmonics". *AIEE Transactions*, 69:735–741, 1950.

[56] J. Kucera. "Single phase induction motor with short circuited auxiliary winding". *Revue Generale de l' Electricite (Paris, France)*, 58:185–191, May 1949.

[57] E. R. Laithwaite. *Induction Machines for Special Purposes.* Newnes, London, 1966.

[58] E. R. Laithwaite. *Transport without Wheels.* Westview Press, Inc, Colorado, 1977.

[59] E. R. Laithwaite. "Linear Induction Motors - A New Species Takes Root". *IEE Electron. & Power*, pages 355–359, 1986.

[60] E. R. Laithwaite. "Adapting a linear induction motor for the acceleration of large masses to high velocities". In *IEE Proc. Electr. Power Appl*, volume 142, No.4, pages 262–268, July, 1995.

[61] K. S. Lock. "Analysis of the Steady State Performance of the Reluctance-Augmented Shaded-Pole Motor". *IEEE Transactions on Power Apparatus and Systems*, PAS-103(9):2625–2632, 1984.

[62] K. S. Lock. "Transient Analysis of the Shaded-Pole Motor by Numerical Solution of the Basic Performance Equations". *IEEE Transactions on Power Apparatus and Systems*, PAS-103(9):2691–2698, 1984.

[63] D. A. Lowther and P. P. Sylvester. *Computer-Aided Design in Magnetics.* Springer-Verlag, New York, 1986.

[64] W. V. Lyon and C. Kingsley Jr. "Analysis of Unsymmetrical Machines". *Electrical Engineering (AIEE Transactions)*, 55:471–476, 1936.

[65] T. C. Lyoyd and Sheldon S. L. Chang. "A Design Method for Capacitor Start Motors". In *AIEE Proceedings*, volume 66, pages 1369–1374, 1947.

[66] K. Makowski. "Calculation of performance characteristics of a single-phase shaded pole induction motor by circuit-field method". In *Proc. Int. Symposium on Electromagnetic fields in Electrical Engineering*, volume ISEF'95, pages 131–134, September, 1995.

[67] T. Matsubara, Y. Ishihara, S. Kitamura, and Y. Inoue. "Magnetic Field Analysis in Shaded-pole Type Induction Motor". *COMPEL - The Int. Journal for Computational and Mathematics in Electrical and Electronic Engineering*, 11(1):97–100(c), 1992.

[68] M. McCormick, P. A. Kuale, and K. A. Foster. "Design of auxiliary phase windings for resistance-start split-phase fractional-horsepower induction motors". In *Proc. IEE*, volume 118, No.12, pages 1755–1758, December 1971.

[69] G. W. McLean. "Review of Recent Progress in Linear Motors". In *Proc. IEE*, volume 135, Part B, No.6, pages 380–416, November,1988.

[70] T.J.E Miller. *Brushless Permanent-Magnet and Reluctance Motor Drives.* Clarendon Press, Oxford, 1989.

[71] E. Morath. "A mathematical theory of shaded-pole motors". *Transactions, Royal Institute of Technology (Stockholm, Sweden)*, .(26):1–47, 1949.

[72] W. J. Morrill. "The Revolving Field Theory of the Capacitor Motor". *AIEE Transactions*, 48:614–629, April 1929.

[73] M. Nagel. "Note on theory of shaded-pole motor". *Arch. Electrotech.*, 43:32–50, 1957.

[74] T. Nakata and N. Takahashi. "Direct Finite Element Analysis of Flux and Current Distributions Under Specified Conditions". *IEEE Transactions on Magnetics*, MAG-18(2):325–330, March 1982.

[75] S. A. Nasar. "Electromagnetic theory of electrical machines". *Proceedings of the IEE*, 111(6):1123–1131, 1964.

[76] S. A. Nasar and I. Boldea. *Linear Motion Electric Machines.* Wiley, New York, 1976.

[77] V. D. Nene. *Advanced Propulsion Systems for Urban Rail Vehicles.* Prentice-Hall Inc, Englewood Cliffs, New Jersey, 1985.

[78] G. F. Nix and E. R. Laithwaite. "Linear induction motors for low-speed and standstill application". *Proc. IEE*, 113(6):1044–1056, June 1966.

[79] S. Nonaka and T. Higuchi. "Design Strategy of Single-sided Linear Induction Motors for Propulsion of Vehicles". In *Proc. of International Conference on Maglevs & Linear drives*, pages 1–5, Las-Vegas, 1987.

[80] S. Nonaka and T. Higuchi. "Design of single-sided linear induction motors for urban transit". In *Proc. of International Conference on Maglevs & Linear drives*, pages 141–148, Vancouver, 1986.

[81] T. A. Nondahl. "Equivalent Circuit Model for a Shaded Pole Induction Motor: One Shading Coil with a Stepped Air Gap". *(IEEE Transactions)*, PAS-100(1):295–302, January 1981.

[82] J.O. Ojo, A. Consoli, and T. A. Lipo. "An Improved Model of Saturated Induction Machines". *(IEEE Trans. on Industry Applications)*, 26(2):212–221, March/April 1990.

[83] H. Okuda, T. Kawamura, and M. Nishi. "Finite-Element Solution of Magnetic Field and Eddy Current Problems in the End Zone of Turbine Generators". *IEEE (P.E.S.)*, 1976.

[84] J. O. Oni and I. E. Davidson. "Electromagnetic Field Simulation By Finite Element Methods". In *Proc. of African Network for Scientific and Technical Institutions Conference*, volume ANSTI-91, 1991.

[85] H. Ooka. "Analysis of the reluctance-augmented shaded pole motor". *Elec. Eng. Japan*, 91:2118–2212, 1971.

[86] H. Ooka. "Distribution of flux, current and torque of a reluctance-augmented shaded pole motor operating under locked rotor conditions". *Elec. Eng. Japan*, 93:46–53, 1973.

[87] R. M. Pai and S. A. Nasar. "A Hybrid Method of Analysis of Low-Speed Linear Induction Motors". *IEEE Transactions on Magnetics*, MAG-23(6), November 1987.

[88] R. Perret and M. Poloujadoff. "Characteristics analysis of saturated shaded pole induction motors". *IEEE Trans. on Power Apparatus and Systems*, PAS-95(4):1347–1353, July/August 1976.

[89] M. Poloujadoff. *The theory of linear induction machinery.* Clarendon Press, Oxford, 1980.

[90] P. G. Potter and G. K. Cambrell. "A Combined Finite Element and Loop Analysis for Nonlinearly Interacting Magnetic Fields and Circuits". *IEEE Transactions on Magnetics*, MAG-19(6):2352 – 2355, November 1983.

[91] A. F. Puchstein and T. C. Llyod. "Capacitor Motors with Windings Not in Quadrature". *Electrical Engineering (AIEE Transactions)*, 54:1235–1239, 1935.

[92] J. Pustola and T. Sliwinski. *Construction and operation of single-phase motors (in Polish).* WNT, Warsaw, 1964.

[93] R. L. Russell and K. H. Norsworthy. "Eddy currents and wall losses in screened rotor induction motors". In *Proc. IEE*, volume 105A, pages 163–175, April 1958.

[94] S. Russenschunk and E. Ch. Andresen. "Mathematical design optimization of a permanent magnet synchronous motor with FD field calculation method". *The International Journal for Computational and Mathematics in Electrical and Electronic Engineering*, 11(1):101–104.

[95] G. V. Sadler and A. W. Davey. "Applications of Linear Induction Motors in Industry". In *Proc. IEE*, volume 118(6), pages 765–776, 1971.

[96] W. Seitz and A. Drehmann. "Dreiphasenasasynchron Machine mit Unsymmetrischer Shaltung". *Arch. Electrotech.*, 30:58–70, 1936.

[97] H. S. Sherer and G. E. Herzog. "The calculation of shaded-pole motor performance by use of a digital computer". *AIEE Transactions*, 78:1607–1610, 1959.

[98] Y. Shoyama, M. Ando, and H. Namikawa. "LIM driven subway railcar with small sectional area". In *Proc. Int. Conf. Maglev Transport*, pages 311–318, 1985.

[99] R. L. Stoll. *The Analysis of Eddy Currents.* Clarendon Press, Oxford, 1974.

[100] F. W. Suhr. "A Theory for Shaded-Pole Induction Motors". *AIEE Transactions*, 77:509–515, August 1958.

[101] M. S. Thacker and G. R. Ranganath. "An analysis of shaded-pole motors by symmetrical components". *Electrotechnics*, 22:104–120, 1950.

[102] P. H. Trickey. "An Analysis of the Shaded Pole Motor". *AIEE Transactions*, 55:1007–1014, September 1936.

[103] P. H. Trickey. "Performance Calculations on Shaded Pole Motors". *AIEE Transactions*, 66:1431–1438, 1947.

[104] D. B. Turner and W. L. Wolf. "Houston WEDWAY people mover control and propulsion system". In *Proc. 32nd IEEE Vehicular Technol. Conf.(San Diego, CA)*, May, 1982.

[105] P. Vaske. "Contributions to the theory of the shaded-pole motors". *Arch. Electrotech.*, 47:1–28, 1962.

[106] C.G. Vienott. *Fractional and subfractional horsepower electric motors.* McGraw-Hill, New York, 1970.

[107] A. K. Wallace and O. I. Butler. "Equivalent Circuit for Nonquadrature, Tapped-Quadrature and Shaded-Pole Single-Phase Induction Motor". *Proceedings of the IEE*, 115(12):1767–1771, December 1968.

[108] S. Williamson. "Induction motor modelling using finite elements". In *Proc. of Int. Conf. on Electrical Machines, Paris, France*, volume 1, pages 1–8, September 1994.

[109] S. Williamson and P. Breese. "Effect of Airgap-Profile Variations on the Performance of Reluctance-Augmented Shaded-Pole Motors". In *Proc. IEE*, volume 124, pages 860–864, October 1977.

[110] S. Williamson and P. Breese. "Evaluation of the reluctance-augmented principle in shaded-pole motors". In *Proc. IEE*, volume 125, pages 831–835, September 1978.

[111] S. Williamson and M. Ostojic. "Reversing shaded-pole motor with effective ring shift". In *Electric Power Applications*, volume 1, pages 31–35, February 1978.

[112] S. Yamamura. *Theory of Linear Induction Motors.* John Wiley & Sons Inc, New York, 2nd edition, 1979.

Appendix A

Table 7.1: B-H Curve for Cold Rolled Steel Primary Core

Magnetic Flux Density (B) (T)	Magnetic Field Intensity (H) (A/m)
0.0	0.0
0.1	45.0
0.2	70.0
0.4	90.0
0.6	115.0
0.8	130.0
0.9	150.0
1.0	165.0
1.1	185.0
1.2	220.0
1.3	275.0
1.4	400.0
1.45	500.0
1.5	740.0
1.6	1350.0
1.65	2100.0
1.7	4200.0
1.8	7500.0
1.9	15000.0
2.0	23000.0
2.1	35000.0
2.2	50000.0
2.3	90000.0

Table 7.2: B - Specific Loss Curve for Cold Rolled Steel Primary Core

Magnetic Flux Density (B) (T)	Specific Loss (ΔP_{Loss}) (W)
0.0	0.0
0.2	0.25
0.4	0.5
0.5	0.7
0.6	0.95
0.7	1.2
0.8	1.56
0.9	1.95
1.0	2.4
1.2	3.6
1.4	4.9
1.5	5.6
1.6	6.4
1.7	7.3
1.8	8.2
1.9	9.1
2.0	10.0
2.1	11.1
2.2	12.2
2.5	16.0
2.8	20.0
3.0	23.0

Table 7.3: H_{Fe}, B_{Fe}, a_R, a_X Data for Solid Steel Secondary

Magnetic field intensity	Magnetic flux density		
H_{Fe}	B_{Fe}	a_R	a_X
(A/m)	(T)		
0.0	0.0	0.83	0.95
100.0	0.016	0.84	0.94
350.0	0.660	0.90	0.90
1000.0	1.257	1.61	0.93
2000.0	1.410	1.72	0.80
4000.0	1.508	1.61	0.78
6000.0	1.583	1.56	0.80
10000.0	1.598	1.52	0.82
16000.0	1.61	1.49	0.85
100000.0	1.63	1.42	0.90
1000000.0	1.68	1.40	0.90

For the 2-D analysis, $\beta = \pi/2$ and,

$$\chi_i = (\alpha_i^2 + \beta^2)^{1/2} = (a_{Ri} + j a_{Xi}) k_i$$

The complex propagation constant, $\alpha_{\nu i}$, is a function of slip s. For the forward travelling magnetic field[41, 42]:

$$\alpha_{\nu i} = \alpha_{\nu i}^{+} = \sqrt{j\omega_{\nu i}^{+} \mu_i \sigma_i}$$

$$= (a_{Ri} + j a_{Xi}) \sqrt{1 - \nu(1-s)} k_i$$

For the backward travelling magnetic field[41, 42]:

$$\alpha_{\nu i} = \alpha_{\nu i}^{-} = \sqrt{j\omega_{\nu i}^{-} \mu_i \sigma_i}$$

$$= (a_{Ri} + j a_{Xi}) \sqrt{1 + \nu(1-s)} k_i$$

Appendix B

Table 7.4: Shaded-Pole Flat Linear Induction Motor Load Test Data - 50Hz

Voltage (V)	Current (A)	$Cos\Theta$	Speed (rpm)	P_{in} (W)	Torque (N-m)	P_{out} (W)	Efficiency $\eta(100\%)$
90	4.94	0.495	70.8	220.08	0.1584	1.1746	0.5337
90	4.94	0.495	66.5	220.08	0.1982	1.3806	0.6273
91	4.95	0.500	62.1	225.23	0.2231	1.4505	0.6440
91	4.96	0.500	59.5	225.68	0.2504	1.5600	0.6912
90	4.90	0.500	52.5	220.50	0.2793	1.5358	0.6965
90	4.91	0.500	47.4	220.95	0.3150	1.5635	0.7076
90	4.91	0.500	42.8	220.95	0.3315	1.4856	0.6724
90	4.92	0.500	36.9	221.40	0.3796	1.4669	0.6625
89	4.89	0.500	25.6	217.60	0.4399	1.1792	0.5419
89	4.87	0.505	11.7	218.88	0.5128	0.6283	0.2871
89	4.85	0.505	5.60	217.98	0.5716	0.3352	0.1538

Table 7.5: Shaded-Pole Flat Linear Induction Motor Load Test Data - 60Hz

Voltage (V)	Current (A)	$Cos\Theta$	Speed (rpm)	P_{in} (W)	Torque (N-m)	P_{out} (W)	Efficiency $\eta(100\%)$
110	5.40	0.480	95.0	285.12	0.2710	2.6960	0.9456
110	5.42	0.482	86.5	287.37	0.2939	2.6625	0.9265
110	5.43	0.485	76.6	289.69	0.3586	2.8762	0.9951
109	5.39	0.492	53.3	289.05	0.4649	2.5947	0.8977
109	5.39	0.500	14.9	293.76	0.6775	1.0571	0.3599
109	5.37	0.500	6.20	292.67	0.7421	0.4818	0.1646

Table 7.6: Shaded-Pole Flat Linear Induction Motor Load Test Data - 75Hz

Voltage	Current	$Cos\Theta$	Speed	P_{in}	Torque	P_{out}	Efficiency
(V)	(A)		(rpm)	(W)	(N-m)	(W)	$\eta(100\%)$
160	6.61	0.455	153.8	481.21	0.2168	3.4918	0.7256
161	6.60	0.458	148.4	486.67	0.2482	3.8579	0.7927
161	6.64	0.460	144.9	491.76	0.2606	3.9540	0.8040
161	6.62	0.458	142.7	488.15	0.2921	4.3643	0.8941
161	6.64	0.461	139.4	492.83	0.3252	4.7473	0.9633
162	6.63	0.460	136.0	494.07	0.3567	5.0798	1.0282
162	6.61	0.462	131.8	494.72	0.3606	4.9776	1.0061
161	6.60	0.470	120.1	499.42	0.4148	5.2174	1.0447
161	6.62	0.470	118.2	500.94	0.4586	5.6767	1.1332
161	6.63	0.470	109.5	501.69	0.5441	6.2389	1.2436
161	6.61	0.480	94.30	510.82	0.6212	6.1346	1.2010
161	6.64	0.480	72.70	513.14	0.7088	5.3960	1.0516
161	6.68	0.481	50.30	517.31	0.8151	4.2934	0.8300
160	6.70	0.482	28.30	516.70	0.8255	2.4465	0.4735
160	6.67	0.484	19.20	516.52	0.8818	1.7730	0.3433

Appendix C

Table 7.7: Magnetic Flux Density Measurements

Pole No.	Reading No.	Flux Density, $\|B\|$ Tesla (T)	Flux Density, $\|B\|$ Tesla (T)
		V = 113.2volts	Rated Voltage
1st Half-Pole			
	1	0.018	0.0377
	2	0.027	0.0565
	3	0.033	0.069
	4	0.033	0.069
1st Full Pole			
	1	0.012	0.0251
	2	0.031	0.0649
	3	0.049	0.1025
	4	0.049	0.1025
	5	0.024	0.0502
	6	0.020	0.0419
Interpole	7	0.014	0.0293
2nd Full Pole			
	1	0.028	0.0586
	2	0.053	0.1109
	3	0.050	0.1046
	4	0.036	0.0753
	5	0.019	0.0398
3rd Full Pole			
	1	0.018	0.0377
	2	0.032	0.067
	3	0.055	0.1151
	4	0.054	0.113
Shaded-pole	5	0.046	0.0962
	6	0.026	0.0544
	7	0.021	0.0439
2nd Half Pole			
	1	0.021	0.0439
	2	0.026	0.0544
	3	0.024	0.0502
	4	0.017	0.0356

Table 7.8: Magnetic Flux Density Vs Voltage ($B \propto V$)

Current	Voltage	Flux Density (B)
I	V	Tesla (T)
2.7	50.4	0.021
4.0	75.3	0.034
5.31	100.5	0.046
6.25	119.4	0.058
11.5	220	0.1165